

Structural characterisation of FACT histone chaperone complex

Gabriele Marcianò, M.Sc. (Hons)

Submitted in fulfilment of the requirements for the Degree
of
Doctor of Philosophy

Beatson Institute for Cancer Research
School of Medicine
College of Medical, Veterinary and Life Sciences
University of Glasgow

May 2015

Supervisor: Dr. Danny T Huang

Abstract

Due to the huge amount of DNA and the small space in which this is stored, cells package DNA into condensed chromatin. During DNA replication, repair or transcription, cells need to reorganize chromatin structure in order to gain access to the DNA. To do so they use a wide range of enzyme that can modify chromatin structure such as acetyltransferases, methyltransferases and others. Chromatin remodelling is also accomplished by ATP dependent and independent histone chaperones. One of the ATP independent histone chaperones is FACT (facilitate chromatin transcription), which is a heterocomplex of SSRP1 and Spt16. Studies on FACT showed that it is implicated in DNA replication, transcription and repair. To date little is known about its mechanism of action; but based on recent structural studies of its individual domains, it has been proposed that FACT reorganizes nucleosome by eviction of the heterocomplex H2A/H2B. Nevertheless, how FACT reorganizes nucleosomes remains elusive. Studies conducted in several cancer cell lines have shown that FACT is overexpressed in these cells and that knockdown of FACT reduces cells proliferation suggesting that FACT may be a cancer therapeutic target.

Here I report the structure of human Spt16 N-terminal domain, which resembles an aminopeptidase domain lacking a catalytic centre. Sequence conservation and electrostatic surface analyses of this domain reveal some acidic regions that might be associated with histone binding. Indeed, ITC analysis showed that this domain binds both histone H2A/H2B and (H3/H4)₂ at mid-low μM affinity. Interestingly, Spt16 N-terminal domain showed a sequential binding event both for *G. gallus* and *X. laevis* histone dimer H2A/H2B.

On the onset of my project there was no structure for Spt16 middle domain. To gain insight into FACT mechanism of action, I determined the structure of *D. rerio* Spt16 middle domain. Surprisingly this domain resembles a double PH domain, which is similar to the POB3 middle domain and RTT106 except for having a U-turn motif at its C-terminus. Sequence conservation and electrostatic surface analyses of this domain reveal two possible surfaces for histone binding. Interestingly, ITC analysis showed Spt16 middle domain has weak binding affinity for both histone H2A/H2B and (H3/H4)₂ with the latter displaying a double binding event. Moreover, ITC analysis showed that Spt16 middle domain binds histone H2A/H2B via the U-turn motif consistent with the recent published data.

Finally, I investigated the solution structure of SSRP1 by using AUC and SAXS analysis. I found that SSRP1 is an elongated homodimer, which assumes an open v conformation. Mutations in PH2 or PH3 domain alone resulted in the formation of monomer suggesting that SSRP1 homodimer may assume an asymmetric conformation. Interestingly, PH2 and PH3 domain mutants displayed weaker histone binding affinity than wild type suggesting that homodimerization plays a role in histone binding.

Acknowledgements

First of all, I would like to thank my wife Erisa Llaka for her support and understanding in these four years. I would like to thank my parents and their effort thanks to which all of this has been possible.

I would like to thank my supervisor Dr. Danny Huang for his helpful and wise advises during these four years of my PhD. I am grateful to my advisor Peter Adams for his advice and discussion of my project. I would like to thank Dr. Olwyn Byron for giving me the opportunity to use and learn the Analytical ultracentrifugation (AUC). I would like to thank postdocs, Mads Gabrielsen and Lori Buetow, for their advice and for sharing their knowledge in this field. I would like to thank Gary Sibbet for his big help in purifying the histone core from chicken blood and from inclusion body and for being such a good friend in supporting me in the lab. I would like to thank Alexander Schüttelkopf for his valuable comments on my ITC results. Thanks also go to the other members of R04 group: Amrita Patel; Dominika Kowalczyk; Marta Klejnot and Hao Dou for their help and friendship. I would also like to thank Giancarlo Tria from DESY synchrotron at Hamburg for giving me the opportunity to analyse my protein by using SAXS.

I would like to thank the Beatson central service, proteomic facility and molecular technology service for their help. I would also like to thank Diamond light source (DLS) at Oxford and EMBL Desy synchrotron at Hamburg for beamtime and assistance.

Last but not least, I am thankful to Cancer Research UK for funding my studies and our research.

Author's Declaration

I declare that I am the sole author of this thesis and the work presented here is entirely my own, except where acknowledged to others. This thesis does not include work that has been submitted for consideration for another degree in this or any other university.

Table of Contents

Abstract	ii
Acknowledgements	iv
Author's Declaration	v
Table of Contents	vi
List of Figures	ix
List of Tables	xii
Abbreviations	xiii
Chapter 1	16
1 Introduction	17
1.1 Epigenetic overview	17
1.1.1 Chromatin architecture	17
1.1.2 Histone post-translational modifications	21
1.1.3 Chromatin remodellers	27
1.1.4 Histone chaperones	31
1.2 Facilitates Chromatin Transcription (FACT)	37
1.2.1 FACT and transcription	37
1.2.2 FACT and DNA damage	38
1.2.3 FACT and DNA replication	38
1.2.4 Suppressor of Ty 16 (Spt16)	41
1.2.4.1 <i>Spt16</i> NTD	41
1.2.4.2 <i>Spt16</i> DD	43
1.2.4.3 <i>Spt16</i> MD	44
1.2.4.4 <i>Spt16</i> CTD	46
1.2.5 Structure-specific recognition protein-1 (SSRP1)	46
1.2.5.1 <i>SSRP1</i> NTD/DD	46
1.2.5.2 <i>SSRP1</i> MD	48
1.2.5.3 <i>HMG domain</i>	49
1.2.6 FACT functions and their regulations	50
1.2.7 FACT activity models	51
1.3 Histone Chaperone and Cancer	54
1.4 Objective	55
Chapter 2	56
2 Materials and methods	57
2.1 Molecular cloning	57
2.1.1 Plasmid source and cDNA	57
2.2 Expression and purification of recombinant proteins	57

2.2.1	Purification of Hu Spt16 NTD	59
2.2.2	Purification of Dr Spt16 MD	59
2.2.3	Purification of SSRP1 constructs	59
2.2.4	Purification of FACT	60
2.2.5	Histone dimer and tetramer purification from <i>Xenopus laevis</i>	60
2.2.5.1	Histone H2A/H2B and H3/H4 refolding	60
2.2.6	Histone octamer purification from <i>Gallus gallus</i>	61
2.3	Crystallization	63
2.3.1	Hu Spt16 NTD ₁₋₅₁₀ crystal	63
2.3.2	Dr Spt16 MD ₆₁₃₋₉₃₀ crystal	63
2.4	Data collection and processing	63
2.5	Structure determination and refinement	64
2.5.1	Structure of Hu Spt16 NTD ₁₋₅₁₀	64
2.5.2	Structure of Dr Spt16 MD ₆₁₃₋₉₃₀	64
2.6	Small angle X-ray scattering (SAXS)	65
2.6.1	Data collection and processing (by Giancarlo Tria)	65
2.7	Analytical Ultracentrifugation (AUC)	65
2.7.1	AUC analysis of SSRP1 constructs	65
2.8	Isothermal titration calorimetry (ITC)	66
2.8.1	ITC data collection and analysis	66
2.9	Surface plasmon resonance (SPR) (by Gary Sibbet)	67
Chapter 3	68
3	Structural and functional analysis of Hu Spt16 N-terminal domain	69
3.1	Aims and objective	69
3.2	Results	70
3.2.1	Hu Spt16 NTD purification and crystallization	70
3.2.2	Structure determination of Hu Spt16 ₁₋₅₁₀	71
3.2.3	A conserved pocket on Spt16 NTD might be responsible for histone binding	73
3.2.4	Functional analysis of Hu Spt16 NTD	75
3.2.4.1	Hu Spt16 NTD binds both histones H2A/H2B and (H3/H4) ₂ with low affinity	75
3.2.4.2	Hu Spt16 N-terminal domain does not bind histone tails H3 and H4	80
3.3	Discussion	83
Chapter 4	86
4	Structural and functional analysis of Dr Spt16 middle domain	87
4.1	Aims and objective	87
4.2	Results	88
4.2.1	Strategies	88
4.2.2	Dr Spt16 MD purification and crystallization	88
4.2.3	Dr Spt16 ₆₁₃₋₉₃₀ structure determination	92

4.2.4	Functional analysis of Dr Spt16 middle domain	94
4.2.5	Dr Spt16 MD binds both histone H2A/H2B and (H3/H4) ₂	97
4.3	Discussions	100
Chapter 5	102
5	Biochemical and biophysical characterization of SSRP1	103
5.1	Aims and objective	103
5.2	Results	104
5.2.1	SSRP1 heterodimerize with Spt16 through conserved sequences.....	104
5.2.2	SSRP1 is a conserved homodimer in solution	114
5.2.2.1	SSRP1 PH2 and PH3 domains are responsible for homodimerization	118
5.2.3	FACT is a heterodimer of SSRP1 and Spt16.....	121
5.2.4	SSRP1 shape revealed by SAXS analysis	123
5.2.5	SSRP1 homodimerization increases histone binding affinity	128
5.3	Discussion	131
Chapter 6	133
6	Summary and future directions	134
6.1	Summary	134
6.1.1	Hu Spt16 NTD and histone binding	134
6.1.2	Dr Spt16 middle domain and histone binding.....	134
6.1.3	SSRP1 homodimerization enhances histone binding	135
6.2	Future directions	136
6.2.1	Hu Spt16 N-terminal domain acidic patches and binding partners.....	136
6.2.2	Dr Spt16 middle domain and histone binding.....	136
6.2.3	Characterization of SSRP1's homodimerization and functions.....	137
Chapter 7	138
7	Appendix	139
7.1	Appendix 1 construct list	139
7.2	Appendix 2 oligo list	152
7.3	Appendix 3 histone peptides	157
7.4	Appendix 4. Purity of SSRP1 and FACT variants	157
8	Bibliography	162

List of Figures

Figure 1-1 Structural representation of histones core with protruding N-terminal tails and nucleosome.	19
Figure 1-2 Graphical representation of the “sequential nucleosome assembly” model.	20
Figure 1-3 Graphical representation of some histones modification crosstalk	26
Figure 1-4 Graphical representation of nucleosomes redistribution models.	28
Figure 1-5 Nucleosome repositioning mechanism.	30
Figure 1-6 Structural representation of a tetrasome (left) and ASF1-H3/H4 complex (right).	33
Figure 1-7 Structural representation of NAP1.	36
Figure 1-8 Schematic representation of FACT.	40
Figure 1-9 Superposition of Spt16 NTD and bacterial prolidase.	42
Figure 1-10 Structural representation of Spt16 DD bound to SSRP1 NTD/DD.	43
Figure 1-11 Structural representation of Spt16 MD and its superposition with POB3 MD and RTT106.	45
Figure 1-12 Structural representation of POB3 first 111 residues.	47
Figure 1-13 Structural representation of <i>S. cerevisiae</i> POB3 MD.	48
Figure 1-14 Structural representation of Nhp6 bound to DNA.	49
Figure 1-15 Schematic diagram showing two possible models for the nucleosome reorganization mediated by FACT.	53
Figure 2-1 Cation exchange chromatography of histone octamer.	62
Figure 3-1 Purity and crystals of Hu Spt16 ₁₋₅₁₀	70
Figure 3-2 Structural representation of Hu Spt16 N-terminal domain.	72
Figure 3-3 Sequence conservation of Spt16 N-terminal domain.	73
Figure 3-4 Electrostatic surface representation of Hu Spt16 ₁₋₅₁₀	74
Figure 3-5 SPR analysis of Hu Spt16 NTD against histone H2A/H2B or (H3/H4) ₂ (by Gary Sibbet).	76
Figure 3-6 ITC profiles and fitting of Hu Spt16 N-terminal domain against histone (H3/H4) ₂ from <i>X. laevis</i> and <i>G. gallus</i>	78
Figure 3-7 ITC profiles and fitting of Hu Spt16 N-terminal domain against histone H2A/H2B from <i>X. laevis</i> and <i>G. gallus</i>	79
Figure 3-8 Spt16 N-terminal domain’s putative binding site for histone tail H4 showing S83 and K86 side chains.	80
Figure 3-9 ITC profiles of Hu Spt16 NTD against histone N-terminal peptides.	82
Figure 3-10 Close up of the putative binding pocket of <i>S. pombe</i> Spt16 NTD.	84
Figure 3-11 Electrostatic surface comparison of <i>S. pombe</i> and Hu Spt16 NTD.	85
Figure 4-1 Purity and crystals of Dr Spt16 ₆₁₃₋₉₃₀	89
Figure 4-2 Purity and optimised crystals of SeMet Dr Spt16 ₆₁₃₋₉₃₀	90

Figure 4-3 Diffraction pattern of a twinned Dr Spt16 MD crystal.....	91
Figure 4-4 Structural representation of Spt16 MD.....	93
Figure 4-5 Sequence conservation of Spt16 middle domain.	95
Figure 4-6 Electrostatic potential mapped onto the surface of Dr Spt16 ₆₁₃₋₉₃₀	96
Figure 4-7 ITC profiles and fitting of Dr Spt16 ₆₁₃₋₉₃₀ against <i>G. gallus</i> histone H2A/H2B and (H3/H4) ₂	98
Figure 4-8 ITC profiles and fitting of Dr Spt16 MD ^{NVIT} against <i>G. gallus</i> histone H2A/H2B and (H3/H4) ₂	99
Figure 4-9 Electrostatic surface representation of Dr Spt16 MD showing the location of <i>S. cerevisiae</i> corresponding mutated residues that affect FACT activity.	101
Figure 5-1 Size exclusion chromatography overlay of SSRP1 N-terminal/DD domain and c-CBL.....	104
Figure 5-2 Structural representation of the symmetry related molecule of the PH1 domain from POB3.	105
Figure 5-3 Size exclusion chromatography of Hu SSRP1 N-terminal/DD wild type and hypothetical homodimerization interface mutants.	106
Figure 5-4 GSH-sepharose pull-downs of SSRP1- Spt16 complex.....	109
Figure 5-5 Examples of quasi-crystals and needle clusters obtained from crystallization trials outlined in table 5-5	112
Figure 5-6 Structural representation of the heterodimer comprising SSRP1 N-terminal/DD domain and Spt16's DD domain.	113
Figure 5-7 Diagram and structure representation of SSRP1/POB3 domains.....	114
Figure 5-8 sd200 10/330GL elution porfile of Hu SRP1 ΔCTD.....	115
Figure 5-9 AUC analysis of Hu and Dd SSRP1 ΔCTD.....	117
Figure 5-10 Structural representation of SSRP1/Spt16 heterodimerization interface showing residues targeted for mutagenesis.	119
Figure 5-11 AUC analysis of Dd FACT ΔCTD	122
Figure 5-12 SAXS analysis of Dd SSRP1 ΔCTD	123
Figure 5-13 Dd SSRP1 ΔCTD homology models predicted by I-TASSER.....	125
Figure 5-14 CRY SOL scattering curve calculation of different Dr SSRP1 ΔCTD model derived from I-TASSER.	126
Figure 5-15 Grafical representation of Dd SSRP1 ΔCTD <i>ab initio</i> and CORAL models.....	127
Figure 5-16 ITC analysis of Dd SSRP1 ΔCTD and mutants against histone (H3/H4) ₂	129
Figure 5-17 ITC analysis of Dd SSRP1 ΔCTD and mutants against histone H2A/H2B	130
Figure 7-1 Purity of Dd and Dr SSRP1 FL and ΔCTD	157
Figure 7-2 Purity of Hu, Dr and Dd SSRP1 N-terminal/DD.....	158
Figure 7-3 Purity of Hu, Dr and Sc SSRP1 N-terminal/DD, MD and ΔCTD.....	159
Figure 7-4 Purity of Hu, Dr and Dd FACT constructs.....	160

Figure 7-5 Purity of Hu FACT constructs161

List of Tables

Table 3-1 Data collection and refinement statistics.	71
Table 4-1 Spt16 MD construct list from different species	88
Table 4-2 Data collection and refinement statistics.	92
Table 5-1 Hu SSRP1 N-terminal domain mutants.	105
Table 5-2 His-tag SSRP1 and GST-tag Spt16's co-expression constructs used in pull-down assays (Fig. 5-4) to map SSRP1-Spt16 interactions.	108
Table 5-3 Sequence alignment of SSRP1 and Spt16 interacting sequences.	110
Table 5-4 Sequence alignment of Spt16 interacting sequences.	110
Table 5-5 SSRP1 and FACT constructs used for crystallization attempts (Appendix 4).	111
Table 5-6 Sedimentation equilibrium analysis of Dd SSRP1 constructs	120
Table 5-7 Data collection and SAXS-derived parameters for Dd SSRP1 ΔCTD.	124

Abbreviations

Å	Angstrom
ABPS	Adaptive Poisson-Boltzmann Solver
ATP	Adenosine triphosphate
AUC	Analytical ultracentrifugation
c-Cbl	Casitas B-lineage lymphoma
CK	Casein kinase
CTD	C-terminal domain
DD	Dimerizing domain
DNA	Deoxyribonucleic acid
DTT	Dithiothreitol
FACT	Facilitate chromatin transcription
GST	Glutathione S-Transferase
h	Hour
His-tag	Histidine tag
HMG	High mobility group
ID	Intrinsically disordered
IPTG	Isopropyl β -D-thiogalactopyr
ITC	Isothermal titration calorimetry
K	Lysine
K_d	Dissociation constant
KDa	Kilo Daltons
LB	Luria broth
M	Molar
MD	Middle domain
mg	Milligram
mg/ml	Milligram per millilitre
min	Minutes

ml	Millilitre
mM	Milli molar
MW	Molecular weight
Nhp6	Non histone protein 6
nM	Nano molar
NMR	NMR Nuclear magnetic resonance
NTD	N-terminal domain
NTD/DD	N-terminal domain/ dimerization domain
OD ₆₀₀	Optical density of a sample measured at 600 nm
ORF	Open reading frame
PCR	Polymerase chain reactions
PDB	Protein Data Bank
PEG	Polyethylene glycol
PH	Pleckstrin homology domain
POB3	Pol1 binding protein 3
Pol	Polymerase
PTM's	Post-translational modifications
Q	Glutamine
r.m.s.d	Root-mean-square deviation
RNA	Ribonucleic acid
rNTP's	Ribonucleotide triphosphate
rpm	Revolution per minute
R.T.	Room temperature
RTT106	Regulator of Ty1 Transposition 106
S	Serine
SAXS	Small-angle X-ray scattering
SDS-PAGE	Sodium dodecyl sulphate polyacrylamide gel electrophoresis
SE	Sedimentation equilibrium

SeMet	Selenomethionine
SERp	Surface entropy reduction prediction
SPR	Surface plasmon resonance
Spt16	Silencing of Ty 16
SSRP1	Structure-specific recognition protein 1
SV	Sedimentation velocity
TEV	Protease found in the tobacco etch virus
Tris-HCl	Tris (hydroxymethyl) aminomethane hydrochloride
WT	Wild type
Δ CTD	Delta carboxyl terminal domain
μ g	Microgram
μ l	Microliter

Chapter 1

Introduction

1 Introduction

1.1 Epigenetic overview

1.1.1 Chromatin architecture

Eukaryotes need to package their huge amount of DNA in higher ordered structures in order to fit it within the nucleus. This is made necessary by the fact that DNA of a single eukaryotic cell is 2m long (1). To package their DNA, eukaryotic cells use four histone proteins, H2A, H2B, H3 and H4. These histone proteins associate in hetero-dimers to form two complexes, H2A/H2B and H3/H4. The latter further associate to form a tetramer $(H3/H4)_2$ (Fig. 1-1 a). Two hetero-dimers H2A/H2B (Fig. 1-1 b) and one tetramer $(H3/H4)_2$ associate to form an octamer around which 147bp of DNA wraps in 1.65 turns (Fig. 1-1 c). This structure is called the nucleosome, and is highly conserved and repeated every 200 ± 40 bp (2,3). The disordered N-terminal histone tails protrude outside the nucleosome and are subjected to post-translational modification (Fig. 1-1). The DNA-histone components are kept in position by several contacts of which at least one salt-bridge between histone and DNA backbone (4).

Previous work has shown that nucleosome reconstitution is a salt-gradient dependent process in which, at high salt strength, a tetramer $(H3/H4)_2$ (or two dimers H3/H4) is deposited onto DNA followed by two H2A/H2B dimers while salt strength is reduced. This process has been called “sequential nucleosome assembly” (5-7) (Fig. 1-2). Histones are highly conserved among species. Besides canonical histones, cells express histone variants that localize in particular loci and are responsible for regulation of different biological functions. Most of these variants are substitutions of the histone H3 and H2A (8). An example is the centromere protein A (CENP-A) a H3 histone variant, important for chromosome segregation and for kinetochore formation at the centrosome (9). An alternative histone variant of the canonical H2A is H2A.Z (10). Its functions are involved in transcription, DNA repair, cancer initiation and progression as well as chromosome segregation and centromeric silencing (11-15).

The nucleosome and histone H1 associate to form a higher-ordered structure called chromatin (16). For decades it was known that chromatin was subdivided into an open and relaxed configuration called euchromatin (EC) and a closed compact configuration called

heterochromatin (HC) (17), which are respectively transcriptionally active and inactive (18). Difference between these two states relies on modifications in the histone tails. Euchromatin is characterized by the presence of histone H3 and H4 acetylation and H3K4 di and tri-methylation (H3K4me_{2/3}), while heterochromatin is hypo-acetylated and H3K9 di and tri-methylated (H3K9me_{2/3}). H3K9me_{2/3} are required to recruit heterochromatin protein 1 (HP1) through its chromo domain (reviewed in (1)). Heterochromatin can be further characterised as constitutive (cHC) or facultative (fHC). In lower eukaryotes, cHC is localized only at telomeres and centromeres, whereas in higher eukaryotes it also includes repetitive and non-coding sequences (19-21). fHC is also transcriptionally inactive but it can be converted into EC when the cells require (22).

A recent work conducted by Filion G.J. and others in 2010 (23) (by using *Drosophila melanogaster* as model system and a genome-wide location of 53 chromatin associated proteins), showed that chromatin can be subdivided in 5 major types: two were identified as distinct types of euchromatin, two as distinct types of heterochromatin and one was classified as repressed chromatin.

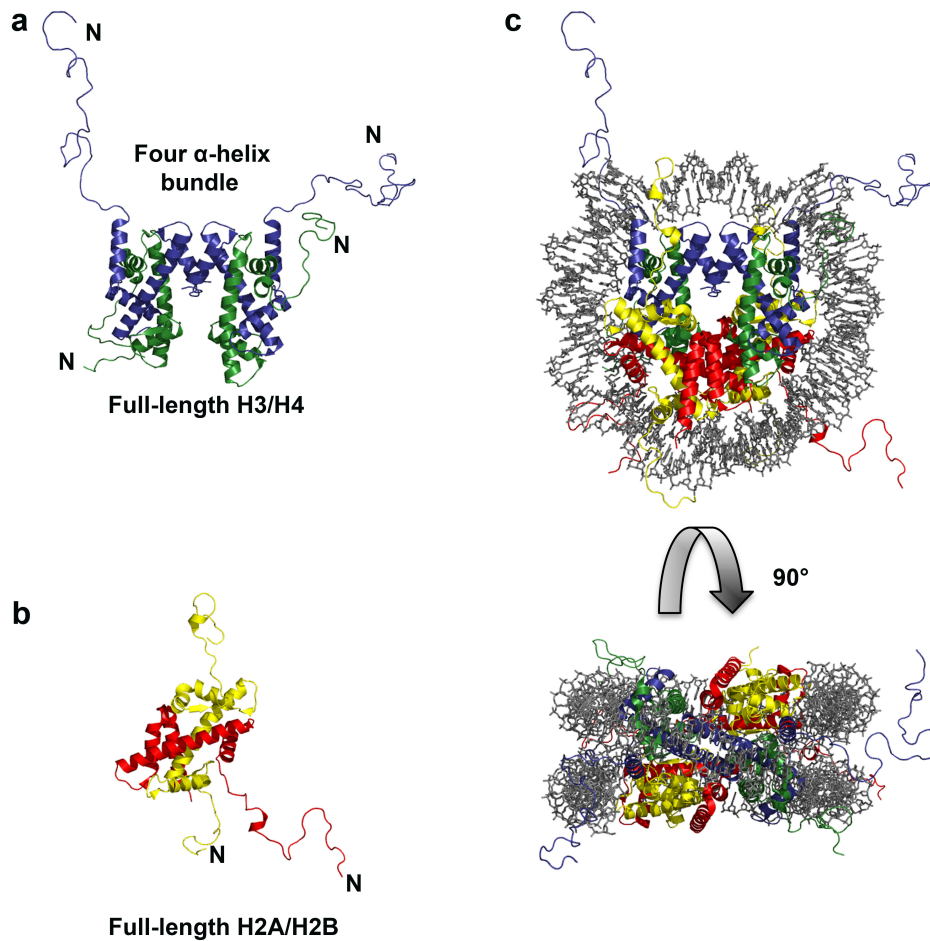


Figure 1-1 Structural representation of histones core with protruding N-terminal tails and nucleosome.

(a) Structure of the tetramer H3/H4, showing the four α -helices bundle required for tetramer interaction, (b) structure of the dimer H2A/H2B and (c) structure of the nucleosome (PDB: 1KX5). Histone N-terminal tails are indicated as N. H3 is in blue, H4 is in green, H2A is in yellow and H2B is in red. The figure was adapted from (7).

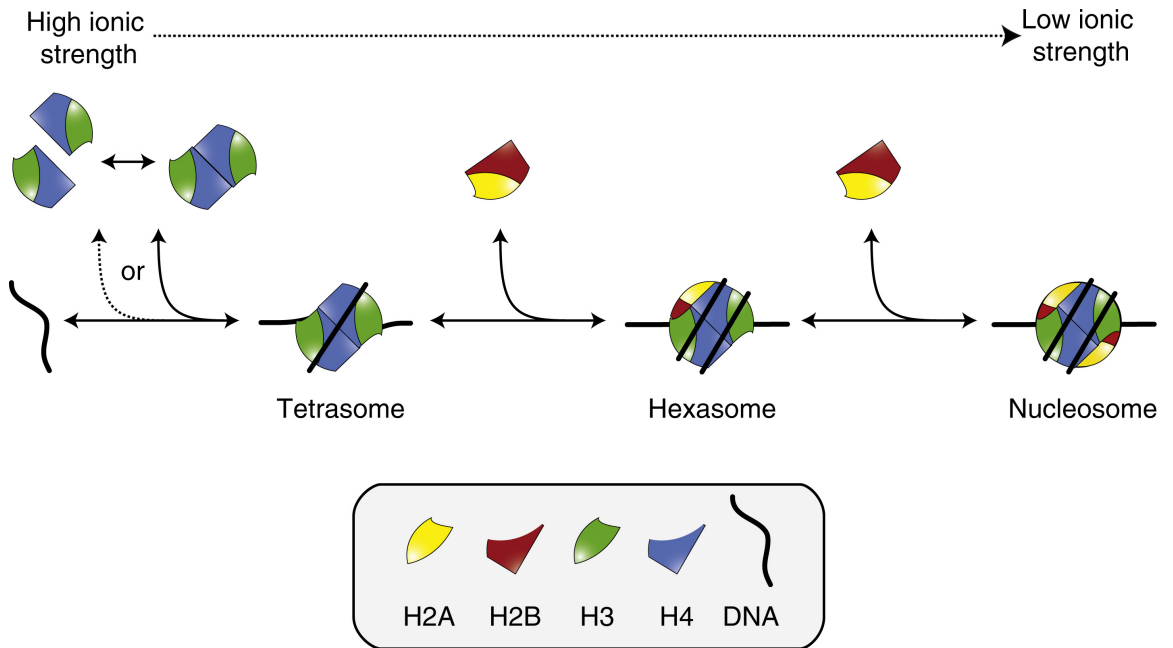


Figure 1-2 Graphical representation of the “sequential nucleosome assembly” model. Two histone dimers H3/H4, or one tetramer (H3/H4)₂, bind DNA to form a tetrasome. Then two H2A/H2B dimers are deposited to form a nucleosome. In this process an intermediate is formed called hexasome, which consists of a tetramer (H3/H4)₂ and a dimer H2A/H2B. The figure was adapted from (7) with permission.

1.1.2 Histone post-translational modifications

Post-translational modifications of histone tails are important in regulating chromatin structure between EC and HC states. Histone acetylation was one of the first histone post-translational modifications discovered by Allfrey in 1964 (24). Since then, 60 other histones residues have been found to be modified. These modifications, described in the following paragraph, are: acetylation, phosphorylation, methylation, deimination, β -N-acetylglucosamineation, ADP ribosylation, ubiquitylation, sumoylation and histone proline isomerization. (25).

1.1.2.1 Histone acetylation

Various enzymes play a role into post-translational modifications (PTMs) of the histones at their N-terminal tails. Histone acetylation is a dynamic process, regulated by histone acetyl-transferases (HATs) and histone deacetylases (HDACs). HATs transfer an acetyl group into the ϵ -amino group of lysine by using acetyl-CoA as a cofactor. This modification neutralizes the positive charge of lysine, weakening the interaction between histones and DNA. HATs are subdivided in two classes: Type A and B. Type A can be classified in three groups based on their acetyl-transferase domain: Gcn5-related N-acetyltransferase; monocytic leukaemia zinc finger protein, Ybf2 now renamed Something about silencing 3 and Tat-interacting protein 60 (MYST) and CREB binding protein/p300 (26). Type A HATs can be also found in complex with other proteins, which control their enzyme specificity, activity and recruitment. Type A HATs are also responsible for histone core acetylation at H3K56 by human general control nonderepressible 5 (hGcn5). This modification of lysine, which point towards DNA's major groove, affects the interactions between histone and DNA by neutralizing lysine charge (27). Type B is mainly cytosolic and acetylates newly synthesized histones at H4K5 and K12, which are important for histone depositions (28). HDACs play an opposite role, by removing lysine acetylation and restoring the positive charge. This may restore chromatin architecture and cause transcriptional silencing. HDACs can be divided into four classes: Class I (*S. cerevisiae* Reduced Potassium Dependency 3-like proteins), class II (*S. cerevisiae* histone deacetylase 1-like protein), class III (also known as sirtuins) are homologous of *S. cerevisiae* Silent Information Regulator 2, which differ from the other by relying on NAD^+ for their activity and class IV, which has only one member HDAC11 (28).

1.1.2.2 Histone phosphorylation

Histone phosphorylation takes place at histone N-terminal tails and core (H3 Y41 (29)) using serine, threonine and tyrosine as acceptors. This process is regulated by kinases and phosphatases (30). During histone phosphorylation kinases transfer phosphate groups, provided by ATPs, to a hydroxyl group of the targeted residue. This, in turn, adds a negative charge that influences chromatin structure (28).

1.1.2.3 Histone methylation

Histone methylation is a PTM that targets lysines and arginines, without altering the charge of the histones. Lysines can be mono-, di- or tri-methylated whereas arginines can be mono- and symmetrically or asymmetrically di-methylated (31). All the histone lysine methyltransferases (HKMT) that methylate N-terminal tails (with exception of disruptor of telomeric silencing that methylates histone core H3K79), harbour the enzyme activity in a Su(var)3-9, Enhancer-of-zeste and Trithorax (SET) domain that transfer a methyl group from S-adenosylmethionine (SAM) to the ϵ -amino group of the lysine (28). Arginine methyltransferases are divided into two classes: Type I generate mono- and asymmetrically di-methylated arginines; type II generates mono- and symmetrically di-methylated arginines. Together these methyltransferases (type I and II) form a family called protein arginine N-methyltransferase (PRMTs), which transfer a methyl group from SAM to the ω -guanidino group (28). Histone methylation was considered a stable modification until 2002, when demethylation reactions were discovered (32). Subsequently a lysine-specific demethylase 1 (LSD1) was characterized and found to use FAD as co-factor (33).

1.1.2.4 Histone deimination and β -N-acetylglucosamine

Deimination is a process that converts arginines into citrullines, neutralizing the positive charge of arginines. In higher eukaryotes this reaction is carried out by Peptidyl arginine deiminase type IV (PADI4), which is also able to convert mono-methyl arginine to citrulline thus acting as a demethylase (34,35).

β -N-acetylglucosamine (O-GlcNAc) is a sugar that is generally added to serine and threonine of non-histone proteins. In mammals there is only one O-GlcNAc transferase that uses UDP-GlcNAc as substrate to transfer the sugar to the protein. Recently it has been shown that O-GlcNAc transferase adds an O-GlcNAc to H2B serine 112, which in

turn enhances ring finger protein 20 (RNF20) binding affinity and therefore H2B monoubiquitination (36). O-GlcNAc transferase counterpart is the β -N-acetylglucosaminidase (O-GlcNAcase), which is responsible of removing the sugar (37).

1.1.2.5 ADP ribosylation

Two enzymes are responsible for histone's ADP-ribosylation: the poly-ADP-ribose polymerase (PARP) and the mono-ADP-ribosyltransferase, which catalyse poly-ADP-ribosylation and mono-ADP-ribosylation respectively. This modification targets arginine and glutamate residues giving them a negative charge, which in turn affect chromatin structure and can be reverted by the poly-ADP-ribose glycohydrolase. It has been shown that the mono-ADP-ribosylation increases during DNA damage suggesting a possible role of the enzyme (38).

1.1.2.6 Ubiquitylation and sumoylation

Ubiquitin is a 8.5 kDa protein of 76 amino acid, which is covalently conjugated to histone lysine by a cascade of enzymes: ubiquitin-activating enzyme (E1), ubiquitin-conjugating enzyme (E2) and ubiquitin-ligase (E3) (39). This enzymatic cascade specifies the substrate and whether the substrate is mono- or poly-ubiquitylated. Histones are mainly mono-ubiquitylated at H2A K119, which is a marker for gene silencing and at H2B K123, which is important for transcriptional initiation and elongation (40-42). Ubiquitylation of histones can be reverted by de-ubiquitinating enzymes (28)

Small ubiquitin-related modifier (SUMO) is an ubiquitin like protein that is covalently linked to histone lysine catalysed by distinct set of E1, E2 and E3 dedicated for SUMO modification. Shiio Y et al (43) showed that UBC9 (an E2 SUMO-conjugating enzyme) sumoylates histone H4 on its N-terminal tail and induces histone deacetylation by recruiting HDAC. They also found that SUMO modification promotes recruitment of HP1 leading to transcription repression (43). It has since been shown that sumoylation occurs not only on H4 but also on H2A, H2B and H3 histone proteins (44).

1.1.2.7 Histone tail clipping and proline isomerization

Histone tail clipping was first discovered in *Tetrahymena* micronuclei where the first six H3 N-terminal residues were removed (45). This PTM is well conserved in yeast and

mammals, where serine proteases removes the first 21 residues, which in turns unpack the repressive structure of the chromatin, favouring transcription (46).

Prolines can assume two possible conformations that differ by 180° called *cis* and *trans*. Little is known about this PTM, which differs from all the others because it does not involve any covalent binding. To date *S. cerevisiae* FKBP Proline Rotamase (ScFpr4) is the only protein known to be correlated with this PTM, which isomerizes H3 P38 (47).

1.1.2.8 Histone PTMs functions and crosstalk

Histone PTMs have two distinct functions. Firstly, they alter chromatin architecture by varying histone charge or structure. Chromatin alterations are achieved where interactions between histones of consecutive nucleosomes or histone and DNA are broken by changes in the charge of these proteins. Among these alterations, acetylation has the biggest effect as it neutralises the basic charge of histones. Another PTM that affects chromatin structure by altering histone charge is phosphorylation, which plays a role in mitosis, apoptosis and gametogenesis (48-50). Secondly these modifications allow recruitment of non-histone proteins with different enzymatic activities for example chromatin remodellers. Each modification recruits different enzymes based on their domains. For example methylation is recognised by the “Royal family” proteins (which consist of chromo, tudor and malignant brain tumor (MBT) domain) and proteins bearing the plant homeodomain (PHD) domains, acetylation is recognised by bromodomains and phosphorylation is recognised by 14-3-3 proteins like domains (25). As a consequence, these enzymes may be in complex with other enzymes that further modify chromatin. An example is Polycomb protein PC2 a protein of the polycomb repressive complex 1 (PRC1) that recognise H3K27me through its chromodomain and is associated with RING1b, an ubiquitin ligase enzyme that mono-ubiquitinate H2A K119 (51,52).

Histone PTMs are used to tightly regulate chromatin structure. This regulation is further increased by crosstalk between different PTMs, which can occur in different ways. For example, a single lysine can be methylated, acetylated or ubiquitylated. Therefore, each of these modifications will compete with the others for the same residues, causing activation of different pathways. Binding of proteins to histone tail modifications can be prevented by other adjacent modifications, e.g. H3 S10 phosphorylation blocks H3K9me binding by HP1 (49). PTMs can also alter the substrate of an enzyme affecting its activity. As an example isomerization of H3 P38 affects methylation of H3 K36 by Set2 (47). Other

modifications can increase the ability of a protein to recognise its substrate, such as the phosphorylation of H3 S10, which increase the affinity of GCN5 (an acetyltransferase) to H3 K14 (53). Crosstalk can even occurs between different histone tails; indeed H2B K123 mono-ubiquitylation is required for H3 K4 and H3 K79 methylation (41) and (25) (Fig. 1-3).

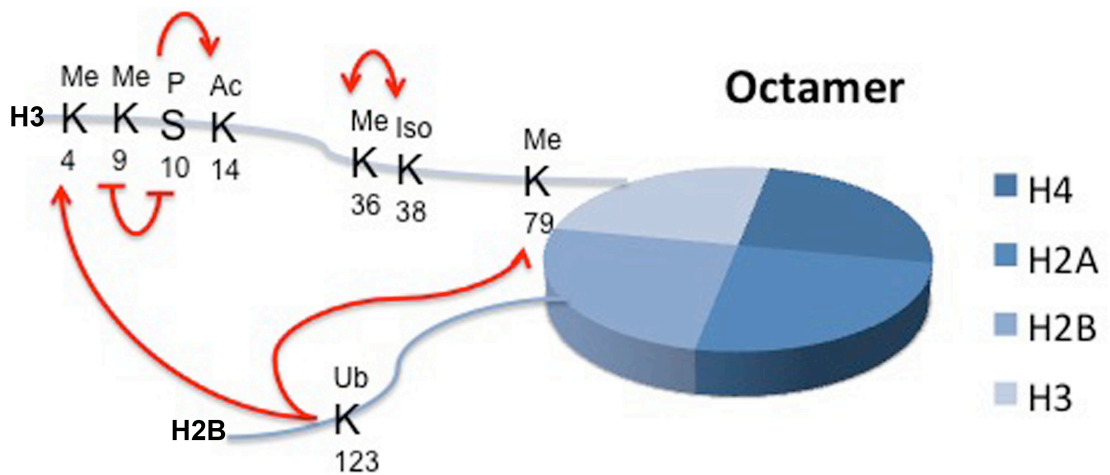


Figure 1-3 Graphical representation of some histones modification crosstalk

Figure shows histones H3 and H2B tails that protude outside the octamer represented as a pie chart. Red arrow indicate the crosstalk amongs some of the post-traslational modified residues. The figure is adapted from review (25).

1.1.3 Chromatin remodellers

Access to the DNA in the chromatin can be achieved in two different ways: by histone PTMs and by chromatin remodelling complexes (CRCs). As previously described histone PMTs and their crosstalk are important factors for chromatin structure alterations. On top of this, chromatin can be reorganized by another class of proteins that uses the energy generated by the hydrolysis of ATPs to alter nucleosome/DNA interactions known as chromatin remodelling complexes (CRCs). Their functions are to rearrange nucleosomes positions along the DNA or remove/exchange nucleosomes in order to grant access to chromatin DNA for other proteins to carry out different cell activities (54).

Chromatin remodelling proteins were first discovered in yeast with two experiments, which identified two mutants defective in mating-type switching and growth on sucrose, called switching defective (*SWI*) and sucrose non-fermenting (*SNF*) (55,56). Further studies showed that mutations in H2A and H2B were able to suppress *swi2* and *snf2* mutants and that these mutations caused a different nuclease digestion pattern of the gene *SUC2*, suggesting that chromatin structure was altered by *SWI/SNF* to activate transcription (57). This class of proteins is conserved among different species. They can be subdivided into four families: Swi/Snf, which includes the subunits Brahma-related gene 1 and human Brahma; inositol requiring 80 (INO80)/Swi Snf-related1 family, which contains ATPases INO80, hDomino and Snf2-related CREB activator protein; Imitation *SWI* (Iswi) family including human Snf2-homolog and human Snf2-like and Chromatin organization modifier, Helicase and DNA-binding (CHD) family with CHD1-9. Some of these proteins can form complexes that alter their ATPase activity *in vitro* (54).

The mechanisms by which nucleosomes are redistributed were not clear. Three models were proposed to explain it: bulk rotation, bulge diffusion and twist defect diffusion (Fig. 1-4). The bulk rotation model can be described in two different ways: the DNA shifts while the octamer rotates within it or the DNA rotates about its axis (Fig. 1-4 a, and b). This model encounters problems, as the histone terminal tails, that protrude outside the nucleosome would effectively block this kind of rotation (58).

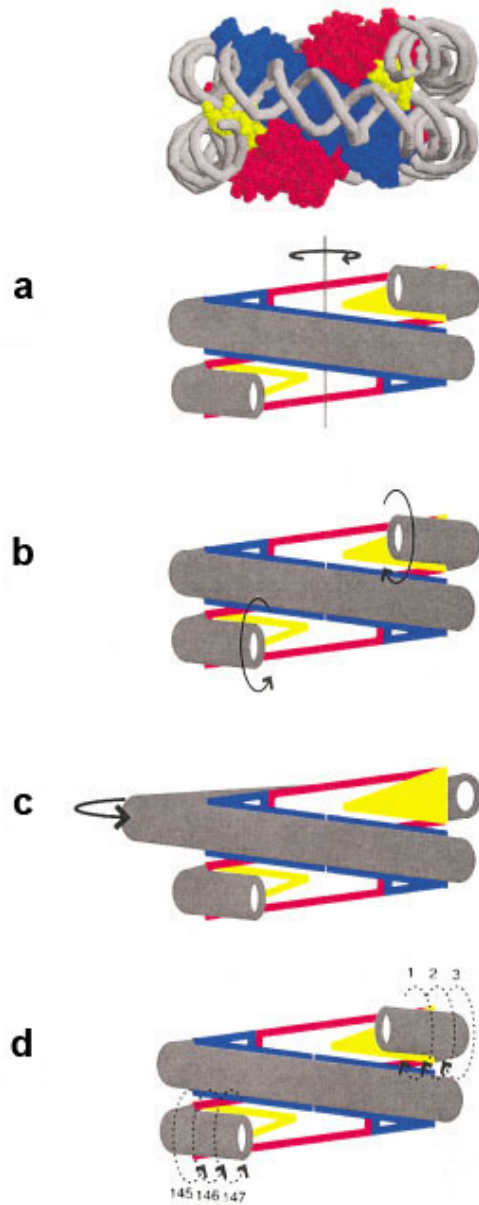


Figure 1-4 Graphical representation of nucleosomes redistribution models.

(a) Bulk rotation of octamer within DNA; (b) bulk rotation of DNA around octamer; (c) planar bulge diffusion and (d) twist defect diffusion. Histones H3/H4 and H2A/H2B are represented in blue and red respectively. H2 N-terminal α -helices are represented in yellow. Figure was taken with permission of (58).

The bulge diffusion model suggests that DNA, following disruption of one or more contacts with histones, forms an “unbound bulge or bend defect” that diffuse around the octamer in both directions. It can be planar or topological. In the planar model the unbound DNA remains in the same plane and therefore it does not have any topological effects. The topological model suggests that the unbound DNA, following torsional stress due to twist and writhe, loop over itself forming a topological bulge (58,59).

The twist defect diffusion model proposes that DNA can twist or untwist to allow a shift of one or more base pairs (Fig.1-4D), which can be propagated between DNA linker and the DNA wrapped around the octamer. This torsion generates a twist defect that can spread from one DNA segment to another, allowing the octamer to shift an equivalent number of twisted DNA pairs (59).

However, ATP-dependent nucleosome sliding activity is not affected in presence of DNA hairpin or biotin crosslinks that otherwise would preclude DNA rotation during sliding (60,61), suggesting that chromatin remodellers uses a different mechanism for nucleosomes sliding.

More recently, Deindl and others (62) showed that ISWI complexes allow nucleosome repositioning by favouring DNA movement of 7 bp toward the exit site (with 1 bp sub-steps) followed by 3 bp step translocation from the entry-side. This data contrasts the aforementioned models where the DNA is drawn into the nucleosome before to being removed (reviewed in (63) Fig. 1-5)

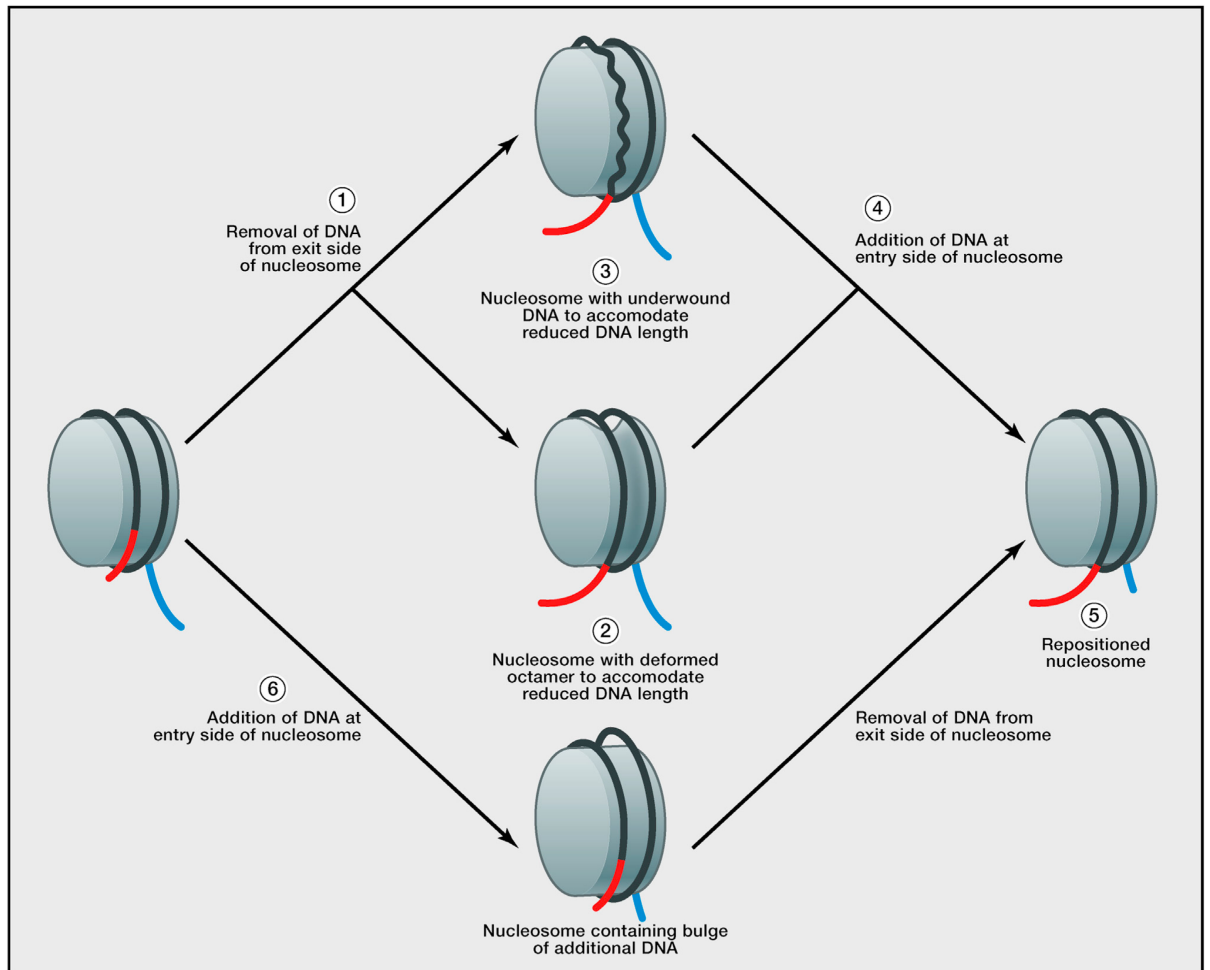


Figure 1-5 Nucleosome repositioning mechanism.

(1) DNA is removed from the nucleosome exit-side (red) (62), generating an intermediate where the 4 to 7 bp deficit is accommodated by conformational changes in the octamer (2), a reduction in DNA twist (3) or their combination. Then DNA is drawn into the nucleosome from the entry-side (blue) (4) allowing a shift of 3 bp along the nucleosomal DNA (5). This model is in contrast with previous models in which DNA was proposed to enter the into the nucleosome before to being removed (6). Figure taken with permission of (63).

1.1.4 Histone chaperones

During synthesis, incorporation in nucleosomes or eviction, histone basicity patches may be exposed and cause nonspecific interactions with other protein's acidic patch or form aggregate causing cell defects (64). To overcome this problem cells synthesize specialized proteins that associate with histones and hide their positive charges, mask the hydrophobic histone-histone interactions, control their transfer during nucleosome assembly and prevent histones from assuming a wrong structure (65). These proteins are known as histone chaperones. This name was first used for nucleoplasmine, which is involved in avoiding histone/DNA aggregation (66). Histone chaperones can be classified in two groups based on their functions: histone storage and histone deposition factor. An example of histone storage, other than nucleoplasmine, is the histone chaperone antisilencing function 1 (ASF1) that binds histone H3/H4 and promotes nucleosome reconstitution *in vitro* by transferring histones to either chromatin assembly factor 1 (CAF-1), or histone regulator A (HIRA) (67,68). CAF-1 and HIRA are, in turn, histone deposition factors that favour nucleosome formation in a DNA synthesis dependent or independent manner, respectively (69,70). Finally, histone chaperones, contrary to the ATP-dependent chromatin remodellers that interact mainly with DNA, are ATP-independent histone binders.

1.1.4.1 Antisilencing function 1 (ASF1)

ASF1 was the first structure determined for a histone chaperone bound to histones (71). It binds H3 residues in the $\alpha 2$ and $\alpha 3$ helices necessary for the formation of a four-helix bundle between two histone H3s, thus preventing H3/H4 tetramerization (Fig. 1-6). ASF1 also cause a conformational change in H4 C-terminal tail, which normally forms a parallel β -sheet with H2A C-terminal tail, by folding it back to make contacts with one of its antiparallel β -sheet (Fig. 1-6). Indeed, during nucleosome disassembly the eviction of H2A/H2B dimer exposes H4 C-terminal tail on the tetramer surface. It is then possible that this tail can be recognised by ASF1 in a "strand capture" way (71).

Despite the fact that ASF1 binds H3/H4 dimers in a way that prevents association with other H3/H4 or H2A/H2B dimers, their N-terminal tails (which differs between H3.1 and H3.3 (72)) remain exposed in solution and therefore can be subjected to PTMs (73). This, in turn, will favour histone H3/H4 differentiations and target them to different deposition pathways, as HIRA and CAF-1 recognise H3.3 and H3.1 respectively (74). Recently, a structure of ASF1 bound to a peptide corresponding to the b-domain present in both HIRA

and CAF-1 shows interactions between the N-terminal region of ASF1 (156 residues) and the b-domain, explaining why the binding of ASF1 to HIRA or CAF-1 is mutually exclusive (Fig. 1-6) (75). A model for ASF1 function in DNA replication suggests that, following nucleosome disassembly, ASF1 recover histones H3/H4, which are subsequently given to histone depositions factors for their assembly into nucleosomes (76).

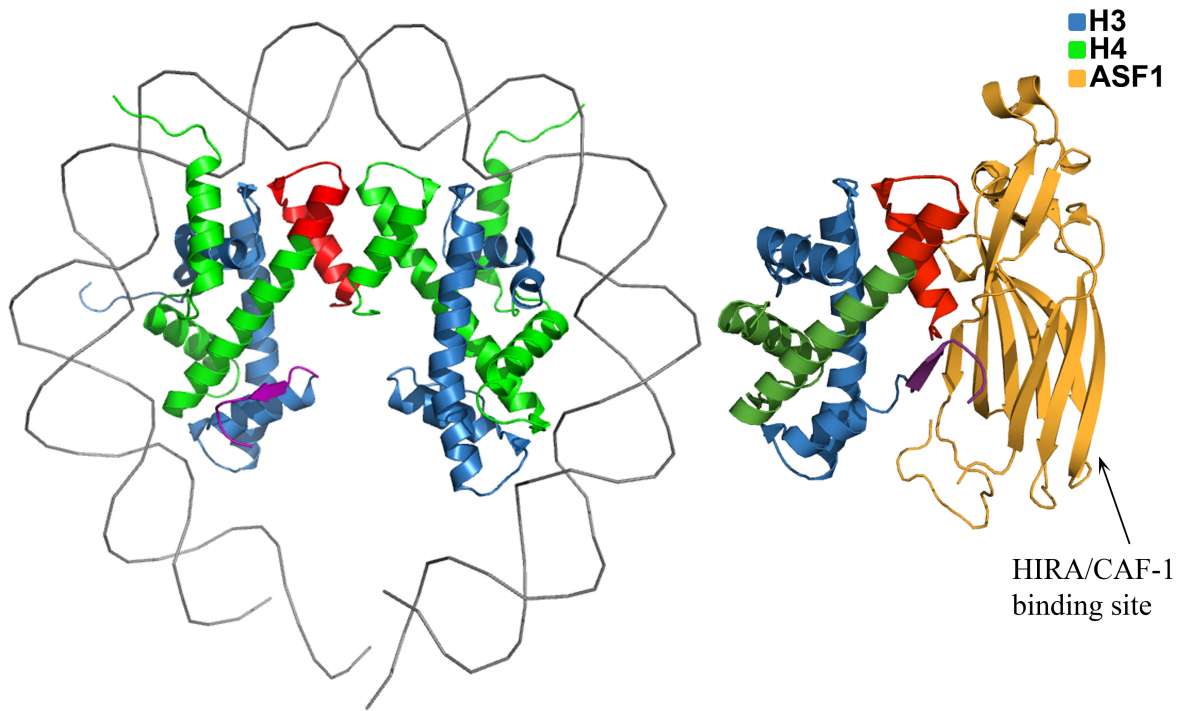


Figure 1-6 Structural representation of a tetrasome (left) and ASF1-H3/H4 complex (right).

Representation of histone tetramer (H3/H4)₂ wrapped by DNA (tetrasome; left panel) (PDB 1ID3) (77) and ASF1 bound to the heterodimer H3/H4 (PDB 2HUE; right panel) (71). H3 α -helix in red is involved in tetramerization and is sequestered by ASF1. H4 β -sheet in purple interacts with H2A C-terminal tail and is sequestered by ASF1.

1.1.4.2 Nucleosome assembly protein 1 (NAP1)

Another histone deposition factor is the nucleosome assembly protein 1 (NAP1), which was initially identified in mammalian cells as a protein that assist nucleosome assembly (78). NAP1 homologues have been found in all eukaryotes, from yeast to human (78-81). Its family consist of different proteins that share a core of 300 amino acid residues, essential for NAP1 homo-dimerization, histone binding and nucleosome formation (82,83). Although the NAP1 C-terminal region is not involved in histone binding, it is required for H2A/H2B dimer removal in order to facilitate nucleosome sliding (84). Crystal structure of NAP1 shows a homo-dimer that adopts a “head-phone” shape with two distinct domains: I and II. Domain I, responsible for the homo-dimerization of NAP1, is delineated by a long α -helix (residues 90-140) that assume an antiparallel “tram-track” motif delimited by two short α -helices. Domain II, responsible for proteins interactions, consists of four antiparallel β -sheets (Fig. 1-7 in green) wrapped by two α -helices (Fig. 1-7 in red) (83).

NAP1 is involved in histone shuttling between nucleus and cytoplasm by localizing in the nucleus during S phase and in the cytoplasm during G2 phase (85). This is supported by the fact that NAP1 mediate the interaction of H2A/H2B with karyopherin (importin) responsible of their nuclear import (86), by the presence of a NLS motif located in a β hairpin in domain II and by a NES-like sequence located in NAP1 domain I (83,87). The mechanism by which NAP1 subcellular localization is regulated is unknown, although some experiments suggest it may be regulated by phosphorylation (88). It was already known that NAP1 associate with all histone protein in *vivo* (89). Studies conducted by Sheena D’Arcy and others (90), showed that Nap1 binds two copies of H2A/H2B in an unconventional tetrameric conformation at the H2A/H2B interface which is normally involved into inter-histone interactions observed in nucleosome structure.

Subsequently, other experiments showed that NAP1 homo-dimer can bind two H3/H4 dimers but this study was not able to distinguish between H3/H4 dimer and tetramer (91). Recently it has been shown that NAP1 (and its homologous vacuolar protein sorting 75 or Vps75) binds histone H3/H4 in a tetrameric conformation both in *vivo* and in *vitro*. Moreover Vps75, which has been found in complex with the acetyl transferase RTT109 causing its nuclear localization and activity, promote histone H3 acetylation (H3K56Ac) in a tetrameric conformation (H3/H4)₂ (92,93). It has also been shown that NAP1 and Vps75 are tetramers at physiological conditions, assuming a ring shaped conformation in solution. In the presence of RTT109 the homo-tetramer dissociate into two dimers that

independently interact with RTT109. This suggests that homo-tetramerization may act as a “self-chaperoning” mechanism to prevent Vps75 aggregation in absence of its histone cargo. (94).

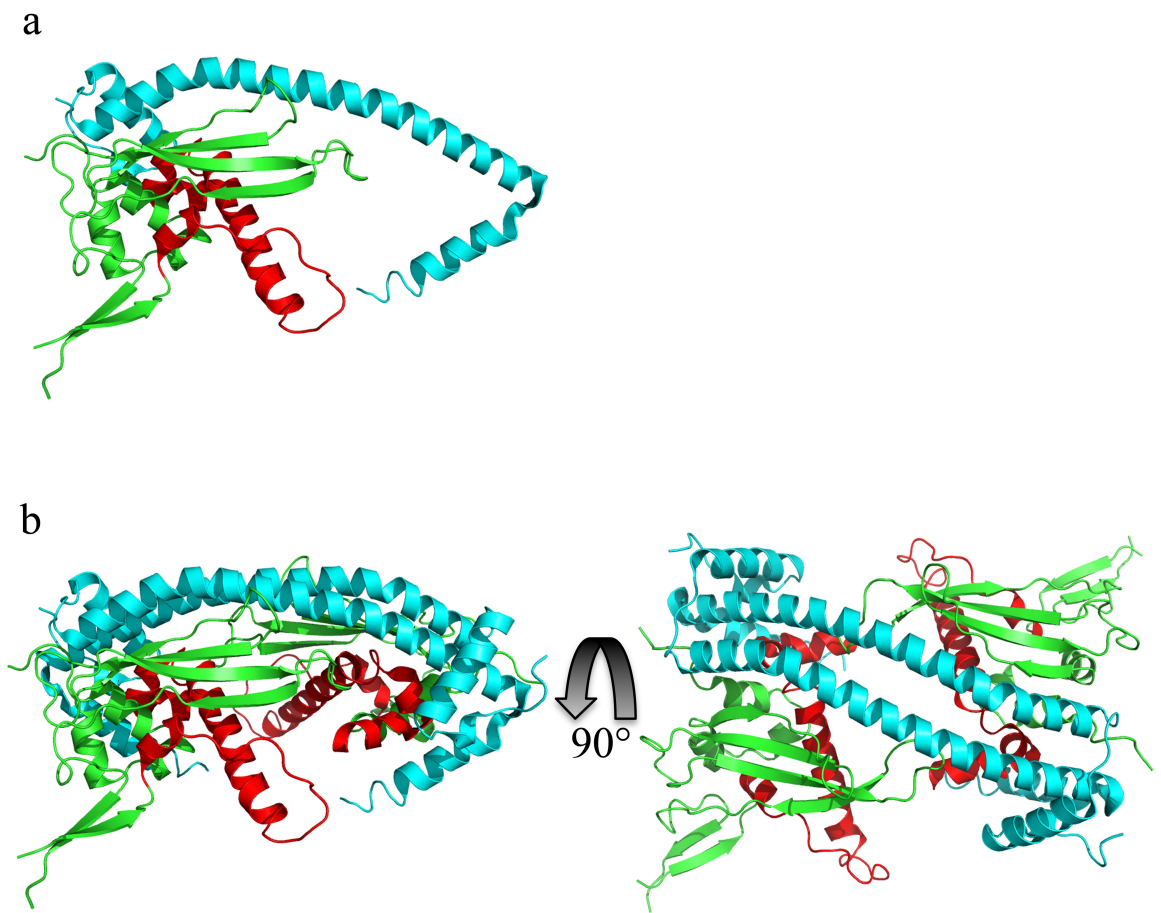


Figure 1-7 Structural representation of NAP1.

(a) NAP1 monomer. (b) NAP1 homodimer displayed in two different angles. Domain I is coloured in cyan. Domain II's amphipathic β -sheets are in green and two α -helices are in red. PDB: 2AYU (83).

1.2 Facilitates Chromatin Transcription (FACT)

In 1998 Orphanides and others (95) have isolated a complex consisting of suppressor of Ty 16 (Spt16) and structure-specific recognition protein-1 (SSRP1); which has an high mobility group (HMG-1) domain that is involved into nucleosomal DNA binding (95,96). By using pulse-chase transcription assays they showed that this heterocomplex was able to facilitate RNA Pol II chromatin transcription, therefore they rename it FACT (Facilitate Chromatin Transcription) (95).

Spt16 was first discovered in two independent experiment: in 1988 as high copy number suppressor of δ insertion mutations (indicated as class 1 in (97)) and in 1989 as Cdc68. Afterwards, a study conducted by Malone and others demonstrated that Spt16 and Cdc68 were the same protein (98).

Yeast SSRP1 counterpart is called Pol1 Binding protein 3 (POB3), which was first characterized in 1997 and it has been shown to form a heterocomplex with yeast Spt16 (ySpt16) *in vivo* (99). Contrary to human, yeast FACT (yFACT) requires an additional protein, called non-histone protein 6 (Nhp6), to carry out its activity (100-102) (Fig. 1-8). Native gel shift assays of human FACT incubated with core histones and DNA at physiological condition showed that FACT is also able to deposit histone heterodimer H2A/H2B and heterotetramer (H3/H4)₂ onto DNA, which classifies it as a histone chaperone (103). Moreover, further studies showed that during transcription reactions, FACT both assists the eviction of a single histone dimer H2A/H2B from the nucleosome (103) and the rapid deposition of the histones proteins during transcriptional elongation, suggesting it may also have a role in nucleosome assembly (104,105).

1.2.1 FACT and transcription

After FACT discovery, researchers investigated its role in transcription. Some of these studies were conducted by using 6-azauracile, which inhibit RNA transcription elongation by affecting the pool of rNTPs, confirming that FACT plays a role in transcription elongation (106,107). Other studies on yFACT also showed genetic interaction with TATA binding protein (TBP) and transcription factor II A (TFIIA) causing an enhancement of their interaction, both *in vivo* and *in vitro* (108), therefore linking FACT to transcription initiation. Other experiments reported that yFACT associate with RNA Pol II, traveling with it throughout its mRNA coding region. In this case the transcription factor IIIH

(TFIIH), which phosphorylate RNA Pol II C-terminal domain (CTD) during elongation, is required for FACT association (109). Moreover, FACT association and nuclear co-localization with RNA Pol II was also identified in plants and flies respectively (110,111). Other studies have shown that yFACT interacts physically or genetically with a set of transcription initiation and elongation factors, suggesting it can perform different functions by cooperating with different complexes (106,112-115). Subsequently, studies on FACT showed that this complex is also involved into DNA damage and replication.

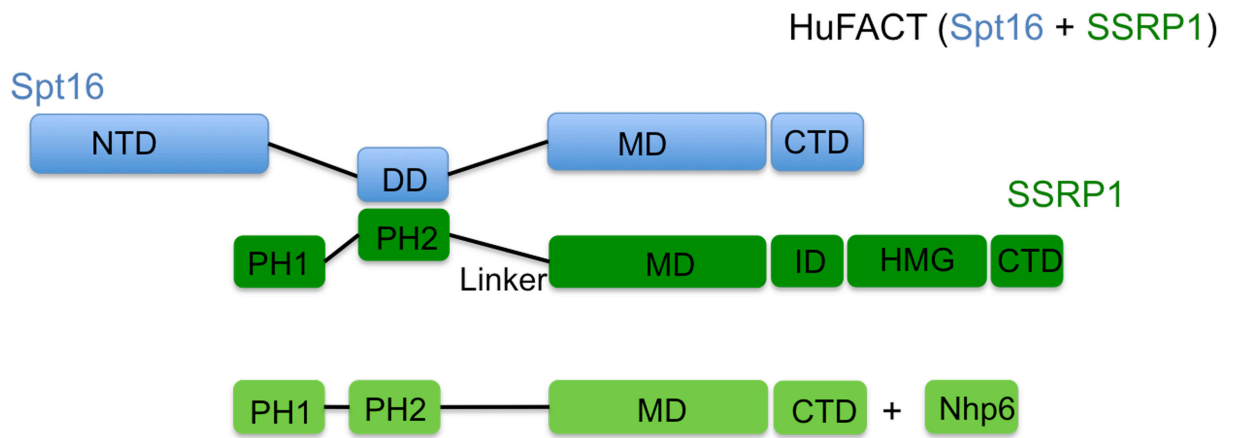
1.2.2 FACT and DNA damage

Cisplatin is an anticancer drug used in chemotherapy, which cause DNA intra-stand crosslinking (GpG and ApG) forcing the DNA to bend towards the major groove and to unwind (116). Studies conducted by using this drug showed that FACT, and particularly SSRP1 HMG domain, interact with cisplatin damaged DNA suggesting a role in DNA repair (117). Other study, conducted by San-Dejmek (118), have recently shown that the DNA-dependent protein kinase (DNA-PK) complex, which plays a role in DNA repair and apoptosis, co-purifies with FACT in cisplatin-treated cells. Furthermore, immunofluorescence of UV laser treated cells did confirm the presence of SSRP1 and Ku68 (a subunit of DNA-PK) at the DNA double strand breaks (DSBs). Finally, this study shows that SSRP1 silencing increase cell sensitivity to the cisplatin drug with decreased appearance of γ H2AX, suggesting that both FACT and DNA-PK plays a role in DNA repair (118). Another study, conducted by Keller and others (119) using murine embryonic testicular carcinoma F9 cells, showed that FACT interacts with CK2 and cause phosphorylation of the conserved p53 Ser392 following UV DNA damage (119); therefore linking FACT activity to the DNA damage. Finally, a recent study showed that FACT causes transcription restart after UV DNA damage. Moreover, this study shows that SSRP1 silencing does not affect Spt16 recruitment, suggesting it is independent of SSRP1, while Spt16 silencing prevent SSRP1 recruitment at site of DNA damage (120).

1.2.3 FACT and DNA replication

Wittmeyer and other showed that both POB3 and Spt16 co-localize with DNA Pol1 in the nucleus and by using different chromatography technique their were also able to co-purifies yFACT with DNA Pol 1 α complex (121). They also showed that the chromosome transmission fidelity (Ctf4) and yFACT were competing to bind Pol1, therefore they suggested that this binding was mutual exclusive (99). They also noticed that Cdc68-1

mutant (Spt16 G132D) was causing the cell to stop in G1, whereas depletion of Ctf4 was causing the cell to arrest at G2; therefore they hypothesized that Pol1 associate with yFACT for DNA replication start and after with Ctf4 to switch to elongation (99). Other studies showed genetic interaction between POB3 and several DNA replication factors (122) as well as interaction between yFACT and replicative helicase Mcm2 (123). Notably, some of the mutation of Spt16 and POB3 cause hydroxyurea (HU) sensitivity, which affect ribonucleotide reductase activity and therefore DNA synthesis (106,122,124). Furthermore, in 2006 VanDemark and others showed genetic interactions between yFACT and the replication protein A (RPA), suggesting that FACT may be important to promote a step in DNA replication (125). They also shown genetic interaction between POB3 Q308K and H4 N-terminal tail mutated residues K5R, K12R that are acetylated in newly deposited nucleosomes during DNA replication (126), therefore linking POB3 to nucleosome deposition (125).



yFACT: Spt16 + SSRP1 (POB3) + Nhp6

Figure 1-8 Schematic representation of FACT.

Diagrams showing human Spt16 (blue) and human SSRP1 (green) domains and the dimerization domain of the two protein. In yeast, SSRP1 consists of two proteins, POB3 and Nhp6 shown in light green (adapted from figure reviewed in (127)).

1.2.4 Suppressor of Ty 16 (Spt16)

Spt16 is a 120 kDa protein consisting of four domains: N-terminal domain (NTD), dimerization domain (DD), middle domain (MD) and C-terminal domain (CTD) (Fig. 1-8) (119,125,128).

1.2.4.1 Spt16 NTD

Spt16 N-terminal domain structures for *S. cerevisiae* and *S. pombe* have been determined (PDB: 3BIP and PDB: 3CB5 respectively). They adopt an aminopeptidase-like domain that resembles a “pita-bred” fold, which has lost its aminopeptidase activity (Fig. 1-9, a) (129,130). An example of an aminopeptidase is the bacterial prolidase from *Pyrococcus furiosus*. In this enzyme five residues (D209, D220, E313, E327 and H284) make its active site; of these the carboxylate group of residues D and E orient the two Zn ions in position (131). In yeast Spt16 NTD those residues are mutated; therefore they cannot longer coordinate the Zn ions. Furthermore, Spt16 NTD presents a longer loop that hides this active site (Fig. 1-9, b). Nevertheless, it has been proposed that this site could be a histone peptide-binding groove (130).

In yeast, deletion of Spt16 NTD or mutations in specific conserved residues on the putative peptide-binding groove is tolerated, but when combined with POB3 Q308K (a mutant that cause defect in DNA replication and transcription in yeast) they are lethal (124,130). Moreover, full length FACT shows high affinity for histone N-terminal tails and their removal strictly reduce FACT/nucleosome binding (129,130,132). Furthermore, work by Stuwe and others show that *S. pombe* Spt16 NTD binds histone H4 tail with an affinity of 3 μ M (129). These results suggest that Spt16 NTD binds the histone tails by the putative peptide-binding groove. However, work by VanDemark and others disfavours this hypothesis, showing that *S. cerevisiae* full length FACT binds nucleosome and/or histone H3 and H4 tails at high affinity, independently of Spt16 NTD (130). Interestingly, analysis of Spt16 NTD and POB3 MD show genetic interactions with the H2A C-terminal “docking domain” (130). H2A docking domain consists of 25 residues at the C-terminal that makes contacts with histone (H3/H4)₂; of these 25 residues the last 6, which are ordered in the crystal structure of the yeast nucleosome (77), might be unstructured in free H2A/H2B (130). Notably, this domain has been shown to be important to prevent nucleosome sliding and dimer dissociation (133,134). Although in yeast Spt16 NTD is not essential for FACT activity, it may be important for destabilization of histone dimer/tetramer interactions.

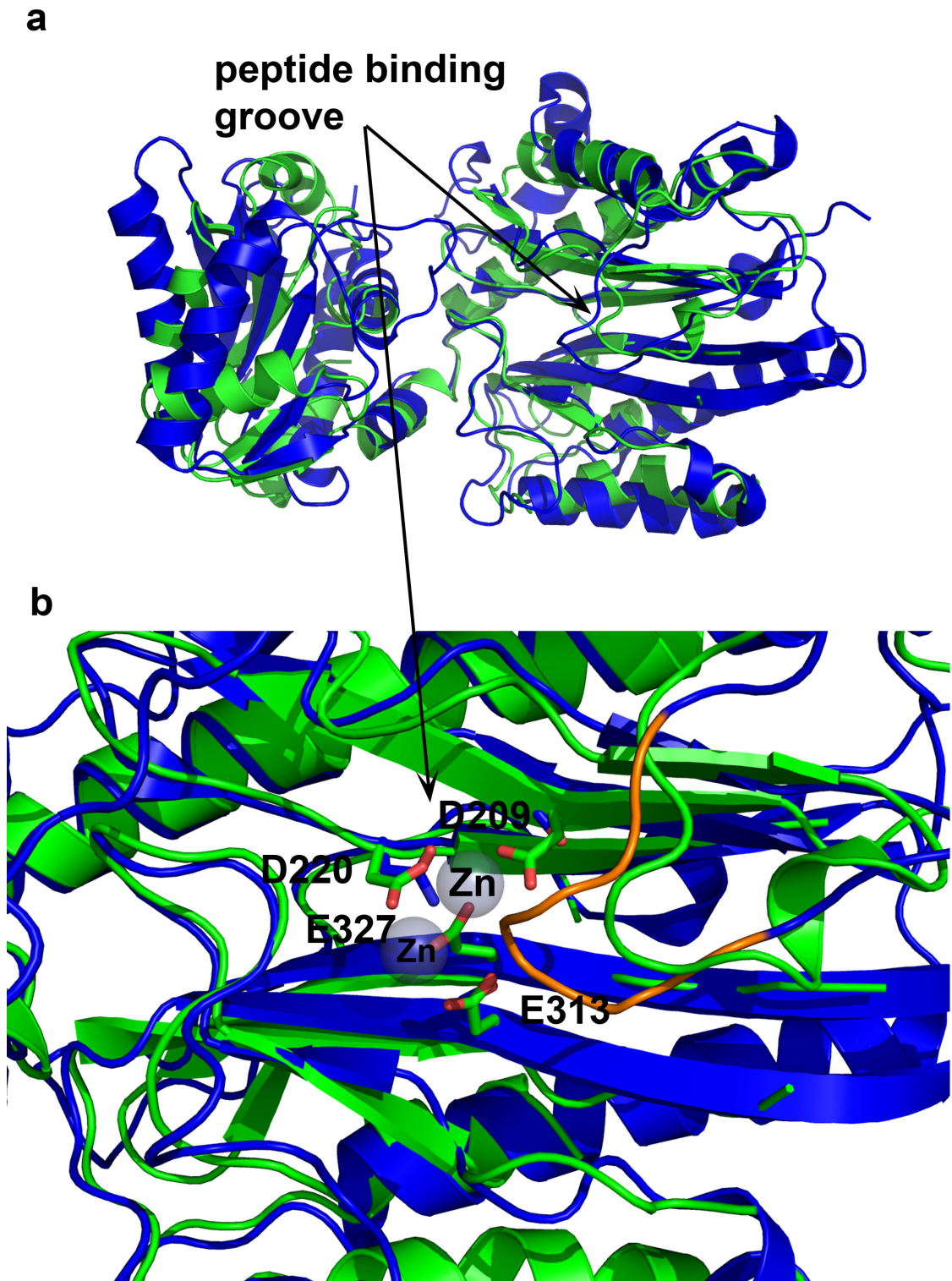


Figure 1-9 Superposition of Spt16 NTD and bacterial prolidase.

(a) Structural representation of Spt16 NTD (blue; PDB: 3BIP (130)) superimposed to the bacterial prolidase domain (green; PDB: 1PV9 (131)) (r.m.s.d of 3 Å). (b) Close up of the hypothetical peptide-binding groove showing side chains of prolidase (green) and Spt16 NTD (blue); Zn ions of the prolidase active site is blocked by Spt16 loop shown in orange. Arrow shows the location of the peptide-binding groove.

1.2.4.2 Spt16 DD

FACT heterodimerization involves the Spt16 dimerization domain and SSRP1/POB3 N-terminal/dimerization domain (NTD/DD) (Fig. 1-8) (119). In 2013, Hondele and others reported the structure of Spt16 DD in complex with SSRP1 NTD/DD (PDB: 4KHB) (135). The structure shows that Spt16 DD adopts a pleckstrin homology-like fold (PH) and interacts with SSRP1 NTD/DD domain, which is a double PH domain (Fig. 1-10). Pull down experiments show that this hetero-complex is able to interact with DNA polymerase α complex (Pol1), suggesting that FACT heterodimerization domain may be responsible for the interaction with the replication machinery (135).

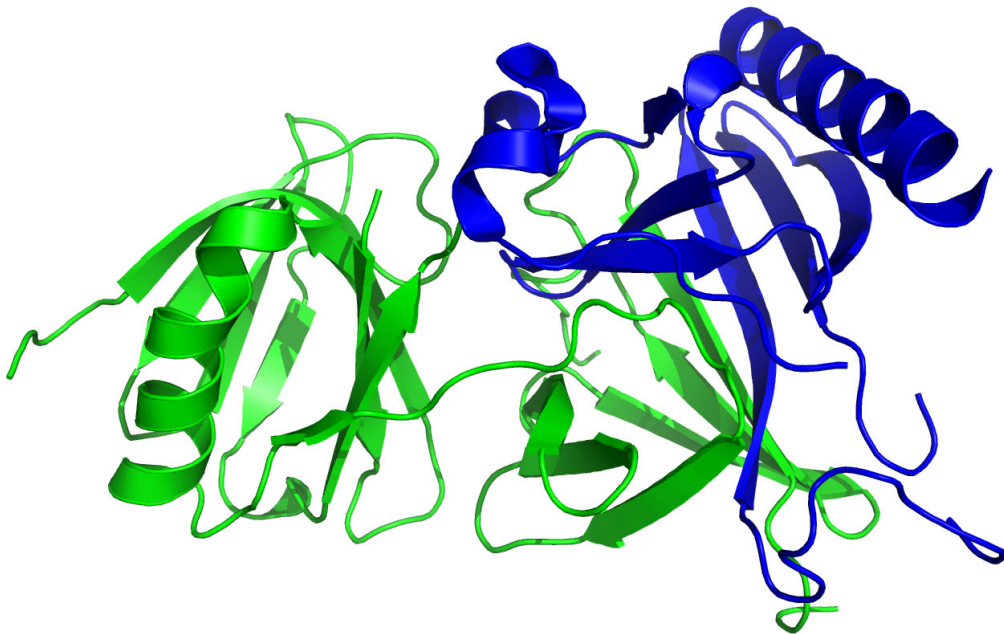


Figure 1-10 Structural representation of Spt16 DD bound to SSRP1 NTD/DD.

Structural representation of the two PH domains of SSRP1 NTD/DD (green) in complex with Spt16 DD (blue), which resemble a PH-like domain (PDB: 4KHB).

1.2.4.3 Spt16 MD

In 2013, the structure of *S. cerevisiae* Spt16 MD (PDB: 4IOY) and *C. thermophilum* Spt16 MD in complex with H2A/H2B were published (4KHA and Fig. 1-11); both resemble two PH-like domains in tandem with a root mean square deviation (rmsd) between them of 0.70 Å. Spt16 MD also shows structure similarity with two other protein structures: POB3 MD and Regulator of Ty1 Transposition (RTT106) with an r.m.s.d of 1.92 Å and 3.4 Å, respectively (Fig. 1-11). It has been shown that this structural architecture displayed H3/H4 binding (135-137). Spt16 MD differs from the other two structures: (1) it has a longer helix in PH1 domain, (2) it lacks the second helix present in POB3 and RTT106 in PH1 domain, and (3) it has three additional α -helices located at the C-terminus of PH2 domain, which forms a U-Turn motif (Fig. 1-11). The three α -helices at the C-terminus of the PH2 interact with the H2A/H2B dimer by hydrophobic interactions with residues on H2B α 1-helix (135). H2B α 1-helix is important for DNA attachment at the super helical location ± 4.5 (helix turns counted from the nucleosome dyad axis), suggesting that Spt16 MD may displace nucleosomal DNA without H2A/H2B eviction (138). Interestingly, most of Spt16 mutations that affect FACT activity are in Spt16 MD domain (100,139). These mutations can be suppressed by destabilizing H2A/H2B and (H3/H4)₂ interactions (139-141), suggesting that Spt16 MD is responsible for establishing important interactions with the nucleosome during FACT activity.

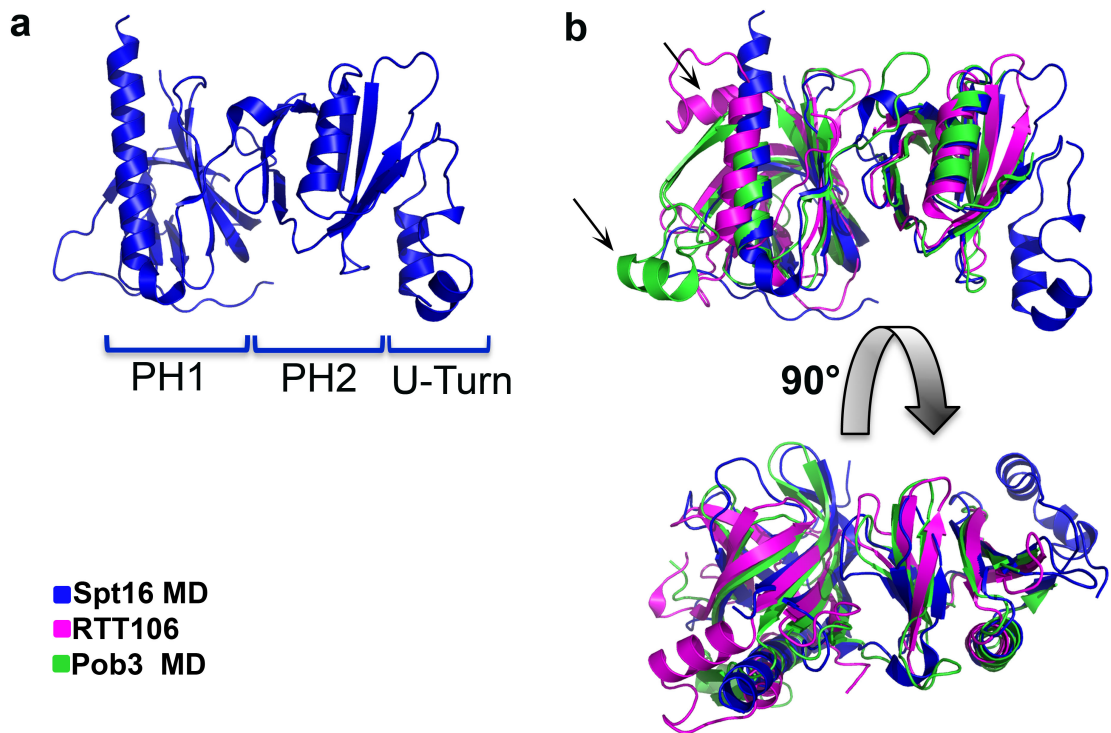


Figure 1-11 Structural representation of Spt16 MD and its superposition with POB3 MD and RTT106.

(a) Crystal structure of *C. thermophilum* Spt16 MD with indicated subdomains (PDB: 4KHA). (b) Superposition of Spt16 MD with POB3 MD (PDB: 2GCL) and RTT106 (PDB: 3GYP) showing structural difference with Spt16 MD. Arrows show the second α -helix present in POB3 and RTT106, which are missing in Spt16 MD.

1.2.4.4 Spt16 CTD

Spt16 CTD consists of a highly acidic intrinsically disordered domain, which has been implicated in H3 interactions and is important for FACT activity (103,139). This domain contains a putative nuclear localization sequence (NLS) responsible for the nuclear localization of Spt16 (135).

1.2.5 Structure-specific recognition protein-1 (SSRP1)

SSRP1 is an 80 kDa protein. It contains three domains identified as the N-terminal/dimerization domain (NTD/DD), a middle domain (MD), and the high mobility group or HMG-1 domain (HMG), which is flanked by two intrinsically disordered regions (ID and CTD) (Fig. 1-8) (125,128). Yeast POB3, a SSRP1 homolog, contains only the NTD/DD and MD domains, followed by the ID region. The HMG domain is synthesized as an individual protein called Nhp6 (101).

1.2.5.1 SSRP1 NTD/DD

The structure of the SSRP1 NTD had been determined (PDB: 3F5R) revealing a PH domain (Fig. 1-12). Characteristic of PH domains is that they bind lipids, protein and peptides (125,142). It remains unknown whether this domain contributes to histone binding. As described above (section 1.2.1), the structure of SSRP1 NTD/DD in complex with Spt16 DD was published whilst this study was undertaken. SSRP1 NTD/DD consists of two PH domains linked together by a loop of 16 residues (Fig. 1-10); the second PH domain is responsible for SSRP1/Spt16 heterodimerization (135).



Figure 1-12 Structural representation of POB3 first 111 residues.

Structural representation of POB3 (residues 1-111) resembling a PH-like fold (PDB: 3F5R).

1.2.5.2 SSRP1 MD

The structure of POB3 MD has been solved (PDB: 2GCJ), which contains two PH domains in tandem (residues 220-477 PH3 and PH4; Fig. 1-13) (125). Surprisingly these two PH domains share structure similarities with the first PH domain of NTD/DD with an r.m.s.d of 2.87 Å for PH3 and 1.31 Å for PH4 (reviewed in (127)). Genetic analysis of POB3 MD reveal that some residues, including the mutant Q308K, show temperature sensitivity, Hu sensitivity and Spt⁻ phenotype, suggesting a possible role in transcription, and DNA replication (125). The structure of POB3 Q308K mutant has been determined (PDB: 2GCL). It exhibits a similar fold as POB3 wild type (WT) showing that the phenotype is not due to a change in structure (125). As aforementioned, studies on POB3 Q308K showed genetic interaction with H4 residues K5 and K12, which are acetylated in newly synthesized histone. Moreover, alteration of the histone pools, particularly deletion of one copy of H3/H4 or histone H2A/H2B overexpression, showed synthetic defect with POB3 Q308K. All together these data suggest a possible role during nucleosome deposition (125).

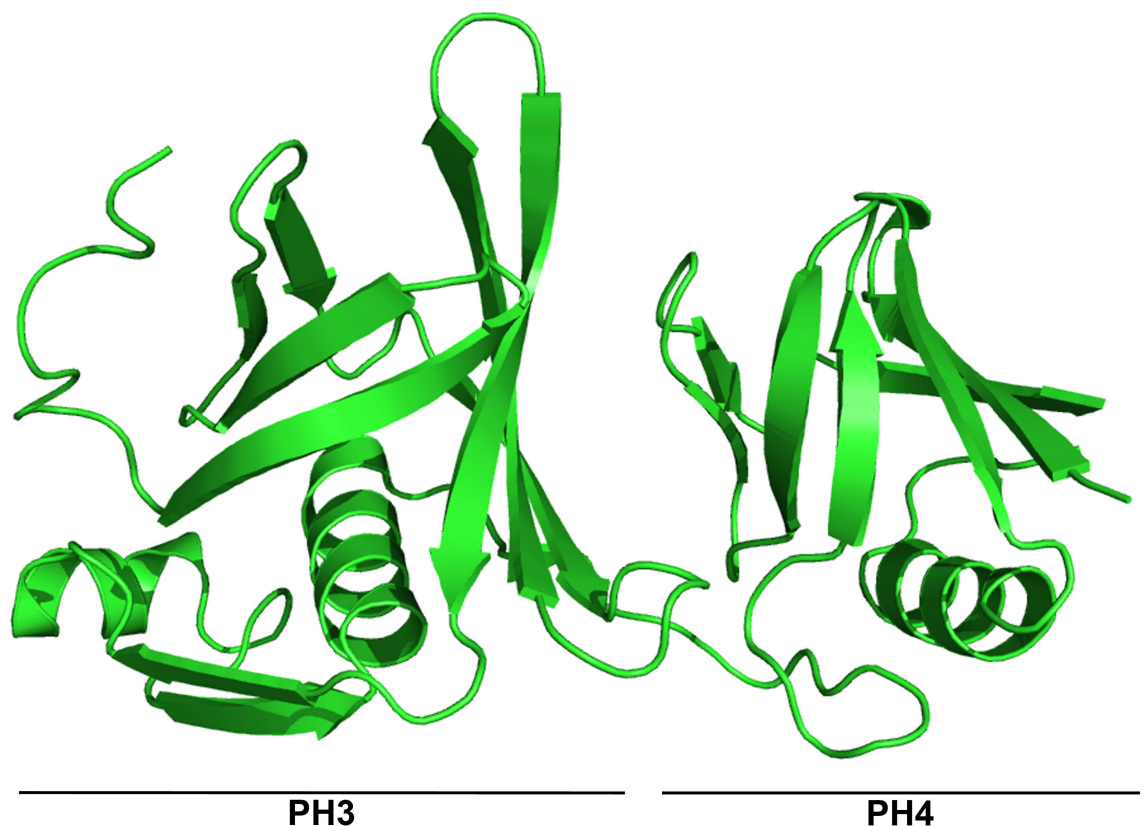


Figure 1-13 Structural representation of *S. cerevisiae* POB3 MD.

S. cerevisiae POB3 MD (PDB: 2GCL).

1.2.5.3 HMG domain

NMR structures of the HMG domain of SSRP1 (PDB 1WXL) and yeast Nhp6a (PDB 1LWM) have been reported (143,144) (Fig. 1-14). Solution structure of Nhp6 in complex with DNA assumes an L-shaped conformation typical of HMG domain. This domain makes interaction with the DNA minor groove through its short α -helix and with the major groove through its extended N-terminal α -helix (144).

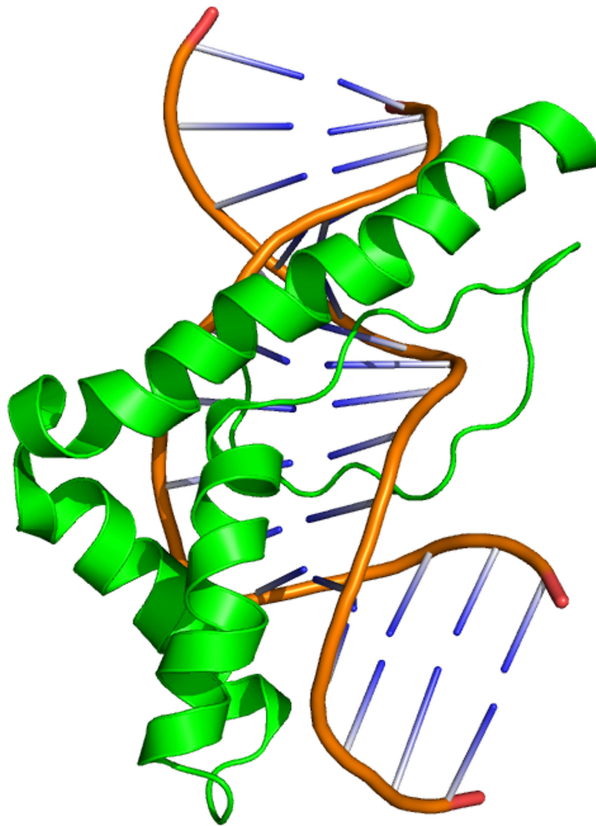


Figure 1-14 Structural representation of Nhp6 bound to DNA

Structural representation of *S. cerevisiae* Nhp6 (green) in complex with DNA (PDB: 1J5N).

1.2.6 FACT functions and their regulations

1.2.6.1 Histone PTMs and FACT activity

As described in Section 1.1.2, histone PTMs can modify chromatin structure by altering histone residue charges, or by recruiting or blocking protein complexes capable of changing it. For example the human but not yeast chromatin remodelling factor Chromatin organization modifier, Helicase, and DNA-binding domain 1 (CHD1) is recruited to the chromatin by binding to the trimethylated histone H3 lysine4 (H3K4me3) (145-147). It has been demonstrated that CHD1 physically interacts and reallocates FACT onto active open reading frame (ORFs) (113,148). Another histone modification is H2B monoubiquitination at lysine 120 (H2BK120ub1) mediated by RNA-Polymerase II Associating Factor (PAF) complex and Rad6/Bre1 (E2/E3) complex, which correlate with transcription elongation (149,150). Moreover, PAF complex has been shown to interact with FACT, suggesting that H2B monoubiquitination is required to promote FACT-mediated transcription (115,151). It has been shown that H2A monoubiquitination at lysine 119 mediated by histone H2A-homologous to ubiquitin (2A-HUB) represses transcription initiation by preventing FACT and RNA Pol II to bind at the GAL4 promoter (152). Finally, studies have shown that FACT can mediate H2AX exchange following its phosphorylation at serine 139 by DNA-PK in response to DNA damage (153).

1.2.6.2 FACT's post-translational modifications

In addition to histone PTMs, there are proteins that can directly modify FACT, and thus its activity. One of them is Poly-ADP-Ribose Polymerase 1 (PARP1), which poly-ADP ribosylate Spt16 and inhibits FACT's activity following DNA damage, so that H2AX cannot be removed from nucleosomes (153). Other studies showed that SSRP1 is influenced by several modifications that occur in different pathways. During apoptosis, SSRP1 is degraded both by ubiquitin-mediated proteolysis and caspase cleavage (154). These processes block genes transcription in order to facilitate apoptosis (154). Casein kinase 2 (CK2), an evolutionarily conserved kinase, phosphorylates the HMG domain of SSRP1 on three different serines: S510, S657 and S688. Phosphorylation of S510 decreases the ability of SSRP1 to bind the DNA (155). Moreover, it has been shown that FACT forms a complex with CK2 and thus alters the specificity of CK2 such that it selectively phosphorylates p53 S392 to enhance p53's activity following UV damage (156). Studies *in vivo* showed that SSRP1 associates with Serum Response Factor and

functions as a transcriptional co-activator with p63 (157,158). Recently it has been shown that SSRP1 is also involved into the regulation of the microtubule growth and gene transcription independent of its partner Spt16 (159,160).

1.2.7 FACT activity models

It is evident that FACT plays an important role during transcription by reorganising the chromatin structure, but how it alters the chromatin structure remains elusive. A recent review by Winkler and Luger (127) suggests two possible models that could explain FACT activity: the “Dimer Eviction Model” and the “Global Accessibility/Non-Eviction Model”. The first model assumes that FACT exerts its chaperone activity by displacing a H2A/H2B dimer thus generating a hexasome to facilitate RNA Pol II transcription (Fig. 1-11). The second model suggests that FACT does not evict H2A/H2B dimer from the nucleosomes but simply makes the structure loosen so that H2A/H2B dimer can exchange freely with the surrounding environment, allowing the formation of the hexasome (127) (Fig.1-11).

In the “Dimer Eviction Model”, FACT associates with the nucleosome at a 1:1 ratio (Fig. 1-11, 1a). FACT then causes H2A/H2B displacement (Fig. 1-11, 2a), followed by its reinsertion after RNA Pol II has gone through the DNA (Fig. 1-11, 3a). This model is supported by experiments showing that FACT not only specifically binds nucleosomes, but also histone dimer H2A/H2B *in vitro* (132). Moreover, during transcription elongation FACT is able to generate the hexasome (103). Similarly, cross-linking of nucleosome histones inhibits FACT activity (96). These results correlate the eviction of the histone heterodimer H2A/H2B, associated with transcription, DNA replication and repair (153,161-163).

“Global Accessibility/Non-Eviction Model” is based on the finding that yFACT can facilitate hydroxyl radical and nuclease accessibility without H2A/H2B displacement *in vitro* and promote transcription *in vivo* (138). According to this model, first Nhp6 binds to the DNA (Fig. 1-11, 1b), causing a conformational change in the nucleosome structure, which favours ySpt16/POB3 recruitment (Fig. 1-11 2b). At this stage, FACT allows nucleosome reorganization by individual histones binding to its domains followed by nucleosome restoration once cell machineries no longer need the DNA access (Fig. 1-11 3b) (138). Recent findings support this model by showing that several copies of Nhp6 are required for yFACT recruitment (102). Furthermore, even though yFACT cause histone dimer H2A/H2B displacement *in vitro*, the amount of dimer released is not consistent with

the level of nucleosome access (138). Finally, only a minimal loss of histone dimer or tetramer occurs following transcription activation of GAL1-10 promoter (138). These findings suggest that nucleosome components are constantly reorganized between FACT and a non-canonical nucleosome while DNA access is required. This reorganization may rely on FACT ability to interact with a wide range of protein through its multiple binding domains.

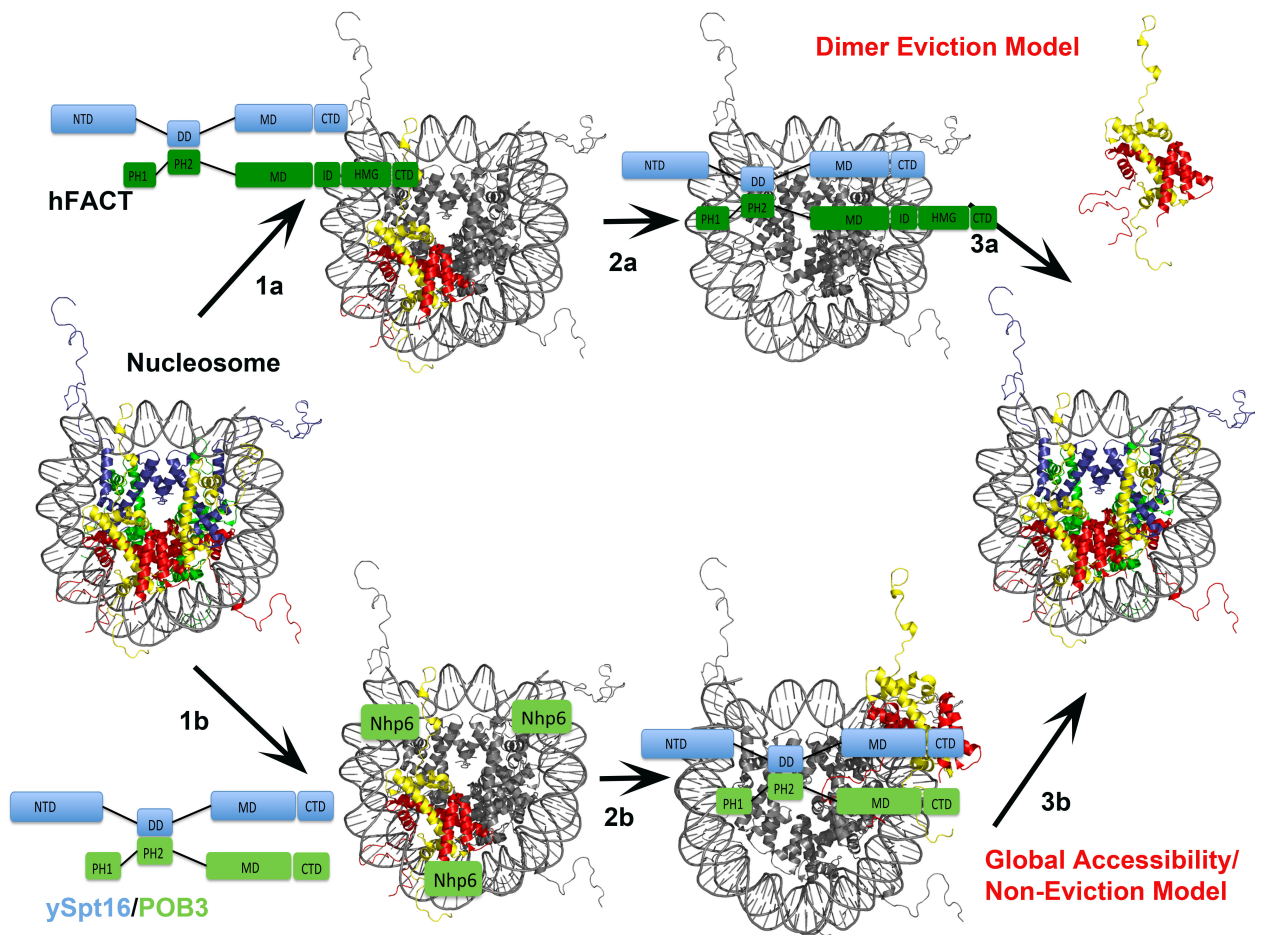


Figure 1-15 Schematic diagram showing two possible models for the nucleosome reorganization mediated by FACT

Dimer eviction model (Top) described in three steps indicated as 1a (FACT/nucleosome docking), 2a (H2A/H2B eviction) and 3a (H2A/H2B reinsertion). Global accessibility/non-eviction model (low) described in three steps indicated as 1b (Nhp6 docking and nucleosome conformational change), 2b (ySpt16/POB3 recruitment and nucleosome reorganization) and 3b (nucleosome restoration). H3 dark blue, H4 green, H2A yellow H2B red (PDB: 1KX5). Figure adapted from (127).

1.3 Histone Chaperone and Cancer

Chromatin conformation and its alterations are two characteristics important for malignant transformation (164,165). Recently, a study showed that the expression level of Asf1b (an isoform of the histone chaperone Asf1 in humans) correlates with cell proliferation. Indeed deletion of this chaperone prevents cell proliferation, thus it can be used as a marker to identify proliferating cells. Furthermore, depletion of Asf1b by siRNA led to aberrant nuclei structure and morphology, micronuclei formation, and inter-nuclear DNA bridges. Analysis on breast cancer samples showed that Asf1b is overexpressed in highly proliferative tumour cells, suggesting a correlation between Asf1b and breast cancer outcome (166). Consistent with this finding, study on other histone chaperone such as tNASP (Nuclear Autoantigenic Sperm Protein) revealed a similar observation. It has been shown that its depletion reduces the proliferation of the prostate cancer PC-3 cells and induces apoptosis (167). Recent studies showed that FACT is overexpressed in several cancers such as lung adenocarcinoma, fibrosarcoma, cervical carcinoma and mouse melanoma. Its knock down in those cell lines reduces cell proliferations (168). Thus, histone chaperones such as FACT may be potential therapeutic targets for treating diseases such as cancer.

1.4 Objective

Hu FACT was first discovered in 1998 (95). Since then, works in cell biology and structural biology have provided insights into its functions and mechanism of action in nucleosome reorganization. However, how FACT reorganizes nucleosome remains elusive, therefore further studies are required to fully understand this process. To this end, the objects of my thesis are:

1. To determine the crystal structure of Hu Spt16 NTD. Comparison of this structure with the *S. cerevisiae* and *S. pombe* structures may provide evidence of Spt16 NTD structure conservation and insight into its mechanism of histone binding.
2. To determine the crystal structure of Spt16 MD. This structure may explain how Spt16 MD interacts with histones.
3. To determine SSRP1 oligomerization state and solution structure, and how this may affect histone binding affinity.

Chapter 2

Materials and methods

2 Materials and methods

2.1 Molecular cloning

2.1.1 Plasmid source and cDNA

Vectors pGEX4T1 and pRSF_Duet-1 were purchased from Novagen and modified in laboratory to introduce a TEV cleavage site to remove the tag. Codon optimised full-length cDNA for *Human* (Hu) *Danio rerio* (Dr) and *Dictyostelium discoideum* (Dd) of Spt16 and SSRP1 were synthesized and cloned into pGEX4T1 for Spt16 or pRSF_Duet-1 for SSRP1 (Genewiz). POB3 and ySpt16 were obtained from yeast cDNA (Stratagene). Several constructs for Spt16 and SSRP1 were then generated by polymerase chain reaction (PCR) by using PFU Ultra II (Stratagene) (see Appendix 1 construct list). PCR product were digested with restriction enzymes (NEB), gel purified (Qiagen) and cloned into pGEX4T1 or pRSF_Duet-1 either by Quick ligase reactions (NEB) or In-Fusion® HD (Clontech), and checked by automated sequencing.

2.2 Expression and purification of recombinant proteins

Plasmid containing Spt16, SSRP1 or Spt16/SSRP1 (FACT complex) constructs were transformed into BL21 (DE3) Gold competent cells. Cells were grown at 37 °C using 6 to 100 L of media, depending on protein yield, to an OD₆₀₀ of ~0.7-0.8 in the presence of antibiotics and then induced with 0.2 mM isopropyl β-D-thiogalactopyranoside (IPTG, Foremedium) overnight at 20 °C. Following day, cells were harvested and resuspended in wash buffer with 1 mM phenylmethylsulfonyl fluoride (PMSF) along with 1 mg of lysozyme per ml of pellet and then subjected to a cycle of freeze-thaw. Before sonication an extra 1.5 mM PMSF was added. Cell were then sonicated using Vibra-Cell VCX 750 (Sonics & Materials, inc.) with a 13 mm probe at 85% amplitude and 8 seconds pulse followed by 8 second pause for 8 times. The lysed cells were then centrifuged at 20,000 rpm for 25 min at 4 °C for two times. Clear lysate was then loaded onto glutathione sepharose (GSH) affinity column or Ni-NTA affinity column depending on the tag. The tag was subsequently removed by incubating with TEV overnight. The protein was then purified by anion exchange or cation exchange (only for Spt16 MD) chromatography (gradient from 5 to 50% buffer B) and size exclusion chromatography (SD75 for Spt16 and SSRP1 single domains; or SD200 for Spt16 FL, SSRP1 ΔCTD and FL and FACT).

Fractions were analysed by SDS gel and pure protein were pooled together, frozen in liquid nitrogen and stored at -80 °C.

Dr Spt16 MD was transformed into BL21 (DE3) Gold competent cells and grown in 1X M9 minima salt base medium (Foremedium). Cells were grown at 37 °C to an OD₆₀₀ of 0.6-0.8; then amino acid mix (-Met) (Foremedium) and selenomethionine (SeMet; L (+)-Seleno Methionine, Foremedium) were added to the media. Cells were subsequently induced as previously described.

Protein concentration were determined by Bradford assay (169) with bovine serum albumin (BSA) as standard. Proteins concentrations for isothermal titration calorimetry (ITC) and histones purification were measured at A₂₈₀ by using NanoDrop 2000c (Thermo scientific). The extinction coefficient for each protein was determined with ProtParam (ExpASy website) (170).

Buffers commonly used for protein purification by affinity column:

Chromatography	Buffer
GSH-affinity	Wash: 50 mM Tris pH 7.6, 200 mM NaCl and 1 mM DTT
	Elution: 50 mM Tris pH 8.0, 200 mM NaCl, 10 mM GSH and 5 mM DTT
Ni ²⁺ -affinity	Wash: 25 mM Tris pH 7.6, 150 mM NaCl, 5 mM β-mercapto ethanol and 20 mM imidazole
	Elution: 25 mM Tris pH 7.6, 150 mM NaCl, 5 mM β-mercapto ethanol and 200 mM imidazole
Size exclusion	Running buffer: 25 mM Tris pH 7.6, 150 mM NaCl and 1 mM DTT

2.2.1 Purification of Hu Spt16 NTD

GST-Hu Spt16 NTD (Hu Spt16₁₋₅₁₀) was purified from lysate by GSH affinity column followed by overnight TEV cleavage and pass-back in order to remove the tag. Cleaved protein was loaded into anion exchange chromatography (SOURCE Q, GE; (Buffer A: 50mM Tris pH7.6 1mM DTT, B: 50mM Tris pH7.6, 1M NaCl and 1mM DTT) and size exclusion chromatography (Superdex 75, GE; running buffer: 25 mM Tris pH 7.6, 150 mM NaCl and 1 mM DTT). Fractions containing Hu Spt16 NTD were pooled together and concentrated using Amicon ultra centrifugal filter (Millipore), with a cut-off of 30KDa, to a final concentration of about 13.31 mg/ml. protein was then frozen in liquid nitrogen and stored at -80°C.

2.2.2 Purification of Dr Spt16 MD

GST- Spt16 MD from *human*, *Danio rerio* and *S. cerevisiae* were purified from lysate by GSH affinity column followed by overnight TEV cleavage. Cleaved protein was loaded into cation exchange chromatography (SOURCE S, GE; Buffer A: 50 mM MES pH 6 1 mM DTT, B: 50 mM MES pH 6, 1 M NaCl and 1 mM DTT) followed by size exclusion chromatography (Superdex 200, GE; running buffer: 25 mM Tris pH 7.6, 250 mM NaCl and 1 mM DTT). Fractions containing Spt16 MD were pooled together and concentrated using Amicon ultra centrifugal filter (Millipore), with a cut-off of 30KDa, to a final concentration of about 9 mg/ml. protein was then frozen in liquid nitrogen and stored at -80°C.

2.2.3 Purification of SSRP1 constructs

Vectors containing SSRP1 in different length or mutations were purified using Ni²⁺ or GSH- affinity column, cleaved overnight with TEV to remove the tag and then loaded onto anion exchange chromatography (Buffer A: 50 mM Tris pH 7.6 1 mM DTT, B: 50 mM Tris pH 7.6, 1 M NaCl and 1 mM DTT). Fractions containing SSRP1 construct were pooled together and concentrated before loading onto the size exclusion chromatography (Superdex 200, GE), using as running buffer 25 mM Tris pH 7.6, 200 mM NaCl and 5 mM DTT. Fractions containing purified proteins were finally concentrate by using Amicon ultra centrifugal filter (Millipore), with a cut-off of 30KDa, to a final concentration of about 6 mg/ml. Then frozen with liquid nitrogen and stored at -80°C.

2.2.4 Purification of FACT

GST-tag Spt16 and His-tag SSRP1 were co-expressed in BL21 (DE3) Gold cells and purified from lysate by GSH affinity column followed by overnight TEV cleavage. Cleaved protein was loaded onto anion exchange chromatography (SOURCE Q, GE; Buffer A: 50 mM Tris pH 7.6 1 mM DTT, B: 50 mM Tris pH 7.6, 1 M NaCl and 1 mM DTT) followed by size exclusion chromatography (Superdex 200, GE; running buffer: 25 mM Tris pH 7.6, 150 mM NaCl and 1 mM DTT). Fractions containing FACT complex were pooled together and concentrated using Amicon ultra centrifugal filter (Millipore), with a cut-off of 30KDa, to a final concentration of about 6 mg/ml. protein was then frozen in liquid nitrogen and stored at -80°C.

2.2.5 Histone dimer and tetramer purification from *Xenopus laevis*

Preparation of histone octamer from *Xenopus laevis* was performed as previously described in (171). Briefly His-tag H2A, H2B, H3 and H4 were cloned into RSF_Duet vector and transformed individually into BL21 (DE3) Gold cells and then grown for 2h at 37°C. Cell were harvest by centrifugation at 2000 rpm for 5 min at R.T., resuspend in wash buffer (50 mM Tris pH 7.5, 100 mM NaCl, 1 mM Na-EDTA, 1 mM benzamidine) and stored at -80°C. The following day the cells were thawed and lysed with a homogenizer, then centrifuged at 20000 g for 20 min at 4°C to collect the inclusion body (white pellet) where the histones are located. Pellet is then washed with wash buffer containing 1% Triton X-100 and resuspend by using a homogeniser. Repeat this step three times (once with Triton and twice without) then dry the pellet and store it at -80°C.

To dissolve the histones add 1 ml DMSO to the pellet for 30 min at R.T. then mince it with a spatula and add 40 ml unfolding buffer (7 M Guanidinium hydrochloride, 20 mM Tris pH 7.5 and 10 mM DTT). Stir it for 1h at R.T. and pass it repeatedly through a pipet to make the solution homogeneous. Then, centrifuge at 20000 g for 10 min at 20°C to remove the undissolved pellet.

2.2.5.1 Histone H2A/H2B and H3/H4 refolding

Mix the two proteins (H2A/H2B or H3/H4) at equimolar ratios to a final concentration of 1 mg/ml by using unfolding buffer and dialyze it for at least three changes with 2 l refolding buffer (2 M NaCl, 10 mM Tris pH 7.5, 1 mM Na-EDTA, 5 mM β -mercaptoethanol). The

last change should be performed overnight. Then you can concentrate the protein and store them at -80°C

2.2.6 Histone octamer purification from *Gallus gallus*

Chicken octamer were purified from chicken blood as described in (172). Briefly, 80 ml chicken erythrocyte nuclei ($2 \times 10^9/\text{ml}$) were quickly swirled with a solution made of 80 ml 4 M NaCl and 40 ml of saturated ammonium sulphate at 4°C and left on ice for 1 h, giving a viscous and cloudy gel. This solution is then centrifuged at 100000 g for 18 h to remove the precipitated non-histone protein. Next the supernatant was concentrated to ~ 10 mg/ml and an equal volume of saturated ammonium sulphate was added dropwise to the solution containing histone protein while stirring on ice. The solution is then centrifuged 100000 g for 1 h and the supernatant discarded. As a further purification step, the pellet was resuspended in 100 ml of 10 mM Tris pH 7.4, 2M NaCl and precipitated again with an equal volume of saturated ammonium sulphate as previously described. At this stage the pellet was resuspended in 2 M KCl, 0.3 M KH_2PO_4 and 0.3 M K_2HPO_4 , concentrated to ~ 20 mg/ml and dialyzed into 2 M KCl, 0.5 M KH_2PO_4 and 0.5 M K_2HPO_4 .

Histone dimer H2A/H2B and tetramer H3/H4 were separated by using cation exchange chromatography (SOURCE S, GE) using a gradient where buffer A was 50 mM KH_2PO_4 , 50 mM K_2HPO_4 , and 1 mM DTT; buffer B was 50 mM KH_2PO_4 , 50 mM K_2HPO_4 , 2 M KCl and 1 mM DTT; with a final pH of 6.5 (see Fig 2-1).

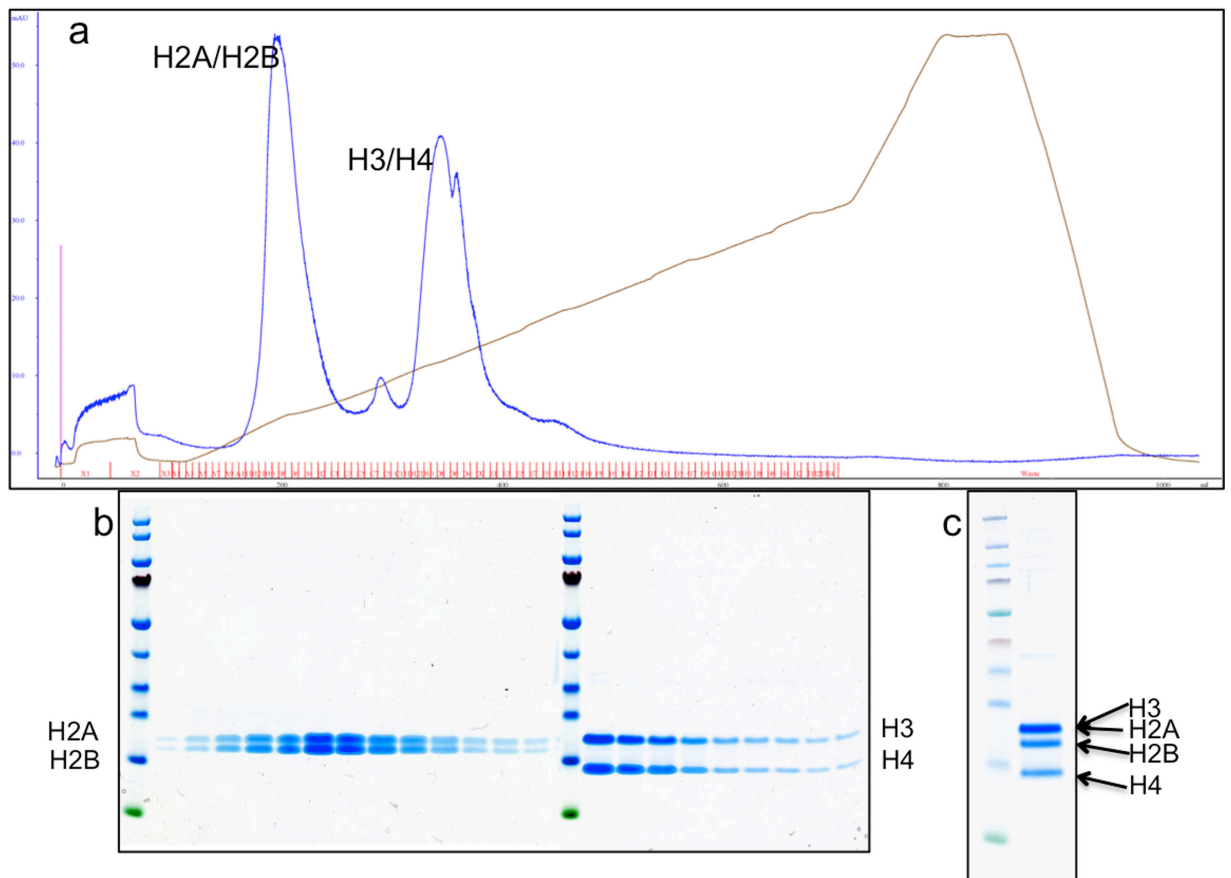


Figure 2-1 Cation exchange chromatography of histone octamer.

(a) Chromatogram showing histone H2A/H2B (eluted at about 500 mM NaCl) and H3/H4 (eluted at about 1 M NaCl) separation. (b) Gel showing fractions of anion exchange chromatography. (c) Gel showing purified octamer before loading onto anion exchange chromatography.

2.3 Crystallization

Initial crystallizations screening were performed in 96-well setting drop trays. Different crystallization kits buffers were used such as: Classic, Index, PEG, MPD, JCSG+, Morpheus, PACT and ProPlex. Mosquito (ttplabtech) was used to set the crystallization drop, which consists of 200 nl well solution and 200 nl of purified protein. Then, trays were sealed with a transparent film (ThermalSeal RT™) and stored in the Formulatrix workstation for image collections at different times. Crystal optimization was carried out in 24-well hanging drop trays.

2.3.1 Hu Spt16 NTD₁₋₅₁₀ crystal

Purified protein was mixed with equal volume of reservoir solution in a sitting drop tray at 4 and 19 °C. Crystals appeared after three days at 19 °C and have been optimized using hanging drop vapour diffusion at the same temperature. Crystallization conditions contained 17% (w/v) PEG 3350, 0.1 M ammonium iodide and 0.1 M sodium acetate pH 5. Crystals were flash frozen with liquid nitrogen in 20% (w/v) PEG 3350, 0.1 M ammonium iodide, 0.1 M sodium acetate pH 5 and 20% (w/v) glycerol.

2.3.2 Dr Spt16 MD₆₁₃₋₉₃₀ crystal

Purified protein was mixed with equal volume of reservoir solution in a sitting drop tray at 4 and 19 °C. Crystals appeared after three days at 19 °C and have been optimized using hanging drop vapour diffusion at the same temperature. Crystallization conditions contained PEG 3350 9% (w/v), 0.1 M ammonium nitrate and 0.1 M sodium citrate pH 5. Crystals were flash frozen with liquid nitrogen in 11% (w/v) PEG 3350, 0.1 M ammonium nitrate, 0.1 M sodium citrate pH 5 and 20% glycerol.

2.4 Data collection and processing

Diffraction data of Hu Spt16 NTD and Dr Spt16 MD were collected at Diamond Light Source (DLS) beamline I02 and I04. Data were integrated by the automated XDS (173) and scaled using CCP4 program suite (174).

2.5 Structure determination and refinement

Statistics of refinement are shown in Table 3.1, and 4.2. Pymol (Schrödinger) has been used to generate all figures.

2.5.1 Structure of Hu Spt16 NTD₁₋₅₁₀

Native Hu Spt16 NTD crystals belong to the space group F432 with one molecule in the asymmetric unit. Initial phase was obtained by automated molecular replacement with PHASER (175) using *S. cerevisiae* Spt16 NTD (PDB: 3BIQ) (130) as initial search model. The model was built and refined by using COOT (176) and PHENIX (177) respectively.

Structure of Hu Spt16 NTD was refined to 1.85 Å resolution. The model contains only chain A (residues 2-432). Residues 433-510 were absent in the electron density. Side chains with poor electron density were built as an alanine.

2.5.2 Structure of Dr Spt16 MD₆₁₃₋₉₃₀

Dr Spt16 MD crystal belongs to the space group P12₁1 with two molecules in the asymmetric unit. To determine the initial phase, multi-wavelength anomalous dispersion (MAD) data of SeMet Dr Spt16 MD crystals were collected. Unfortunately, both native and SeMet crystals exhibit pseudo-merohedral twinning as indicated by PHENIX Xtriage analyses (See Section 4.2.2). Due to twinning, we were unable to determine the SeMet sites and hence the phase information. After several attempts of crystal optimization I managed to obtain a dataset of the native Dr Spt16 MD that was not twinned. During that time, the structure of *S. cerevisiae* Spt16 MD was published. Initial phase was obtained by molecular replacement PHASER (175) using this structure (PDB: 4YOI) as the search model. The model was then built by using COOT (176). The structure of native Dr Spt16 MD₆₁₃₋₉₃₀ (chain A and B) was refined to 2.3 Å resolution using PHENIX. The model contained chain A (residues 660-927) and chain B (residues 648-927). Side chain residues with poor electron density were built as an alanine.

2.6 Small angle X-ray scattering (SAXS)

2.6.1 Data collection and processing (by Giancarlo Tria)

SAXS data collection of purified Dd SSRP1 Δ CTD was done at EMBL P12 beamline (DESY, Hamburg), using a wavelength of 1.24 Å and a PILATUS 2M pixel with an s range of 0.2 x 0.12 mm². An exposure time of 0.05 sec per frame was applied for a total of 20 frames.

Samples at a concentration range of 0.7-9.7 mg/ml were loaded (50µl) into the sample charger. Scattering intensity changes between the first and last frame were evaluated to assess sample radiation damage. Data were then processed with PRIMUS (178). Data were first averaged, then buffer subtracted and finally scaled based on sample concentration. Scaled data were finally checked for interparticle interference or protein aggregation. GNOM (178,179) was used to generate a p(r) analysis. DAMMIF (180) was used to generate 20 *Ab initio* models, which were subsequently superimposed and averaged using DAMAVER (181). Homology model of SSRP1 Δ CTD generated by I-TASSER (182) were first modelled into the scattering curve using CORAL (183) and then superimposed with the averaged *AB initio* model using SUPCOMB (184)

2.7 Analytical Ultracentrifugation (AUC)

2.7.1 AUC analysis of SSRP1 constructs

Sedimentation velocity (SV) analysis was carried out in a Beckman Coulter (Palo Alto, CA, USA) Optima XL-I analytical ultracentrifuge at 4 °C with a rotor speed of 49k rpm to determine sample monodispersity. Samples (typically 360µl) at a range of concentrations, which have previously been dialysed in 25mM Tris 200mM NaCl and 2mM TCEP, were loaded into 7 double sector centrepieces. 120 scans were taken every 7 minutes using interference optics and/or absorbance optics. SEDNTERP (185) was used to calculate partial specific volume of each protein and viscosity and density of the buffer used. SV data were then analysed by using SEDFIT (186) with a “continuous c(s) distribution” model. Sedimentation coefficient at 20°C in water ($S_{20,w}$) was calculated using the following equation:

$$S_{20,w} = S_{obs} \left(\frac{\eta_{t,w}}{\eta_{20,w}} \right) \left(\frac{\eta_b}{\eta_w} \right) \left(\frac{1 - \bar{V}\rho_{20,w}}{1 - \bar{V}\rho_{t,b}} \right)$$

Where S_{obs} is the sedimentation coefficient measured in the experimental buffer at temperature T; $\eta_{t,w}$ and $\eta_{20,w}$ are viscosity in water at experimental temperature (t,w) and at 20°C (20,w); η_b and η_w are viscosities of buffer (b) or water (w) at a common temperature; $\rho_{20,w}$ and $\rho_{t,b}$ are water density at 20 °C and buffer density at the experimental temperature respectively.

In order to determine protein oligomeric state, sedimentation equilibrium (SE) experiments were performed at 4 °C at two different speeds accordingly to the predicted MW. 90µl of sample, at various concentrations, were loaded into 7 double sector centrepieces. For each speed scans were taken every 3h until equilibrium had been reached. SE data were then analysed using SEDPHAT (187) with a “species analysis” model.

2.8 Isothermal titration calorimetry (ITC)

Isothermal titration calorimetry is a gold standard technique used to measure interactions between proteins, peptides, lipids and drugs. Usually, a macromolecule is placed into the cell and the ligand, such as peptide; protein etc. (which is in the same buffer as the molecule in the ITC cell) will go into the injection syringe. When the ligand is injected into the ITC cell (one injection at a time, usually 20) it will interact with the macromolecule generating or absorbing heat depending on the type of interaction. The same buffer will be also placed into the reference cell that is used to measure temperature difference between ITC cell and reference cell following ligand injection. If the interaction is exothermic it will generate heat, therefore the instrument will use less energy to heat the reference cell; if the interaction is endothermic it will absorb heat and the ITC instrument will use more energy to heat the reference cell. Energy measured by the instrument will then be plotted in a graph and will be used to calculate associating constant (K_a), enthalpy (ΔH), entropy (ΔS), and stoichiometry (n).

2.8.1 ITC data collection and analysis

All ITC experiments have been run at 25°C by using ITC200 (GE Life Science, MicroCal) with a buffer containing: 20 mM Hepes pH7.5, 200 mM NaCl and 1 mM TCEP for Dd SSRP1 and Hu Spt16 NTD; 20 mM Hepes pH7.5, 250 mM NaCl and 1 mM TCEP for

Spt16 MD and 20 mM Tris pH7.6, 150 mM NaCl and 1 mM TCEP for H3 and H4 peptides (Generon Ltd., see Appendix 3). Histone dimers H2A/H2B or tetramers (H3/H4)₂ were loaded into the cell at a concentration of 20-30 μM. Ligands, SSRP1 or Spt16 constructs, were loaded into the injection syringe at a concentration 10 times higher than cell. 20 injections, 2μl each, of ligand were then added every 180 seconds into the cell. ITC raw data were analysed using Origin software (version 7) with “one set of site” or “sequential binding” model. For histones peptides assays 50 μM of Hu Spt16 NTD was loaded into the cell while histone H3 or H4 peptides were loaded into the syringe at a concentration 10 times higher than cell.

2.9 Surface plasmon resonance (SPR) (by Gary Sibbet)

Experiments were conducted at 25 °C using a Biacore T100/T200 SPR instrument with a NTA sensor chip for His-tag proteins. All the protein were buffered exchanged in 25mM Tris pH7.6, 150 mM NaCl, 0.1 mg/ml BSA, 1mM DTT and 0.005% (v/v) Twenn-20. His-tag proteins (H3/H4)₂ or H2A/H2B were directly couple to the Ni-NTA chip at a response unit between 1000-2000. Hu Spt16 NTD was serially titrated and then flowed on top of the chip. Data were analysed by steady-state affinity analysis using Biacore T100 and T200 evaluation software package (Biacore Life Sciences).

Chapter 3

Structural and functional analysis of Hu Spt16 NTD

3 Structural and functional analysis of Hu Spt16 N-terminal domain

3.1 Aims and objective

At the onset of this project the structures of Spt16 NTD from *S. cerevisiae* and *S. pombe* were available (PDB: 3BIP and 3CB5 respectively) (129,130). Both resemble an amino peptidase like domain, which have lost the activity (see section 1.2.1). Studies on *S. cerevisiae* show that yFACT binds the nucleosome preferentially the tails of the histones, with high affinity (130). Whereas studies on *S. pombe*, conducted by Stuwe and others, showed that Spt16 NTD binds histone (H3/H4)₂; specifically, they showed that this interaction occurs between histone N-terminal tails H3 and H4 and serine 83 and lysine 86, with a K_d of 11 μ M (H3 N-tail) and 3 μ M (H4 N-tail) (129).

The aims of this project where: to investigate whether Spt16 NTD is conserved among different species; to test whether also Hu Spt16 NTD is able to bind histone dimer and/or tetramer or H3, H4 N-tails.

In this chapter I report the structure of Hu Spt16 NTD. By using ITC I show that Hu Spt16 NTD binds histone dimers and tetramers purified from *Gallus gallus* and *Xenopus laevis* in μ M range. Finally, ITC analysis of Hu Spt16 NTD against histone N-terminal tails H3 and H4 show no interaction.

3.2 Results

3.2.1 Hu Spt16 NTD purification and crystallization

Before I started my PhD, Danny and Gary performed a limited proteolysis analysis of Spt16 in complex with SSRP1 in order to identify the heterodimerization domain in both proteins. Based on this assay and on previous published structure of *S. cerevisiae* and *S. pombe* Spt16 NTD (129,130), Danny did generated different construct for human Spt16 NTD, which I cloned and purified for crystallization. Of these, only Hu Spt16₁₋₅₁₀ yielded crystals.

Protein expression and purification of Hu Spt16 NTD (Hu Spt16₁₋₅₁₀) was carried out as described in **chapter 2**. Purity of the protein before setting crystallization trays is shown in Fig. 3-1; crystal did grow in a cubic shape at 19 °C after 1day.

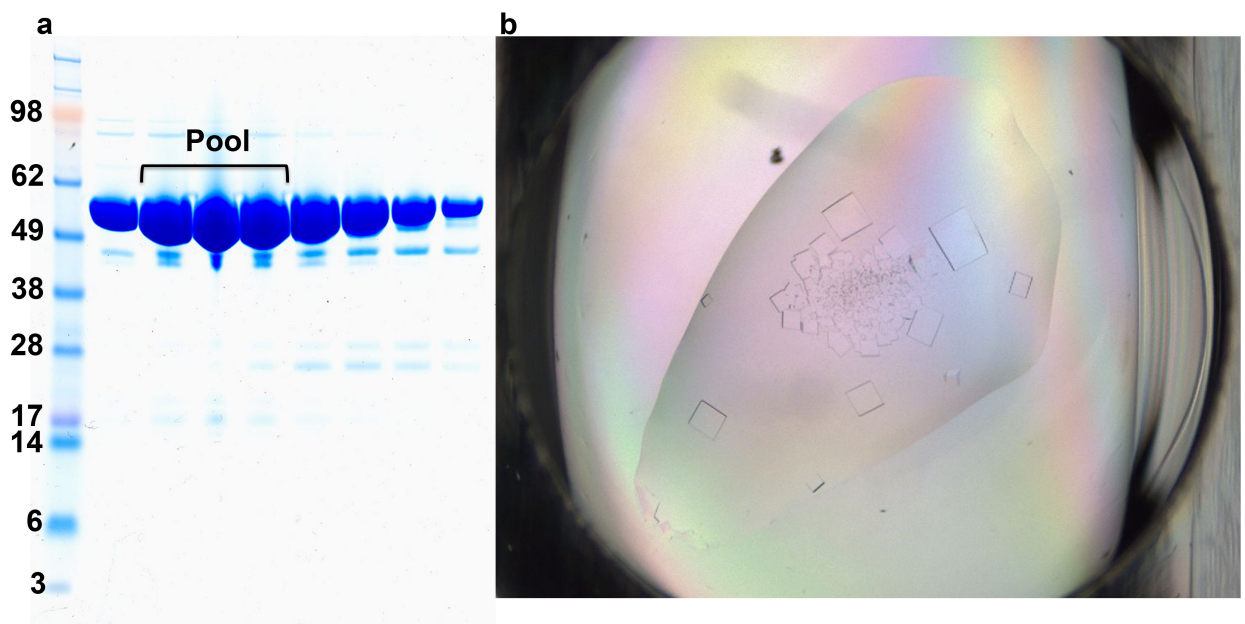


Figure 3-1 Purity and crystals of Hu Spt16₁₋₅₁₀

(a) SDS gel showing fractions of Hu Spt16₁₋₅₁₀ after SD75 gel filtration chromatography.

(b) Crystals of Hu Spt16₁₋₅₁₀.

3.2.2 Structure determination of Hu Spt16₁₋₅₁₀

Crystals of Hu Spt16₁₋₅₁₀ diffracted to a resolution of 1.84 Å with a space group of *F*432 and one molecule per asymmetric unit. Data collection and refinement statistics are reported in Table 3-1.

Table 3-1 Data collection and refinement statistics.

Hu Spt16 N-terminal domain	
Data collection	
Space group	<i>F</i> 432
Cell dimensions	
a, b, c (Å)	246.57, 246.57, 246.57
α , β , γ (°)	90, 90, 90
Resolution (Å)	87.18-1.84 (8.21-1.84)
R_{merge}	0.082 (0.779)
$I/\sigma(I)$	28.1 (4.2)
Completeness (%)	100 (100.0)
Multiplicity	20.0 (17.6)
Wilson B factor (Å ²)	23.3
Refinement	
Resolution (Å)	61.67-1.84
No. reflections	56309
$R_{\text{free}}/R_{\text{work}}$	0.184/0.163
No. atoms	
Protein	3459
Water	449
<i>B</i> -factors	
Protein (Å ²)	27.6
Water (Å ²)	37.6
r.m.s. deviation	
Bond length (Å)	0.008
Bond angles (°)	1.254

Note: Highest-resolution shell is shown in parenthesis. $R_{\text{work}} = \sum |F_0 - F_c| / \sum F_0$. $R_{\text{merge}} = \sum_h \sum_{i=1}^N |I_{(h)i} - \bar{I}_{(h)}| / \sum_h \sum_{i=1}^N I_{(h)i}$. R_{free} is the cross validation of *R* factor without 5% of the total reflections against which the model was not refined.

Hu Spt16₁₋₅₁₀ consists of two lobes: N-lobe (comprising residues 1-175) and C-lobe (comprising residues 176-432). Similarly to *S. cerevisiae* and *S. pombe*, Hu Spt16₁₋₅₁₀ adopts an aminopeptidase fold where the C-lobe resembles pita bread fold (Fig. 3-2, a and b) (129,130).

Structure superposition of Hu Spt16₁₋₅₁₀ onto the homologous from *S. cerevisiae* (r.m.s.d of 1.22 across C α) and *S. pombe* (r.m.s.d of 0.86 across C α) show subtle difference except for some loops in the N- and C-lobe due to sequence insertion (see Fig. 3-2, c and d). Moreover, superposition of Hu Spt16 N- or C-lobe against *S. cerevisiae* and *S. pombe* N- or C-lobe, respectively, shows small difference in the overall structure suggesting the two lobes are locked in position.

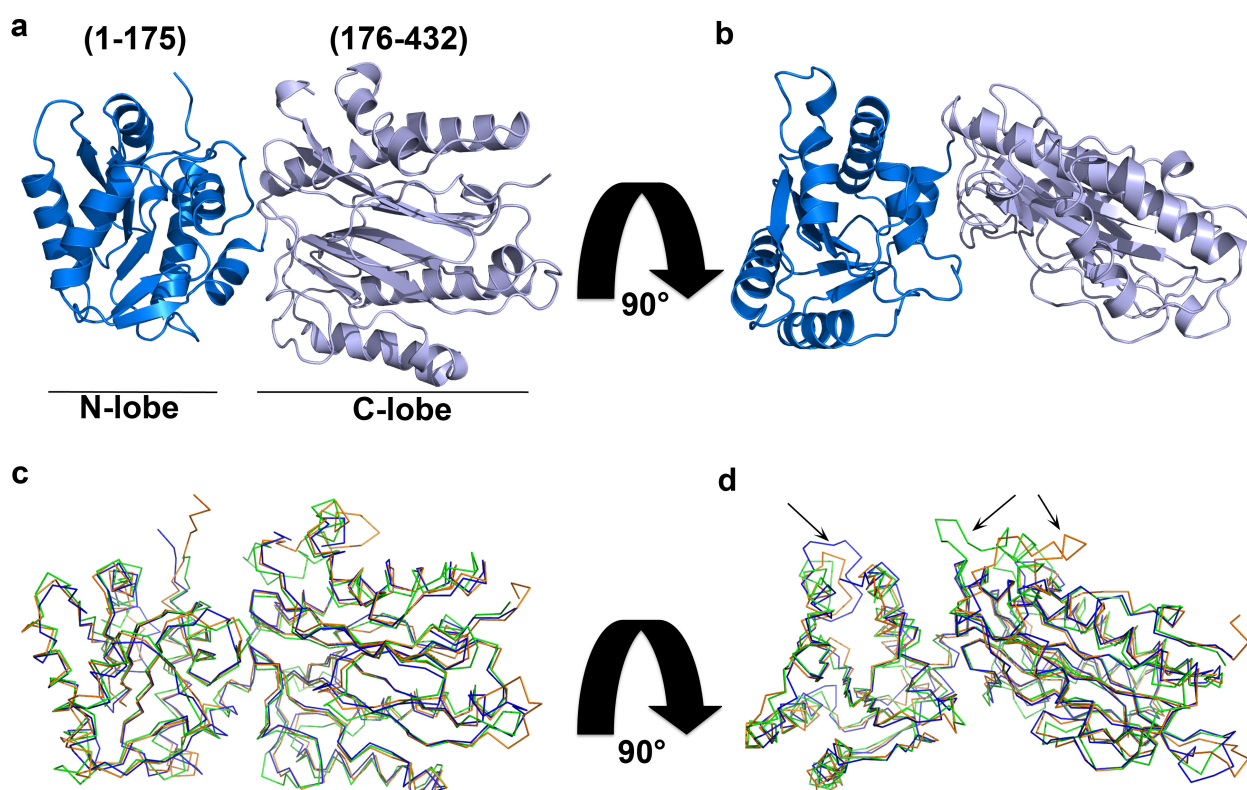


Figure 3-2 Structural representation of Hu Spt16 N-terminal domain.

(a and b) Structure of Hu Spt16₁₋₅₁₀ in two orientations. The domain consists of an N-terminal lobe (1-175 in blue) and a C-terminal lobe (176-432 in light blue). (c and d) Superposition of Hu (blue), *S. cerevisiae* (green) (PDB: 3BIP) and *S. pombe* (orange) (PDB: 3CB5) Spt16 NTD. c and d are displayed in same orientations as in a and b, respectively. Arrows indicate variation in the loops due to sequence insertion.

3.2.3 A conserved pocket on Spt16 NTD might be responsible for histone binding

Due to structure similarity, I did a sequence conservation analysis of Spt16 NTD in order to highlight a possible conserved region of this domain that may be involved in histone binding. I performed sequence alignment of Spt16 NTD from *Human*, *Danio rerio*, *S. cerevisiae*, *Drosophila melanogaster*, *Xenopus laevis*, *Dictyostelium discoideum* and *Chaetomium thermophilum* and generated a map that shows the conserved residues exposed on the surface (Fig. 3-3).

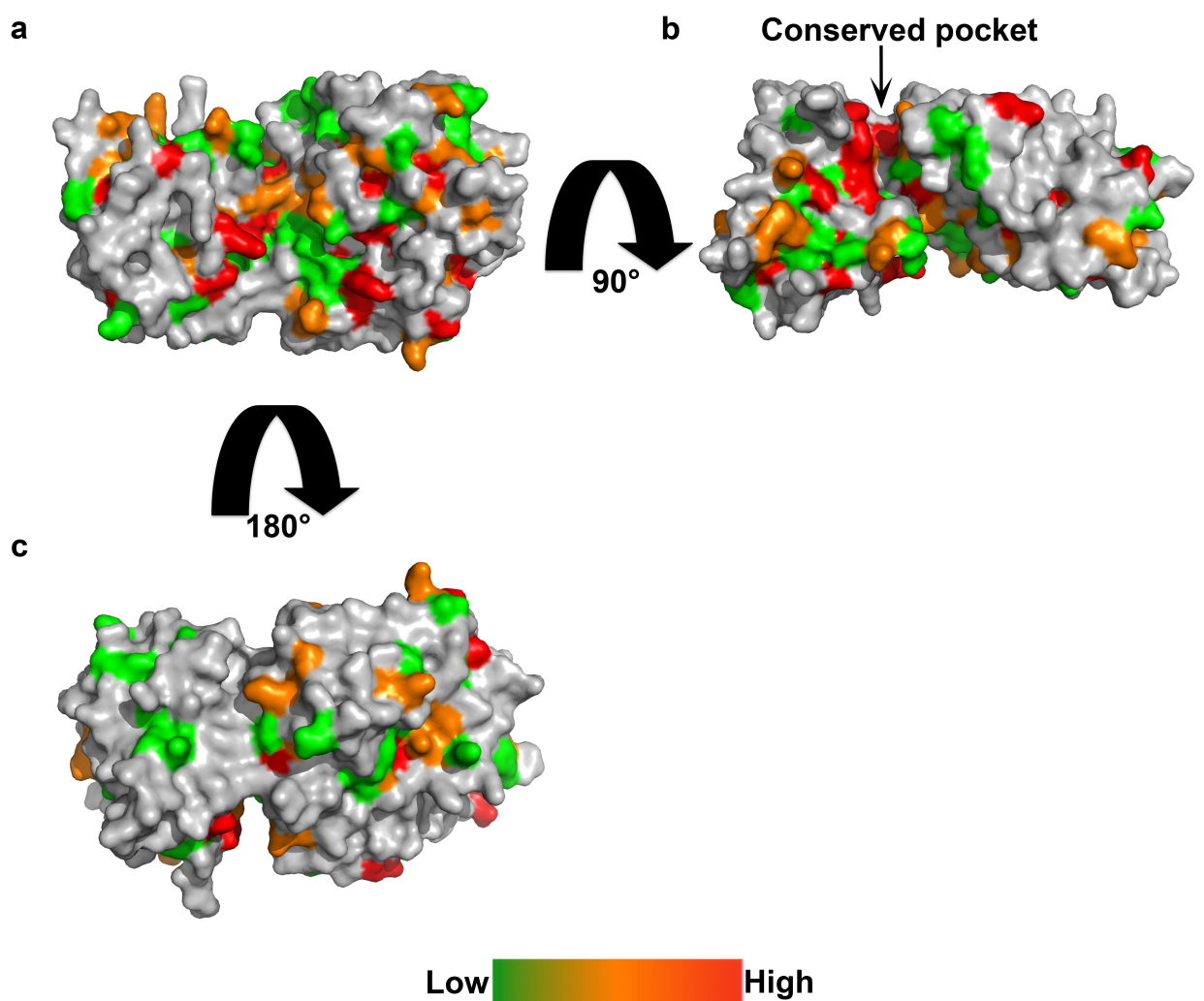


Figure 3-3 Sequence conservation of Spt16 N-terminal domain.

Sequence conservation map of Spt16 N-terminal domain (a) front side view, (b) side view and (c) back side view, showing a conserved pocket (arrow).

The sequence conservation map showed very low conservation on the backside of the domain. Interestingly, most of the conserved residues cluster on the C-lobe and in a pocket between the N-lobe and C-lobe, suggesting that this pocket might be involved in histone binding. Furthermore, electrostatic surface analysis of Hu Spt16 NTD showed an acidic patch that co-localize within the conserved pocket, which may interact favourably with the histones (Fig. 3-4, a and b). The electrostatic maps also show acidic patches at the bottom of the C-lobe and on the top of the N-lobe that might also be involved in histone binding (Fig. 3-4, d and e).

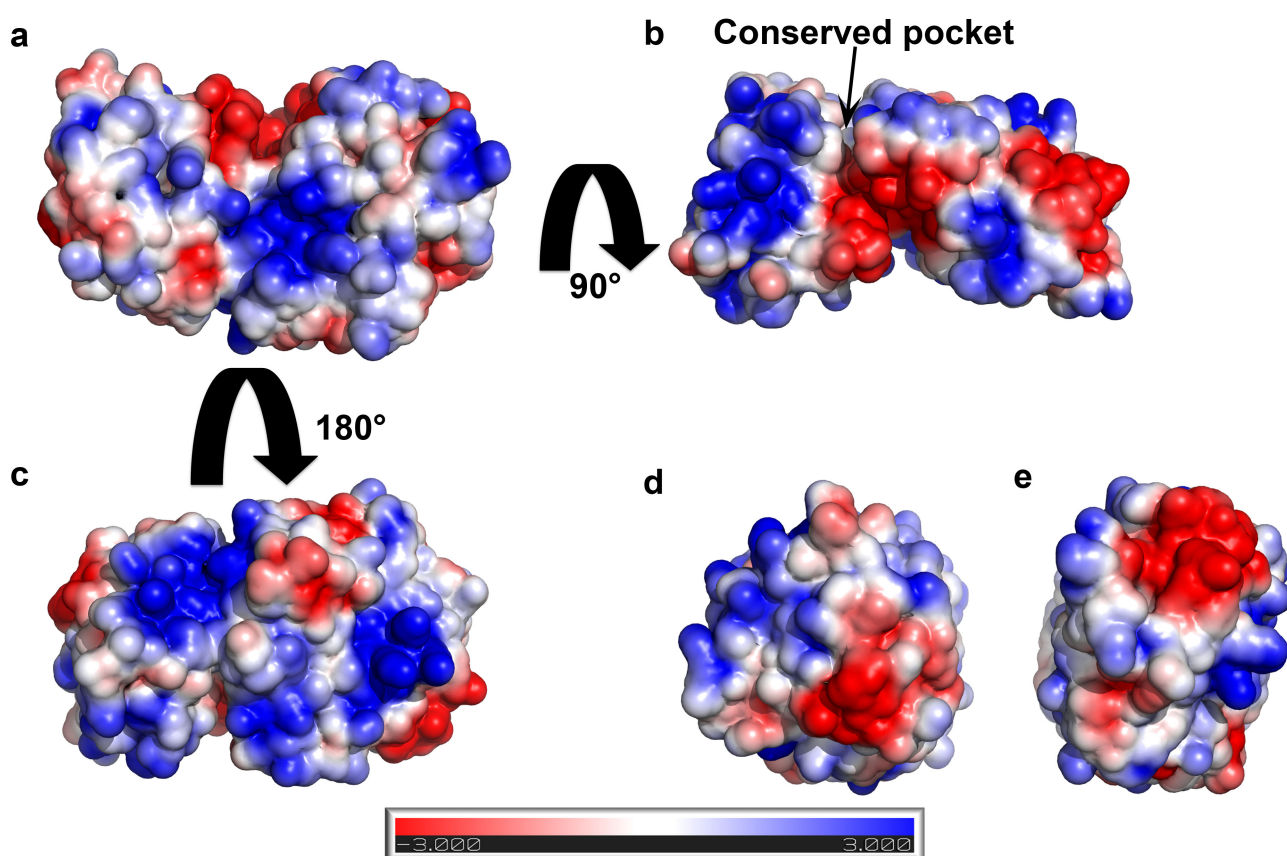


Figure 3-4 Electrostatic surface representation of Hu Spt16₁₋₅₁₀.

Electrostatic surface representation of Hu Spt16₁₋₅₁₀ at different angles generated using pymol APBS (188). (a) front; (b) side; (c) back; (d) top and (e) bottom. Arrow shows the location of the conserved pocket identified in Figure 3-3.

3.2.4 Functional analysis of Hu Spt16 NTD

3.2.4.1 Hu Spt16 NTD binds both histones H2A/H2B and (H3/H4)₂ with low affinity

Studies on yeast, conducted by VanDemark and others (130), showed that Spt16 NTD deletion is well tolerated by cells but when in complex with POB3 Q308K it causes severe synthetic defects. They also showed that yFACT bind the nucleosome primarily through the histone tails; indeed their removal by Trypsin digestion prevent nucleosome binding by yFACT (130). Furthermore, they showed genetic interaction between Spt16 NTD and the H2A docking domain, suggesting a possible interaction between these two domains. Other studies on *S. pombe* show that Spt16 NTD binds histone (H3/H4)₂ through their N-terminal tails with weak affinity (see section 3.1). Together these data suggest that Spt16 NTD has a role in histone binding that does not necessarily involve their N-terminal tails. To test whether this binding event is conserved in human, Gary Sibbet performed surface plasmon resonance (SPR) analyses to assess the binding affinity of *X. laevis* His-tag (H3/H4)₂ or His-tag H2A/H2B (coupled on the Ni-NTA chip) for Hu Spt16 NTD. SPR analyses showed weak interaction between Hu Spt16 NTD and histone dimer and tetramer (Table 3-2 and Fig. 3-5).

Table 3-2 SPR analysis of the binding interaction between Hu Spt16 N-terminal domain and histone H2A/H2B or (H3/H4)₂ (by Gary Sibbet).

Proteins	Kd
<i>X. Laevis</i> (H3/H4) ₂	225 ± 29 μM
<i>X. Laevis</i> H2A/H2B	361 ±110 μM

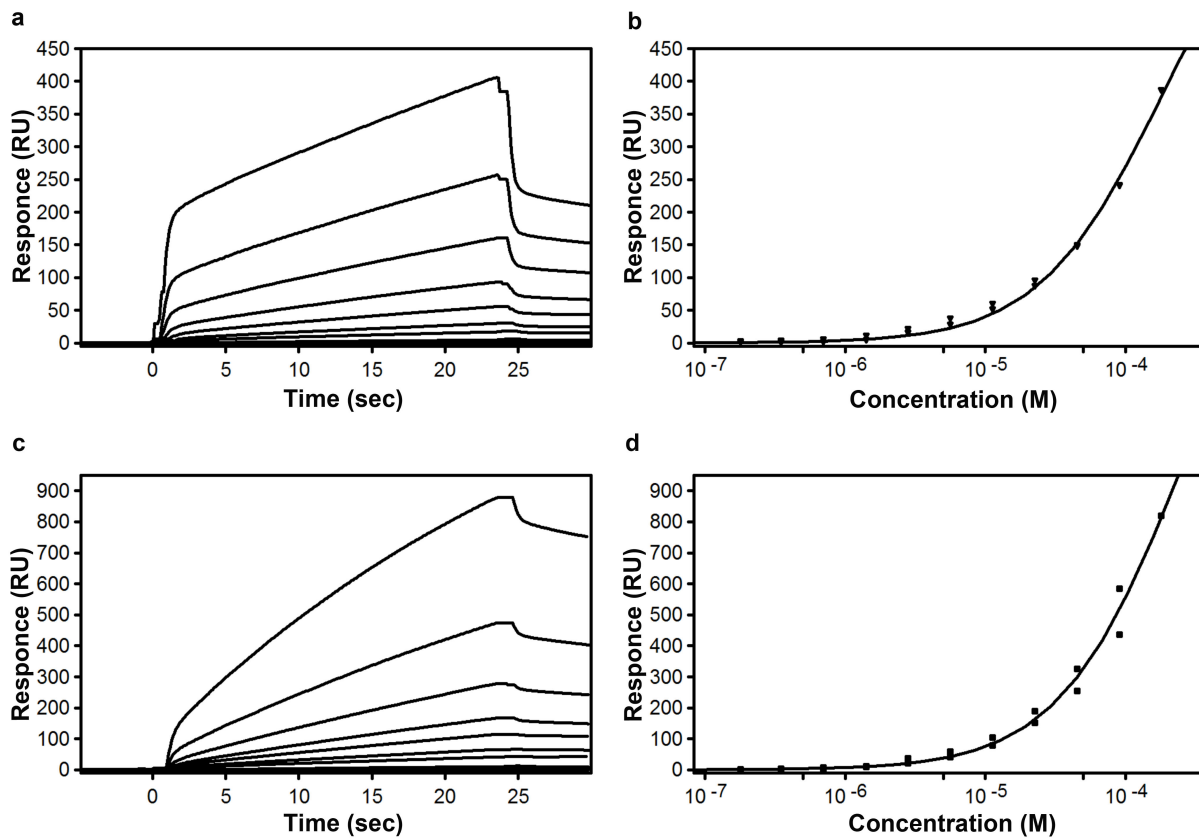


Figure 3-5 SPR analysis of Hu Spt16 NTD against histone H2A/H2B or (H3/H4)₂ (by Gary Sibbet).

Graphical representation of the sensorgram (a and c) and binding affinity plot (b and d) of Hu Spt16 NTD against histone (H3/H4)₂ (a and b) and histone H2A/H2B (c and d).

In order to validate SPR results and to further characterise the binding between Spt16 NTD and histones, I performed ITC analyses. Since human, *X. laevis* and *G. gallus* show high sequence conservation (sequence identity between *X. laevis* and human: H2A 93%, H2B 84%, H3 100%, H4 100%; sequence identity between *G. gallus* and human: H2A 95%, H2B 86%, H3 99%, H4 100%) for this assays I did used histones purified from *X. laevis* and *G. gallus*. Unfortunately, due to weak binding affinity, all ITC experiments did not reach saturation. Nonetheless, I was able to approximate the binding affinities by fitting the curve using the available data points.

Hu Spt16 NTD binds *X. laevis* (H3/H4)₂ with a K_d of 57.1 μM in a 1:2 molar ratio (Fig. 3-6a). Similarly, ITC titration of Hu Spt16 NTD against *G. gallus* (H3/H4)₂ shows a K_d of 52.35 μM with a 1:1 molar ratio (Fig. 3-6b). It is noteworthy that estimation of the molar ratio may not be accurate here because the binding curve is not saturated. Nevertheless, the ITC results suggest that Spt16 NTD binds histone (H3/H4)₂ with mid-low μM affinity.

Subsequently, I tested whether Hu Spt16 NTD is also able to bind histone H2A/H2B. ITC analysis of Hu Spt16 NTD against *X. laevis* H2A/H2B (Fig. 3-7a) gave a profile that could only be fitted with a “sequential binding site” with K_{d1} of 23.8 μM and K_{d2} of 456 μM . Likewise, ITC analysis of Hu Spt16 NTD against *G. gallus* H2A/H2B revealed an unusual and repeatable profile showing a biphasic binding event with similar K_d values as *X. laevis* (K_{d1} of 13.26 μM and K_{d2} of 746 μM) (Fig. 3-7b). Together my results are in line with previous published data, where Spt16 NTD displayed weak histones binding affinities.

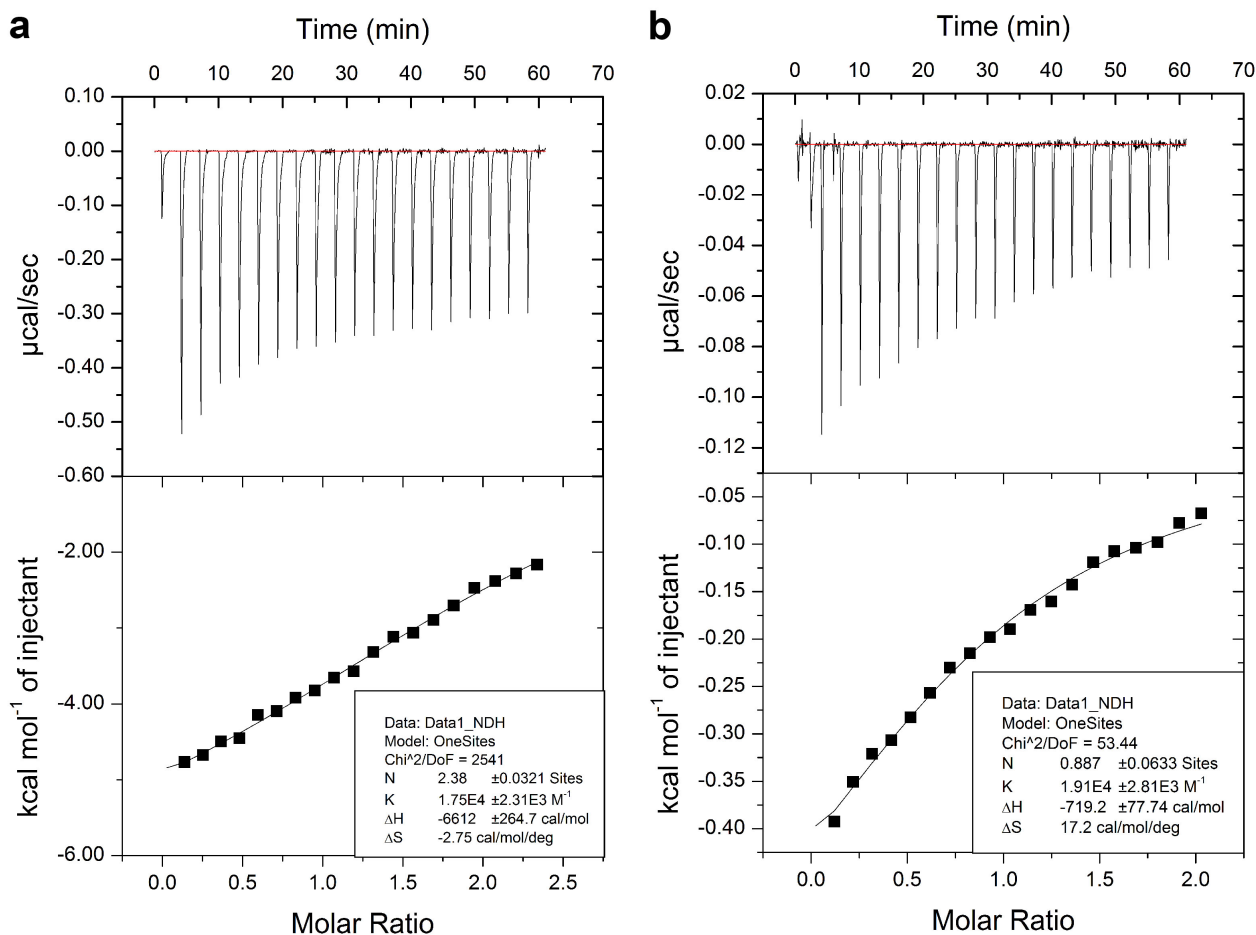


Figure 3-6 ITC profiles and fitting of Hu Spt16 N-terminal domain against histone (H3/H4)₂ from *X. laevis* and *G. gallus*.

(a) ITC profile showing raw data (upper panel) and normalised data (lower panel) plotted against the molar ratio between the ligand *X. laevis* (H3/H4)₂ and Hu Spt16 N-terminal domain. (b) ITC profile showing raw data (upper panel) and normalised data (lower panel) plotted against the molar ratio between the ligand *G. gallus* (H3/H4)₂ and Hu Spt16 N-terminal domain. Inset box shows stoichiometry (n), association constant (K_a), enthalpy (ΔH) and entropy (ΔS).

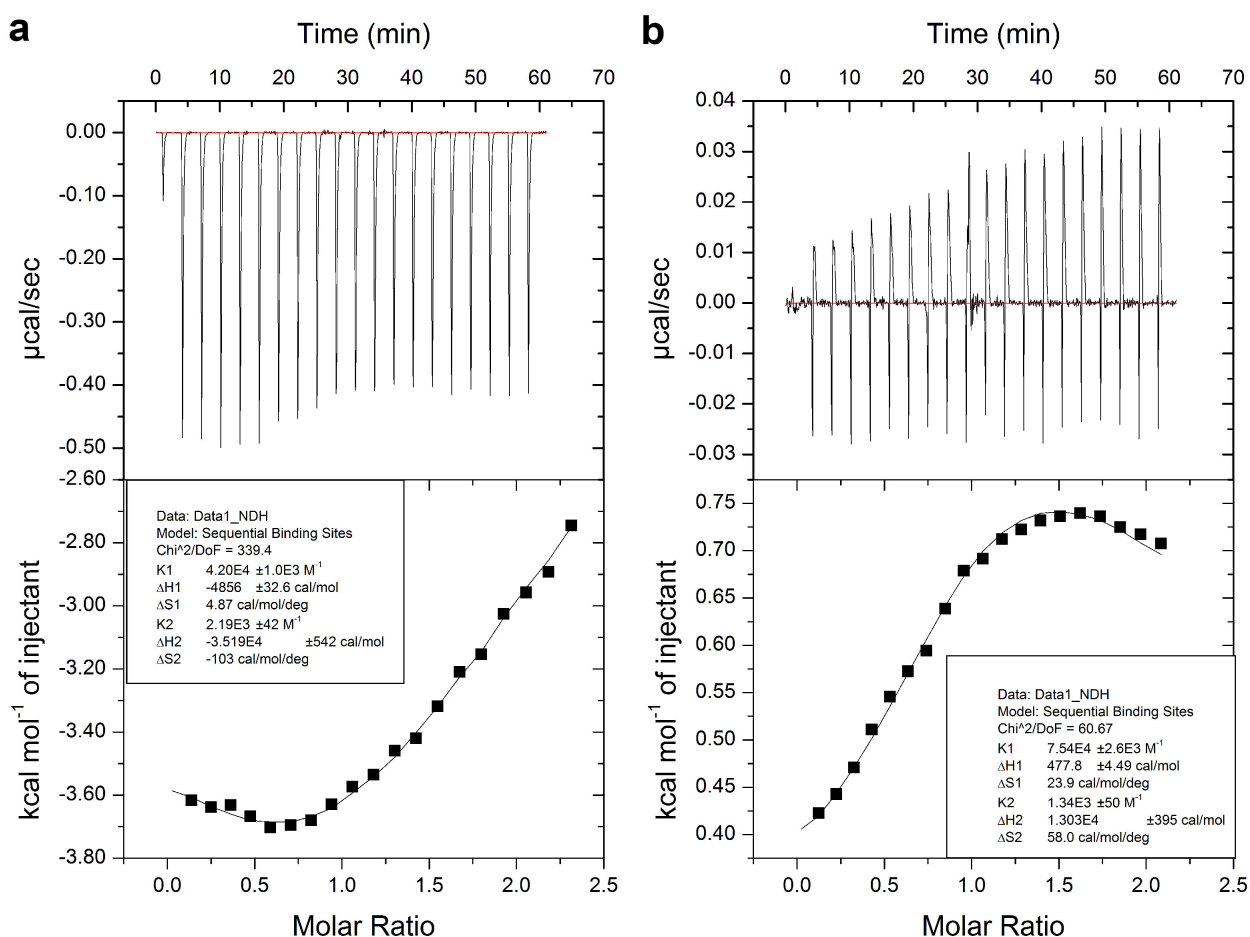


Figure 3-7 ITC profiles and fitting of Hu Spt16 N-terminal domain against histone H2A/H2B from *X. laevis* and *G. gallus*.

(a) ITC profile showing raw data (upper panel) and normalised data (lower panel) plotted against the molar ratio between the ligand *X. laevis* H2A/H2B and Hu Spt16 N-terminal domain. (b) ITC profile showing raw data (upper panel) and normalised data (lower panel) plotted against the molar ratio between the ligand *G. gallus* H2A/H2B and Hu Spt16 N-terminal domain. Inset box shows stoichiometry (n), association constant (K_a), enthalpy (ΔH) and entropy (ΔS).

3.2.4.2 *Hu Spt16 N-terminal domain does not bind histone tails H3 and H4*

As mentioned previously, Stuwe and others (129) showed that *S. pombe* Spt16 NTD binds histone tail H4 through two conserved residues K86 and S83 located on the $\alpha 3$ helix of the N-lobe. Mutations of those two residues to alanine reduce the affinity between Spt16 NTD and H4 peptide by 10-fold (129). These residues are conserved both in *Hu* and *S. cerevisiae* and adopt similar orientations as in *S. pombe*, suggesting that *Hu* and *S. cerevisiae* may also bind histone H4 tails (Fig. 3-8). In the previous section I showed that *Hu* Spt16 NTD binds both histone H2A/H2B and (H3/H4)₂ with low affinity. Based on these results I wanted to test whether *Hu* Spt16 NTD binds histone (H3/H4)₂ via their N-terminal tails. Hence, I purified *Hu* Spt16 NTD and tested its binding affinity against histone tails H3 or H4 (sequence shown in appendix 3).

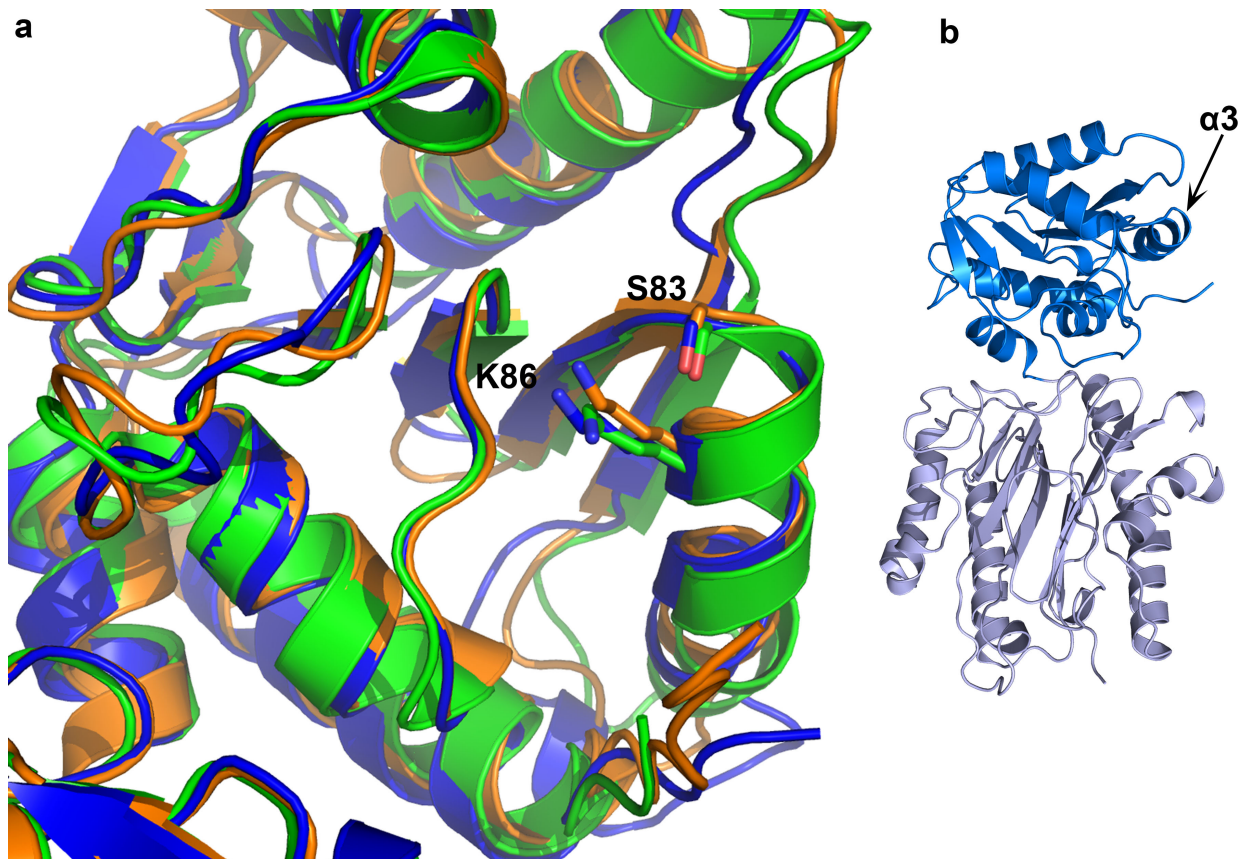


Figure 3-8 Spt16 N-terminal domain's putative binding site for histone tail H4 showing S83 and K86 side chains.

(a) Close up of the putative binding site on Spt16 N-lobe, showing S83 and K86 side chain in the $\alpha 3$ helix of *S. pombe* (orange) (PDB: 3CB5) and corresponding residues of *Hu* (blue) and *S. cerevisiae* (green) (PDB: 3BIP). (b) Structural representation of *Hu* Spt16 NTD showing the location of the $\alpha 3$ helix.

ITC experiments showed that Hu Spt16 NTD does not bind histone H4 or H3 tails peptide (see Figs. 3-9a and 3-9b). This result is in agreement with VanDemark's data where ySpt16 NTD does not bind histone tails (see section 3.1); it also suggests that residues S83 and K86 of this pocket, although conserved, might not be involved in histone binding or that this binding in human is too weak to be detected at the concentrations used on this assay.

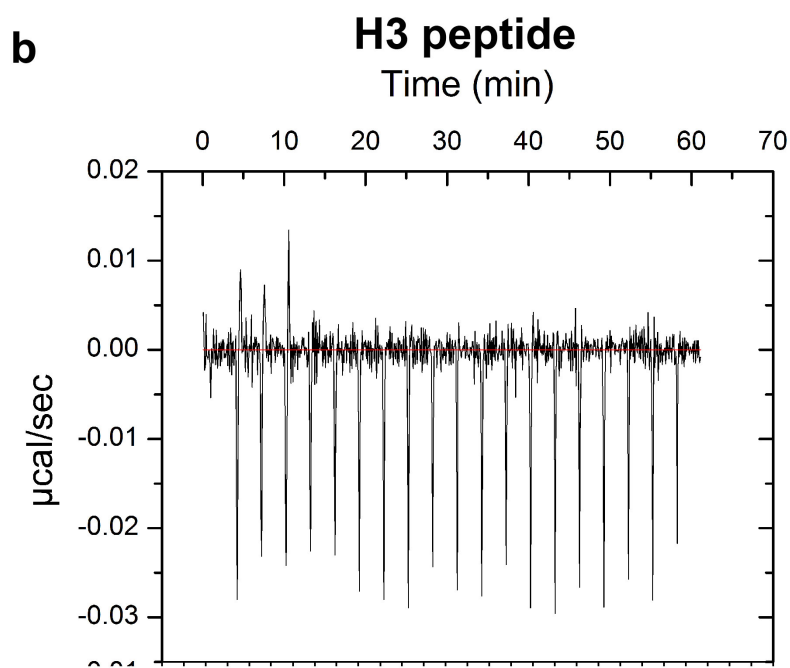
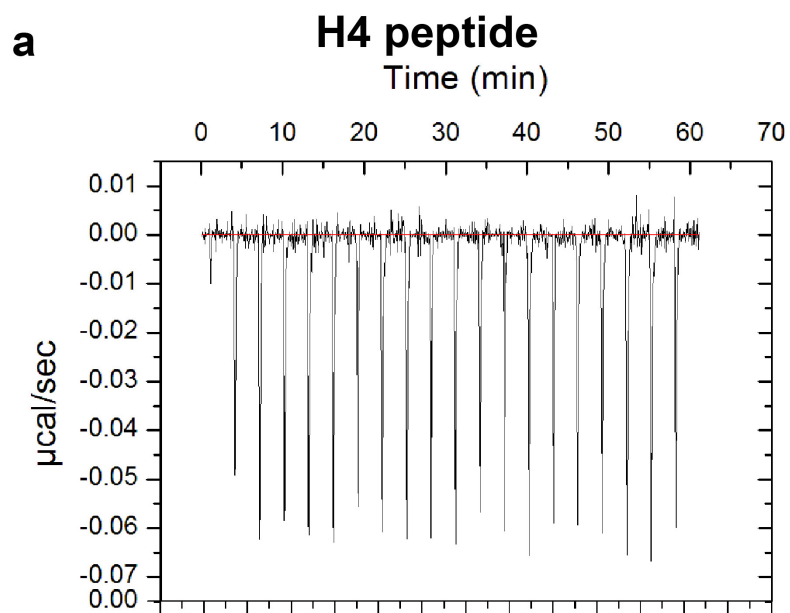


Figure 3-9 ITC profiles of Hu Spt16 NTD against histone N-terminal peptides.

(a) ITC raw data titration between the ligand H4 peptide (26 mer) and Hu Spt16 NTD.

(b) ITC raw data titration between the ligand H3 peptide (38 mer) and Hu Spt16 NTD.

3.3 Discussion

Little is known about Spt16 NTD and its functions. In this chapter I reported that Hu Spt16 NTD adopts a similar conformation compared to yeast and pombe Spt16 NTD (PDB: 3BIP and 3CB5). Analysis of residues conservation and electrostatic surface of this domain, highlight the presence of an acidic pocket that may be involved in histone binding (Fig. 3-4). Moreover, SPR and ITC experiments showed that Hu Spt16 NTD binds both histone H2A/H2B and (H3/H4)₂ with low affinity, which is consistent with previously published data (129,130). While ITC analysis of Spt16 against H2A/H2B exhibited profiles that can only be fitted with two binding sites, it is important to note that these binding curves were not saturated and will require further studies to validate these results. Spt16 N-terminal domain contains an acidic patch at the top of the N-lobe and at the bottom of the C-lobe (Fig. 3-4, d and e). It is speculative that these acidic patches may contribute to the weak histone binding. Furthermore the weaker binding affinities obtained by using SPR likely due to direct coupling of histones onto the CM5 chip which may alter histones accessibility.

Previous study showed that *S. pombe* Spt16 NTD binds H3 and H4 N-terminal tails with K_d of 11 and 3 μ M, respectively (129). This interaction primarily involves two conserved residues, S83 and K86 (see section 3.2.4.2), in Spt16 NTD's N-lobe. My ITC analyses of Hu Spt16 NTD against histone H3 or H4 peptides showed no interaction between them. Comparison of the electrostatic surface of *S. pombe* and Hu Spt16 NTD showed that S83 and K86 are located in a basic patch of the N-lobe (Fig. 3-10), suggesting that this region may not be favourable for histone tails interaction. Future structural studies on Spt16 and histones complexes are required to elucidate how Spt16 binds histone core and tails.

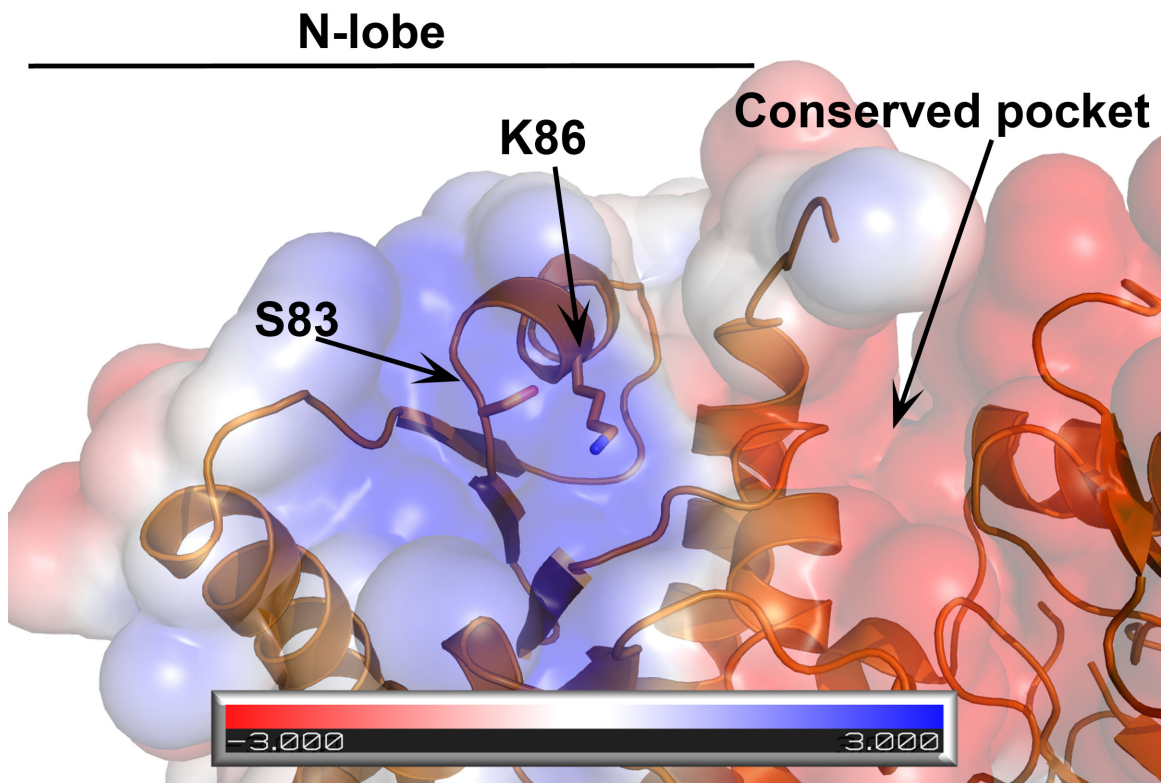


Figure 3-10 Close up of the putative binding pocket of *S. pombe* Spt16 NTD.

Electrostatic surface and structural (orange) representation of: *S. pombe* Spt16 N-lobe (PDB: 3CB5). Side chain of S83 and K86 and conserved pocket are shown.

Moreover, due to the low sequence conservation, *S. cerevisiae* and *S. pombe* show electrostatic surface differences compared to human. Particularly, *S. pombe* shows a larger acidic surface around the conserved pocket between the two lobes of the domain (Fig. 3-11). It is possible that *S. pombe* bind histone H4 N-tail with stronger affinity compared to human, because of this acidic patch. The acidic pocket between the N- and C-lobe is well conserved, and therefore it might be involved in histone binding as shown in section 3.2.4.1. Interestingly, some of the mutations of Spt16 NTD that, together with POB3 Q308K, affect yFACT activity cluster in a region near the conserved pocket. All together my result suggest that Hu Spt16 NTD has a role in histone binding, but that its function is dispensable for FACT activity.

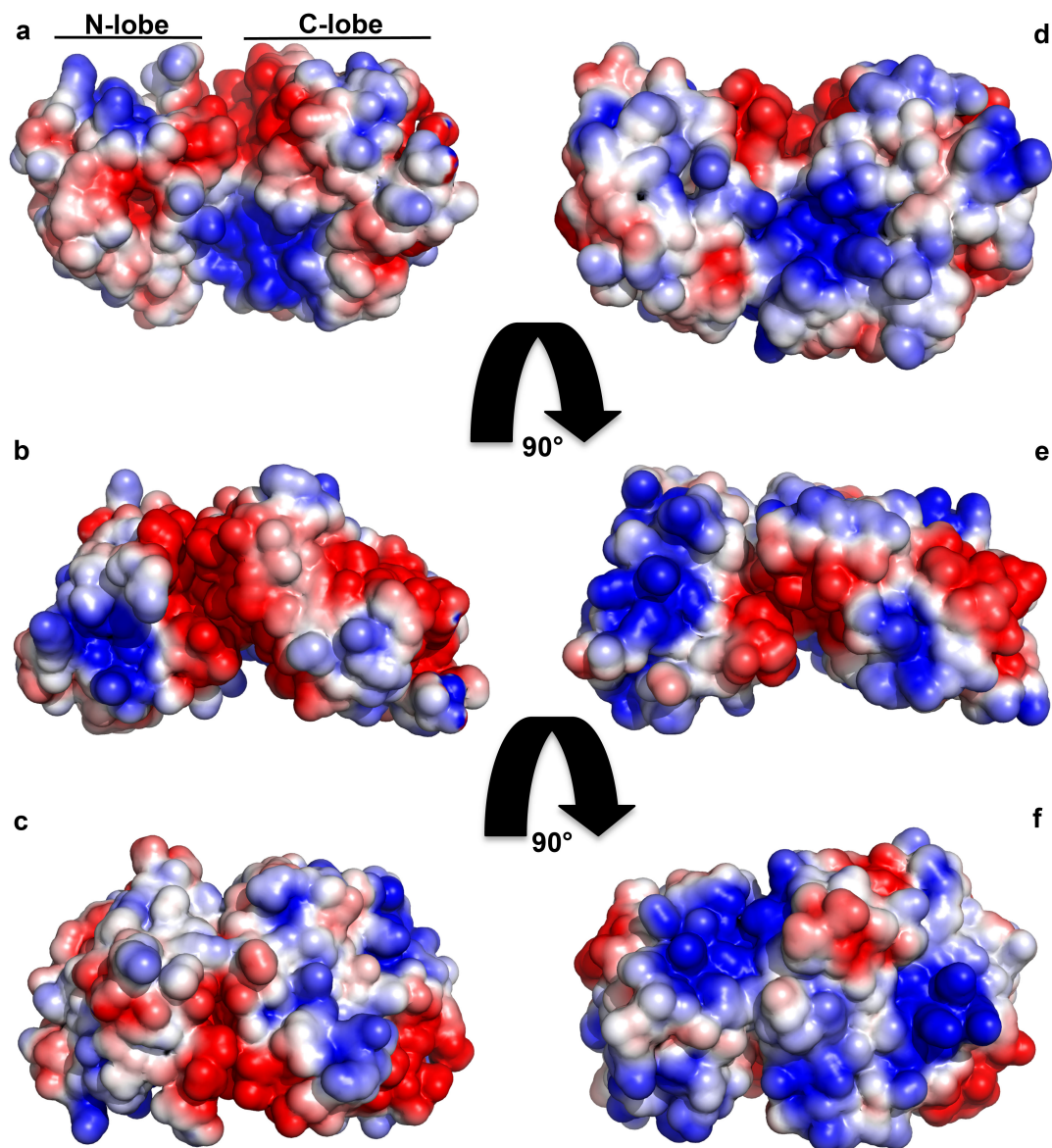


Figure 3-11 Electrostatic surface comparison of *S. pombe* and Hu Spt16 NTD.

Electrostatic surface representation of: *S. pombe* (from a to c) and Hu Spt16 NTD (from d to f) at different angles. It is possible to notice that *S. pombe* expose more acidic surface compared to human.

Chapter 4

Structural and functional analysis of Dr Spt16 middle domain

4 Structural and functional analysis of Dr Spt16 middle domain

4.1 Aims and objective

When I started my PhD the structure of Spt16 MD was not available. However, Spt16 studies had shown that most FACT-affecting mutations clustered on Spt16 MD (100,139). In addition, other studies had shown that Spt16 MD mutant effects could be suppressed by mutating the binding interface between H2A/H2B and (H3/H4)₂, and H3 mutant effects could be suppressed by Spt16 MD mutations (139-141). These results suggested a possible role for Spt16 MD in histone binding, but the absence of a structure for this domain precludes understanding its mechanism of action, including whether or not it is competent to bind (H3/H4)₂, and the impact of mutations within this domain on function.

The aims of this project are to crystallize and determine the structure of Spt16 MD and to test its binding affinity with histone H2A/H2B and (H3/H4)₂.

Here I report the structure of *Danio rerio* Spt16 MD (Dr Spt16₆₁₃₋₉₃₀) and, its binding affinity with *Xenopus laevis* histone H2A/H2B and (H3/H4)₂ as determined by ITC.

4.2 Results

4.2.1 Strategies

To optimize my chances of successfully determining the structure of Spt16, I generated several constructs of Spt16 MD for crystallization attempts. I performed a sequence alignment analysis of Spt16 from several species including human, *Danio rerio*, *S. cerevisiae*, *Drosophila melanogaster*, *Xenopus laevis* and *Dictyostelium discoideum*. Based on this analysis I cloned and purified different constructs from human, *S. cerevisiae* and *D. rerio* for crystallization (Table 4-1). Only Dr Spt16₆₁₃₋₉₃₀ yielded crystals.

Table 4-1 Spt16 MD construct list from different species

Species	Protein sequence
<i>S. cerevisiae</i>	619-833
	633-833
	633-816
	633-918
	633-955
Human	589-888
	589-927
	611-888
	611-927
<i>D. rerio</i>	590-895
	590-930
	613-895
	613-930

4.2.2 Dr Spt16 MD purification and crystallization

Protein expression and purification of native Dr Spt16 MD (Dr Spt16₆₁₃₋₉₃₀) was carried out as described in **Chapter 2**. The purified protein used for crystallization screens is shown in Fig. 4-1 a. The crystals grew as plates at 19 °C (Fig. 4-1, b), diffracted to a resolution of about 2-3 Å, and were twinned.

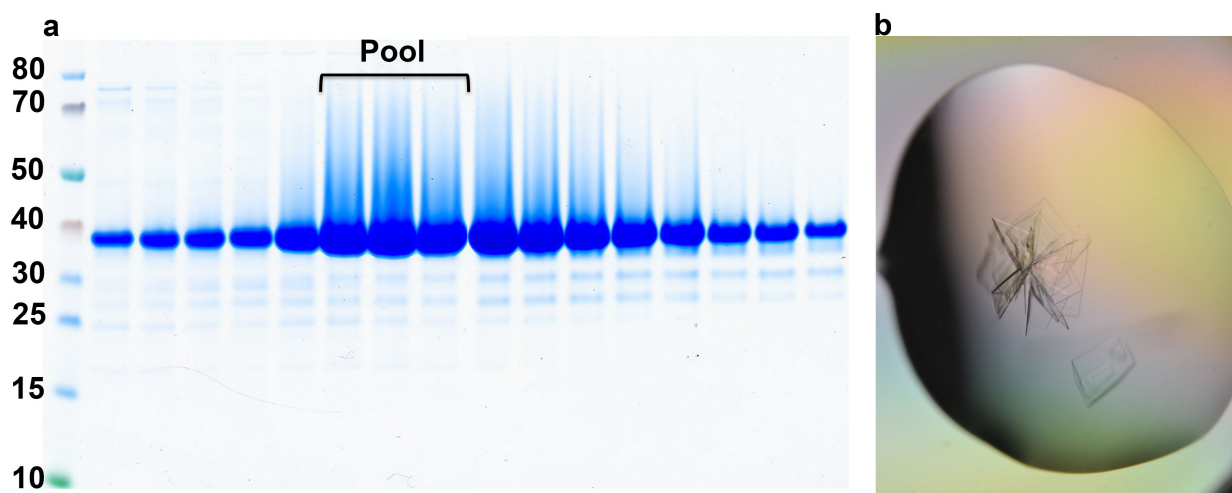


Figure 4-1 Purity and crystals of Dr Spt16₆₁₃₋₉₃₀.

(a) SDS gel showing fractions of Dr Spt16₆₁₃₋₉₃₀ after size exclusion chromatography (SD75 GE). (b) Crystals of Dr Spt16₆₁₃₋₉₃₀ before optimization.

Since there was no previously reported structure of this domain, I also expressed and purified selenomethionine labelled (SeMet) Dr Spt16₆₁₃₋₉₃₀ for multiwavelength anomalous dispersion (MAD) data collection (Fig. 4-2, a). SeMet crystals grew in conditions similar as native Dr Spt16 MD and had comparable morphology (Fig. 4-2, b). These crystals were also twinned (Fig. 4-3), making structure determination difficult. Hence, I tried to further optimize my crystals to eliminate twinning. Examination of the crystals with a microscope showed that they were made of several layers of plates (Fig. 4-2, b and c), which might account for the crystal twinning. To improve crystal diffraction and eliminate twinning, I planned to use surface entropy reduction predictions software (SERp) (189) to identify residues that potentially would enhance crystallizability if mutated. In the interim, I continued additional optimization methods as well as seeding and successfully obtained a crystal that was not twinned. Unfortunately, while I was struggling to optimize my crystals, the structures of *S. cerevisiae* Spt16 MD and *C. thermophilum* Spt16 MD in complex with histone H2A/H2B were published (135,136). These published structures of Spt16 MD together with the non-twinned crystal helped me determine the structure of Dr Spt16₆₁₃₋₉₃₀.

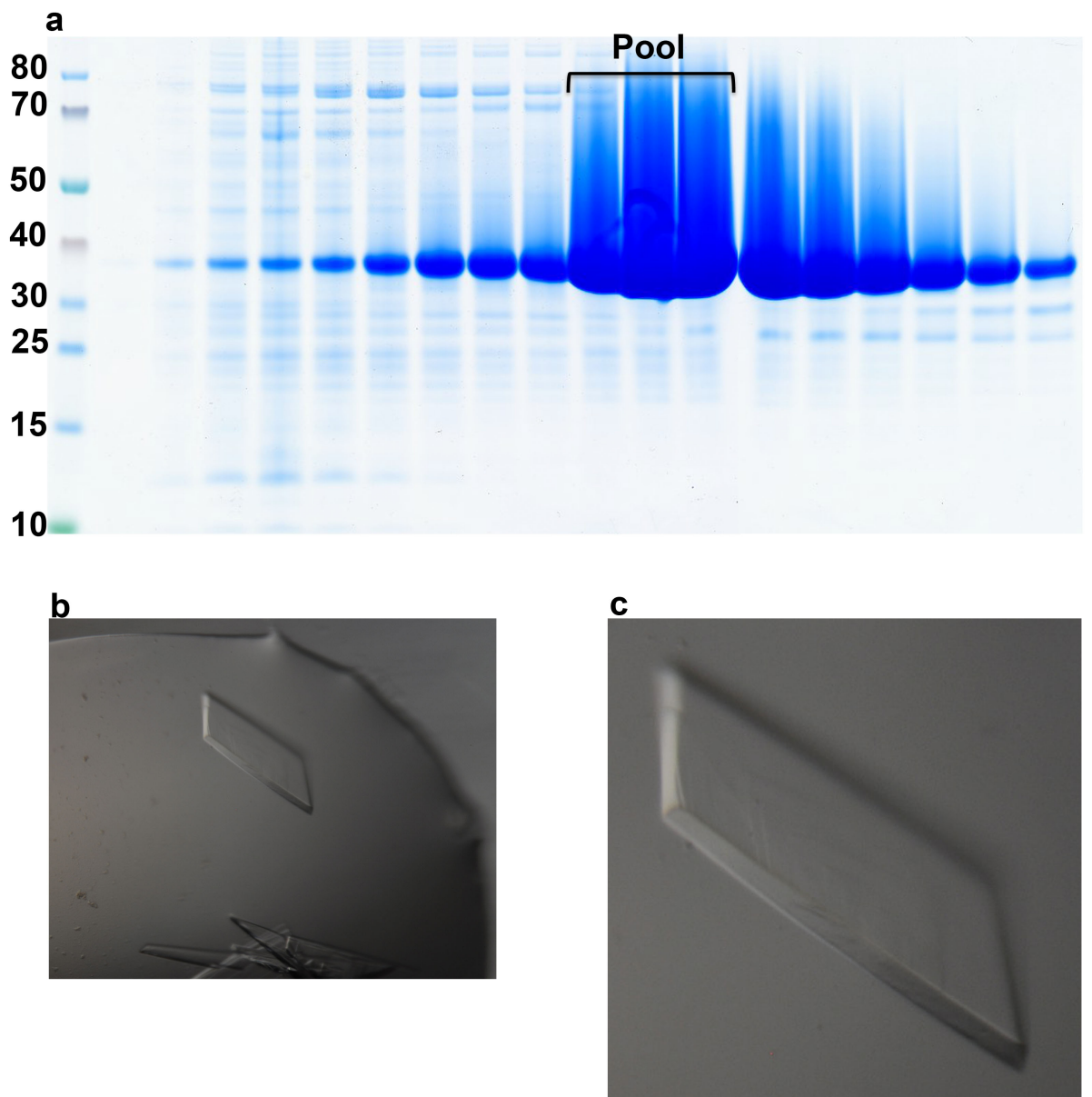


Figure 4-2 Purity and optimised crystals of SeMet Dr Spt16₆₁₃₋₉₃₀.

(a) SDS gel showing fraction of SeMet Dr Spt16₆₁₃₋₉₃₀ after size exclusion chromatography (SD75 GE). (b) Optimized crystals of SeMet Dr Spt16₆₁₃₋₉₃₀. (c) Close up of the optimized crystals where multiple layers are evident.

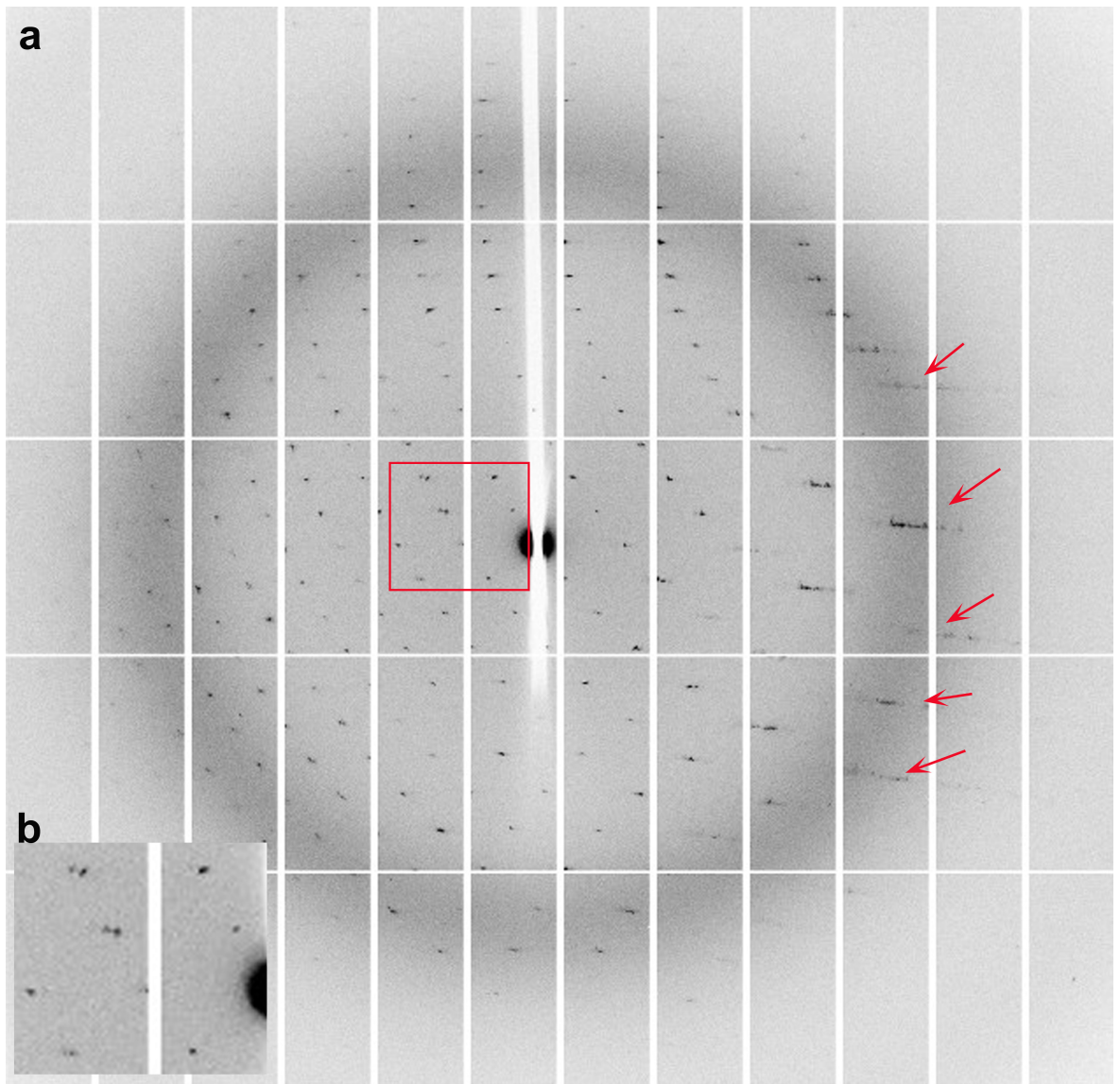


Figure 4-3 Diffraction pattern of a twinned Dr Spt16 MD crystal.

(a) Diffraction pattern showing split and smearing spots (arrow) taken with a resolution edge of 2.6 Å and omega oscillation 0.1°, suggesting the presence of twinning. (b) Close up view of the red square showing the presence of split spots.

4.2.3 Dr Spt16₆₁₃₋₉₃₀ structure determination

Crystals of Dr Spt16₆₁₃₋₉₃₀ diffracted to a resolution of 2.17 Å and belonged to space group $P2_1$. Two molecules of the monomeric domain were present per asymmetric unit. Both molecules are similar to each other (0.42 Å r.m.s.d. for $C\alpha$ atoms). My discussion focuses on one molecule in the asymmetric unit. Data collections and refinement statistics are reported in Table 4-2.

Table 4-2 Data collection and refinement statistics.

Dr Spt16 middle domain	
Data collection	
Space group	$P2_1$
Cell dimensions	
a, b, c (Å)	39.98, 49.52, 172.21
α , β , γ (°)	90, 96.16, 90
Resolution (Å)	42.87-2.17 (9.70-2.17)
R_{merge}	0.059 (0.508)
$I/\sigma(I)$	10.1 (2.1)
Completeness (%)	95.9 (76.8)
Multiplicity	2.9 (1.8)
Wilson B factor (Å ²)	33.3
Refinement	
Resolution (Å)	27.6-2.3
No. reflections	34315
$R_{\text{free}}/R_{\text{work}}$	0.25/0.20
No. atoms	
Protein	4320
Water	89
B-factors	
Protein (Å ²)	46.77
Water (Å ²)	40.97
r.m.s. deviation	
Bond length (Å)	0.008
Bond angles (°)	1.208

Note: Highest-resolution shell is shown in parenthesis. $R_{\text{work}} = \sum |F_0 - F_c| / \sum F_0$. $R_{\text{merge}} = \sum_h \sum_{i=1}^N |I_{(h)i} - \bar{I}_{(h)}| / \sum_h \sum_{i=1}^N I_{(h)i}$. R_{free} is the cross validation of R factor without 5% of the total reflections against which the model was not refined.

Dr Spt16₆₁₃₋₉₃₀ resembles *S. cerevisiae* and *C. thermophilum* Spt16 MD (r.m.s.d 0.851 and 0.867 Å across Cα respectively). It has two PH domains at the N-terminus connected by an extensive α-helix (α1) (PH1) and a U-turn at its C-terminus (Fig. 4-4). Spt16 is structurally homologous to POB3 MD and RTT106, suggesting it might bind histones using a similar mechanism (136). These homologs lack the extended α1 helix and U-turn motif (see section 1.2.1.3).

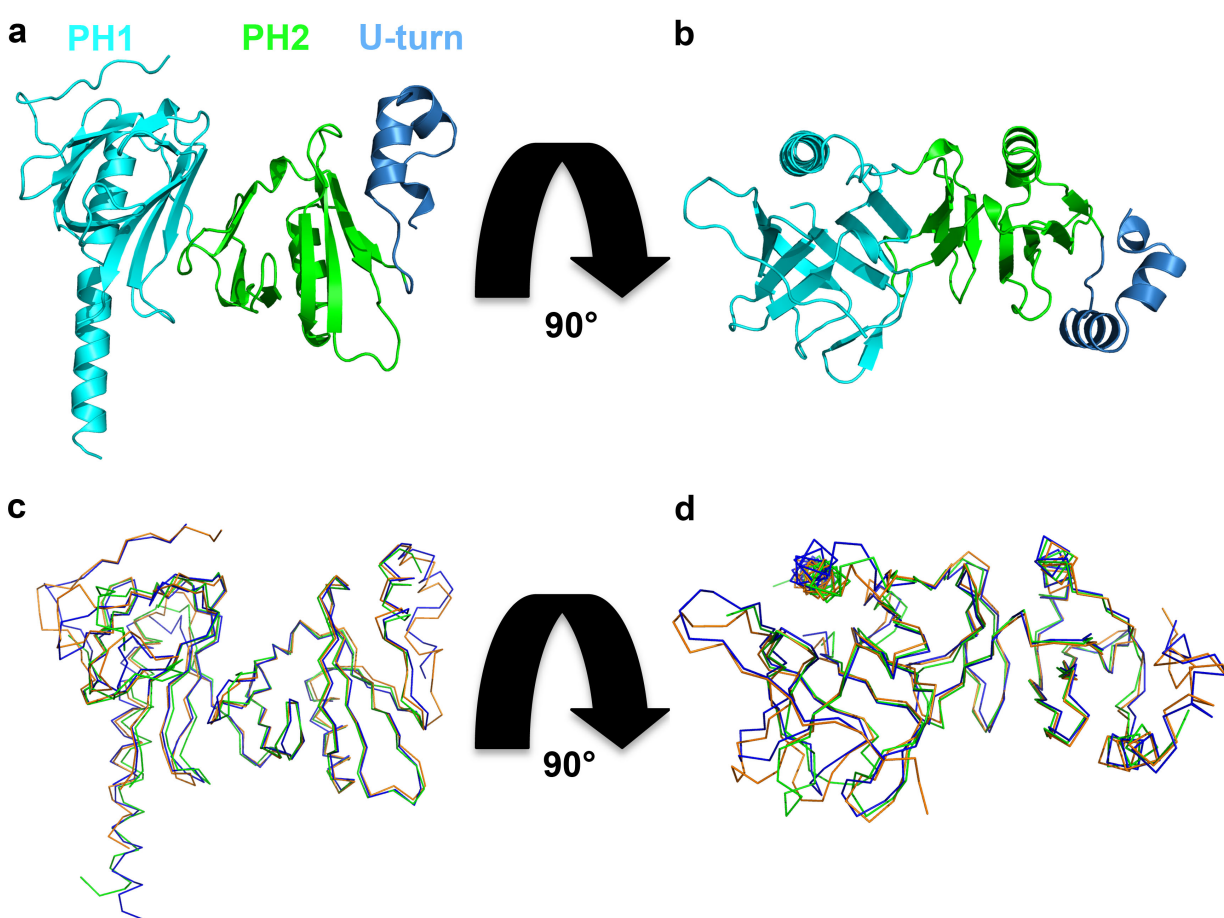


Figure 4-4 Structural representation of Spt16 MD.

(a and b) Cartoon representation of the structure of Dr Spt16₆₁₃₋₉₃₀ in two different orientations. The PH-like domains are coloured cyan and green followed by a U-turn motif in blue. (c and d) Superposition of Spt16 MD from Dr (blue); *S. cerevisiae* (green) (PDB: 4IOY) and *C. thermophilum* (orange) (PDB: 4KHA) in two orientations.

4.2.4 Functional analysis of Dr Spt16 middle domain

ySpt16 MD binds histone (H3/H4)₂ with a K_d of 2.5 μ M (136). To investigate the mechanism of action and histone binding of Spt16 MD, I generated a surface view of Dr Spt16 MD showing electrostatic potential and sequence conservation to help identify a potential histone binding site.

I analysed sequences of Spt16 MD from human, *D. rerio*, *S. cerevisiae*; *D. melanogaster*; *X. laevis*; *Dictyostelium discoideum* and *Chaetomium thermophilum* to create a surface view of conserved residues (Fig. 4-5). Most of the conserved residues are located on the PH2 domain, suggesting it might contribute to Spt16 function(s). There is also a conserved patch on the U-turn motif surface, which has been demonstrated to be involved in histone H2B binding (Fig. 4-5, e) (135). Interestingly, another conserved patch is localized at the end of the extended α 1 helix, suggesting a possible role for this surface as well.

The electrostatic surface potential map of Dr Spt16₆₁₃₋₉₃₀ shows a basic patch on one face and an acidic patch on the opposite face (Fig. 4-6). Most of the acidic surfaces are located at the end of the α 1 helix, between PH1 and PH2 domains (covering more PH2 domain) and at the U-turn motif (involved in histone H2A/H2B binding) (Fig. 4-6, b). These observations suggest that both the PH2 domain and U-turn motif might contribute to histone binding. Indeed, published data by Hondele and others show that Spt16's PH2 domain and U-turn motif are involved in histone H2A/H2B binding (135). Interestingly, on α 1 there is an acidic surface with a conserved sequence across species, suggesting another histone binding surface may be present.

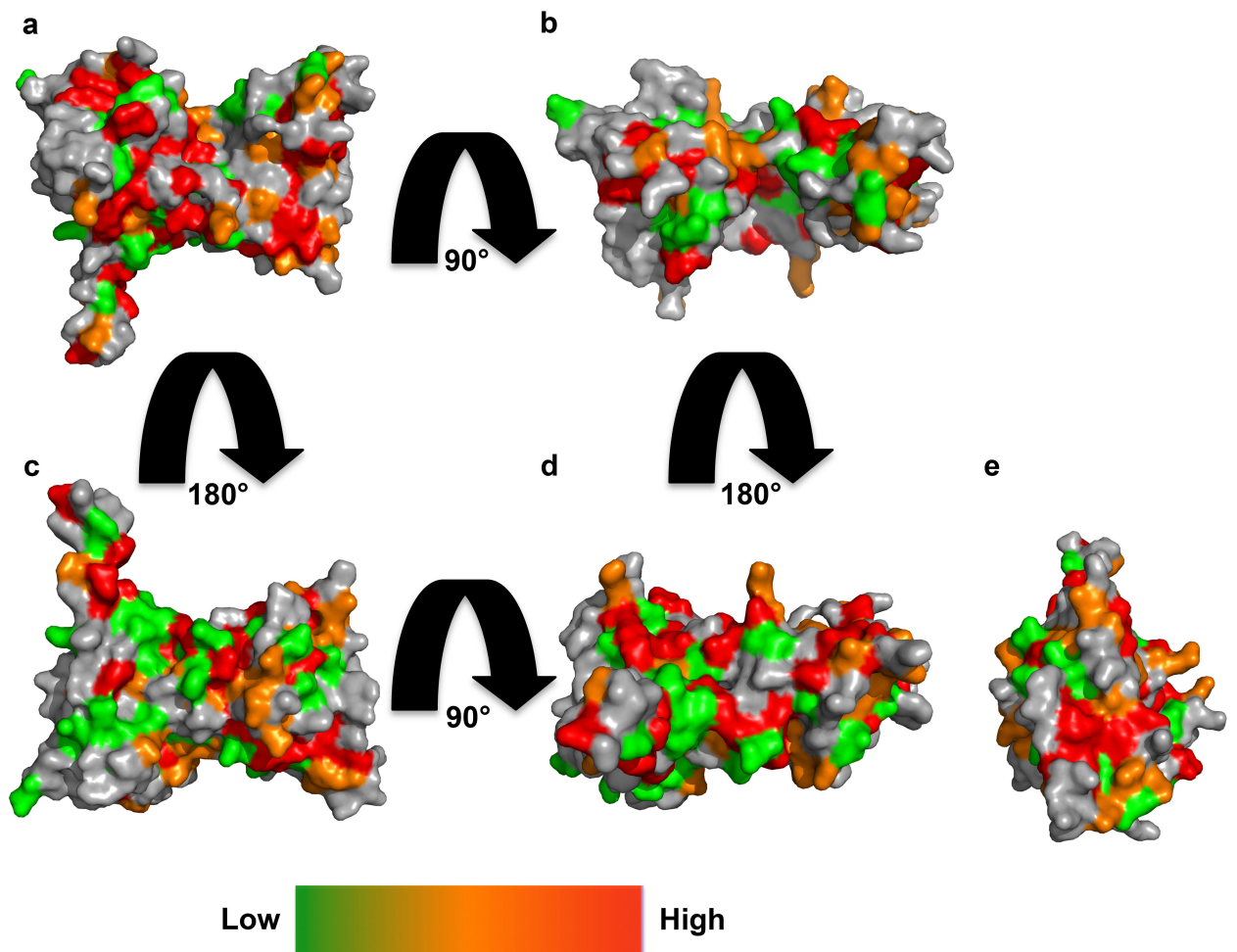


Figure 4-5 Sequence conservation of Spt16 middle domain.

Surface representation of Spt16 MD showing residues conserved amongst different species. (a) as in 4-4 (a), (b) as in 4-4 (b), (c and d) rotated 180° about the horizontal axis from a and b, respectively (e) C-terminus extremity rotated 90° about the vertical axis from c. Low conserved residues are coloured green, medium conserved residues orange, and high conserved residues red.

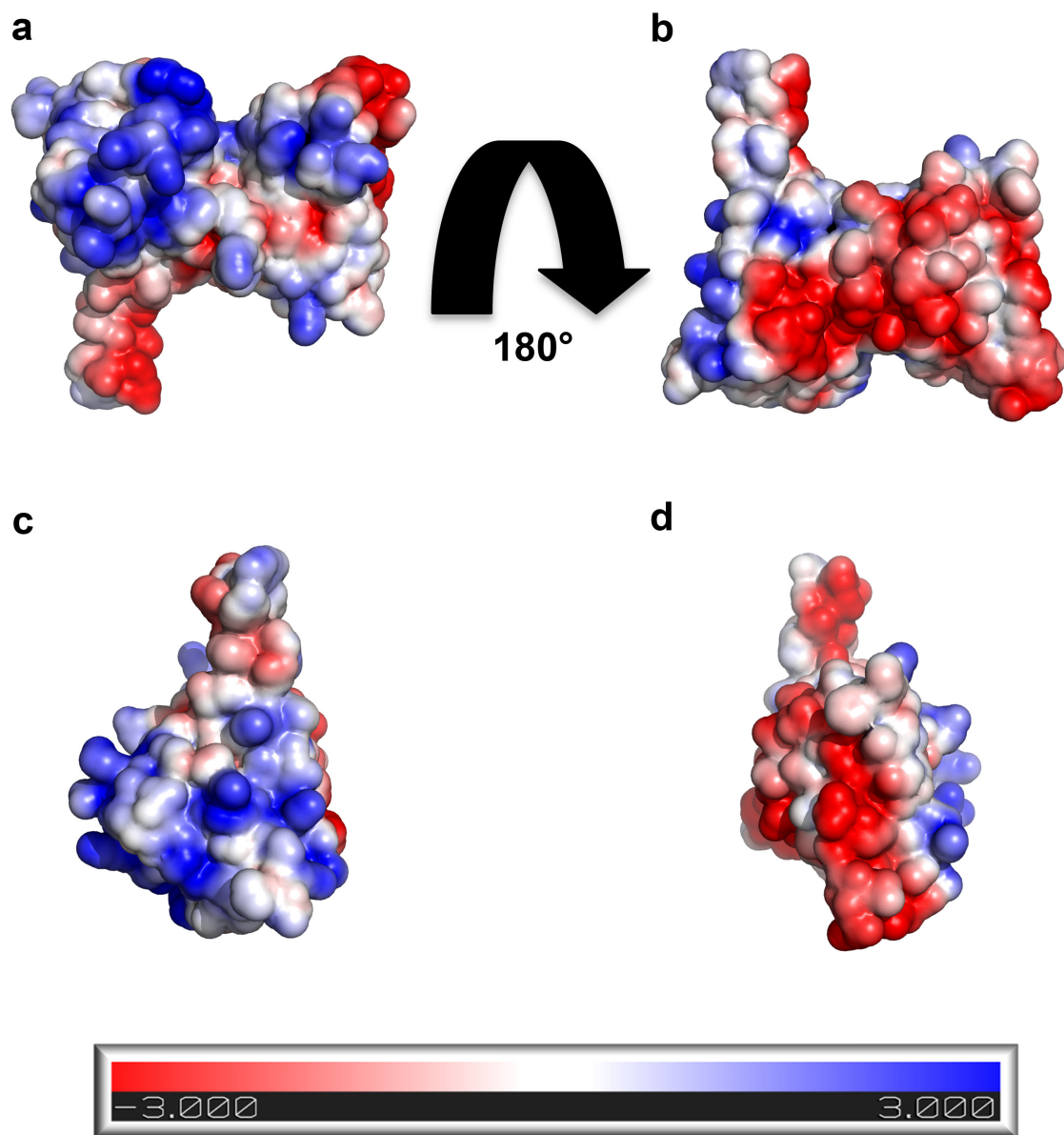


Figure 4-6 Electrostatic potential mapped onto the surface of Dr Spt16₆₁₃₋₉₃₀.

Electrostatic surface potential map of Dr Spt16₆₁₃₋₉₃₀ generated using Pymol APBS plugin (188). (a) in the same orientation as Fig. 4-4 a; (b) in the same orientation as Fig 4-5 b; (c) N-terminal view rotated 90° about the vertical axis from b; (d) in the same orientation as in Fig. 4-5 e.

4.2.5 Dr Spt16 MD binds both histone H2A/H2B and (H3/H4)₂

Although Spt16 MD is conserved, previous studies suggest there may be differences in histone binding abilities across species. One study has shown that γ Spt16 MD binds histone tetramer with a K_d of 2.5 μ M but no binding to histone dimer was observed (136). In contrast, studies on *C. thermophilum* Spt16 MD report that this domain binds histone dimer with nanomolar affinity and is able to pull down histone tetramer as well (135). Thus, my next step was to investigate whether Dr Spt16 MD was able to bind histone dimers and tetramers with ITC using *Gallus gallus* histone H2A/H2B and (H3/H4)₂.

ITC analyses showed Dr Spt16 MD binds both H2A/H2B and (H3/H4)₂, but Dr Spt16 MD binds H2A/H2B with a considerably weaker binding affinity (K_d of 22.57 μ M (Fig. 4-7, a)) than *C. thermophilum* Spt16 MD. Interestingly, for Dr Spt16 MD binding to (H3/H4)₂, the ITC profile showed the presence of two binding events that can only be fit with a “sequential binding site” model, where K_{d1} is 65 μ M and a K_{d2} is 2.3 μ M (Fig.4-7, b). Notably, K_{d2} is similar to the one reported for the *S. cerevisiae* Spt16 MD-(H3/H4)₂ interaction (136).

In *C. thermophilum*, binding between Spt16 MD and H2A/H2B occurs through the conserved residues N916, V919, I920 and T923 (Spt16 MD^{NVIT}) located at the U-turn motif (135). To investigate whether Dr Spt16 MD uses a similar mechanism of histone H2A/H2B and (H3/H4)₂ binding as *C. thermophilum*, I mutated the corresponding residues in Dr Spt16 MD and measured its binding affinity to histones dimers and tetramers using ITC.

ITC analysis of Dr Spt16 MD^{NVIT} against histone H2A/H2B yields a dissociation constant of 123 μ M (Fig. 4-8, a), confirming that Dr Spt16 MD also uses the U-turn motif to bind histone H2A/H2B. Interestingly, ITC analysis of Dr Spt16 MD^{NVIT} binding to histone (H3/H4)₂ gave a profile similar to wild type Dr Spt16 MD. This time, ITC raw data have been fitted with a “two binding site” model where the first binding site gave N_1 of 1.72 and K_{d1} of 0.32 μ M whereas the second binding site gave N_2 of 0.678 and K_{d2} of 0.21 μ M (Fig. 4-8, b). Both wild type and mutant Dr Spt16 MD gave a profile of a double binding events with different fitting, suggesting that even though the calculated K_d 's are different (probably because Dr Spt16 MD wild type was less stable at high concentration compared to the mutant), the mechanism of binding may be similar.

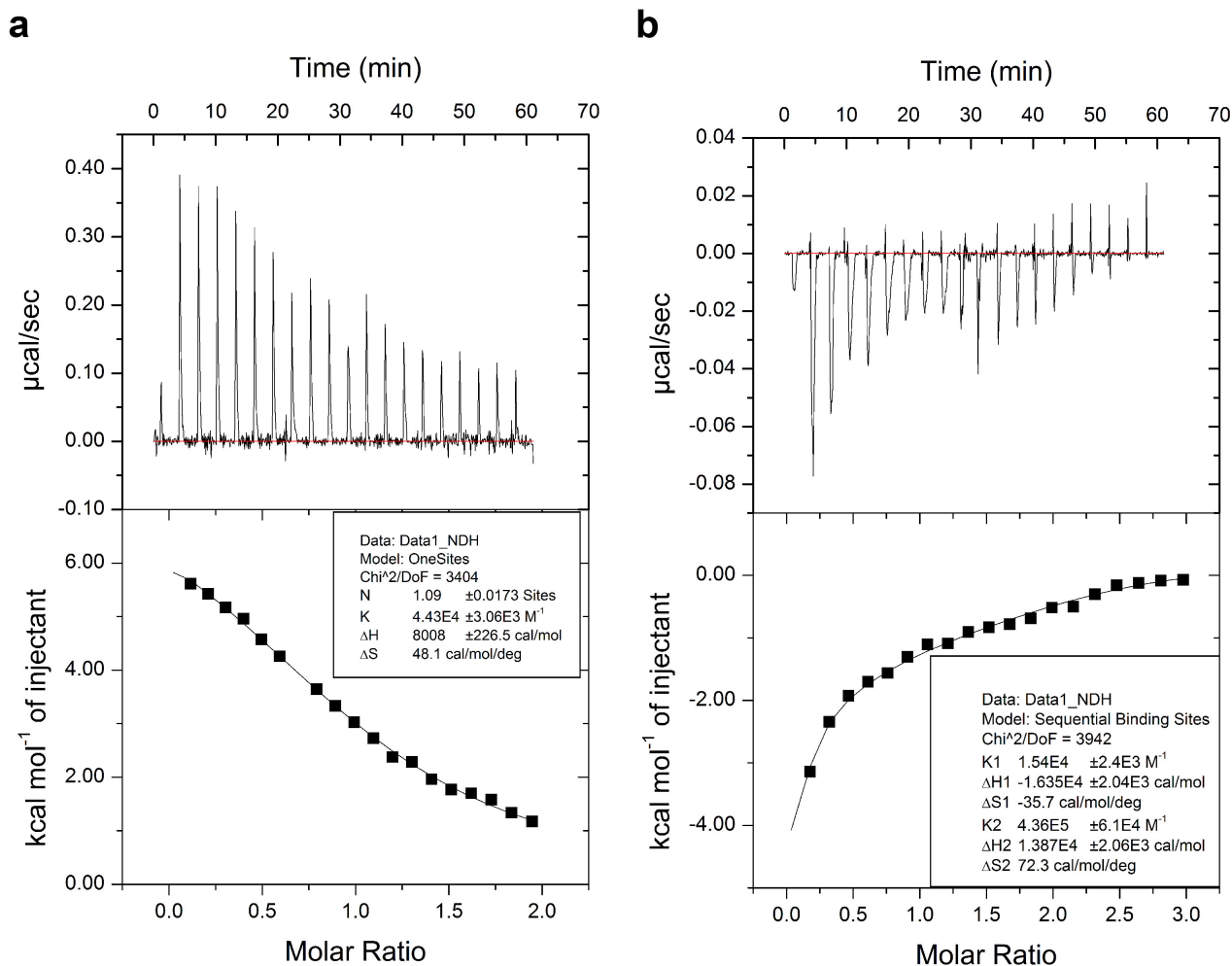


Figure 4-7 ITC profiles and fitting of Dr Spt16₆₁₃₋₉₃₀ against *G. gallus* histone H2A/H2B and (H3/H4)₂.

(a) ITC profile showing raw data (upper panel) and normalised data (lower panel) plotted against the molar ratio between the ligand *G. gallus* H2A/H2B and Dr Spt16613-930.

(b) ITC profile showing raw data (upper panel) and normalised data (lower panel) plotted against the molar ratio between the ligand *G. gallus* (H3/H4)₂ and Dr Spt16₆₁₃₋₉₃₀. Inset box shows stoichiometry (n), association constant (K_a), enthalpy (ΔH) and entropy (ΔS).

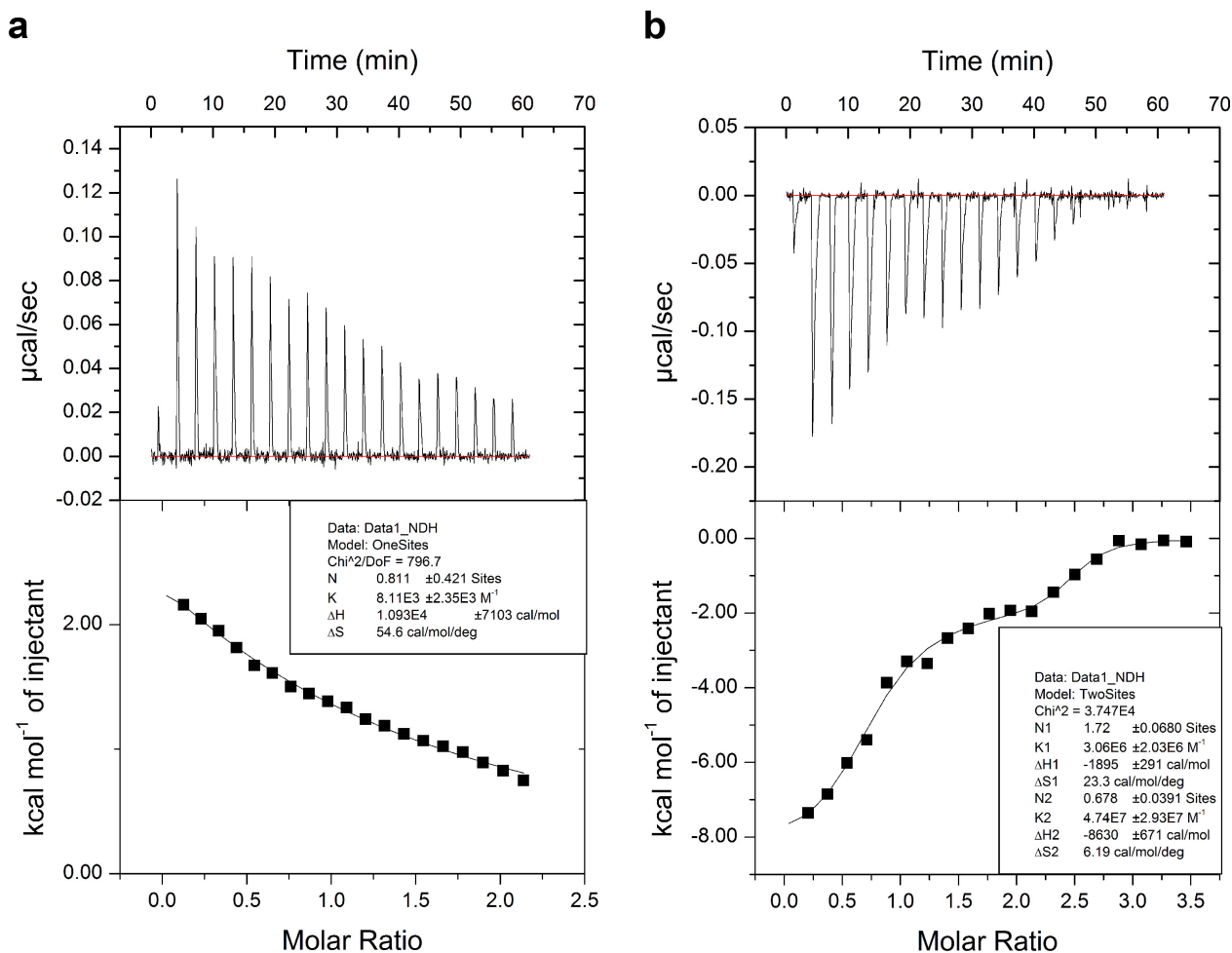


Figure 4-8 ITC profiles and fitting of Dr Spt16 MD^{NVIT} against *G. gallus* histone H2A/H2B and (H3/H4)₂.

(a) ITC profile showing raw data (upper panel) and normalised data (lower panel) plotted against the molar ratio between the ligand *G. gallus* H2A/H2B and Dr Spt16 MD^{NVIT}.

(b) ITC profile showing raw data (upper panel) and normalised data (lower panel) plotted against the molar ratio between the ligand *G. gallus* (H3/H4)₂ and Dr Spt16 MD^{NVIT}. Inset box shows stoichiometry (n), association constant (Ka), enthalpy (ΔH) and entropy (ΔS).

4.3 Discussions

Here I show that Dr Spt16 MD adopts a similar fold to yeast and *C. thermophilum* Spt16 MD. POB3 and RTT106 (136) resemble Spt16 MD except for the presence of the U-turn motif in Spt16 MD. This structural similarity suggests that, this structure conformation might be required for the interaction with the four histones in a nucleosome context. Moreover, Spt16 MD shows wide sequence conservation across different species and presence of localized acidic patches on the PH2 domain, U-turn motif and α 1 helix. These results, together with the Spt16 mutational effects on yFACT activity highlighted in section 4.1 (Fig. 4-9), suggest that an important function of Spt16 MD is to bind histones.

ITC analysis of H2A/H2B binding to Dr Spt16 MD gave a binding affinity of 123 μ M for the U-turn mutant and 22 μ M for the wild type. Strikingly, Dr Spt16 MD wild type binds histone H2A/H2B 55-fold more weakly than *C. thermophilum* Spt16 MD (135) despite having similar folds and 46.4% sequence conservation. A possible explanation for this binding difference may arise from the fact that these are two evolutionarily distant species. This result confirms that the Spt16 MD-H2A/H2B interaction is mediated by the U-turn motif, the weak binding in Dr Spt16 MD suggests additional FACT domains are required to perform its functions.

Finally, ITC analysis of wild type Dr Spt16 MD and a mutant that disrupts histone (H3/H4)₂ binding showed the presence of two binding events. Although ITC titrations of (H3/H4)₂ with Dr Spt16 MD were conducted under equivalent conditions, Spt16 MD mutant exchanged more heat compared to the wild type (Fig. 4-7 and 4-8, b). This may be due to stabilization of the Spt16 mutant in solution. Interestingly, the stabilizing effects of H3 L61W on the histone H3-H4 interaction is suppressed by Spt16 MD mutations localized in the PH1, α 1 helix and PH2 domains (136,139). These data together with the electrostatic surface potential analysis and ITC experiments, suggest that the interaction between Spt16 MD and histone (H3/H4)₂ is not only mediated by the PH2 domain and U-turn motif but also by the PH1 domain and α 1 helix.

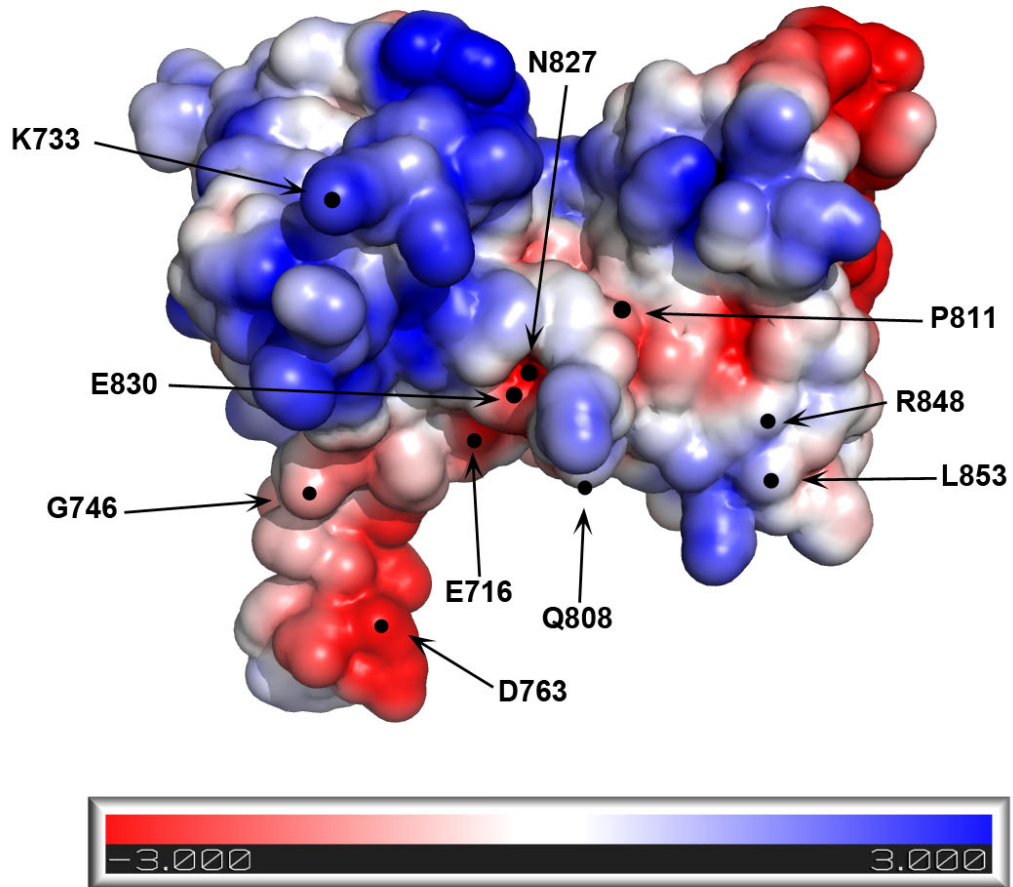


Figure 4-9 Electrostatic surface representation of Dr Spt16 MD showing the location of *S. cerevisiae* corresponding mutated residues that affect FACT activity.

Electrostatic surface representation of Dr Spt16 MD as showed in figure 4-6 a. Arrow indicate localization of *S. cerevisiae* Spt16 MD corresponding mutated residue that affect FACT activity (139,141).

Chapter 5

Biochemical and biophysical characterization of SSRP1

5 Biochemical and biophysical characterization of SSRP1

5.1 Aims and objective

As described in section 1.2, FACT is a hetero complex of Spt16 and SSRP1(96). SSRP1 consists of three ordered domains: the N-terminal/DD, the MD and the HMG-1 domain, which is flanked by two intrinsically disordered regions (ID) (125,128,135). When I started my PhD only the structures of SSRP1 N-terminal domain/DD (PH1) and MD (PH3/4) were available (PDB: 3F5R and 3GCL respectively) (Fig. 1-9). Moreover, limited proteolysis revealed that Spt16 DD heterodimerize with SSRP1 N-terminal/DD domain (125), but little was known about their interaction.

In vivo studies showed that the HMG-1 domain (residues Ser510, ser657 and Ser688) of SSRP1 is phosphorylated by CK2; notably, phosphorylation of Ser510 inhibits SSRP1's ability to bind DNA (155). During apoptosis SSRP1 is degraded both by ubiquitin-mediated proteolysis and caspase cleavage (154). It also associates with p63 as a co-transcriptional activator (158). Recent studies suggest that SSRP1 may have FACT-independent functions in transcription and microtubule growth (159). However, distinguishing between SSRP1-independent and FACT-dependent functions *in vivo* is complicated by a number of factors. First, deletion of SSRP1 causes cell mortality (99). Moreover, SSRP1 and Spt16 co-localize in the nucleus (121). Hence, little is known about SSRP1-independent functions *in vivo* and SSRP1 alone remains poorly characterized *in vitro*. Therefore, the aims of this project were to understand how SSRP1 and Spt16 interact with each other and to characterize SSRP1-independent functions by using biochemical and biophysical analysis.

In this chapter, I report the identification of the minimum sequence required for SSRP1 and Spt16 heterodimerization and, by using AUC and SAXS analysis, I have determined the oligomeric state of SSRP1 in solution. Furthermore, using mutagenesis, I show SSRP1's PH1 and PH3 domains contribute to homodimerization. Lastly, with ITC, I show for the first time that SSRP1 binds histone H2A/H2B in addition to (H3/H4)₂ and that homodimerization plays a role in histone binding.

5.2 Results

5.2.1 SSRP1 heterodimerize with Spt16 through conserved sequences

When I started my PhD the structure of the first 111 residues from POB3 (yeast SSRP1) was published (PDB: 3F5R). In addition, biochemical analysis revealed that Spt16 DD domain interacted with SSRP1 N-terminal/DD domain (see section 5.1), but the absence of an Spt16/SSRP1 complex structure made understanding the mechanism of their interaction difficult. To gain insight into the SSRP1/Spt16 complex, I purified and crystallized Hu SSRP1 N-terminal/DD domain. During size exclusion chromatography I noticed that SSRP1 N-terminal/DD domain (1-197, ~22 kDa) eluted much earlier than the N-terminal fragment of c-Cbl, an ~45 kDa monomer (Fig. 5-1). This suggested that SSRP1's DD might oligomerize or be in an elongated state.

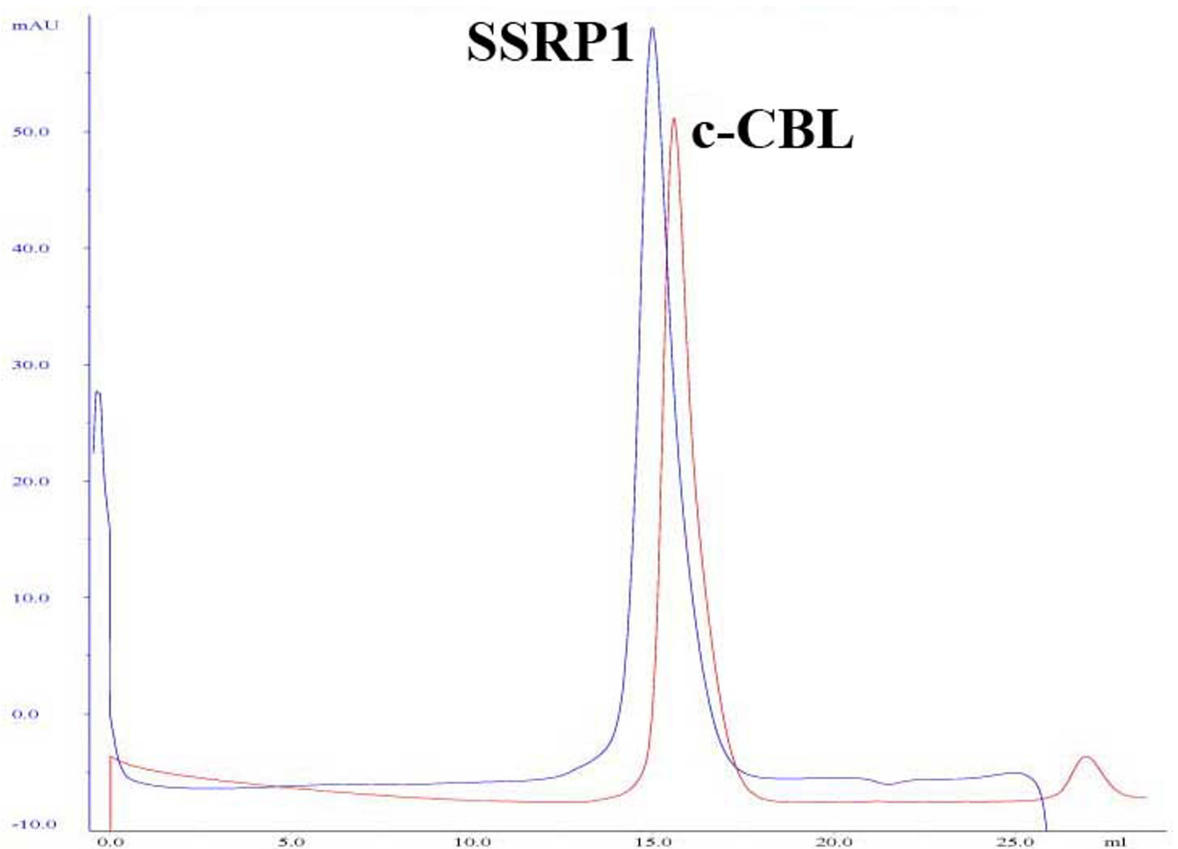


Figure 5-1 Size exclusion chromatography overlay of SSRP1 N-terminal/DD domain and c-CBL

Overlaid size exclusion elution profiles of SSRP1 N-terminal/DD domain (blue) and a control protein, c-CBL (red). SSRP1 1-197 and the N-terminal fragment of c-CBL have theoretical molecular weights of 22 and 45 kDa, respectively.

In the aforementioned structure of POB3, this domain appears as a monomer, although crystal packing suggests this domain might dimerize via a symmetry-related molecule. To test this hypothesis, I generated two SSRP1 N-terminal/DD mutants along this putative dimer interface (Fig. 5-2 and Table 5-1) and used size exclusion chromatography to assess the oligomeric state. Unfortunately, none of these mutants affected SSRP1's elution profile (Fig. 5-3), suggesting there was no effect on the shape or oligomeric state.

Table 5-1 Hu SSRP1 N-terminal domain mutants.

Mutations of SSRP1 N-terminal domain ¹
Hu SSRP1 1-199 Q52A, K63A, V71A
Hu SSRP1 1-199 Q52A, K63A, V71E

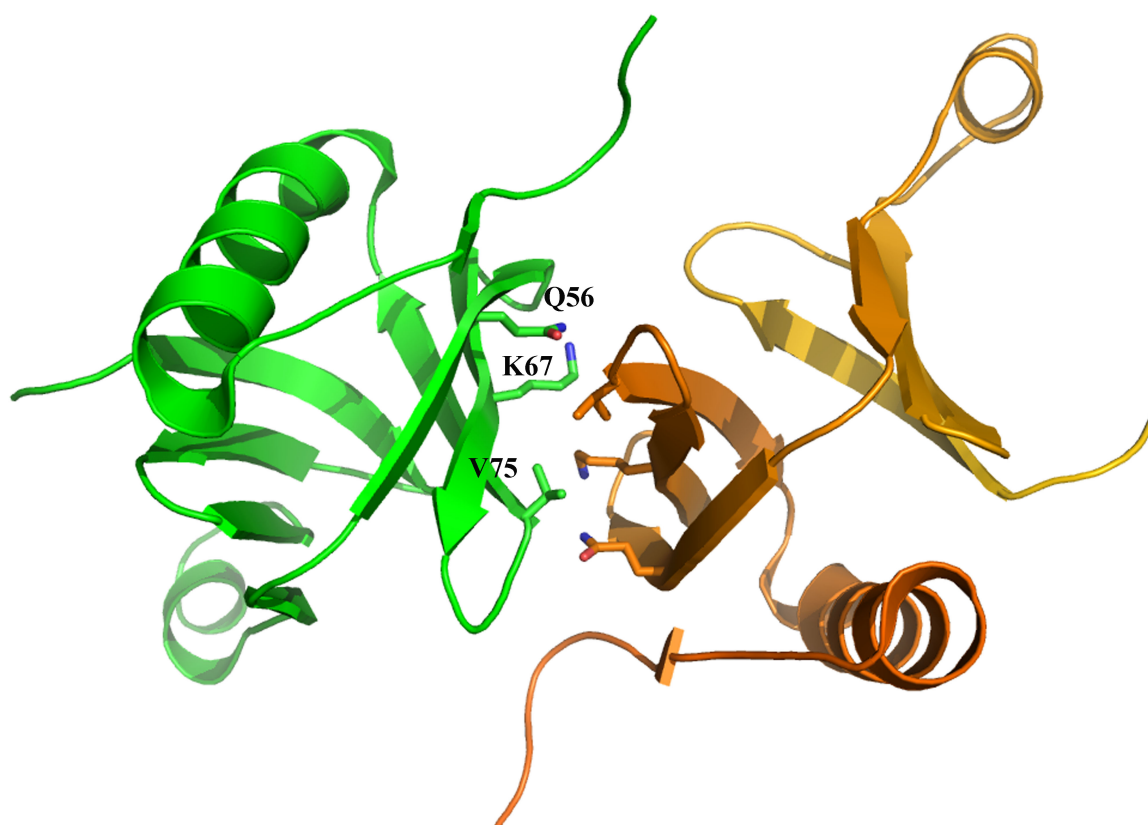


Figure 5-2 Structural representation of the symmetry related molecule of the PH1 domain from POB3.

Structure of the N-terminal domain of POB3 (green) and a symmetry related molecule in the crystal packing (orange). Glu56, Lys67 and Val75 are located at the interface of the two molecules.

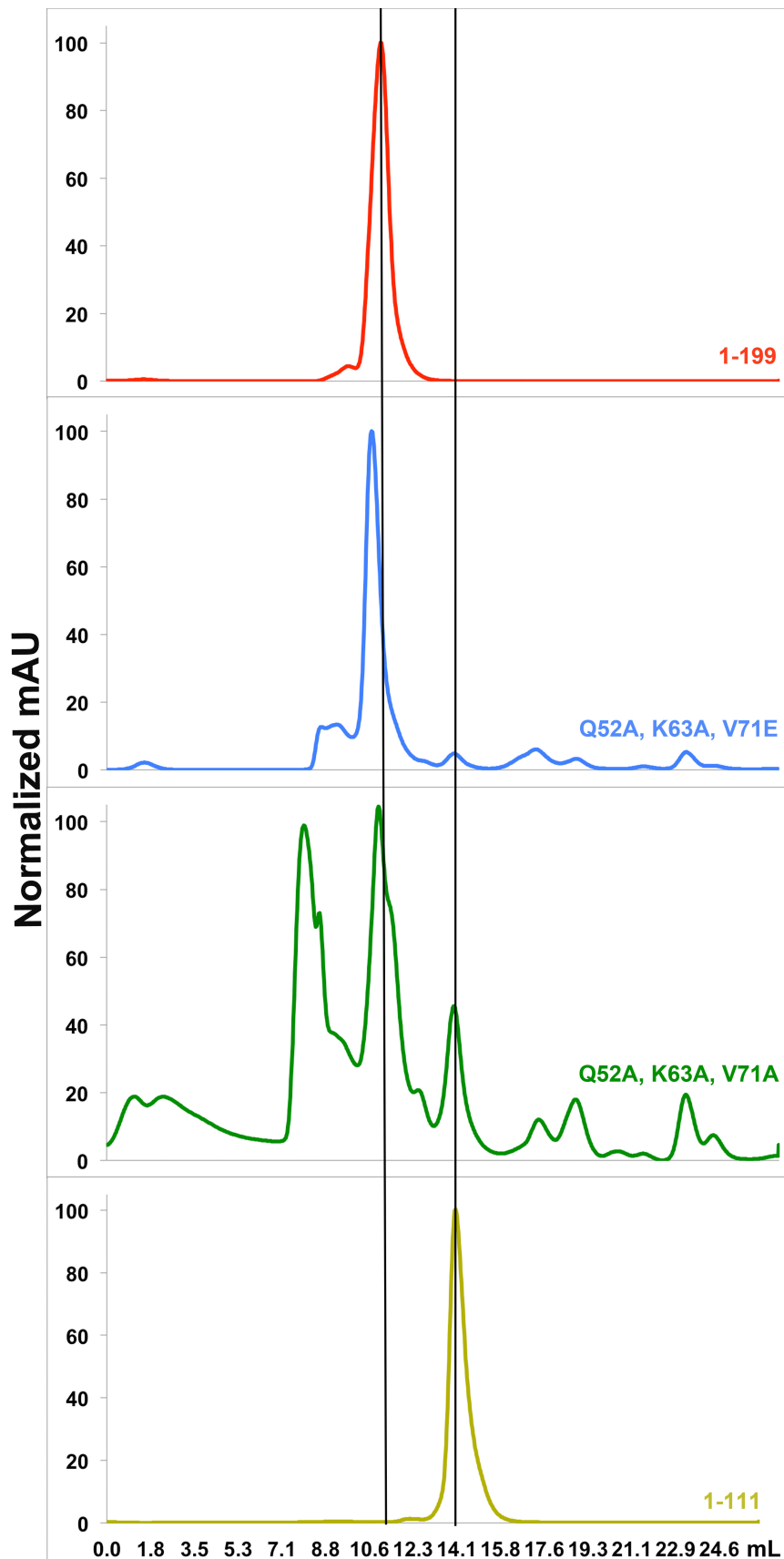


Figure 5-3 Size exclusion chromatography of Hu SSRP1 N-terminal/DD wild type and hypothetical homodimerization interface mutants.

Size exclusion profiles of: purified Hu SSRP1 1-199 (red, 22 KDa) as control, Hu SSRP1 1-111 (yellow, 13 KDa) as standard, Ni-NTA pull down of Hu SSRP1 1-199 Q52A, K63A, V71A (green) and Hu SSRP1 1-199 Q52A, K63A, V71E (blue).

Before my arrival, my supervisor Danny Huang and our scientific officer Gary Sibbet mapped a small peptide sequence in the Spt16 DD domain (509-581), important for interaction with SSRP1. To further characterize SSRP1/Spt16 heterodimerization, I used GST-Spt16 and His-SSRP1 pull down assays to map the minimum region involved in this interaction. Hence, I did a Ni-NTA pull down of His-SSRP1 104-199 alone (Fig. 5-4 lane 1) and co-expressed with GST-Spt16 509-581 (Fig. 5-4 lane 2). Lane 2 shows an extra band between 28 and 38 KDa that match GST-Spt16 509-581 MW, suggesting that SSRP1 104-199 is able to pull down Spt16 509-581. To further characterize this interaction I performed another Ni-NTA pull down of His-SSRP1 1-199 co-expressed with GST-Spt16 509-581 (lane 3) GST-Spt16 519-581 (lane 4) GST-Spt16 557-581 (lane 5). In this case as control I did use His-SSRP1 1-199 (lane 6). As shown in Fig. 5-4, SSRP1 1-199 was able to pull down both GST-Spt16 509-581 and 519-581 (see extra band between 28 and 38 KDa in Fig. 5-4 lane 3, 4 compared to lane 6). Unfortunately, both His-SSRP1 1-199 and GST-Spt16 557-581 (lane 5) have similar molecular weight, which makes it difficult to distinguish between SSRP1 and Spt16 bands. To this end I cleaved the tag, using TEV, which helped me to separate the two bands (Fig. 5-4 c), which confirmed the presence of Spt16 557-581. I also performed a GSH-sepharose pull down assay of His-SSRP1 1-199 co-expressed with GST-Spt16 564-799 (Fig. 5-4 b, lane 7) and His-SSRP1 1-160 co-expressed with GST-Spt16 509-581 (Fig. 5-4 b, lane 9). As we can see from Fig 5-4 b GST-Spt16 564-799 was able to pull down SSRP1 1-199 (see lane 6 and 7), whereas GST-Spt16 509-581 was not able to pull down SSRP1 1-160 (see lane 8 and 9).

All together my pull downs shows that SSRP1's residues 160-199 and Spt16's residues 557-580 are the minimal sequences required for SSRP1/Spt16 heterodimerization (Table 5-2). Surprisingly, alignment of these sequence from SSRP1 and Spt16 showed sequence conservation (Table 5-3 and 5-4).

Based on these mapped interactions, I designed different constructs of SSRP1 and Spt16 (Table 5-5) to determine the structure of SSRP1 dimerizing domain and Spt16 DD. After generating and purifying these constructs, I screened thousands of different conditions at 4 and 19°C. Unfortunately I only got quasi-crystals or needle clusters that did not diffract (Fig. 5-5).

Table 5-2 His-tag SSRP1 and GST-tag Spt16's co-expression constructs used in pull-down assays (Fig. 5-4) to map SSRP1-Spt16 interactions.

Lane	His-SSRP1	GST-Spt16	Pull-down
2	104-199	509-581	Yes
3	1-199	509-581	Yes
4	1-199	519-581	Yes
5	1-199	557-581	Yes
7	1-199	564-799	Yes
9	1-160	509-581	No

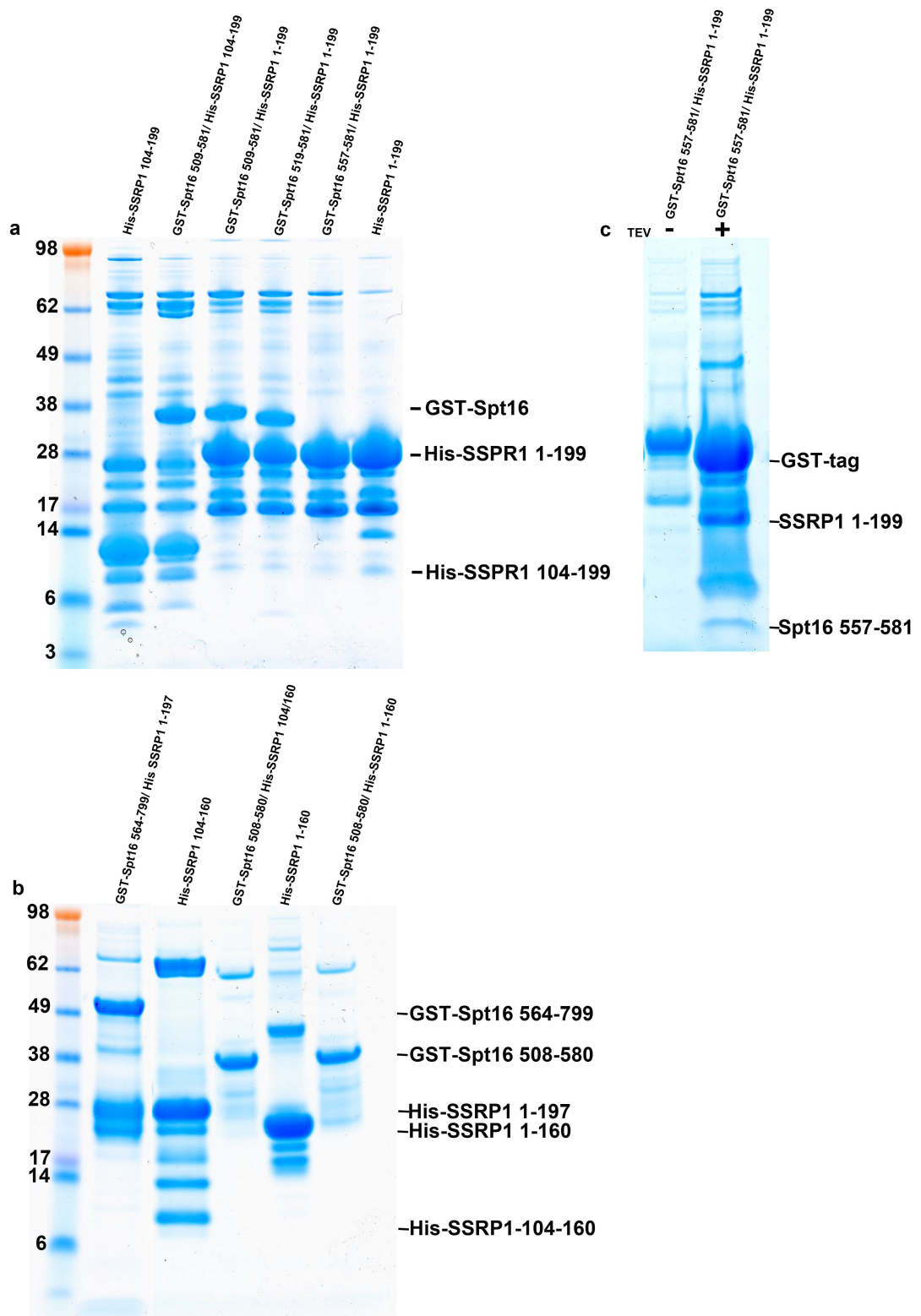


Figure 5-4 GSH-sepharose pull-downs of SSRP1- Spt16 complex.

(a) Ni-NTA pull down of His-SSRP1 104-199 (lane 1), co-expression of His-SSRP1 104-199 and Spt16 509-581 (lane 2), co-expression of His-SSRP1 1-199 and Spt16 509-581 (lane 3), co-expression of His-SSRP1 1-199 and Spt16 519-581 (lane 4), co-expression of His-SSRP1 1-199 and Spt16 557-581 (lane 5) and His-SSRP1 1-199 (lane 6). (b) GSH-sepharose gel pull down of co-expressed His-SSRP1 1-199 and GST-Spt16 564-799 (lane 7), control for His-SSRP1 1-160 (lane 8) and co-expressed His-SSRP1 1-160 and GST-Spt16 508-580 (lane 9). (c) TEV cleavage of GST-Spt16 557-581/His-SSRP1 1-199 from gel (a) lane 5. Protein standard markers are indicated.

Table 5-3 Sequence alignment of SSRP1 and Spt16 interacting sequences.

Human (Hu), *Saccaromyces cerevisiae* (Sc) and *Danio Rerio* (Dr) SSRP1 and Spt16 sequences are indicated. Polar uncharged residues (**red**), hydrophobic residues (**green**) and basic residues (**orange**) are highlighted.

Species and protein	Sequence	Conservation
Hu SSRP1	158-166	V S L M E V R F Y
Sc POB3	167-175	DEL V E M R F Y
Dr SSRP1	158-166	V S L M E V R F Y
Hu Spt16	565-573	Y T Y L R I N F Y

Table 5-4 Sequence alignment of Spt16 interacting sequences.

Human (Hu), *Saccaromyces cerevisiae* (Sc) and *Danio rerio* (Dr) Spt16 sequences are indicated. Polar uncharged residues (**red**), hydrophobic residues (**green**) and basic residues (**orange**) are highlighted.

Species and proteins names	Sequences	Conservation
Hu Spt16	565-573	Y T Y L R I N F Y
Sc Spt16	589-597	Y T Y L R L N F N
Dr Spt16	566-574	Y T Y L R I N F F

Table 5-5 SSRP1 and FACT constructs used for crystallization attempts (Appendix 4).

SSRP1 constructs	
Dr 1-173	Dd SSRP1 ΔCTD
Dr 1-199	Dd SSRP1 FL
Hu 1-160	Dd SSRP1 6-187
Hu 1-174	Dd SSRP1 6-187-T4
Hu 1-197	Dd SSRP1 T4-6-187
Hu 1-433	Dd SSRP1 ΔCTD in situ proteolysis
Hu 1-111	Dd SSRP1 ΔCTD + histones
Sc 1-241	Dd SSRP1 FL + histones
Dr FL	Dr FL disulfide bonded
Dr FL + histone octamer	
FACT constructs	
Dr SSRP1 1-424/Spt16 FL	Dd SSRP1 FL/Spt16FL
Dr 1-199/Spt16 519-930	Dd FACT ΔCTD
Hu SSRP1 1-197/Spt16 456-919	Hu SSRP1 1-197/Spt16 408-1005*
Hu SSRP1 1-197/Spt16 518-919	Hu SSRP1 1-433/Spt16 456-799*
Hu SSRP1 1-197/Spt16 518-952	Hu SSRP1 1-197/Spt16 456-799*
Hu SSRP1 1-433/Spt16 522-799*	Hu SSRP1 1-433/Spt16 498-799*

* Proteins purified by Danny and Gary

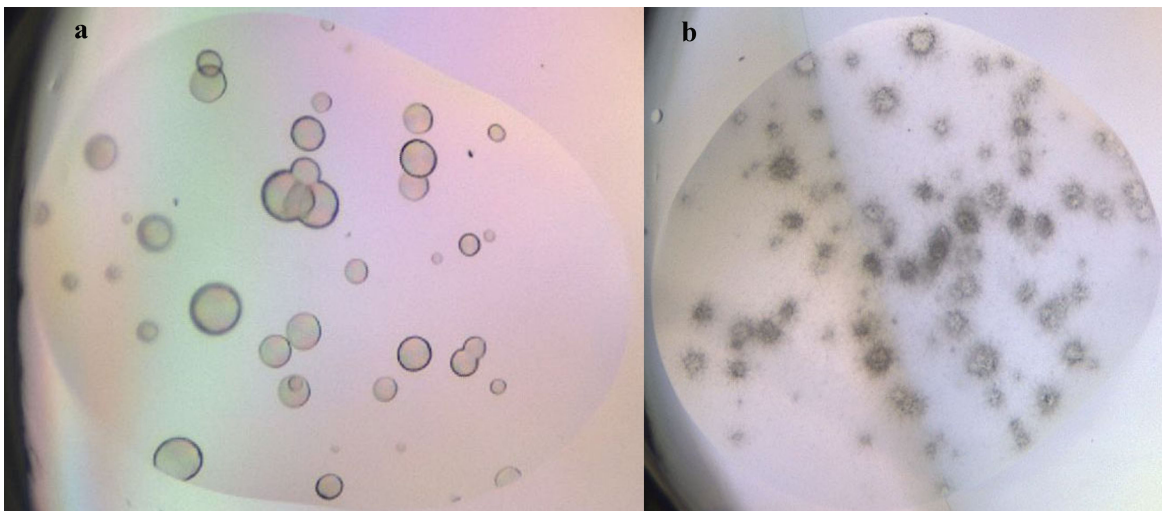


Figure 5-5 Examples of quasi-crystals and needle clusters obtained from crystallization trials outlined in table 5-5

(a) Quasi-crystals and (b) needle cluster.

Unfortunately, while I was working on this project the structure of *C. thermophilum* SSRP1 N-terminal/DD domain in complex with Spt16 DD domain was determined (see section 1.2.1). This structure clearly shows the two proteins interact using the conserved sequence that I identified. These sequences are part of β -strands from SSRP1 and Spt16 that form a continuous β -sheet in the heterodimer (Table 5-3 and 5-4 and Fig. 5-6 red rectangle). The complex structure also shows that the N-terminal/DD domain from SSRP1 and DD domain from Spt16 both adopt PH-like folds (Fig.5-5) (135).

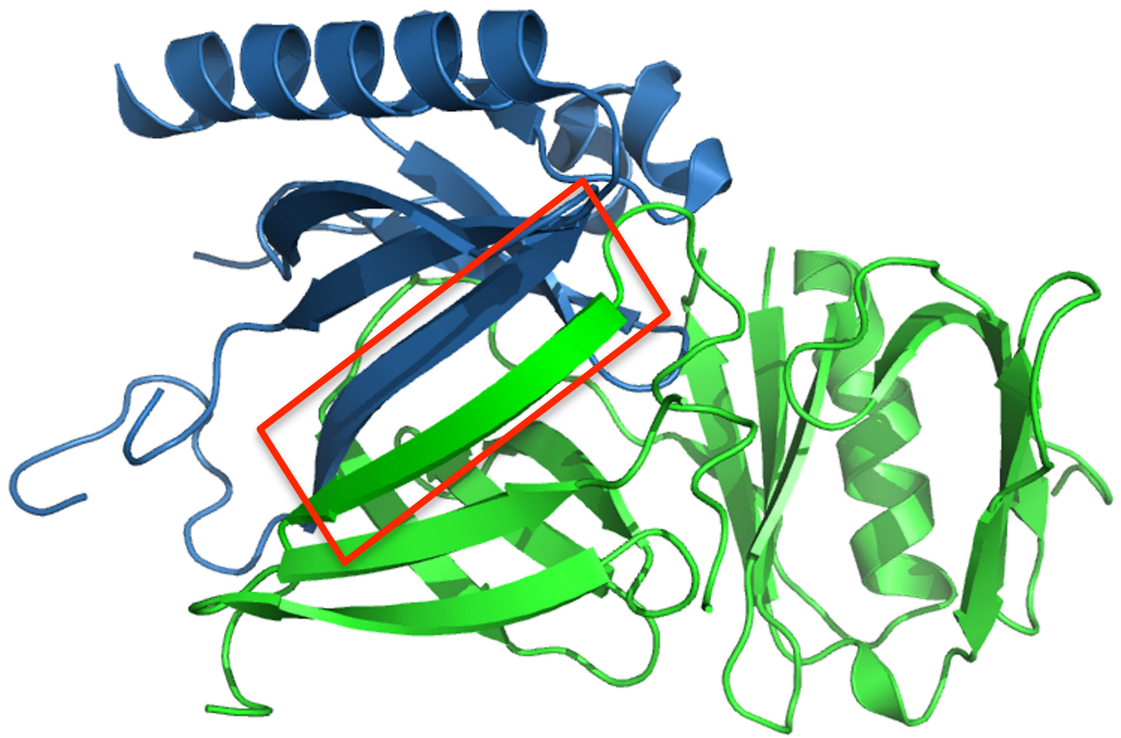


Figure 5-6 Structural representation of the heterodimer comprising SSRP1 N-terminal/DD domain and Spt16's DD domain.

Structure of *C. thermophilum* SSRP1 N-terminal/DD domain (in green) in complex with Spt16 DD domain (in blue) (PDB: 4KHB). Red rectangle highlights SSRP1 and Spt16 β -sheet involved into the heterodimerization comprising the sequences showed in table 5-2.

5.2.2 SSRP1 is a conserved homodimer in solution

In section 5.1 I highlighted some studies that suggest SSRP1 functions independently from FACT complex. Moreover, in section 5.2.1 I presented evidence suggesting SSRP1 N-terminal/DD domain forms a homodimer, but I was not able to identify a homodimerization interface. Therefore, in order to further investigate SSRP1's oligomeric state and to gain insight into its functions, I expressed and purified Hu SSRP1 without the intrinsically disordered region at the C-terminus (SSRP1 Δ CTD) (Fig. 5-7).

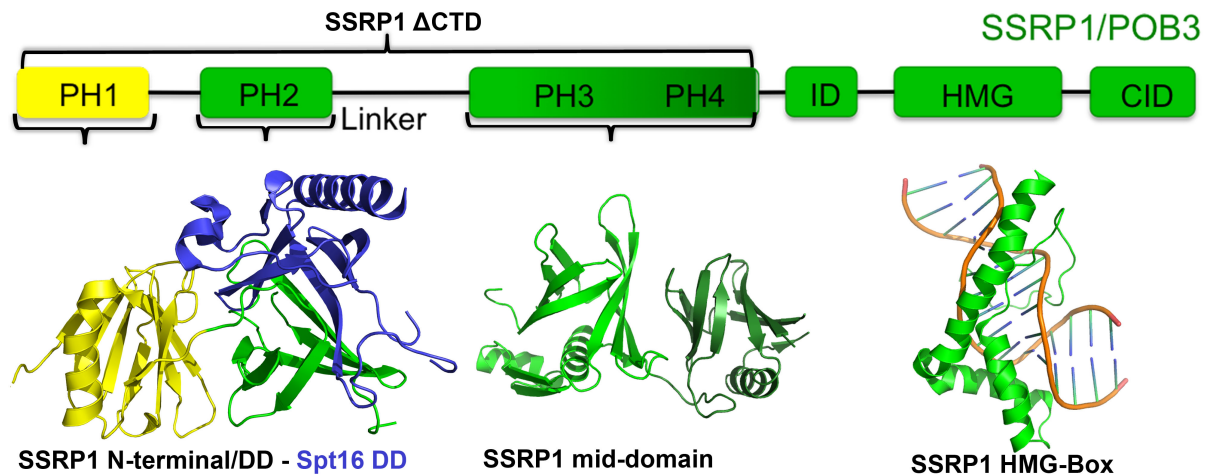


Figure 5-7 Diagram and structure representation of SSRP1/POB3 domains

(Top) Diagram representation of SSRP1 domains (PH1 in yellow, PH4 in dark green and all other domains in green). Curly brackets indicate domains and sub-domains used in this study. (low) Structural representation of SSRP1 N-terminal/DD domain (PH1 yellow, PH2 green) in complex with Spt16 DD domain (blue) (PDB: 4KHB); MD (PH3 green, PH4 dark green) (PDB: 2GCL) and HMG-1 domain bound to DNA (1J5N).

During the last step of purification I noticed that Hu SSRP1 Δ CTD (~50KDa) eluted from the size exclusion chromatography column earlier than expected for its molecular weight (Fig. 5-8 lower panel). The elution volume was between the 150 and 75 KDa molecular markers (Fig. 5-8 upper panel). This result is consistent with the size exclusion profiles observed for SSRP1 N-terminal/DD domain, suggesting that SSRP1 might be an oligomer or in an elongated conformation.

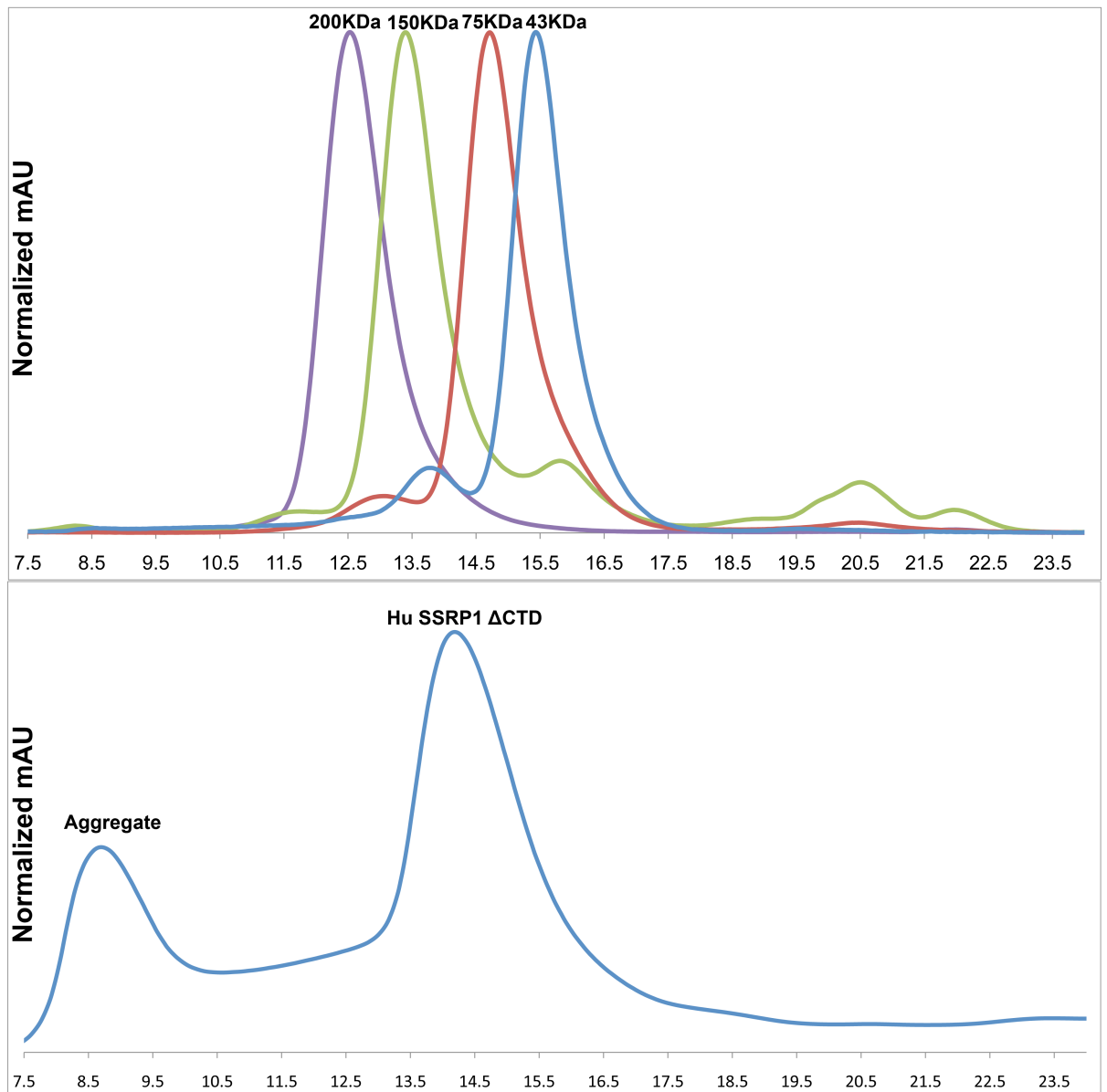


Figure 5-8 sd200 10/330GL elution profile of Hu SRP1 Δ CTD.

Top panel shows the elution profile for the following protein standards: β -amylase (200KDa), alcohol dehydrogenase (150KDa), ovalbumin (43KDa) and conalbumin (75KDa). Lower panel shows Hu SSRP1 Δ CTD elution profile. Hu SSRP1 Δ CTD aggregate is indicated and the elution volume corresponds to the void volume of the column.

I also noticed that a fraction of my protein eluted in the void volume, suggesting this protein might aggregate or form higher-order oligomers. Based on this preliminary result, I decided to further investigate the oligomeric state of Hu SSRP1 Δ CTD in solution by using analytical ultracentrifugation (AUC). Sedimentation velocity (SV) is an AUC technique that uses high centrifugation speeds (usually 49 krpm) to determine a protein's sedimentation coefficient, monodispersity and shape. SV analysis of Hu SSRP1 Δ CTD showed a single peak with a sedimentation coefficient in water at 20°C of $3.32 \pm 0.21 S_{20,w}$ and a frictional ratio of 1.63 (f/f_0) (Fig.5-9 a). Frictional ratio is used to characterize protein shape. Globular proteins have a frictional ratio between 1.2 and 1.3, asymmetric or glycosylated proteins have a ratio between 1.5 and 1.8 and very asymmetric proteins or linear chains will show a bigger value (190,191). To determine the molecular weight (MW) and oligomeric state of Hu SSRP1 Δ CTD, I used another AUC technique called sedimentation equilibrium (SE). This allows accurate determination of a protein's MW by using a particular centrifugation speed (selected based on the predicted MW of the protein of interest and its oligomeric state) for a period of time that allows your protein to stay in equilibrium between centrifugal and diffusion force in solution. This analysis is dependent only on a protein's MW but not its shape. SE analysis of Hu SSRP1 Δ CTD fitted with "species analysis model" gave only one MW of $91795 \pm 3673\text{Da}$ (Fig. 5-9 b), which correlates with the predicted MW of a homodimer (99615Da). Together, the SE and SV AUC analyses showed that Hu SSRP1 Δ CTD self-associates to generate an elongated homodimer in solution.

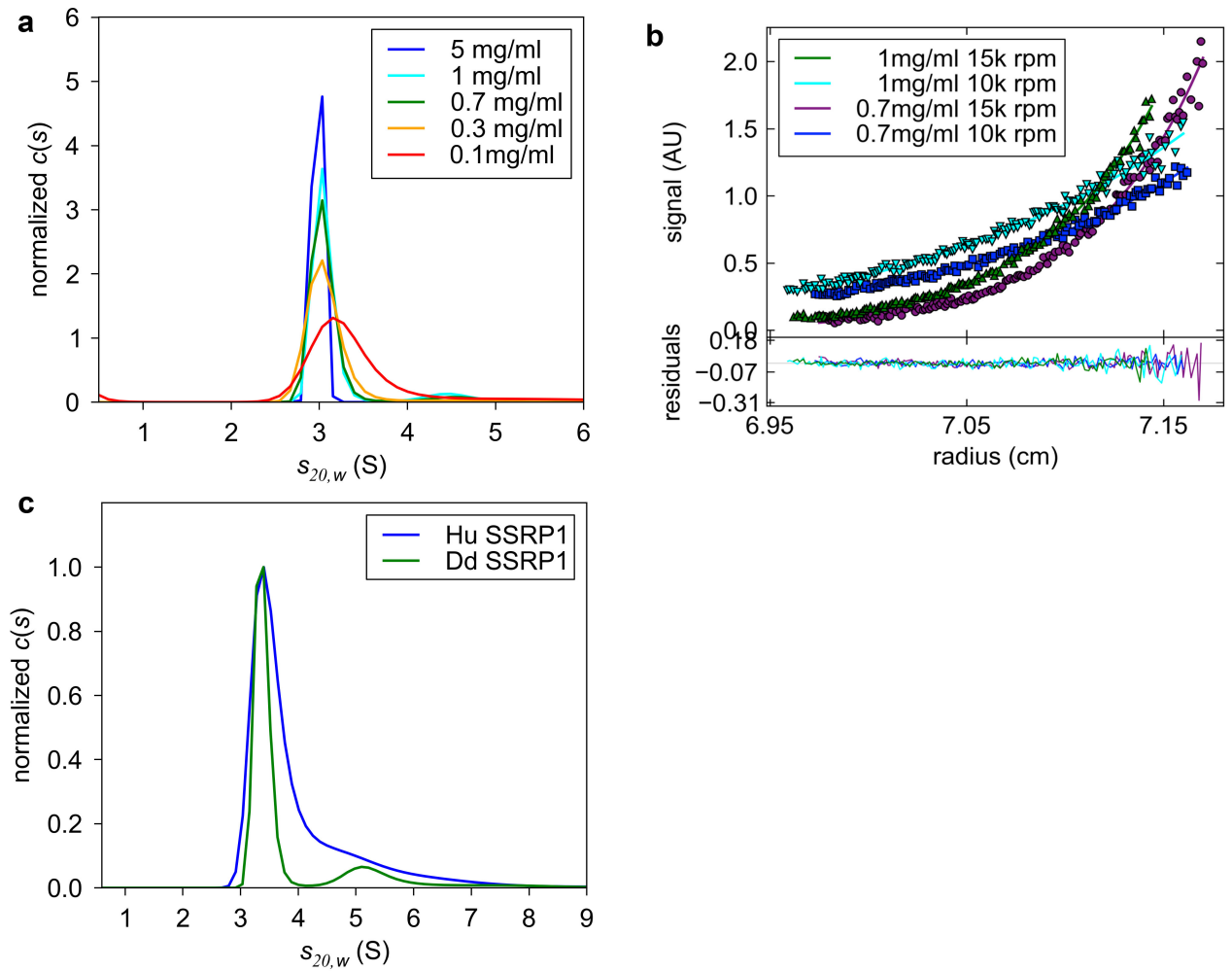


Figure 5-9 AUC analysis of Hu and Dd SSRP1 Δ CTD

(a) Sedimentation velocity plot of $S_{20,w}$ of Hu SSRP1 Δ CTD at different concentrations (from 5 to 0.1 mg/ml). (b) Sedimentation equilibrium at 10 and 15 Krpm of Hu SSRP1 Δ CTD at 1 and 0.7 mg/ml. (c) Sedimentation velocity comparison of Hu (blue) and Dd SSRP1 Δ CTD (green).

Next, I investigated whether SSRP1 homodimerization is conserved among different species. Hence, I cloned and purified *Dictyostelium discoideum* SSRP1 Δ CTD (Dd SSRP1 Δ CTD). SV confirmed that Dd SSRP1 Δ CTD is monodispersed in solution and has a similar $S_{20,w}$ to Hu SSRP1 Δ CTD (Fig. 5-8 c); SE yielded a molecular weight of 104794 ± 22685 , consistent with a homodimer. Conservation of SSRP1 homodimerization across species suggests that it might be required for SSRP1 function.

5.2.2.1 SSRP1 PH2 and PH3 domains are responsible for homodimerization

In section 5.2.1 I showed that SSRP1 N-terminal/DD domain interacts with Spt16 DD and that both proteins adopt PH-like folds (Fig. 5-6 and 5-7). I also showed that SSRP1 N-terminal/DD domain behaves as a dimer or elongated protein, suggesting it might be involved into homodimerization. In section 5.2.2 I showed that SSRP1 is a conserved elongated homodimer in solution. From these results, I predicted that SSRP1 PH2 domain (responsible for the heterodimerization with Spt16) might use the same surface to homodimerize. Based on the crystal structure of SSRP1 N-terminal/DD and Spt16 DD domains (PDB: 4KHB) I generated a mutant containing 6 mutations within the SSRP1 PH2 domain that contribute to the heterodimerization interface (C112A/N113A/W114A F135R/M172R/M175R, also referred to as Dd SSRP1 Δ CTD N-terminal mutant) (Fig. 5-10).

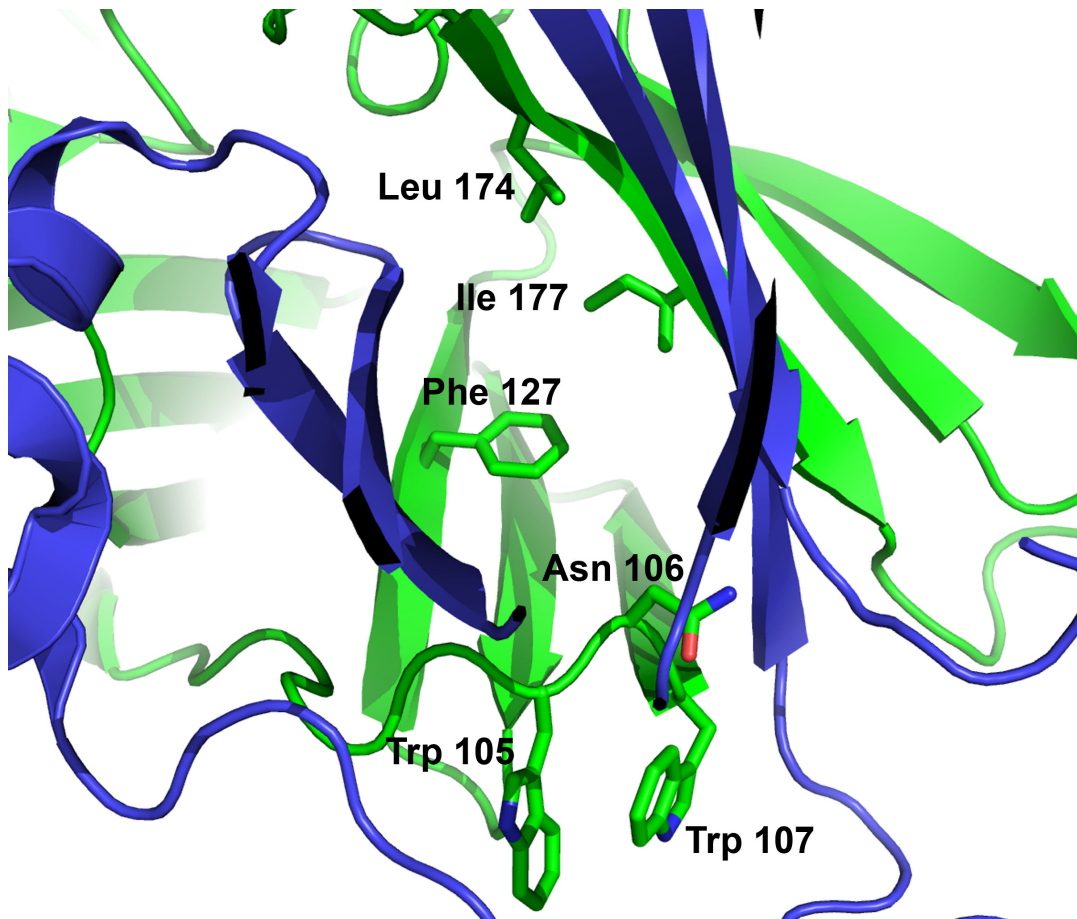


Figure 5-10 Structural representation of SSRP1/Spt16 heterodimerization interface showing residues targeted for mutagenesis.

Structural representation of *C. thermophilum* SSRP1 PH2 domain (green) and Spt16 DD domain (cyan) heterodimerization interface (PDB: 4HKB) showing corresponding residues (in stick) of Dd SSRP1 N-terminal/DD targeted for mutagenesis.

Interestingly, AUC analysis showed that this mutant is monodispersed and has a MW corresponding to a monomer as shown in Table 5-6. These results suggest that SSRP1 homodimerization involves its second PH domain as predicted. If my hypothesis is true, then SSRP1 N-terminal/DD domain (PH1 and 2) should be detected as a dimer in solution by AUC. To test this, I cloned and purified wild-type Dd SSRP1 N-terminal/DD. Unexpectedly, AUC analysis demonstrated that Dd SSRP1 N-terminal/DD is an elongated monomer (Table 5-6), suggesting that the homodimerization is not mediated only by PH2 domain but may involve other SSRP1 domains. Interestingly, studies on POB3 middle domain showed that a mutation on the PH3 domain to a highly conserved glutamine, Q308K, caused defects in transcription initiation and DNA replication (125). I therefore hypothesized that the corresponding residue, Q306K, in Dd SSRP1 Δ CTD might be involved in homodimerization. Hence, I generated and purified this mutant and performed AUC, which showed that Dd SSRP1 Q306K is a monomer (Table 5-6). Together, these results show that the PH2 domain is not interacting with another PH2 as previously hypothesized to form a homodimer; instead, SSRP1 homodimerization involves both SSRP1 PH2 and PH3 domains in an asymmetric interaction.

Table 5-6 Sedimentation equilibrium analysis of Dd SSRP1 constructs

Protein	MW (Da)	σ	MW expected (Da)
Dd SSRP1 Δ CTD N-term mutant	58417.56	5346.65	54102.16
Dd SSRP1 N-terminal/DD domain	20249.15	2808.91	20481.08
Dd SSRP1 Δ CTD Q306K	54827.28	4626.82	54223.44

5.2.3 FACT is a heterodimer of SSRP1 and Spt16

My results have shown that SSRP1 is a homodimer that asymmetrically self-associates by using both the PH2 and PH3 domains. Moreover, SSRP1 PH2 domain is involved in heterodimerization with Spt16 DD. Hence, SSRP1 homodimerization and SSRP1/Spt16 heterodimerization require the same surface. Based on these findings, I expect that SSRP1 binds Spt16 as a monomer. To test this hypothesis I cloned and purified Hu FACT for AUC analysis. Unfortunately I was unable to purify human FACT from *E. coli*. Fortunately, Dd FACT protein was more stable so I used this complex instead.

Sedimentation velocity data showed that Dd FACT Δ CTD is homogeneous in solution with a $S_{20,w}$ of 6.09 ± 0.52 and a frictional ratio of 1.51, suggesting that this protein adopts an elongated shape. Sedimentation equilibrium data gave a MW of 162585 ± 18843 Da, which correlates with the predicted MW of a heterodimer (MW of 162856Da) (Fig. 5-11 a and b). This result is consistent with previous published data that showed yFACT is a heterodimer of SSRP1 and Spt16 (121).

All together my data show that both Hu and Dd SSRP1 are elongated homodimers in solutions. Moreover, I showed that SSRP1 homodimerization and SSRP1/Spt16 heterodimerization are mutual exclusive.

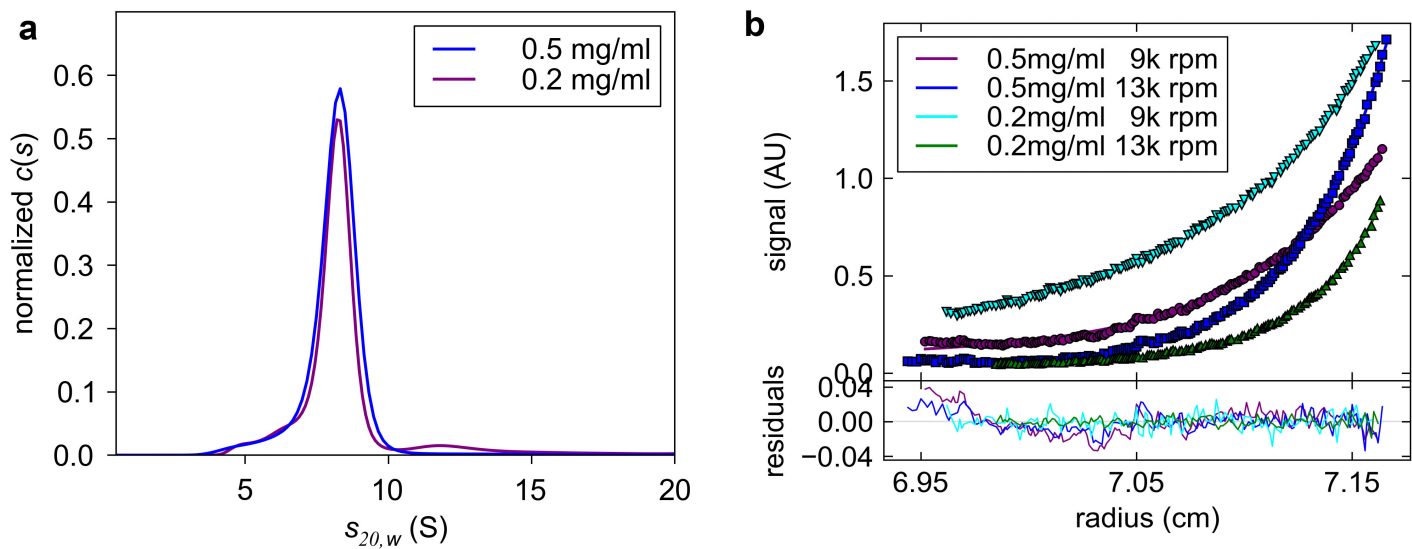


Figure 5-11 AUC analysis of Dd FACT Δ CTD

(a) Sedimentation velocity plot showing $S_{20,w}$ for Dd FACT Δ CTD at two concentrations (0.5 and 0.2 mg/ml). (b) Sedimentation equilibrium at 9 and 13 Krpm of Dd FACT Δ CTD at 0.5 and 0.2 mg/ml.

5.2.4 SSRP1 shape revealed by SAXS analysis

AUC analysis and size exclusion chromatography showed that SSRP1 is an elongated protein. To gain further insights into SSRP1's structure and because it was refractory to crystallization attempts, I then decided to use SAXS. SAXS is a technique used to determine proteins' solution structure at mid-low resolution. Hence, I cloned and purified Dd SSRP1 Δ CTD and sent it to Giancarlo Tria for SAXS analysis. Analysis of the Kratky plot and Pair-distance distribution function $P(r)$ demonstrate that Dd SSRP1 Δ CTD is an elongated homodimer with some flexible regions (Fig. 5-12). Dd SSRP1 Δ CTD has a MW of ~105-130KDa and a D_{max} of 18nm (Table 5-7). All together these data correlate with my AUC analysis showing SSRP1 is an elongated homodimer structure with some intrinsic flexibility.

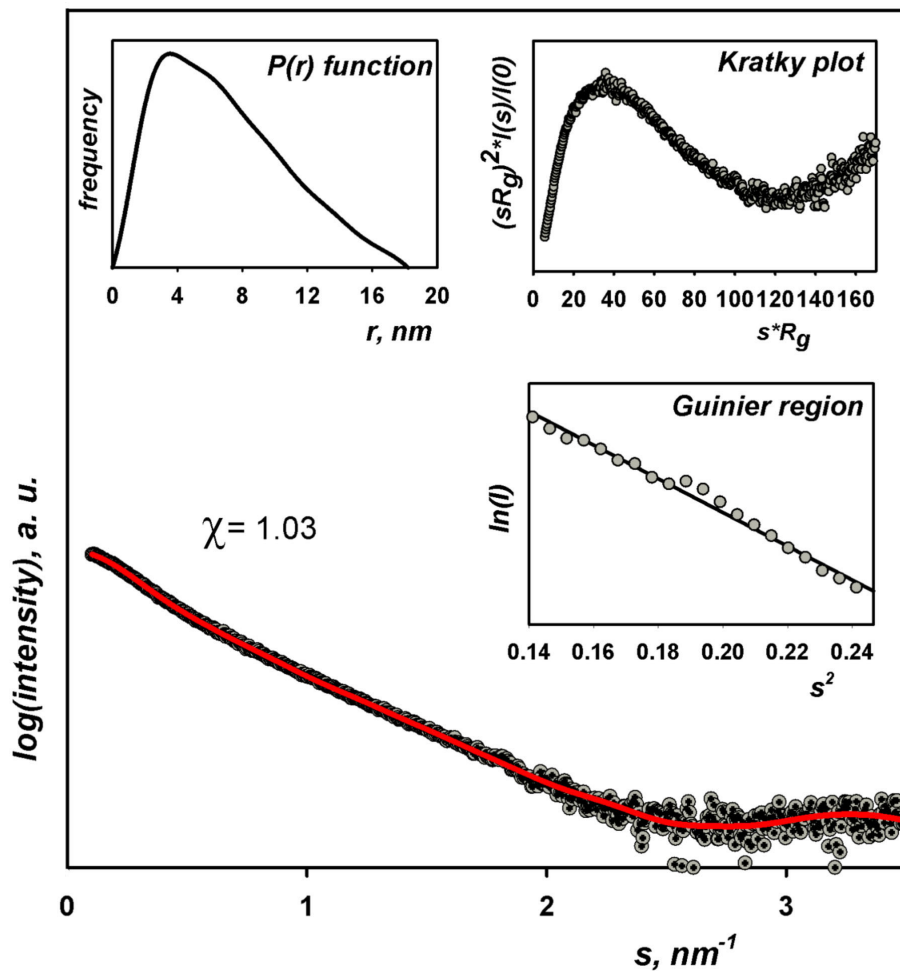


Figure 5-12 SAXS analysis of Dd SSRP1 Δ CTD

Experimental SAXS data vs. theoretical scattering (red). Pair-distance distribution function $P(r)$, Kratky plot and Guinier region are also shown.

Table 5-7 Data collection and SAXS-derived parameters for Dd SSRP1 Δ CTD.

Data-collection parameters		
	Data source	PETRA III (DESY)
	Instrument (beamline)	EMBL P12
	Instrument (detector)	PILATUS 2M pixel
	Beam geometry (mm ²)	0.2 x 0.12
	Wavelength (Å)	1.24
	<i>s</i> range (nm ⁻¹)	0.02-4.5
	Exposure time (sec)	1 (20 frames x 0.05sec)
	Concentration range (mg ml ⁻¹)	0.7 – 9.7
	Temperature (K)	283.15
Structural parameters		
	<i>I</i> (0) (cm ⁻¹) [from <i>P</i> (<i>r</i>)]	2766±50
	<i>R</i> _g (nm) [from <i>P</i> (<i>r</i>)]	5.5±0.3
	<i>I</i> (0) (cm ⁻¹) [from Guinier approximation]	2750±50
	<i>R</i> _g (nm) [from Guinier approximation]	5.3±0.3
	<i>D</i> _{max} (nm)	18±1
	Porod volume estimate (nm ³)	194±15
	Dammif excluded volume (nm ³)	248±15
Molecular-mass determination		
	Molecular mass <i>M</i> _r (kDa) [from <i>Porod invariant</i>]	115±10
	Molecular mass <i>M</i> _r (kDa) [from <i>excluded volume</i>]	120±10
	Calculated monomeric <i>M</i> _r (kDa) [from sequence]	~54
Software employed		
	Primary data reduction	PIPELINE
	Data processing	PRIMUS
	<i>Ab initio</i> analysis	DAMMIF
	Validation and averaging	DAMAVR
	Computation of model intensities	CRYSOL
	Rigid Body Modelling	CORAL
	Model Superimposition	SUPCOMB
	Three-dimensional representations	VMD

An *ab initio* model generated from the scattering curve with P1 symmetry shows that SSRP1 adopts an open V-conformation in solution. Since the structure of SSRP1 Δ CTD is not available I used I-TASSER to generate homology models. The two models yielding the highest scores were predicted to be globular (model 1) and elongated (model 2) (Fig. 5-13).

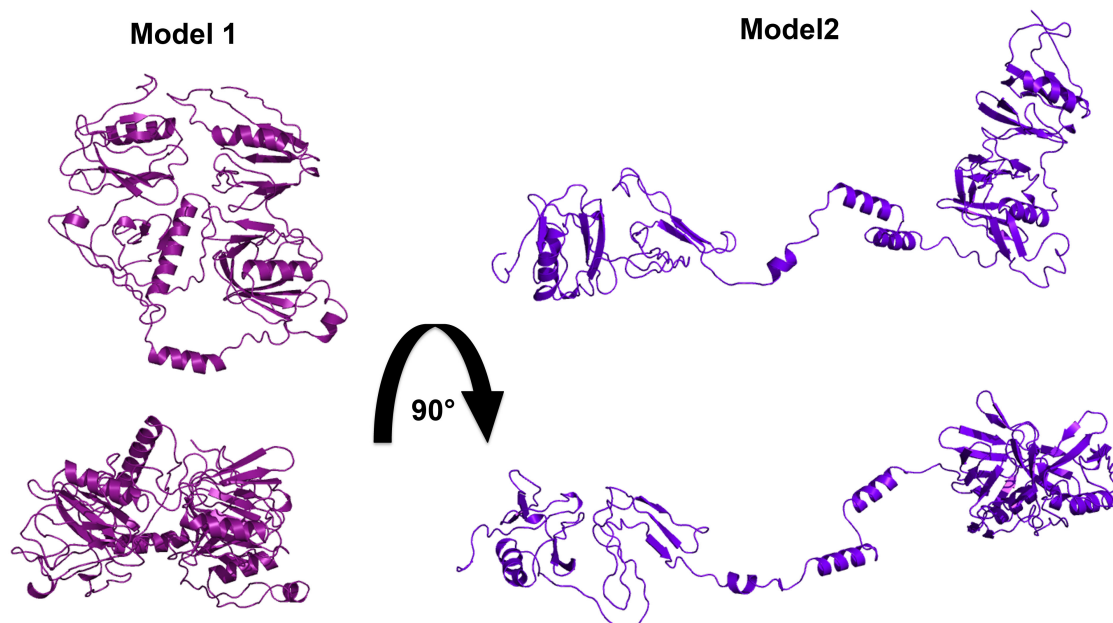


Figure 5-13 Dd SSRP1 Δ CTD homology models predicted by I-TASSER

Model 1 globular; Model 2 elongated

I then used CORAL to do rigid body modelling of the two models (as monomers) into the scattering curve followed by CRY SOL evaluation to compare the predicted scattering curve of the I-TASSER models into the experimental scattering data. As shown in Fig. 5-13 globular and elongated models gave χ^2 values of 52 and 8 respectively, suggesting that SSRP1 Δ CTD is elongated rather than globular. Based on these results I tested whether the SSRP1 Δ CTD elongated model gave a better fit as homodimer. I ran CORAL again using model 2 looking for P2 symmetry (dimer). Remarkably, an elongated dimer model of Dd SSRP1 Δ CTD fit the experimental curve with a χ^2 of 1.4. The homodimer in this model is asymmetrical (Fig. 5-14 and 5-15 E and F), which is consistent with my previous data.

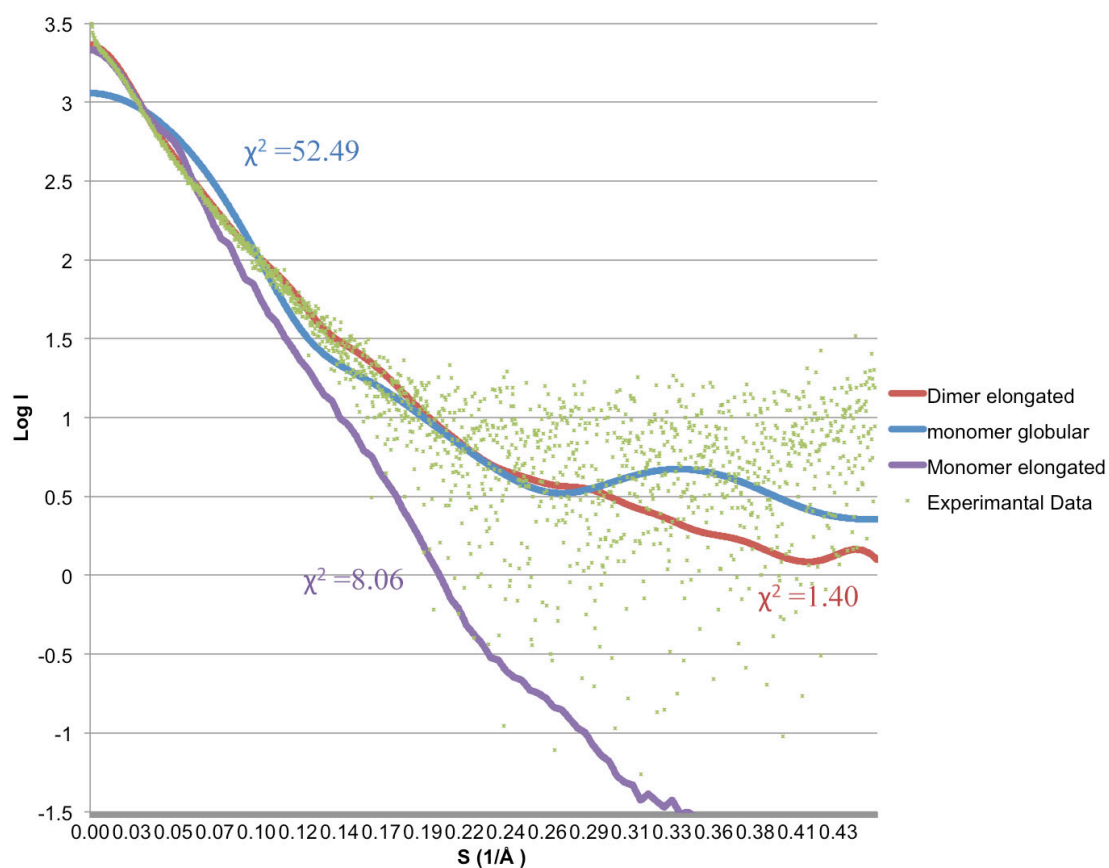


Figure 5-14 CRY SOL scattering curve calculation of different Dr SSRP1 Δ CTD model derived from I-TASSER.

Comparison of the scattering curve of Dd SSRP1 Δ CTD (green) with a CRY SOL calculated scattering curve derived from I-TASSER models of a globular monomer (blue), elongated monomer (purple) and elongated dimer (red).

Finally, I used SUPCOM to superimpose the homodimer model generated by CORAL onto the averaged *ab initio* model (Fig.5-15). Notably, even though the elongated homodimer model gave the best result, Gln308 did not contribute to the homodimer interface, in contrast to my AUC results presented in section 5.2.3. Nevertheless, these results provide a foundation for further investigations into SSRP1 oligomerization.

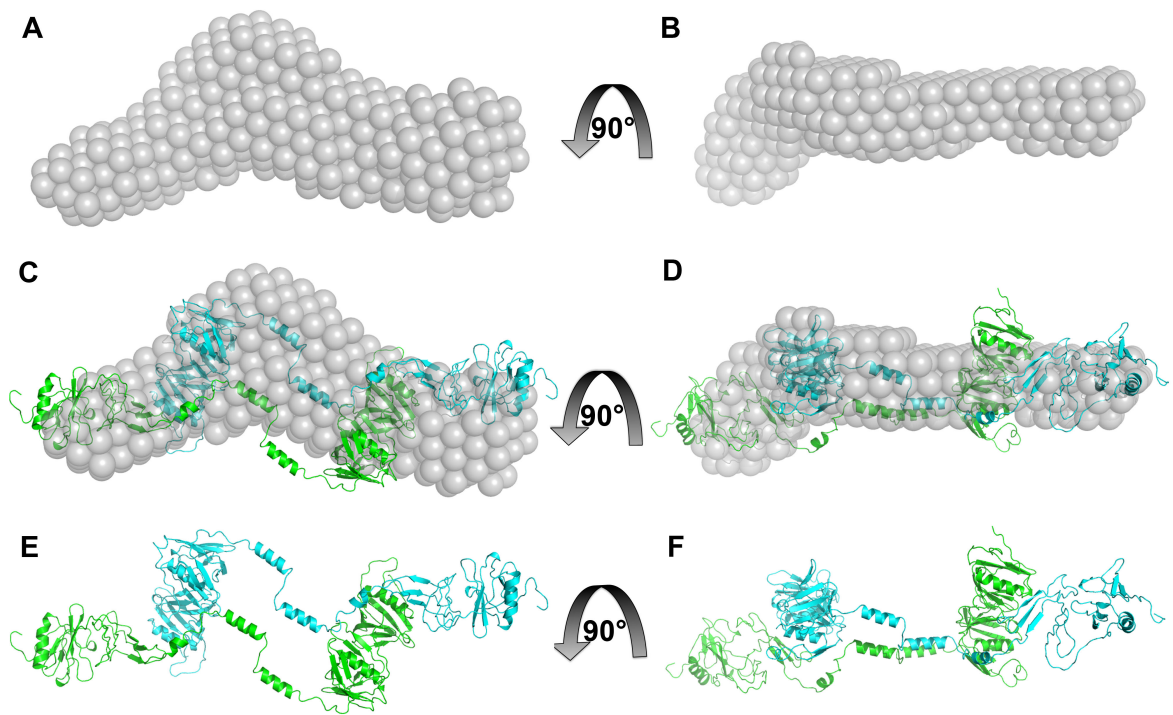


Figure 5-15 Grafical representation of Dd SSRP1 Δ CTD *ab initio* and CORAL models

(A and B) *Ab initio* bead-model that fits the experimental scattering curve (P1 symmetry). (C and D) Superposition of *ab initio* model (from DAMAVER) and elongated homodimer model (from CORAL). (E and F) Dd SSRP1 Δ CTD elongated homodimer model generated by CORAL to fit the experimental scattering curve.

5.2.5 SSRP1 homodimerization increases histone binding affinity

Several pieces of data hint at a role for homodimerization in histone binding. As mentioned in section 5.1, some studies suggest SSRP1 might have independent functions *in vivo*. In addition, an *in vitro* study has shown that SSRP1 binds nucleosomes with high affinity, showing a preference for histone (H3/H4)₂ (132). In order to understand SSRP1-independent functions I performed ITC analysis against histones dimers and tetramer purified from chicken. To validate my hypothesis, I first tested Dd SSRP1 Δ CTD, Dd SSRP1 Δ CTD Q306K and Dd SSRP1 Δ CTD N-terminal mutant (section 5.2.3) against histone (H3/H4)₂. If homodimerization were involved in histone binding I expected a decrease in binding affinity in the mutants. ITC analysis showed that Dd SSRP1 Δ CTD binds histone (H3/H4)₂ with a K_d of 0.562 μ M, which is comparable to the previously determined binding affinity of Hu SSRP1 for (H3/H4)₂ (132) (Fig. 5-16). Strikingly, the two monomeric mutants, Dd SSRP1 Δ CTD Q306K and Dd SSRP1 Δ CTD N-terminal mutant, showed lower binding affinities of 1.37 and 2.99 μ M, respectively, for (H3/H4)₂ (Fig. 5-16), suggesting that SSRP1 homodimerization plays a role in histone (H3/H4)₂ binding .

I also tested Dd SSRP1 Δ CTD binding affinity against histone chicken H2A/H2B as well. Astonishingly, Dd SSRP1 Δ CTD bound H2A/H2B with a K_d of 0.819 μ M (Fig. 5-17). I then tested whether my monomeric Dd SSRP1 Δ CTD mutants were able to decrease this binding affinity. As expected, Dd SSRP1 Δ CTD N-terminal mutant showed a 2-fold decrease in binding (K_d of 1.56 μ M) (Fig. 5-17). Surprisingly, Dd SSRP1 Δ CTD Q306K showed a biphasic profile that could only be fit with a sequential binding site model (Fig. 5-17). The first binding site gave a positive change in enthalpy (endothermic) with a K_{d1} of 3.58 μ M, while the second binding site gave a negative change in enthalpy (exothermic) with a K_{d2} of 38 μ M. The second binding site may be nonspecific due to charge alteration introduced by the Q306K mutation and SSRP1 homodimerization interface exposure.

All together my ITC results showed that once SSRP1 dissociates to a monomer, its histone binding affinity decreases, suggesting that homodimerization somehow affects histone binding. Hence, SSRP1 homodimerization might be important for its independent functions.

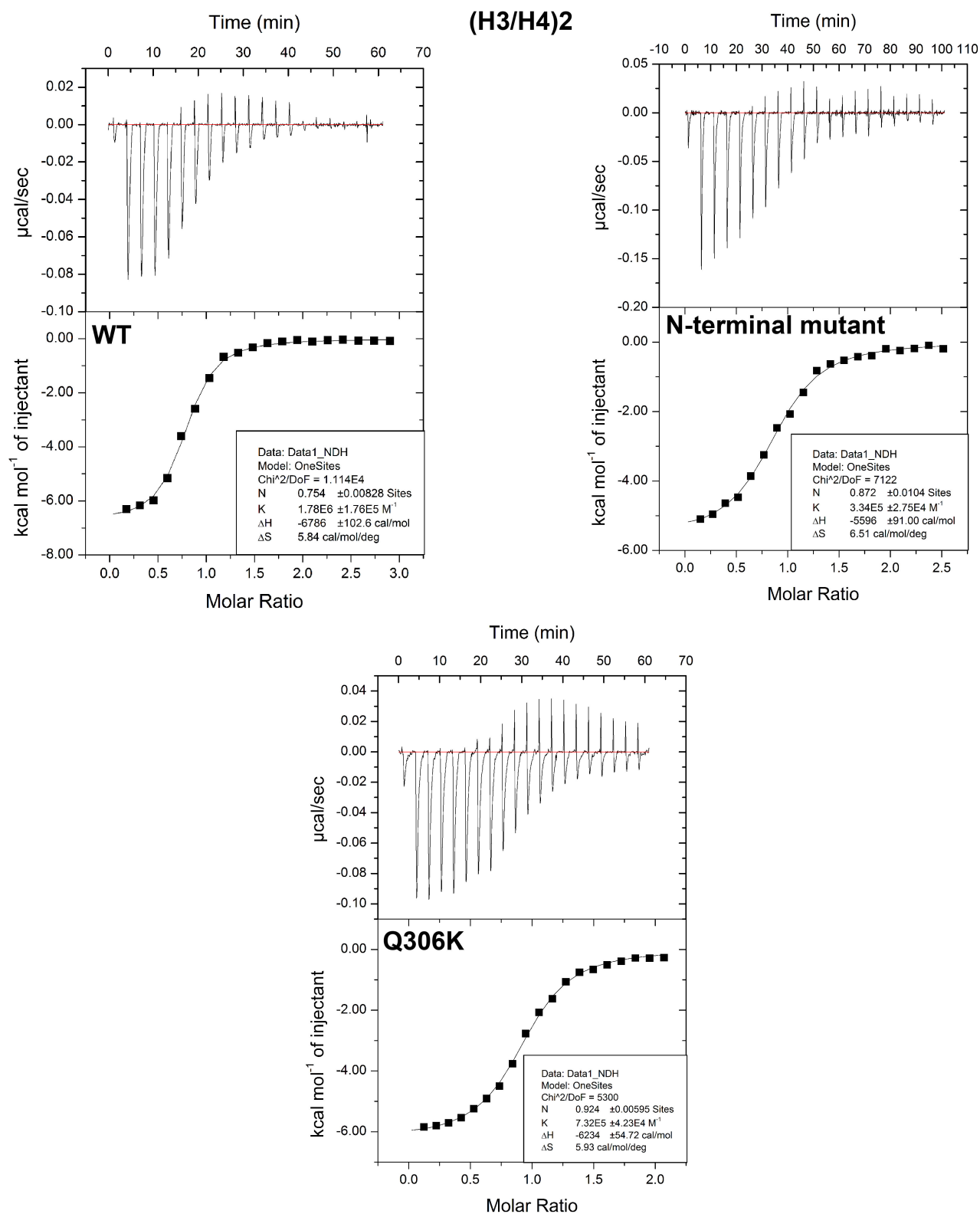


Figure 5-16 ITC analysis of Dd SSRP1 Δ CTD and mutants against histone (H3/H4)₂
 ITC profile showing raw data (upper panel) and normalised data (lower panel) plotted against the molar ratio between the ligand (H3/H4)₂ and SSRP1 protein (as indicated). Inset box shows stoichiometry (n), association constant (K_a), enthalpy (ΔH) and entropy (ΔS).

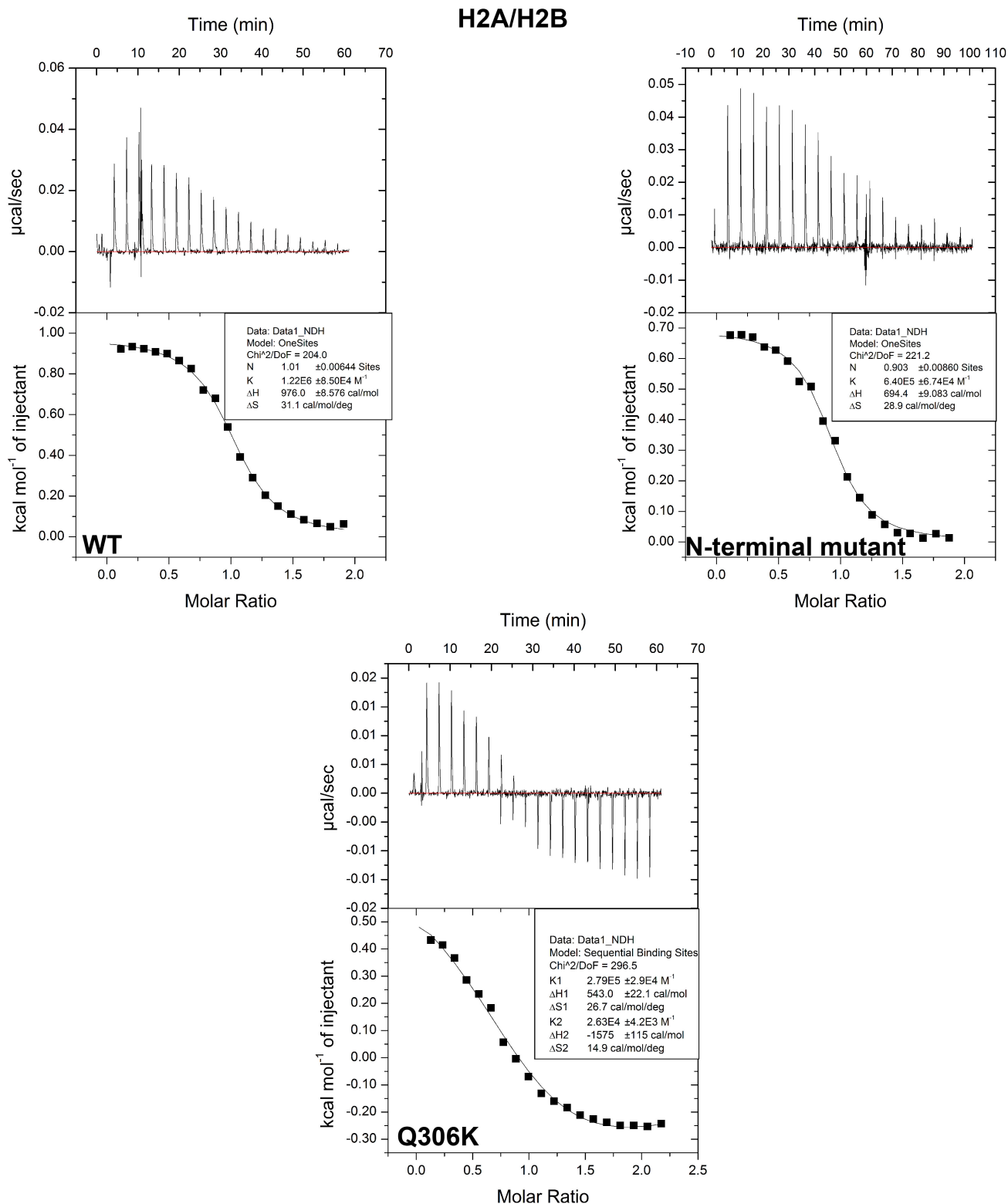


Figure 5-17 ITC analysis of Dd SSRP1 Δ CTD and mutants against histone H2A/H2B
ITC profile showing raw data (upper panel) and normalised data (lower panel) plotted against the molar ratio between the ligand H2A/H2B and SSRP1 protein (as indicated). Inset box shows stoichiometry (n), association constant (K_a), enthalpy (ΔH) and entropy (ΔS).

5.3 Discussion

In this chapter I show that SSRP1 heterodimerize with Spt16 by means of a conserved sequence located on a β -sheet of the SSRP1 PH2 domain and on another β -sheet located on Spt16 DD. Furthermore, AUC analysis of the FACT Δ CTD complex shows that SSRP1 and Spt16 form a flexible and elongated heterodimer in a 1:1 ratio. This result is consistent with other published data (121). The published structure of SSRP1 N-terminal/DD domain in complex with Spt16 DD (135) confirms my pull down data and provides further information regarding this binding. From the structure it is clear that in order to heterodimerize, both proteins need to form a pocket, which is generated by two hydrophobic halves located in SSRP1 and Spt16 dimerizing interface.

To date, nothing is known about SSRP1's full-length structure. Current SSRP1 structures involve fragments of the full-length protein (125,128,135) and do not offer substantial insights into SSRP1's mechanism of action. Unfortunately I couldn't crystallize the full-length protein, but by using AUC and SAXS analysis I elucidated the oligomeric state of SSRP1 in solution. In section 5.2.2 AUC analysis demonstrates that SSRP1 self-associates in solution as an elongated homodimer, which is conserved among species. Also, AUC analysis shows that mutation of either of SSRP1's PH2 or PH3 domains disrupts homodimerization, suggesting that both domains are required for SSRP1 oligomerization. Furthermore, SAXS analysis complements these AUC findings, showing that SSRP1 is a flexible elongated homodimer that adopts an open V conformation in solution. The flexibility and propensity to oligomerize (see Fig. 5-8) provide clues on SSRP1's mechanism of action both as a homodimer and as part of FACT complex. If we suppose SSRP1's homodimeric mechanism of action is similar to FACT complex, then both proteins need to be flexible and elongated in order to interact with all histones within nucleosomes. This hypothesis is supported by my ITC results where I show for the first time that Dd SSRP1 Δ CTD binds both histone dimers and tetramers. When mutations that disrupt the dimer interface are introduced, SSRP1 Δ CTD binding affinity for histone dimers and tetramers is reduced, suggesting that homodimerization might be important for SSRP1 independent functions.

In yeast POB3 Q308K causes defects in transcription and replication; introduction of Spt16 R706T can only rescue the replication defect (125). Based on my results I speculate that POB3 Q308K impairs both FACT and SSRP1 functions by altering an important charge on the surface that might be involved in FACT histone binding and SSRP1

homodimerization. In this scenario, Spt16 R706T (which is located on the middle domain) might be able to partially restore a FACT histone binding surface and, as a consequence, restore its activity to rescue the replication defect. Therefore, yeast double mutant POB3 Q308K and Spt16 R706T only shows a transcription effect. Interestingly, yeast POB3 F133S also only shows a transcription defect (125). Based on my results, I speculate that POB3 F133S may be a monomer that has lost SSRP1-independent activity but can still associate with Spt16 to form an active hetero-complex showing, as a result, only one phenotype.

POB3 T252E has defects in replication and transcription similar to POB3 Q308K whereas POB3 T252E Q308K restores both phenotypes (192). I have shown that the PH3 domain is involved in SSRP1 homodimerization and that charge alterations in this domain affect the oligomeric state. Both Thr252 and Glu308 are opposite one another on the POB3 PH3 domain. Based on my findings, I speculate that individually, both, cause a shift in charge in the PH3 domain that disrupts homodimerization, thereby producing similar phenotypes; the POB3 double mutant T252E Q308K restores the global charge of this patch and rescues SSRP1 functions.

Other studies have shown that mutations at histone tetramer and dimer-tetramer interfaces are able to suppress replication defects but not transcription (193,194). These mutations make the histone octamer less stable such that it can dissociate easily. In this way FACT Q308K can still function but SSRP1 Q308K, which is a monomer, cannot. This may explain why histone mutants can only rescue replication defective phenotypes and not transcription. Interestingly, SSRP1 shares structural similarities with other histone chaperones such as the homodimer RTT106 and Spt16 middle domain (135-137). These similarities suggest a possible role of SSRP1 as a histone chaperone independent from its function in FACT.

Identifying SSRP1 independent functions and the role of homodimerization on its biological activity remain elusive and require further investigation.

Chapter 6

Summary and future directions

6 Summary and future directions

6.1 Summary

6.1.1 Hu Spt16 NTD and histone binding

The structure of Hu Spt16 NTD shows similarity to the previously published structures from *S. cerevisiae* and *S. pombe* (129,130). Like an aminopeptidase domain, it consists of an N-lobe and a C-lobe that appear to be locked into position and inflexible relative to one another.

Sequence and electrostatic surface potential analysis of Hu Spt16 NTD highlights the presence of conserved acidic pocket between the N- and C-lobes, suggesting this pocket may be involved in histone binding. Moreover, this analysis reveals two additionally conserved acidic patches located on the top of the N-lobe and at the bottom of the C-lobe. I speculate that these patches may also contribute to histone binding.

Finally, ITC analysis of Hu Spt16 NTD against histone *X. laevis* H2A/H2B best fit a “sequential binding site” model with weak binding affinity where K_d1 and K_d2 are 23.8 and 456.6 μM , respectively. In contrast, ITC titrations with Hu Spt16 NTD and *X. laevis* histone (H3/H4)₂ gave a K_d of 57 μM . These data are consistent with results obtained by titrating purified histone from *G. gallus* with Hu Spt16; here, ITC analysis also fits a sequential binding site model with K_d1 of 13.2 and K_d2 of 746 μM for histone H2A/H2B and a K_d of 52.3 μM for (H3/H4)₂.

6.1.2 Dr Spt16 middle domain and histone binding

The structure of Dr Spt16 MD resembles recently published structures from *S. cerevisiae* and *C. thermophilum*, consisting of a double PH domain followed by a U-turn motif. Sequence alignment followed by electrostatic surface potential analysis demonstrates the surface of Spt16 MD is conserved especially at the PH2 domain and U-turn motif.

Analysis of the electrostatic surface potential of this domain shows the presence of several acidic patches. Some of these acidic patches are located on the U-turn motif, which has previously been shown to bind histone H2A/H2B (135), whereas others are located on the PH1 domain and on the $\alpha 1$ helix. Interestingly, some of the Spt16 MD mutations that

suppress the H3/H4 stabilizing mutant H3L61W (139) map on the PH1 domain and its $\alpha 1$ helix. These data together with the sequence conservation analysis suggest that both PH1 and $\alpha 1$ helix may have a role in histone binding.

Lastly ITC analysis of Dr Spt16 MD wild type and mutant against H2A/H2B confirm that this interaction is mediated by the U-turn motif as recently published (135) but with a weaker binding affinity. Interestingly, ITC analysis against (H3/H4)₂ showed a double binding event, which support the hypothesis that PH1 and $\alpha 1$ helix might play a role in this binding.

6.1.3 SSRP1 homodimerization enhances histone binding

Characterization of Hu SSRP1 Δ CTD by analytical ultracentrifugation (AUC) revealed several features about its oligomeric state. Sedimentation velocity (SV) analysis showed only one peak, indicating that SSRP1 is monodispersed at all the concentrations evaluated, suggesting that SSRP1 Δ CTD's oligomeric state is independent of protein concentration. The frictional ratio was determined to be 1.63, classifying this protein as elongated. Sedimentation equilibrium (SE) analysis gave a MW of 91795 Da, which is close to the expected molecular weight of a 99615 Da homodimer. AUC analysis of Dd SSRP1 Δ CTD showed results similar to Hu SSRP1 Δ CTD, suggesting that this oligomeric state is conserved across different species. Moreover, mutations within the PH2 (N-terminal mutant) or PH3 (Q306K) domains cause SSRP1 to dissociate into monomers, suggesting an asymmetric oligomer. Finally, AUC analysis of Dd FACT Δ CTD showed the presence of one SSRP1 molecule, suggesting that SSRP1 dissociates when in the presence of Spt16 to generate the heterodimer FACT.

Using SAXS, I determined the molecular envelope of SSRP1 Δ CTD and showed that SSRP1 is an elongated and flexible protein with a predicted MW between 115 and 120 KDa, a Dmax of 18 nm and Rg of 5.5 nm. *Ab initio* modelling of the molecular envelope of SSRP1 Δ CTD revealed an open v-conformation. In short AUC and SAXS results showed that SSRP1 Δ CTD is an elongated and flexible homodimer.

Lastly, ITC analysis was carried out to evaluate the binding affinity of SSRP1 with histones H2A/H2B and (H3/H4)₂. Wild type Dd SSRP1 Δ CTD bound both histone H2A/H2B and (H3/H4)₂ with K_d 's of 0.819 and 0.562 μ M, respectively whereas the N-

terminal mutant and Q306K bound both histones more weakly, suggesting that SSRP1 homodimerization plays a role in histone binding.

6.2 Future directions

The initial goal of my project was to determine the structure of FACT alone or in complex with the nucleosome in order to gain insight into its mechanism of action. Unfortunately, my attempts to crystallize this complex failed. Subsequently, I moved forward by trying to understand the implication of FACT domains into histone binding. My studies suggest that each FACT domains play a role in histone binding and that nucleosome reorganization might be orchestrate by their coordination. Since crystallization of FACT alone or in complex with nucleosome is challenging other technique can be used to determine this structure such as cryo-electron microscopy.

6.2.1 Hu Spt16 N-terminal domain acidic patches and binding partners

To gain insights into how Hu Spt16 NTD binds histone H2A/H2B and (H3/H4)₂, alanine scans of the conserved and /or acidic residues located in the pocket between the N- and C-lobes could be performed. This experiment may help us understand whether all parts of the pocket contribute to both types of histone binding or whether some pocket residues only interact with histone dimer or tetramer.

The Spt16 N-lobe has been proposed to act as a “protein-protein interaction domain” with other FACT-interacting proteins (130). Immunoprecipitation coupled with mass spectrometry (IP/MS) of Spt16 NTD from cell lines synchronized at various stage of the cell cycle may help us identify other protein partners that preferentially interact with this domain.

6.2.2 Dr Spt16 middle domain and histone binding

Knowing how Spt16 MD binds histones will help us understand its mechanism of action. To date, how Spt16 MD binds histone (H3/H4)₂ remains elusive. My hypothesis is that both the PH1 domain and α 1 helix play a role in histone binding. To this end, I can set trays of Dr Spt16 MD in complex with full length histone (H3/H4)₂ or lacking its N-terminal tails. If crystallization does not work other techniques can be applied determine if PH1 and α 1 helix contribute to histone (H3/H4)₂ binding. Examples include alanine scans

followed by ITC analysis, pulse electron-electron double resonance (PELDOR), NMR and electron microscopy.

6.2.3 Characterization of SSRP1's homodimerization and functions.

Crystal structure of homodimeric SSRP1 can help to understand how SSRP1 oligomerize. However, attempts to crystallize full length SSRP1 have not been successful. Nevertheless, my results suggest that SSRP1 homodimerization requires both the PH2 and PH3 domains. Based on this knowledge, I can purify SSRP1 N-terminal/DD and middle domain and by using AUC I can test whether they are able to form a homodimer. If they dimerize, by using ITC, I can test whether these two domains bind histones like wild type SSRP1. I could also use this homodimer fragment alone and in complex with histone H2A/H2B or (H3/H4)₂ to set up crystallization trays.

If crystallization does not work, the use of other technique such as PELDOR and SAXS can be applied to further characterize SSRP1's homodimerization symmetry, histone binding and mechanism of action.

Recent studies have shown that SSRP1 together with Topoisomerase II α and other proteins constitute a complex called Toposome. Within this complex SSRP1 may enhance the Topoisomerase II α decatenation reaction on chromosomal DNA (195,196). These studies suggest a possible role for SSRP1 as a histone chaperone, independent from its role in the FACT heterodimer. To this end, I could test SSRP1's ability to exchange histones *in vitro* in a nucleosome context. It is also of interest to elucidate how SSRP1 interacts with Topoisomerase II α and to investigate if SSRP1 has protein partners other than Spt16.

Chapter 7

Appendix

7 Appendix

7.1 Appendix 1 construct list

Vector	Protein	construct	R.E.	oligo F	oligo R
RSF_D uet His- TEV	D.d SSRP1	FL	BamH1/ EcoR1		
pET3a	D.d. Spt16	20-955 KEK488-490AAA	Nde1/ BamHI	GM130	GM131
pGEX4 T1 GST- TEV	D.d. Spt16	FL KEK488-490AAA	BamH1/ EcoR1	GM132	GM133
pGEX4 T1 GST- TEV	D.d. Spt16	ggsg538-606	BamH1/ EcoR1	GM201	GM196
pGEX4 T1 GST- TEV	D.d. Spt16	FL	BamH1/ EcoR1		
pET3a	D.d. Spt16	20-955	Nde1/ BamHI	GM130	GM131
RSF_D uet His- TEV	D.d. SSRP1	FL KEK192-194AAA	BamH1/ EcoR1	GM134	GM135
RSF_D uet His- TEV	D.d. SSRP1	1-478 KEK192-194AAA	BamH1/ EcoR1	GM134	GM135
RSF_D uet His- TEV	D.d. SSRP1	SSRP1 FL Q306K	BamH1/ EcoR1	GM138	GM139
RSF_D uet His- TEV	D.d. SSRP1	6-478 KEK192-194AAA	BamH1/ EcoR1	GM147	GM149
RSF_D uet His- TEV	D.d. SSRP1	6-187	BamH1/ EcoR1	GM147	GM148
pCAL-n Th	D.d. SSRP1	6-187	BamH1/ EcoR1	GM147	GM148
RSF_D uet His- TEV	D.d. SSRP1	SSRP1 1-478 M172E	BamH1/ EcoR1	GM150	GM151
RSF_D uet His- TEV	D.d. SSRP1	1-478 F135A M172E	BamH1/ EcoR1	GM150	GM151
RSF_D uet His- TEV	D.d. SSRP1	SSRP1 1-478 V173D	BamH1/ EcoR1	GM152	GM153

RSF_D uet His- TEV	D.d. SSRP1	1-478 F135A V173D	BamH1/ EcoR1	GM152	GM153
RSF_D uet His- TEV	D.d. SSRP1	1-478 F177D	BamH1/ EcoR1	GM154	GM155
RSF_D uet His- TEV	D.d. SSRP1	1-478 F135A F177D	BamH1/ EcoR1	GM154	GM155
RSF_D uet His- TEV	D.d. SSRP1	SSRP1 1-478 F135Y	BamH1/ EcoR1	GM156	GM157
RSF_D uet His- TEV	D.d. SSRP1	SSRP1 1-478 F135E	BamH1/ EcoR1	GM158	GM159
RSF_D uet His- TEV	D.d. SSRP1	1-478 F135A	BamH1/ EcoR1	GM160	GM161
RSF_D uet His- TEV	D.d. SSRP1	1-478 F177E	BamH1/ EcoR1	GM162	GM163
RSF_D uet His- TEV	D.d. SSRP1	1-478 F126A	BamH1/ EcoR1	GM167	GM168
RSF_D uet His- TEV	D.d. SSRP1	1-478 F126A F135A F177D	BamH1/ EcoR1	GM167	GM168
RSF_D uet His- TEV	D.d. SSRP1	1-478 F126A F135A V173D	BamH1/ EcoR1	GM167	GM168
RSF_D uet His- TEV	D.d. SSRP1	1-478 F126A F135A M172E	BamH1/ EcoR1	GM167	GM168
RSF_D uet His- TEV	D.d. SSRP1	1-478 F126A F135A	BamH1/ EcoR1	GM167	GM168
RSF_D uet His- TEV	D.d. SSRP1	SSRP1 1-478 Q306K	BamH1/ EcoR1	GM169	GM149
RSF_D uet His- TEV	D.d. SSRP1	1-478 C112,N113,W114A	BamH1/ EcoR1	GM184	GM185
RSF_D uet His- TEV	D.d. SSRP1	1-478 C112,N113,W114A;F135R	BamH1/ EcoR1	GM186	GM187
RSF_D uet His- TEV	D.d. SSRP1	1-478 C112,N113,W114A;F135,M172 ,175R	BamH1/ EcoR1	GM188	GM189
RSF_D uet His- TEV	D.d. SSRP1	200-478	BamH1/ EcoR1	GM192	GM149

RSF_D uet His- TEV	D.d. SSRP1	200-478 Q306K	BamH1/ EcoR1	GM192	GM149
RSF_D uet His- TEV	D.d. SSRP1	200-527	BamH1/ EcoR1	GM192	GM204
pGEX4 T1 GST- TEV	D.d. SSRP1	200-478	BamH1/ EcoR1	GM192	GM207
RSF_D uet His- TEV	D.d. SSRP1	116-478	BamH1/ EcoR1	GM197	GM149
RSF_D uet His- TEV	D.d. SSRP1	116-478 Q306K	BamH1/ EcoR1	GM197	GM149
RSF_D uet His- TEV	D.d. SSRP1	116-478 KEK192-194AAA	BamH1/ EcoR1	GM197	GM149
RSF_D uet His- TEV	D.d. SSRP1	100-187	BamH1/ EcoR1	GM199	GM148
RSF_D uet His- TEV	D.d. SSRP1	ggsg100-187	BamH1/ EcoR1	GM202	GM148
RSF_D uet His- TEV	D.d. SSRP1	479-527	BamH1/ EcoR1	GM203	GM204
pGEX4 T1 GST- TEV	D.d. SSRP1	FL	BamH1/ EcoR1		
RSF_D uet His- TEV	D.d. SSRP1	1-478	BamH1/ EcoR1	GM169	GM149
pGEX4 T1 GST- TEV	D.r. Spt16	509-581	BamH1/ EcoR1	DTH10 12	DTH10 15
pGEX4 T1 GST- TEV	D.r. Spt16	519-581	BamH1/ EcoR1	DTH10 13	DTH10 15
pGEX4 T1 GST- TEV	D.r. Spt16	557-581	BamH1/ EcoR1	DTH10 14	DTH10 15
pGEX4 T1 GST- TEV	D.r. Spt16	1-930	BamHI/ EccoR1	DTH55 5	GM72

RSF_D uet	D.r. spt16	1-924	Bam HI/ EcoR1	DTH55 5	GM35
pET3a	D.r. Spt16	509-581	Nde1/ BamH1	DTH67 4	DTH10 07
pET3a	D.r. Spt16	557-581	Nde1/ BamH1	DTH67 6	DTH10 07
pET3a	D.r. Spt16	1-930	Nde1/ BamHI	GM128	GM129
pGEX4 T1 GST- TEV	D.r. Spt16	613-930 N888A S889A D891A	BamHI/ EccoR1	GM209	GM210
pGEX4 T1 GST- TEV	D.r. Spt16	613-930 N902S K905S I906S T909S	BamHI/ EccoR1	GM211	GM212
pGEX4 T1 GST- TEV	D.r. Spt16	F573A	Bam HI/ EcoR1	GM26	GM27
pGEX4 T1 GST- TEV	D.r. Spt16	583-813	BamHI/ EcoR1	GM41	GM44
pGEX4 T1 GST- TEV	D.r. Spt16	583-800	BamHI/ EcoR1	GM41	GM43
pGEX4 T1 GST- TEV	D.r. Spt16	801-C	BamHI/ EcoR1	GM42	GM46
pGEX4 T1 GST- TEV	D.r. Spt16	590-813	BamHI/ EccoR1	GM68	GM70
pGEX4 T1 GST- TEV	D.r. Spt16	590-895	BamHI/ EccoR1	GM68	GM71
pGEX4 T1 GST- TEV	D.r. Spt16	590-930	BamHI/ EccoR1	GM68	GM72
pGEX4 T1 GST- TEV	D.r. Spt16	613-813	BamHI/ EccoR1	GM69	GM70
pGEX4 T1 GST-	D.r. Spt16	613-895	BamHI/ EccoR1	GM69	GM71

TEV					
pGEX4 T1 GST- TEV	D.r. Spt16	613-930	BamHI/ EccoR1	GM69	GM72
RSF_D uet His- TEV	D.r. Spt16	519-930	BamHI/ EccoR1	GM77	GM78
pGEX4 T1 GST- TEV	D.r. Spt16	519-930	BamHI/ EccoR1	GM77	GM72
pGEX4 T1 GST- TEV	D.r. Spt16	590-895 K793,E794,E795A	BamHI/ EccoR1	GM79	GM80
pGEX4 T1 GST- TEV	D.r. Spt16	613-895 K793,E794,E795A	BamHI/ EccoR1	GM79	GM80
pGEX4 T1 GST- TEV	D.r. Spt16	590-930 K793,E794,E795A	BamHI/ EccoR1	GM79	GM80
pGEX4 T1 GST- TEV	D.r. Spt16	613-930 K793,E794,E795A	BamHI/ EccoR1	GM79	GM80
pGEX4 T1 GST- TEV	D.r. Spt16	1-924	BamHI/ EcoR1	GM96	GM97
pGEX4 T1 GST- TEV	D.r. Spt16	FL	BamHI/ EcoR1		
RSF_D uet His- TEV	D.r. SSRP1	104-429	Bgl II/ Not I	DTH10 02	DTH10 03
RSF_D uet His- TEV	D.r. SSRP1	104-199	Bam HI/ EcoR1	DTH10 04	DTH67 9
RSF_D uet His- TEV	D.r. SSRP1	1-109	Bam HI/ EcoR1	DTH56 1	GM5
RSF_D uet His- TEV	D.r. SSRP1	1-132	Bam HI/ EcoR1	DTH56 1	GM6
RSF_D uet His- TEV	D.r. SSRP1	1-170	BamHI/ EcoR1	DTH56 1	GM21

pGEX4 T1 GST- TEV	D.r. SSRP1	1-424	BamHI/ EcoR1	DTH56 1	GM33
pGEX4 T1 GST- TEV	D.r. SSRP1	1-472	BamHI/ EcoR1	DTH56 1	GM34
RSF_D uet	D.r. SSRP1	1-472	BamHI/ EcoR1	DTH56 1	GM34
RSF_D uet	D.r. SSRP1	1-424	BamHI/ EcoR1	DTH56 1	GM33
RSF_D uet His- TEV	D.r. SSRP1	1-430	BamHI/ EcoR1	DTH56 1	GM73
RSF_D uet His- TEV	D.r. SSRP1	1-199 C-S Q52A, K63A, I71A	BamHI/ EcoR1	DTH56 1	DTH67 9
RSF_D uet His- TEV	D.r. SSRP1	1-199 C-S Q52A, K63A, I71E	BamHI/ EcoR1	DTH56 1	DTH67 9
RSF_D uet His- TEV	D.r. SSRP1	1-199 Q52A, K63A, I71A	BamHI/ EcoR1	DTH56 1	DTH67 9
RSF_D uet His- TEV	D.r. SSRP1	1-199 Q52A, K63A, I71E	BamHI/ EcoR1	DTH56 1	DTH67 9
RSF_D uet His- TEV	D.r. SSRP1	100-175 WT	BamHI/ EcoR1	GM124	GM125
RSF_D uet His- TEV	D.r. SSRP1	100-175 C139S	BamHI/ EcoR1	GM124	GM125
RSF_D uet C- Term- His	D.r. SSRP1	1-430	NcoI/ EcoR1	GM126	GM127
RSF_D uet His- TEV	D.r. SSRP1	1-173 C57,C103,C139S	BamHI/ EcoR1	DTH56 1	DTH67 8
RSF_D uet His- TEV	D.r. SSRP1	1-199 C57,C103,C139S	BamHI/ EcoR1	DTH56 1	DTH67 9
pGEX4 T1 GST- TEV	Hu Spt16	508-580	BamHI/ EcoR1	DTH10 08	DTH10 11
pGEX4 T1 GST- TEV	Hu Spt16	518-580	BamHI/ EcoR1	DTH10 09	DTH10 11

pGEX4 T1 GST- TEV	Hu Spt16	518-919	BamHI/ NotI	DTH10 09	GM31
pGEX4 T1 GST- TEV	Hu Spt16	518-952	BamHI/ NotI	DTH10 09	GM30
pGEX4 T1 GST- TEV	Hu Spt16	518-1013	BamHI/ NotI	DTH10 09	GM32
pGEX4 T1 GST- TEV	Hu Spt16	556-580	BamHI/ EcoRI	DTH10 10	DTH10 11
pGEX4 T1 GST- TEV	Hu Spt16	456-919	BamHI/ NotI	DTH24 6	GM31
pGEX4 T1 GST- TEV	Hu Spt16	456-952	BamHI/ NotI	DTH24 6	GM30
pET3a	Hu Spt16	508-580	NdeI/ BamHI	DTH66 4	DTH10 06
pET3a	Hu Spt16	556-580	NdeI/Ba mHI	DTH66 6	DTH10 06
pGEX4 T1 GST- TEV	Hu Spt16	564-799	Bam HI/ NotI	GM10	DTH24 9
pGEX4 T1 GST- TEV	Hu Spt16	556-580, Y567A	BamHI/ EcoRI	GM11	GM12
pGEX4 T1 GST- TEV	Hu Spt16	556-580, R569A	BamHI/ EcoRI	GM13	GM14
pGEX4 T1 GST- TEV	Hu Spt16	1-510 Y243D I246D	BamHI/ NotI	GM136	GM137
pGEX4 T1 GST- TEV	Hu Spt16	556-580, F572A	BamHI/ EcoRI	GM15	GM16
pGEX4 T1 GST- TEV	Hu Spt16	556-580, Y567A; R569A; F572A	BamHI/ EcoRI	GM17	GM18

pGEX4 T1 GST- TEV	Hu Spt16	F572A	BamHI/ NotI	GM24	GM25
pGEX4 T1 GST- TEV	Hu Spt16	589-888	BamHI/ NotI	GM61	GM65
pGEX4 T1 GST- TEV	Hu Spt16	589-927	BamHI/ NotI	GM61	GM66
pGEX4 T1 GST- TEV	Hu Spt16	611-888	BamHI/ NotI	GM62	GM65
pGEX4 T1 GST- TEV	Hu Spt16	611-927	BamHI/ NotI	GM62	GM66
pGEX4 T1 GST- TEV	Hu Spt16	937-C	BamHI/ EcoRI	GM63	GM67
pGEX4 T1 GST- TEV	Hu Spt16	899-C	BamHI/ EcoRI	GM64	GM67
RSF_D uet His- TEV	Hu Spt16	518-927	BamHI/ NotI	GM75	GM76
pGEX4 T1 GST- TEV	Hu Spt16	1-923	BamHI/ NotI	GM90	GM91
pGEX4 T1 GST- TEV	Hu Spt16	1-927	BamHI/ NotI	GM90	GM66
pGEX4 T1 GST- TEV	Hu Spt16	FL	BamHI/ NotI		
RSF_D uet	Hu Spt16	582-812	BamHI/ NotI	DTH54 7	DTH54 9
RSF_D uet His- TEV	Hu SSRP1	1-433	BglIII/ XhoI	DTH14 9	DTH25 2
RSF_D uet His- TEV	Hu SSRP1	1-197 C-S Q52A, K63A, I71A	BglIII/ NotI	DTH14 9	DTH66 9

RSF_D uet His- TEV	Hu SSRP1	1-197 C-S Q52A, K63A, I71E	BglIII/ NotI	DTH14 9	DTH66 9
RSF_D uet His- TEV	Hu SSRP1	1-197 Q52A, K63A, I71A	BglIII/ NotI	DTH14 9	DTH66 9
RSF_D uet His- TEV	Hu SSRP1	1-197 Q52A, K63A, I71E	BglIII/ NotI	DTH14 9	DTH66 9
pCAL-n Th	Hu SSRP1	1-174 C103,C139S	BglII/ XhoI	DTH14 9	GM123
RSF_D uet	Hu SSRP1	FL C-S	BglII/ XhoI	DTH67 2	DTH67 3
RSF_D uet His- TEV	Hu SSRP1	100-174 C139S	BamHI/ XhoI	GM122	GM123
RSF_D uet His- TEV	Hu SSRP1	100-174 WT	BamHI/ XhoI	GM122	GM123
RSF_D uet His- TEV	Hu SSRP1	104-197	Bgl II/ Not I	DTH10 02	DTH66 9
RSF_D uet His- TEV	Hu SSRP1	104-428	Bgl II/ Not I	DTH10 02	DTH10 03
RSF_D uet His- TEV	Hu SSRP1	104-160	Bgl II/ Not I	DTH10 02	GM7
RSF_D uet His- TEV	Hu SSRP1	1-174 C103,C139S	BglII/ XhoI	DTH14 9	GM123
RSF_D uet His- TEV	Hu SSRP1	1-197 C103,C139S	Bgl II/ Not I	DTH14 9	DTH66 9
RSF_D uet His- TEV	Hu SSRP1	1-102	Bgl II/ Not I	DTH14 9	GM3
RSF_D uet His- TEV	Hu SSRP1	1-122	Bgl II/ Not I	DTH14 9	GM4
RSF_D uet His- TEV	Hu SSRP1	1-160	Bgl II/ Not I	DTH14 9	GM7
RSF_D uet His- TEV	Hu SSRP1	1-158	Bgl II/ Not I	DTH14 9	GM18b
RSF_D uet His- TEV	Hu SSRP1	1-170	Bgl II/ Not I	DTH14 9	GM19
RSF_D uet His- TEV	Hu SSRP1	196-433	Bgl II/ Xho I	GM8	DTH25 2

RSF_D uet His- TEV	Hu SSRP1	150-433	Bgl II/ Xho I	GM9	DTH25 3
pGEX4 T1 GST- TEV	HU-spt16	456-799	BamHI/ Not1	DTH24 6	DTH24 9
pGEX4 T1 GST- TEV	Sc Asf1	1-169	BamHI/ EcoR1	GM92	GM93
RSF_D uet His- TEV	Sc H2A	16-106	BamHI/ EcoR1	GM98	GM99
RSF_D uet His- TEV	Sc H2A/H2B	16-106/37-128	Nco1/ Xho1	GM106	GM107
pET Duet-1	Sc H2A/H2B	16-106/37-128	Nco1/ Xho1	GM106	GM107
pET Duet-1	Sc H2A/H2B	FL	Nco1/ Xho1	GM81	GM82
RSF_D uet His- TEV	Sc H2B	37-128	BglIII/ Xho1	GM100	GM101
RSF_D uet His- TEV	Sc H3 HHT2	38-134	BamHI/ EcoR1	GM102	GM103
RSF_D uet His- TEV	Sc H3 HHT2/H4	38-134/20-104	Nco1/ Xho1	GM108	GM109
pET Duet-1	Sc H3 HHT2/H4	38-134/20-104	Nco1/ Xho1	GM108	GM109
pET Duet-1	Sc H3 HHT2/H4	FL	Nco1/ Xho1	GM83	GM84
RSF_D uet His- TEV	Sc H4	20-104	BglIII/ Xho1	GM104	GM105
pGEX4 T1 GST- TEV	Sc Nap1	1-365	BamHI/ Not1	GM94	GM95
RSF_D uet His- TEV	Sc POB3	1-474	BamHI/ EcoR1	DTH42 3	GM74
RSF_D uet His- TEV	Sc Pob3	1-167	BamHI/ EcoR1	DTH42 3	GM22
RSF_D uet His- TEV	Sc Pob3	1-180	BamHI/ EcoR1	DTH42 3	GM23
RSF_D uet His- TEV	Sc Pob3	1-187 C61S	BamHI/ EcoR1	DTH42 3	DTH68 6

TEV					
RSF_D uet His- TEV	Sc Pob3	1-241 C61S	BamHI/ EcoR1	DTH42 3	DTH68 7
pGEX4 T1 GST- TEV	Sc Spt16	F596A	BamHI/ Xho1	GM28	GM29
pGEX4 T1 GST- TEV	Sc Spt16	619-833	BamHI/ EcoR1	GM49	GM51
pGEX4 T1 GST- TEV	Sc Spt16	633-833	BamHI/ EcoR1	GM50	GM51
pGEX4 T1 GST- TEV	Sc Spt16	633-918	BamHI/ EccoR1	GM57	GM59
pGEX4 T1 GST- TEV	Sc Spt16	633-955	BamHI/ EccoR1	GM57	GM60
pGEX4 T1 GST- TEV	Sc Spt16	1-958	BamHI/ Not1	GM85	GM86
pGEX4 T1 GST- TEV	Sc Spt16	1-955	BamHI/ Not1	GM85	GM87
pGEX4 T1 GST- TEV	Sc Spt16	FL	BamHI/ Xho1	DTH42 1	DTH42 2
pGEX4 T1 GST- TEV	Sc Spt16	633-816	BamHI/ EccoR1	GM57	GM58
RSF_D uet His- TEV	T4 D.d. SSRP1	1-187 3A T4	BamHI/ EcoR1	GM169	GM183
RSF_D uet His- TEV	T4 D.d. SSRP1	1-187 4A T4	BamHI/ EcoR1	GM169	GM182
RSF_D uet His- TEV	T4 D.d. SSRP1	T4 1-187	BamHI/ EcoR1	GM172	GM148
RSF_D uet His- TEV	T4 D.d. SSRP1	T4 2A 1-187	BamHI/ EcoR1	GM172	GM148

TEV					
RSF_D uet His- TEV	T4 D.d. SSRP1	T4 2A 1-187 3A T4	BamHI/ EcoR1	GM172	GM183
RSF_D uet His- TEV	T4 D.d. SSRP1	T4 2A 1-187 4A T4	BamHI/ EcoR1	GM172	GM182
RSF_D uet His- TEV	T4 D.d. SSRP1	T4 1-187/3A T4	BamHI/ EcoR1	GM173	GM183
RSF_D uet His- TEV	T4 D.d. SSRP1	T4 1-187/4A T4	BamHI/ EcoR1	GM173	GM182
RSF_D uet His- TEV	T4 D.d. SSRP1	T4 2A 6-187	BamHI/ EcoR1	GM174	GM148
RSF_D uet His- TEV	T4 D.d. SSRP1	T4 2A 6-187 3A T4	BamHI/ EcoR1	GM174	GM183
RSF_D uet His- TEV	T4 D.d. SSRP1	T4 2A 6-187 4A T4	BamHI/ EcoR1	GM174	GM182
RSF_D uet His- TEV	T4 D.d. SSRP1	T4 6-187	BamHI/ EcoR1	GM175	GM148
RSF_D uet His- TEV	T4 D.d. SSRP1	T4 6-187 3A T4	BamHI/ EcoR1	GM175	GM183
RSF_D uet His- TEV	T4 D.d. SSRP1	T4 6-187 4A T4	BamHI/ EcoR1	GM175	GM182
RSF_D uet	Widom 601	1, 2 or 4 insert EcoRV	EcoRV	GM37	GM38
pGEM3 Z-601	Widom 601		EcoRV	GM39	GM40
RSF_D uet His- TEV	X1 H2A	16-106	BamHI/ EcoR1	GM110	GM111
RSF_D uet His- TEV	X1 H2A/H2B	16-106/36-127	Nco1/ Xho1	GM118	GM119
pET Duet-1	X1 H2A/H2B	16-106/36-127	Nco1/ Xho1	GM118	GM119
RSF_D uet His- TEV	X1 H2B	36-127	BglIII/ Xho1	GM112	GM113
RSF_D uet His- TEV	X1 H3	38-137	BamHI/ EcoR1	GM114	GM115
RSF_D uet His-	X1 H3/H4	38-137/20-104	Nco1/ Xho1	GM120	GM121

TEV					
pET Duet-1	X1 H3/H4	38-137/20-104	NcoI/ XhoI	GM120	GM121
RSF_D uet His- TEV	X1 H4	20-104	BglII/ XhoI	GM 116	GM 117

7.2 Appendix 2 oligo list

code	oligo sequence
DTH687	cgGAATTCcatgcatcaccagcgacttccccg
DTH686	cgGAATTCcagttttcatcgacgtttgttgaataac
DTH679	cgGAATTCcaagcgtctccagtagcttgaatg
DTH678	cgGAATTCcagtctccagtgtttggcgggac
DTH561	cgGGATCCatgggagacactctggagttaacg
DTH549	atagttaGCGCCGttacatataggagctccgttaaatccc
DTH547	cgGGATCCaatgaaggcaacatcttcctaacc
DTH423	cgGGATCCatgagtaccgactttgatagaatttac
DTH422	ccgCTCGAGctaattctctaaagttgcaccctatc
DTH421	cgGGATCCatggaagagctgaatattgattttgac
DTH249	atagttaGCGCCGttacacttcaaattccagttcctcc
DTH246	cgGGATCCcgggcagcattacttacagaaag
DTH1039	aatccatctagtggatTTCaccttgatttttggtat
DTH1038	atacaaaaatcaaggtGAAatccaactagatggatt
DTH1037	tttttggtatttatCGCcaagtcgtaacccc
DTH1036	ggggttacgacttgGCGataaatacaaaaa
DTH1035	ccatctagttggatCGCaccttgatttttg
DTH1034	caaaaaatcaaggtGCGatccaactagatgg
DTH1033	agcccactccaCGCgacggtagataat
DTH1032	attatctaccgtcGCGtgtagtaggggct
DTH1031	gccatcatacttgtaTTCatggccattctttgt
DTH1030	acaagaatggccatGAAatacaagtatgatggc
DTH1029	tctttgtaagcagCGCaagtccatggccc
DTH1028	gggcatggacttGCGctgcttacaaga
DTH1027	ccatcatacttgtaCGCatggccattctttg
DTH1026	caaagaatggccatGCGtacaagtatgatgg
DTH1025	aacacggcgccaGGCaccttctgttaa
DTH1024	ttaacagaaggtGCctggcgccgtgtt
DTH1023	ccgtcatatttgtaTTCgtgtccagtgtg
DTH1022	cagcactggacacGAAatacaaatatgacgg
DTH1021	tggtggccagCGCgagcccatga
DTH1020	tcatgggctcGCGctggccacca
DTH1019	cgatcatatttgtaGGCgtgtccagtgtg
DTH1018	cagcactggacacGCtacaaatatgacg
DTH1017	ctcgacgccaCGCggcctcggag
DTH1016	ctccgaggccGCGtggtcgtcag
DTH1015	cgGAATTCctaccccagagagctgcctggc
DTH1014	cgGGATCCggcggcagcaacatcagtatgtctgtggaagg
DTH1013	cgGGATCCggcggcagcatgccaaggagaaggacatcag
GM37	ctggagaatcccgtgccc
GM38	acaggatgtatataatctgacacg
GM39	atcgagaatcccgtgccc
GM40	atcggatgtatataatctgacacg

GM41	cgGGATCCcagagggcaacatcttccta
GM42	cgGGATCCccttcagagatcttgggttc
GM43	cgGAATTCctaacctcgaactccagctcct
GM44	cgGAATTCctacctgtagggggcgccc
GM45	cgGAATTCctacctggcctcctcctcc
GM46	cgGAATTCctattaatgtcgcctcttcttctgctg
GM47	cgGGATCCcggaaactgaaagatctatacattcgcc
GM48	cgGGATCCaaccagacagaaattccaaaattttaagaa
GM49	cgGGATCCgacaatcaattgtacgttcgattacac
GM50	cgGGATCCggtgaccgcatgagtgaaacct
GM51	cgGAATTCtagcccaaatctctaaatgtattctcc
GM52	atagttaGCGGCCGctagcccaaatctctaaatgtattctcc
GM53	AGATCTCAATTGgatatcCGGGATCCTAATGACCAAGG
GM54	GTCATTAGGATCCCGgatatcGGGAGCTCGGAACACTATCC
GM55	GTGTTCCGAGCTCCCgatatcCGGGATCCTAATGACCAAGG
GM56	GCGTGGCCGGCCgatatcGGGAGCTCGGAACACTATCC
GM57	GTATTTTCAGGGATCCGGTGACCGCATGAGTGAAACCT
GM58	GTCGACCCGGAATTCCTATGCGATTGCGTCTGCAAATAC
GM59	GTCGACCCGGAATTCCTAATCCATATCTGTTAACCCTGCTTC
GM60	GTCGACCCGGAATTCCTAAGTAGCCAGAAAATCCAACCACC
GM61	GTATTTTCAGGGATCCAACCCTGAAGCGACTTTTGTCAAGG
GM62	GTATTTTCAGGGATCCCAGACAGTACCAGCCTTGAACC
GM63	GTATTTTCAGGGATCCGGGATTCAGAGTCTGAAATTGAAG
GM64	GTATTTTCAGGGATCCTCCCTCAACTGGACTAAAATCATGA
GM65	AGTCACGATGCGGCCGCTAGGAATTCAACCATTCTTGATGGG
GM66	AGTCACGATGCGGCCGCTAAGGCTCCAGGAAAGACCAG
GM67	GTCGACCCGGAATTCctattactcctcttttcttgggTgg
GM68	GTATTTTCAGGGATCCAATCCCGAGGCCACATTTGTCA
GM69	GTATTTTCAGGGATCCTCTGTGCCCTCCACCAACC
GM70	GTCGACCCGGAATTCCTACCTGTAGGGGGCGCC
GM71	GTCGACCCGGAATTCCTAAGTGATTTGATATCACACGAGTTG
GM72	GTCGACCCGGAATTCCTAACTCTCAGGGTCCAGGAAAG
GM73	cgGAATTCtatcctctgttcttgatagtcagc
GM74	cgGAATTCtaattctcacccttaggttttagac
GM75	GTATTTTCAGGGATCCATGCCTAAGGAACCGCATATTC
GM76	AAGCATTATGCGGCCGCTAAGGCTCCAGGAAAGACCAG
GM77	GTATTTTCAGGGATCCATGCCCAAGGAGAAGGACATCA
GM78	CGCCGAGCTCGAATTCCTAACTCTCAGGGTCCAGGAAAG
GM79	tcgctcaccGcgGcgGcgctggagttc
GM80	gaactccagcGccGccGCggtgagcga
GM81	AGGAGATATACCATGGCGTCCGGTGGTAAAG
GM82	CTTTACCAGACTCGAGCTATTATGCTTGAGT
GM83	AGGAGATATACCATGGCCAGAACTAAACAAA
GM84	CTTTACCAGACTCGAGCTATTAACCACCGAA
GM85	GTATTTTCAGGGATCCATGGAAGAGCTGAATATTGATTTTGACG
GM86	AGTCACGATGCGGCCGCTAATCTGAACCAGTAGCCAGAAAATTC
GM87	AGTCACGATGCGGCCGCTAAGTAGCCAGAAAATCCAACCACCA

GM88	GTATTTTCAGGGATCCATGAGTACCGACTTTGATAGAATTTACTT
GM89	CGCCGAGCTCGAATTCCTATAGGTTTTAGACTTTAGGAATTGTTT
GM90	GTATTTTCAGGGATCCATGGCTGTGACTCTGGACAAAG
GM91	AGTCACGATGCGGCCGCCTAAGACCAGCCACCTTGTTCTGAAG
GM92	GTATTTTCAGGGATCCATGTCAATTGTTTCACTGTTAGGCA
GM93	GTCGACCCGGGAATTCCTATACGCCGGGCTGTTTCTGAG
GM94	GTATTTTCAGGGATCCATGTCAGACCCTATCAGAACGAAAC
GM95	AGTCACGATGCGGCCGCCTACAAGGCTGCGCCGGTAAA
GM96	GTATTTTCAGGGATCCATGGCGGTGAGTCTGGATAAA
GM97	GTCGACCCGGGAATTCCTAAGACCAGCCGCCCTGCT
GM98	GTATTTTCAGGGATCCtctcaatctagatctgctaaggctg
GM99	CGCCGAGCTCGAATTCCTAttgggcaatggtaacgttacccaat
GM100	TACATATGGCAGATCTTAGAAAGGAAACATACTCTTCTTACATT
GM101	CTTTACCAGACTCGAGCTAAGAGGAAGAGTACTTGTTAACAGCT
GM102	GTATTTTCAGGGATCCaagcctcacagatataagccaggta
GM103	CGCCGAGCTCGAATTCCTAttcacctcttagtcttctggccaat
GM104	TACATATGGCAGATCTtagaaagattctaagagataacatccaag
GM105	CTTTACCAGACTCGAGCTAaccaccgaaaccgtataaggttcta
GM106	AGGAGATATACCATGGCGtctcaatctagatctgctaaggctg
GM107	CTTTACCAGACTCGAGCTAAGAGGAAGAGTACTTGTTAACAGCT
GM108	AGGAGATATACCATGGCGaagcctcacagatataagccaggta
GM109	CTTTACCAGACTCGAGCTAaccaccgaaaccgtataaggttcta
GM110	GTATTTTCAGGGATCCaagactcgctcatctcggggc
GM111	CGCCGAGCTCGAATTCCTAgccctgggcatggtga
GM112	TACATATGGCAGATCTtgagagctacgccatctacgt
GM113	CTTTACCAGACTCGAGCTActtggcgctggtgtacttg
GM114	GTATTTTCAGGGATCCaaacccatcgctatcgccc
GM115	CGCCGAGCTCGAATTCCTAagccctctctcctcggatc
GM116	TACATATGGCAGATCTtaggaaggtgctcagggataac
GM117	CTTTACCAGACTCGAGCTAtccgccgaagccgtagag
GM118	AGGAGATATACCATGGCGaagactcgctcatctcggggc
GM119	CTTTACCAGACTCGAGCTActtggcgctggtgtacttg
GM120	AGGAGATATACCATGGCGaaacccatcgctatcgccc
GM121	CTTTACCAGACTCGAGCTAtccgccgaagccgtagag
GM122	GTATTTTCAGGGATCCaaggaccttgtgtgaagggt
GM123	CTTTACCAGACTCGAGCTAaccatctcctgggtgggtggg
GM124	GTATTTTCAGGGATCCaaggacatgtgtgaagggt
GM125	CGCCGAGCTCGAATTCCTAgccgtcgtctccagtgtt
GM126	AGGAGATATACCATGGgCgacactctggagttaacg
GM127	CGCCGAGCTCGAATTCCTAggtgatgatggtgatgTCCTCTGTTCTTGATAGTCAGC
GM128	AAGGAGATATACATATGGCGGTGAGTCTGGATAAAG
GM129	GTTAGCAGCCGGATCCCTAACTCTCAGGGTCCAGGAAAG
GM130	AAGGAGATATACATATGGGTCCTCGTGAAGCTACCT
GM131	GTTAGCAGCCGGATCCCTAGCCGCTGTCCTCTTCTTCT
GM132	CGCACCATTGAAACAgcGGcAgcGTCTAAGAGCGTG
GM133	CACGCTCTTAGACgcTgCCgcTGTTTCAATGGTGCG
GM134	GAAGAAGGTGGCgcGGcAgcGAAAGTGGGCGA

GM135	TCGCCCACTTTGgcTgCCgcGCCACCTTCTTC
GM136	ctgtggaaatgtgtGaTcctcctGATattcagagtgggtgg
GM137	ccaccactctgaatATCaggaggAtCacacatttccacag
GM138	CCTCCAATCCGCaAaGGCCAAACCAAA
GM139	TTTGGTTTGGCCtTtGCGGATTGGAGG
GM140	CCACTGACCAAGGTGGACAT
GM141	ATTGGTATCGAGTTCCAGGAGA
GM142	GACCGTGCTGTTTCCAATTT
GM143	GCAATTCTATATTGAGATCAGCGA
GM144	AAGAAGAAGAGGACAGCGGC
GM145	TATTCGCCCTAGCAAAGAGG
GM146	CAACTCCAGAGCGACAGC
GM147	GTATTTTCAGGGATCCAACCCTGTGTCTCAGTTCAACAATA
GM148	CGCCGAGCTCGAATTCCTACCCCTCTTTGCTAGGGCG
GM149	CGCCGAGCTCGAATTCCTAGCCGGTTGTAACAGGGTTC
GM150	ATGACGATGAGACCgaaGTTGAGATGCGCTT
GM151	AAGCGCATCTCAACTtcGGTCTCATCGTCAT
GM152	GATGAGACCATGgatGAGATGCGCTTC
GM153	GAAGCGCATCTCatcCATGGTCTCATC
GM154	TGTTGAGATGCGCgatTTCACCCCTATTTCG
GM155	CGAATAGGGGTGAAatcGCGCATCTCAACCA
GM156	GCAAAGTGGGTTaCGAGTTCCCAAT
GM157	ATTGGGAACTCGtAACCCTTTGC
GM158	ATGGCAAAGTGGGTgaaGAGTTCCCAATCAG
GM159	CTGATTGGGAACTctcACCCACTTTGCCAT
GM160	GCAAAGTGGGTgcCGAGTTCCCAAT
GM161	ATTGGGAACTCGgcACCCACTTTGC
GM162	TGTTGAGATGCGCgaaTTCACCCCTATTTCG
GM163	CGAATAGGGGTGAAttcGCGCATCTCAACCA
GM165	GTATTTTCAGGGATCCATGGCGGCAATTGAAAGTTTTGATC
GM166	CGCCGAGCTCGAATTCCTAGGTCCCCGGGATGTAGAA
GM167	CCTATGATCCAGgcCACCACAGATCAT
GM168	ATGATCTGTGGTGgcCTGGATCATAGG
GM169	GTATTTTCAGGGATCCATGAGCAGCTCTAGCAACCC
GM170	GTATTTTCAGGGATCCatgaatatatttgaatgttacgtatagatCa
GM171	CGCCGAGCTCGAATTCCTAatacgcgtcccaagtgccca
GM172	acttgggacgcgtatGCTGCAATGAGCAGCTCTAGCAACCC
GM173	acttgggacgcgtatATGAGCAGCTCTAGCAACCC
GM174	acttgggacgcgtatGCTGCAAACCCTGTGTCTCAGTTCAACAATA
GM175	acttgggacgcgtatAACCCCTGTGTCTCAGTTCAACAATA
GM176	GCTAGAGCTGCTCATTGCAGCatacgcgtcccaagtgccca
GM177	GCTAGAGCTGCTCATatacgcgtcccaagtgccca
GM178	CTGAGACACAGGGTTTGCAGCatacgcgtcccaagtgccca
GM179	CTGAGACACAGGGTTatacgcgtcccaagtgccca
GM180	CCTAGCAAAGAGGGGGCTGCAGCCGCCatgaatatatttgaatgttacgtatagatCa
GM181	CCTAGCAAAGAGGGGGCAGCCGCCatgaatatatttgaatgttacgtatagatCa
GM182	ttcaaatatattcatGGCGGCTGCAGCCCCCTCTTTGCTAGGGCGAA

GM183	ttcaaatatattcatGGCGGCTGCCCCCTCTTTGCTAGGGCGAA
GM184	TGAGCAGCAAGGGTgcCgcggcGGGCGAAGTGAAGGT
GM185	ACCTTCACTTCGCCGccgcGgcACCCTTGCTGCTCA
GM186	CATGGCAAAGTGGGTcgcGAGTTCCCAATCAGC
GM187	GCTGATTGGGAACtCgcACCCACTTTGCCATG
GM188	GATGACGATGAGACCgcGTTGAGcgcCGCTTCTTCACCCCT
GM189	AGGGGTGAAGAAGCGcgcCTCAACcgcGGTCTCATCGTCATC
GM190	GATGACGATGAGACCgcGTTGcGcgcgCCTTCTTCACCCCTATTGCC
GM191	GGCGAATAGGGGTGAAGAAGgcgcgCgCAACgcgGGTCTCATCGTCATC
GM192	GTATTTTCAGGGATCCGGTGAAGAGGATGAAGAGGAC
GM193	AAGGAGATATACATATGACCAAACtGCAGCCTATTTATAGCA
GM194	GTTAGCAGCCGGATCCCTATTGGGTGTAGCTGGTAGGG
GM195	GTATTTTCAGGGATCCACCAAACtGCAGCCTATTTATAGCA
GM196	GTCGACCCGGGAATTCTTATTGGGTGTAGCTGGTAGGG
GM197	GTATTTTCAGGGATCCGAAGTGAAGGTGAACGGCC
GM198	CGCCGAGCTCGAATTCGCCAGGAATGGTGATCTTCTTGCCGGTCAAGGCC
GM199	GTATTTTCAGGGATCCAGCCCTTTGGAGATTATTGAACTGA
GM200	CGCCGAGCTCGAATTCGCCAACGTTGCTACCATGTC
GM201	GTATTTTCAGGGATCCggcggcagcggcACCAAACtGCAGCCTATTTATAGCA
GM202	GTATTTTCAGGGATCCggcggcagcggcAGCCCTTTGGAGATTATTGAACTGA
GM203	GTATTTTCAGGGATCCCCTGCCATGATCATCGATGATGA
GM204	CGCCGAGCTCGAATTCCTATTACTTTTTCTGCTTCTTCTTGCC
GM205	GTCGACCCGGGAATTCTTAGCCAACGTTGCTACCATGTC
GM206	GTCGACCCGGGAATTCTTACCCTCTTTGCTAGGGCG
GM207	GTCGACCCGGGAATTCTTAGCCGGTTGTAACAGGGTTC
GM208	CGCCGAGCTCGAATTCCTAGCCAGGAATGGTGATCTTCTTGCCGGTCAAGGCC
GM209	atcaaagagtggctcGCGGcgtgtgCGatCaaatacactgaaggc
GM210	gccttcagtgtatttGatCGcacacGCCGcgagccactctttgat
GM211	tctttgaGctggaccaGCaGcatgaagaGcatagtg
GM212	cactatgCtctcatgCtGcTggtccagCtcaaaga

7.3 Appendix 3 histone peptides

Peptide	Sequence
H4	MSGRGKGGKGLGKGGAKRHRKVLVDN
H3	MARTKQTARKSTGGKAPRKQLATKAARKSAPSTGGVKK

7.4 Appendix 4. Purity of SSRP1 and FACT variants.

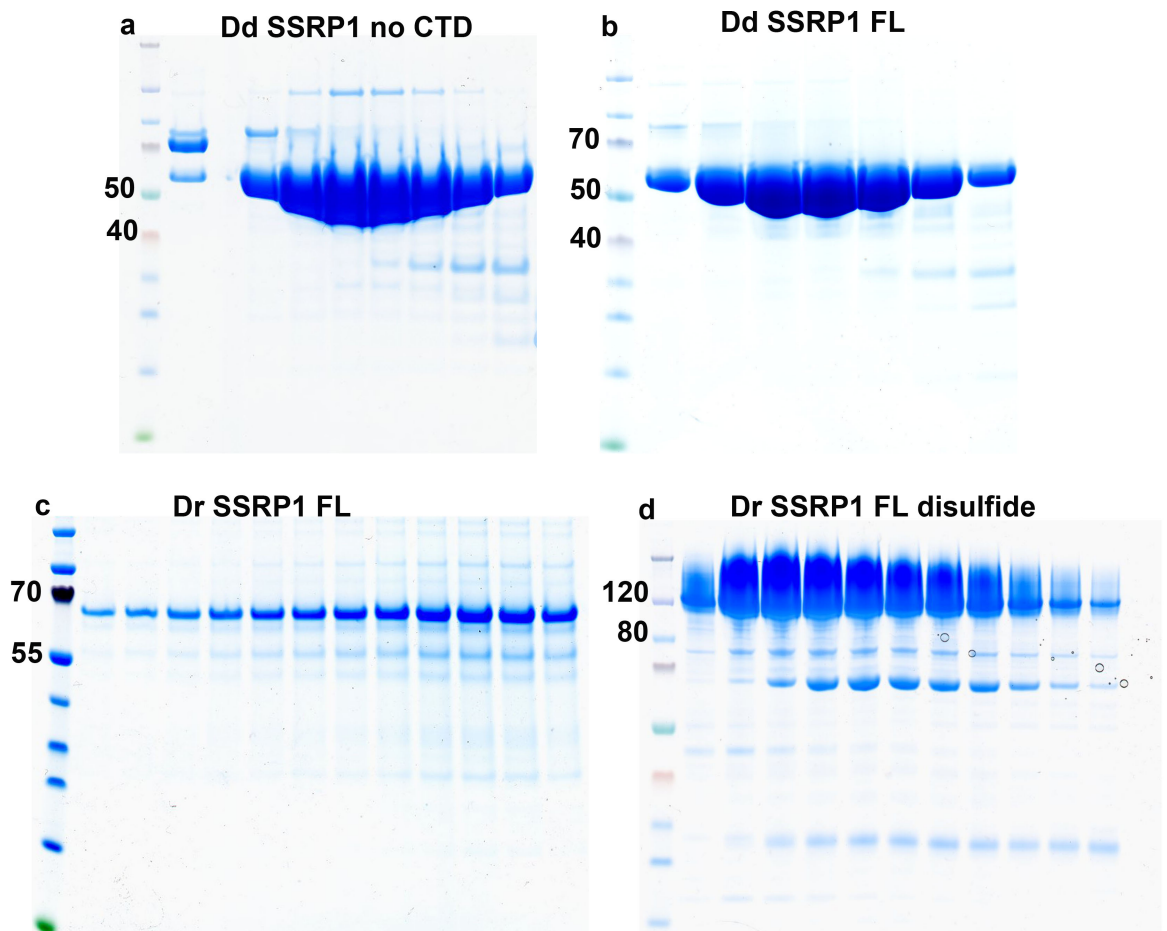


Figure 7-1 Purity of Dd and Dr SSRP1 FL and Δ CTD

Gels show the purity of the proteins after the final step, size-exclusion chromatography (SD200). (a) Purification of Dd SSRP1 Δ CTD, (b) purification of Dd SSRP1 FL, (c) purification of Dr SSRP1 FL and (d) purification of Dr SSRP1 FL with oxidised.

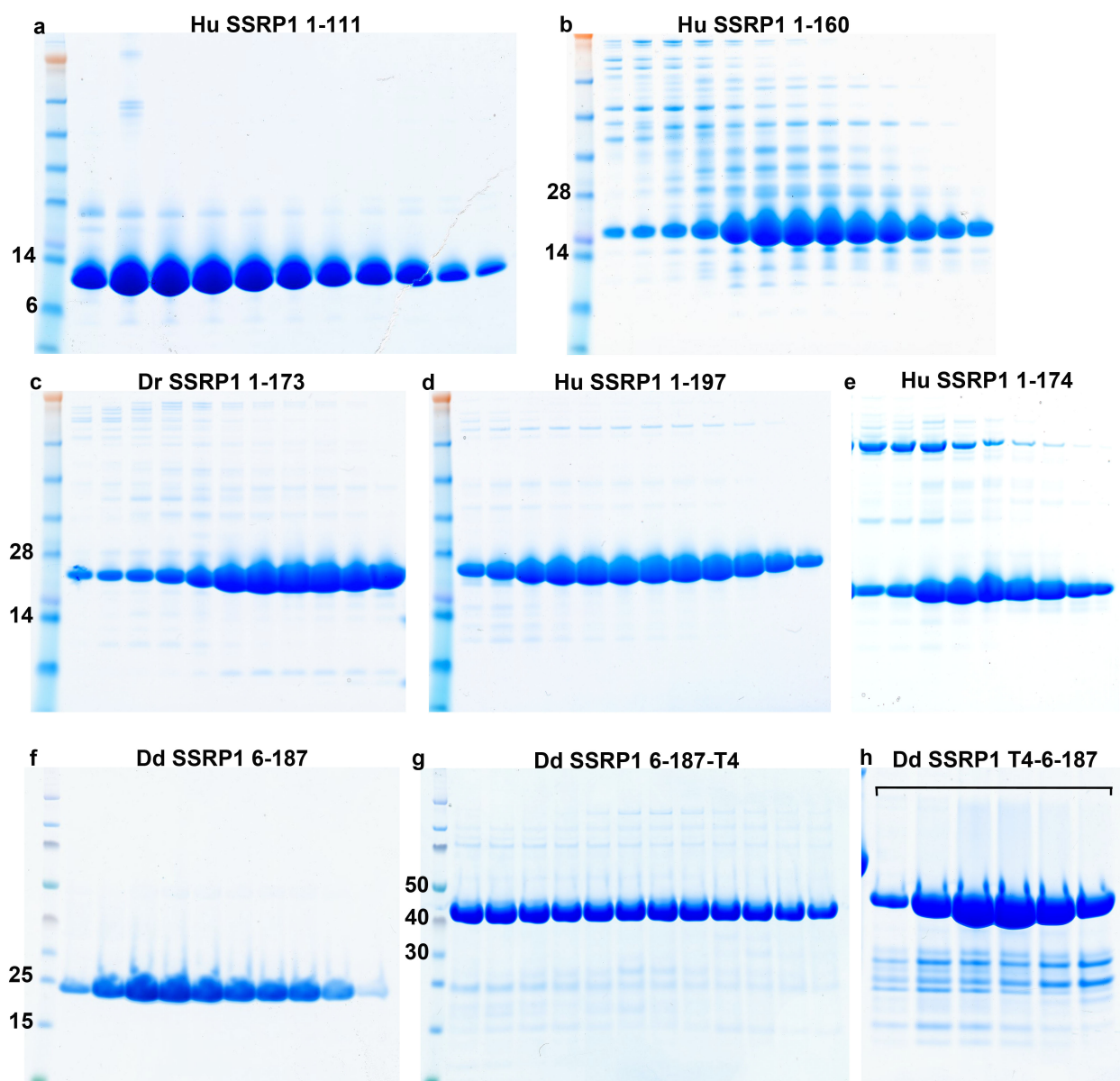


Figure 7-2 Purity of Hu, Dr and Dd SSRP1 N-terminal/DD.

Gels show the purity of the proteins after the final step, size-exclusion chromatography (SD200). (a) Purification of Hu SSRP1 1-111, (b) purification of Hu SSRP1 1-160, (c) purification of Dr SSRP1 1-173, (d) purification of Hu SSRP1 1-197, (e) purification of Hu SSRP1 1-174, (f) purification of Dd SSRP1 6-187, (g) purification of Dd SSRP1 6-187-T4 and (h) purification of Dd SSRP1 T4-6-187.

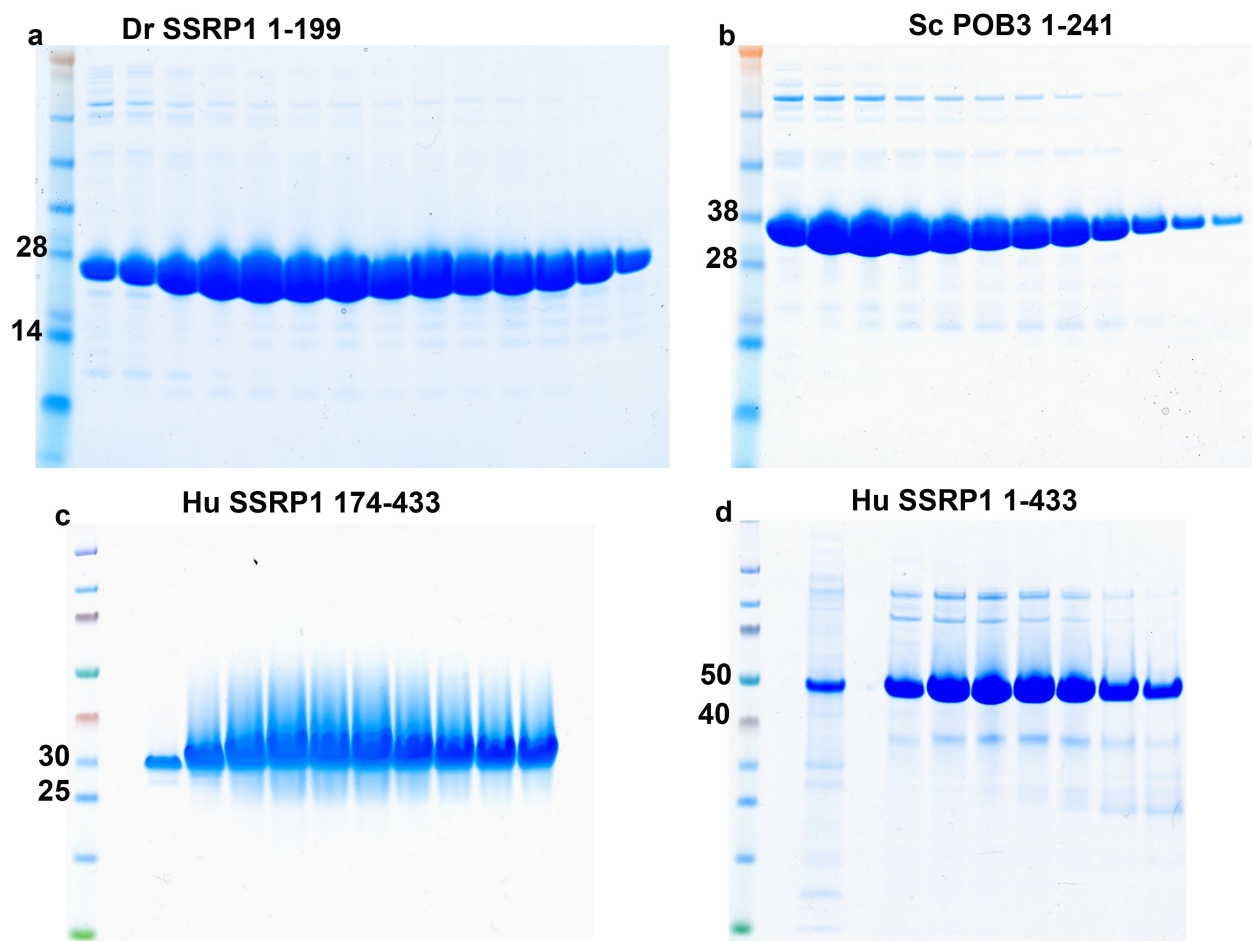


Figure 7-3 Purity of Hu, Dr and Sc SSRP1 N-terminal/DD, MD and Δ CTD

Gels show the purity of the proteins after the final step, size-exclusion chromatography (SD200). (a) Purification of Dr SSRP1 1-199, (b) purification of Sc SSRP1 1-241, (c) purification of Hu SSRP1 174-433 and (d) purification of Hu SSRP1 1-433.

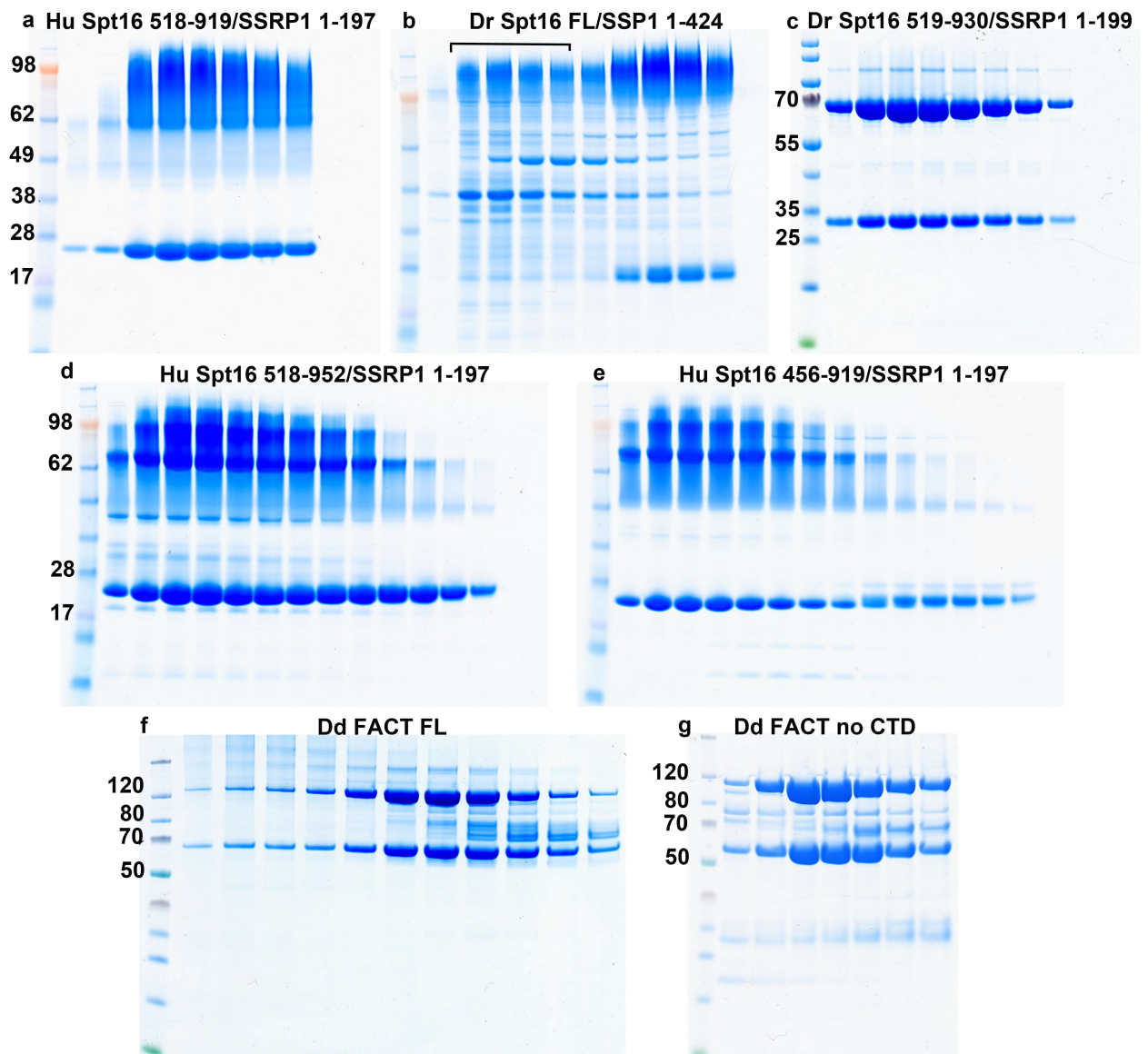


Figure 7-4 Purity of Hu, Dr and Dd FACT constructs.

Gels show the purity of the proteins after the final step, size-exclusion chromatography (SD200). (a) Purification of Hu Spt16 518-919/SSRP1 1-197, (b) purification of Dr Spt16 FL/SSRP1 1-424, (c) purification of Dr Spt16 519-930/SSRP1 1-199, (d) purification of Hu Spt16 518-952/SSRP1 1-197, (e) purification of Hu Spt16 456-919/SSRP1 1-197, (f) purification of Dd Spt16 FL/SSRP1 FL and (g) purification of Dd Spt16 Δ CTD /SSRP1 Δ CTD.

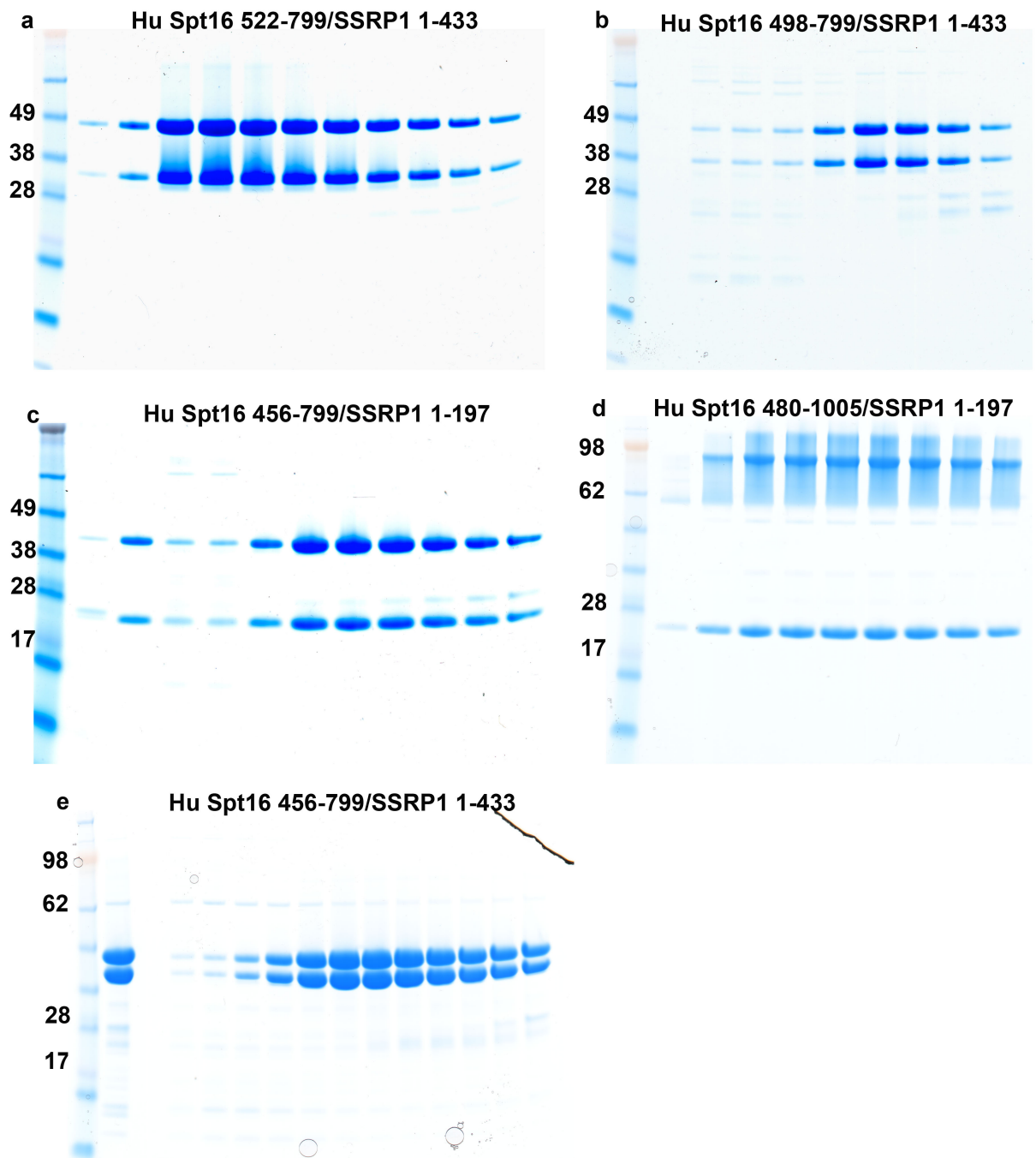


Figure 7-5 Purity of Hu FACT constructs

Gels show the purity of the proteins after the final step, size-exclusion chromatography (SD200). (a) Purification of Hu Spt16 522-799/SSRP1 1-433, (b) purification of Hu Spt16 498-799/SSRP1 1-433, (c) purification of Hu Spt16 456-799/SSRP1 1-197, (d) purification of Hu Spt16 480-1005/SSRP1 1-197 and (e) purification of Hu Spt16 456-799/SSRP1 1-433. Samples Hu Spt16 456-799/SSRP1 1-197, Hu Spt16 498-799/SSRP1 1-433 and 456-799/SSRP1 1-433 had a fraction of aggregated protein, probably due to the fact that residues 799 is cutting Spt16 MD on its second PH domain.

8 Bibliography

1. Bjerling, A. R. a. P. (2013) The links between chromatin spatial organization and biological function. *Biochemical Society Transactions* **41**, (1634–1639)
2. Luger, K., Mader, A. W., Richmond, R. K., Sargent, D. F., and Richmond, T. J. (1997) Crystal structure of the nucleosome core particle at 2.8 Å resolution. *Nature* **389**, 251-260
3. McGhee, J. D., and Felsenfeld, G. (1980) Nucleosome structure. *Annu Rev Biochem* **49**, 1115-1156
4. Richmond, T. J., and Davey, C. A. (2003) The structure of DNA in the nucleosome core. *Nature* **423**, 145-150
5. Oohara, I., and Wada, A. (1987) Spectroscopic studies on histone-DNA interactions. II. Three transitions in nucleosomes resolved by salt-titration. *J Mol Biol* **196**, 399-411
6. Wilhelm, F. X., Wilhelm, M. L., Erard, M., and Duane, M. P. (1978) Reconstitution of chromatin: assembly of the nucleosome. *Nucleic Acids Res* **5**, 505-521
7. Elsasser, S. J., and D'Arcy, S. Towards a mechanism for histone chaperones. *Biochim Biophys Acta* **1819**, 211-221
8. Malik, H. S., and Henikoff, S. (2003) Phylogenomics of the nucleosome. *Nat Struct Biol* **10**, 882-891
9. Allshire, R. C., and Karpen, G. H. (2008) Epigenetic regulation of centromeric chromatin: old dogs, new tricks? *Nat Rev Genet* **9**, 923-937
10. Skene, P. J., and Henikoff, S. (2013) Histone variants in pluripotency and disease. *Development* **140**, 2513-2524
11. Kalocsay, M., Hiller, N. J., and Jentsch, S. (2009) Chromosome-wide Rad51 spreading and SUMO-H2A.Z-dependent chromosome fixation in response to a persistent DNA double-strand break. *Mol Cell* **33**, 335-343
12. Hua, S., Kallen, C. B., Dhar, R., Baquero, M. T., Mason, C. E., Russell, B. A., Shah, P. K., Liu, J., Khramtsov, A., Tretiakova, M. S., Krausz, T. N., Olopade, O. I., Rimm, D. L., and White, K. P. (2008) Genomic analysis of estrogen cascade reveals histone variant H2A.Z associated with breast cancer progression. *Mol Syst Biol* **4**, 188
13. Hou, H., Wang, Y., Kallgren, S. P., Thompson, J., Yates, J. R., 3rd, and Jia, S. (2010) Histone variant H2A.Z regulates centromere silencing and chromosome segregation in fission yeast. *J Biol Chem* **285**, 1909-1918
14. Conerly, M. L., Teves, S. S., Diolaiti, D., Ulrich, M., Eisenman, R. N., and Henikoff, S. (2010) Changes in H2A.Z occupancy and DNA methylation during B-cell lymphomagenesis. *Genome Res* **20**, 1383-1390
15. Santisteban, M. S., Kalashnikova, T., and Smith, M. M. (2000) Histone H2A.Z regulates transcription and is partially redundant with nucleosome remodeling complexes. *Cell* **103**, 411-422
16. Kornberg, R. D. (1977) Structure of chromatin. *Annu Rev Biochem* **46**, 931-954
17. Heitz, E. (1928) Das Heterochromatin der Moose. *Jahrb. Wiss. Bot* **69**, 762-818
18. Heitz, E. (1929) heterochromatin, Chromocentren, Chromomeren (Vorläufige Mitteilung). *Ber. Dtsch. Bot. Ges.* **47**, 274-284

19. Grewal, S. I., and Jia, S. (2007) Heterochromatin revisited. *Nat Rev Genet* **8**, 35-46
20. Grunstein, M. (1998) Yeast heterochromatin: regulation of its assembly and inheritance by histones. *Cell* **93**, 325-328
21. Kent, W. J., Sugnet, C. W., Furey, T. S., Roskin, K. M., Pringle, T. H., Zahler, A. M., and Haussler, D. (2002) The human genome browser at UCSC. *Genome Res* **12**, 996-1006
22. Trojer, P., and Reinberg, D. (2007) Facultative heterochromatin: is there a distinctive molecular signature? *Mol Cell* **28**, 1-13
23. Filion, G. J., van Bommel, J. G., Braunschweig, U., Talhout, W., Kind, J., Ward, L. D., Brugman, W., de Castro, I. J., Kerkhoven, R. M., Bussemaker, H. J., and van Steensel, B. (2010) Systematic protein location mapping reveals five principal chromatin types in *Drosophila* cells. *Cell* **143**, 212-224
24. Allfrey, V. G., Faulkner, R., and Mirsky, A. E. (1964) Acetylation and Methylation of Histones and Their Possible Role in the Regulation of Rna Synthesis. *Proc Natl Acad Sci U S A* **51**, 786-794
25. Kouzarides, T. (2007) Chromatin modifications and their function. *Cell* **128**, 693-705
26. Sterner, D. E., and Berger, S. L. (2000) Acetylation of histones and transcription-related factors. *Microbiology and molecular biology reviews : MMBR* **64**, 435-459
27. Tjeertes, J. V., Miller, K. M., and Jackson, S. P. (2009) Screen for DNA-damage-responsive histone modifications identifies H3K9Ac and H3K56Ac in human cells. *EMBO J* **28**, 1878-1889
28. Bannister, A. J., and Kouzarides, T. (2011) Regulation of chromatin by histone modifications. *Cell research* **21**, 381-395
29. Dawson, M. A., Bannister, A. J., Gottgens, B., Foster, S. D., Bartke, T., Green, A. R., and Kouzarides, T. (2009) JAK2 phosphorylates histone H3Y41 and excludes HP1alpha from chromatin. *Nature* **461**, 819-822
30. Oki, M., Aihara, H., and Ito, T. (2007) Role of histone phosphorylation in chromatin dynamics and its implications in diseases. *Sub-cellular biochemistry* **41**, 319-336
31. Ng, S. S., Yue, W. W., Oppermann, U., and Klose, R. J. (2009) Dynamic protein methylation in chromatin biology. *Cellular and molecular life sciences : CMLS* **66**, 407-422
32. Bannister, A. J., Schneider, R., and Kouzarides, T. (2002) Histone methylation: dynamic or static? *Cell* **109**, 801-806
33. Shi, Y., Lan, F., Matson, C., Mulligan, P., Whetstine, J. R., Cole, P. A., Casero, R. A., and Shi, Y. (2004) Histone demethylation mediated by the nuclear amine oxidase homolog LSD1. *Cell* **119**, 941-953
34. Cuthbert, G. L., Daujat, S., Snowden, A. W., Erdjument-Bromage, H., Hagiwara, T., Yamada, M., Schneider, R., Gregory, P. D., Tempst, P., Bannister, A. J., and Kouzarides, T. (2004) Histone deimination antagonizes arginine methylation. *Cell* **118**, 545-553
35. Wang, Y., Wysocka, J., Sayegh, J., Lee, Y. H., Perlin, J. R., Leonelli, L., Sonbuchner, L. S., McDonald, C. H., Cook, R. G., Dou, Y., Roeder, R. G., Clarke, S., Stallcup, M. R., Allis, C. D., and Coonrod, S. A. (2004) Human PAD4 regulates histone arginine methylation levels via demethyliminination. *Science* **306**, 279-283
36. Fujiki, R., Hashiba, W., Sekine, H., Yokoyama, A., Chikanishi, T., Ito, S., Imai, Y., Kim, J., He, H. H., Igarashi, K., Kanno, J., Ohtake, F., Kitagawa, H., Roeder, R. G., Brown, M., and Kato, S. (2011) GlcNAcylation of histone H2B facilitates its monoubiquitination. *Nature* **480**, 557-560

37. Sakabe, K., Wang, Z., and Hart, G. W. (2010) Beta-N-acetylglucosamine (O-GlcNAc) is part of the histone code. *Proc Natl Acad Sci U S A* **107**, 19915-19920
38. Hassa, P. O., Haenni, S. S., Elser, M., and Hottiger, M. O. (2006) Nuclear ADP-ribosylation reactions in mammalian cells: where are we today and where are we going? *Microbiology and molecular biology reviews : MMBR* **70**, 789-829
39. Hershko, A., and Ciechanover, A. (1998) The ubiquitin system. *Annu Rev Biochem* **67**, 425-479
40. Wang, H., Wang, L., Erdjument-Bromage, H., Vidal, M., Tempst, P., Jones, R. S., and Zhang, Y. (2004) Role of histone H2A ubiquitination in Polycomb silencing. *Nature* **431**, 873-878
41. Lee, J. S., Shukla, A., Schneider, J., Swanson, S. K., Washburn, M. P., Florens, L., Bhaumik, S. R., and Shilatifard, A. (2007) Histone crosstalk between H2B monoubiquitination and H3 methylation mediated by COMPASS. *Cell* **131**, 1084-1096
42. Kim, J., Guermah, M., McGinty, R. K., Lee, J. S., Tang, Z., Milne, T. A., Shilatifard, A., Muir, T. W., and Roeder, R. G. (2009) RAD6-Mediated transcription-coupled H2B ubiquitylation directly stimulates H3K4 methylation in human cells. *Cell* **137**, 459-471
43. Shiio, Y., and Eisenman, R. N. (2003) Histone sumoylation is associated with transcriptional repression. *Proc Natl Acad Sci U S A* **100**, 13225-13230
44. Nathan, D., Ingvarsdottir, K., Sterner, D. E., Bylebyl, G. R., Dokmanovic, M., Dorsey, J. A., Whelan, K. A., Krsmanovic, M., Lane, W. S., Meluh, P. B., Johnson, E. S., and Berger, S. L. (2006) Histone sumoylation is a negative regulator in *Saccharomyces cerevisiae* and shows dynamic interplay with positive-acting histone modifications. *Genes Dev* **20**, 966-976
45. Allis, C. D., Bowen, J. K., Abraham, G. N., Glover, C. V., and Gorovsky, M. A. (1980) Proteolytic processing of histone H3 in chromatin: a physiologically regulated event in *Tetrahymena* micronuclei. *Cell* **20**, 55-64
46. Santos-Rosa, H., Kirmizis, A., Nelson, C., Bartke, T., Saksouk, N., Cote, J., and Kouzarides, T. (2009) Histone H3 tail clipping regulates gene expression. *Nature structural & molecular biology* **16**, 17-22
47. Nelson, C. J., Santos-Rosa, H., and Kouzarides, T. (2006) Proline isomerization of histone H3 regulates lysine methylation and gene expression. *Cell* **126**, 905-916
48. Ahn, S. H., Cheung, W. L., Hsu, J. Y., Diaz, R. L., Smith, M. M., and Allis, C. D. (2005) Sterile 20 kinase phosphorylates histone H2B at serine 10 during hydrogen peroxide-induced apoptosis in *S. cerevisiae*. *Cell* **120**, 25-36
49. Fischle, W., Tseng, B. S., Dormann, H. L., Ueberheide, B. M., Garcia, B. A., Shabanowitz, J., Hunt, D. F., Funabiki, H., and Allis, C. D. (2005) Regulation of HP1-chromatin binding by histone H3 methylation and phosphorylation. *Nature* **438**, 1116-1122
50. Krishnamoorthy, T., Chen, X., Govin, J., Cheung, W. L., Dorsey, J., Schindler, K., Winter, E., Allis, C. D., Guacci, V., Khochbin, S., Fuller, M. T., and Berger, S. L. (2006) Phosphorylation of histone H4 Ser1 regulates sporulation in yeast and is conserved in fly and mouse spermatogenesis. *Genes Dev* **20**, 2580-2592
51. Margueron, R., Trojer, P., and Reinberg, D. (2005) The key to development: interpreting the histone code? *Current opinion in genetics & development* **15**, 163-176
52. McGinty, R. K., Henrici, R. C., and Tan, S. (2014) Crystal structure of the PRC1 ubiquitylation module bound to the nucleosome. *Nature* **514**, 591-596

53. Clements, A., Poux, A. N., Lo, W. S., Pillus, L., Berger, S. L., and Marmorstein, R. (2003) Structural basis for histone and phosphohistone binding by the GCN5 histone acetyltransferase. *Mol Cell* **12**, 461-473
54. Hargreaves, D. C., and Crabtree, G. R. (2011) ATP-dependent chromatin remodeling: genetics, genomics and mechanisms. *Cell research* **21**, 396-420
55. Neigeborn, L., and Carlson, M. (1984) Genes affecting the regulation of SUC2 gene expression by glucose repression in *Saccharomyces cerevisiae*. *Genetics* **108**, 845-858
56. Peterson, C. L., and Herskowitz, I. (1992) Characterization of the yeast SWI1, SWI2, and SWI3 genes, which encode a global activator of transcription. *Cell* **68**, 573-583
57. Hirschhorn, J. N., Brown, S. A., Clark, C. D., and Winston, F. (1992) Evidence that SNF2/SWI2 and SNF5 activate transcription in yeast by altering chromatin structure. *Genes & Development* **6**, 2288-2298
58. Flaus, A., and Owen-Hughes, T. (2003) Mechanisms for nucleosome mobilization. *Biopolymers* **68**, 563-578
59. Bowman, G. D. (2010) Mechanisms of ATP-dependent nucleosome sliding. *Curr Opin Struct Biol* **20**, 73-81
60. Aoyagi, S., and Hayes, J. J. (2002) hSWI/SNF-catalyzed nucleosome sliding does not occur solely via a twist-diffusion mechanism. *Molecular and cellular biology* **22**, 7484-7490
61. Strohner, R., Wachsmuth, M., Dachauer, K., Mazurkiewicz, J., Hochstatter, J., Rippe, K., and Langst, G. (2005) A 'loop recapture' mechanism for ACF-dependent nucleosome remodeling. *Nature structural & molecular biology* **12**, 683-690
62. Deindl, S., Hwang, W. L., Hota, S. K., Blosser, T. R., Prasad, P., Bartholomew, B., and Zhuang, X. (2013) ISWI remodelers slide nucleosomes with coordinated multi-base-pair entry steps and single-base-pair exit steps. *Cell* **152**, 442-452
63. Narlikar, G. J., Sundaramoorthy, R., and Owen-Hughes, T. (2013) Mechanisms and functions of ATP-dependent chromatin-remodeling enzymes. *Cell* **154**, 490-503
64. Gurard-Levin, Z. A., Quivy, J. P., and Almouzni, G. (2014) Histone chaperones: assisting histone traffic and nucleosome dynamics. *Annu Rev Biochem* **83**, 487-517
65. Laskey, R. A., Honda, B. M., Mills, A. D., and Finch, J. T. (1978) Nucleosomes are assembled by an acidic protein which binds histones and transfers them to DNA. *Nature* **275**, 416-420
66. Earnshaw, W. C., Honda, B. M., Laskey, R. A., and Thomas, J. O. (1980) Assembly of nucleosomes: the reaction involving *X. laevis* nucleoplasmin. *Cell* **21**, 373-383
67. Sharp, J. A., Fouts, E. T., Krawitz, D. C., and Kaufman, P. D. (2001) Yeast histone deposition protein Asf1p requires Hir proteins and PCNA for heterochromatic silencing. *Current biology : CB* **11**, 463-473
68. Mello, J. A., Sillje, H. H., Roche, D. M., Kirschner, D. B., Nigg, E. A., and Almouzni, G. (2002) Human Asf1 and CAF-1 interact and synergize in a repair-coupled nucleosome assembly pathway. *EMBO reports* **3**, 329-334
69. Quivy, J. P., Grandi, P., and Almouzni, G. (2001) Dimerization of the largest subunit of chromatin assembly factor 1: importance in vitro and during *Xenopus* early development. *EMBO J* **20**, 2015-2027
70. Ray-Gallet, D., Quivy, J. P., Scamps, C., Martini, E. M., Lipinski, M., and Almouzni, G. (2002) HIRA is critical for a nucleosome assembly pathway independent of DNA synthesis. *Mol Cell* **9**, 1091-1100

71. English, C. M., Adkins, M. W., Carson, J. J., Churchill, M. E., and Tyler, J. K. (2006) Structural basis for the histone chaperone activity of Asf1. *Cell* **127**, 495-508
72. Szenker, E., Ray-Gallet, D., and Almouzni, G. (2011) The double face of the histone variant H3.3. *Cell research* **21**, 421-434
73. Natsume, R., Eitoku, M., Akai, Y., Sano, N., Horikoshi, M., and Senda, T. (2007) Structure and function of the histone chaperone CIA/ASF1 complexed with histones H3 and H4. *Nature* **446**, 338-341
74. Tagami, H., Ray-Gallet, D., Almouzni, G., and Nakatani, Y. (2004) Histone H3.1 and H3.3 complexes mediate nucleosome assembly pathways dependent or independent of DNA synthesis. *Cell* **116**, 51-61
75. Malay, A. D., Umehara, T., Matsubara-Malay, K., Padmanabhan, B., and Yokoyama, S. (2008) Crystal structures of fission yeast histone chaperone Asf1 complexed with the Hip1 B-domain or the Cac2 C terminus. *J Biol Chem* **283**, 14022-14031
76. Corpet, A., and Almouzni, G. (2009) Making copies of chromatin: the challenge of nucleosomal organization and epigenetic information. *Trends in cell biology* **19**, 29-41
77. White, C. L., Suto, R. K., and Luger, K. (2001) Structure of the yeast nucleosome core particle reveals fundamental changes in internucleosome interactions. *EMBO J* **20**, 5207-5218
78. Ishimi, Y., Hirosumi, J., Sato, W., Sugawara, K., Yokota, S., Hanaoka, F., and Yamada, M. (1984) Purification and initial characterization of a protein which facilitates assembly of nucleosome-like structure from mammalian cells. *European journal of biochemistry / FEBS* **142**, 431-439
79. Ishimi, Y., and Kikuchi, A. (1991) Identification and molecular cloning of yeast homolog of nucleosome assembly protein I which facilitates nucleosome assembly in vitro. *J Biol Chem* **266**, 7025-7029
80. Ito, T., Bulger, M., Kobayashi, R., and Kadonaga, J. T. (1996) Drosophila NAP-1 is a core histone chaperone that functions in ATP-facilitated assembly of regularly spaced nucleosomal arrays. *Molecular and cellular biology* **16**, 3112-3124
81. Steer, W. M., Abu-Daya, A., Brickwood, S. J., Mumford, K. L., Jordanaires, N., Mitchell, J., Robinson, C., Thorne, A. W., and Guille, M. J. (2003) Xenopus nucleosome assembly protein becomes tissue-restricted during development and can alter the expression of specific genes. *Mechanisms of development* **120**, 1045-1057
82. Fujii-Nakata, T., Ishimi, Y., Okuda, A., and Kikuchi, A. (1992) Functional analysis of nucleosome assembly protein, NAP-1. The negatively charged COOH-terminal region is not necessary for the intrinsic assembly activity. *J Biol Chem* **267**, 20980-20986
83. Park, Y. J., and Luger, K. (2006) The structure of nucleosome assembly protein 1. *Proc Natl Acad Sci U S A* **103**, 1248-1253
84. Park, Y. J., Chodaparambil, J. V., Bao, Y., McBryant, S. J., and Luger, K. (2005) Nucleosome assembly protein 1 exchanges histone H2A-H2B dimers and assists nucleosome sliding. *J Biol Chem* **280**, 1817-1825
85. Marheineke, K., and Krude, T. (1998) Nucleosome assembly activity and intracellular localization of human CAF-1 changes during the cell division cycle. *J Biol Chem* **273**, 15279-15286
86. Mosammamarast, N., Ewart, C. S., and Pemberton, L. F. (2002) A role for nucleosome assembly protein 1 in the nuclear transport of histones H2A and H2B. *EMBO J* **21**, 6527-6538

87. Miyaji-Yamaguchi, M., Kato, K., Nakano, R., Akashi, T., Kikuchi, A., and Nagata, K. (2003) Involvement of nucleocytoplasmic shuttling of yeast Nap1 in mitotic progression. *Molecular and cellular biology* **23**, 6672-6684
88. Rodriguez, P., Pelletier, J., Price, G. B., and Zannis-Hadjopoulos, M. (2000) NAP-2: histone chaperone function and phosphorylation state through the cell cycle. *J Mol Biol* **298**, 225-238
89. Krogan, N. J., Cagney, G., Yu, H., Zhong, G., Guo, X., Ignatchenko, A., Li, J., Pu, S., Datta, N., Tikuisis, A. P., Punna, T., Peregrin-Alvarez, J. M., Shales, M., Zhang, X., Davey, M., Robinson, M. D., Paccanaro, A., Bray, J. E., Sheung, A., Beattie, B., Richards, D. P., Canadien, V., Lalev, A., Mena, F., Wong, P., Starostine, A., Canete, M. M., Vlasblom, J., Wu, S., Orsi, C., Collins, S. R., Chandran, S., Haw, R., Rilstone, J. J., Gandi, K., Thompson, N. J., Musso, G., St Onge, P., Ghanny, S., Lam, M. H., Butland, G., Altaf-Ul, A. M., Kanaya, S., Shilatifard, A., O'Shea, E., Weissman, J. S., Ingles, C. J., Hughes, T. R., Parkinson, J., Gerstein, M., Wodak, S. J., Emili, A., and Greenblatt, J. F. (2006) Global landscape of protein complexes in the yeast *Saccharomyces cerevisiae*. *Nature* **440**, 637-643
90. D'Arcy, S., Martin, K. W., Panchenko, T., Chen, X., Bergeron, S., Stargell, L. A., Black, B. E., and Luger, K. (2013) Chaperone Nap1 shields histone surfaces used in a nucleosome and can put H2A-H2B in an unconventional tetrameric form. *Mol Cell* **51**, 662-677
91. Andrews, A. J., Chen, X., Zevin, A., Stargell, L. A., and Luger, K. (2010) The histone chaperone Nap1 promotes nucleosome assembly by eliminating nonnucleosomal histone DNA interactions. *Mol Cell* **37**, 834-842
92. Bowman, A., Ward, R., Wiechens, N., Singh, V., El-Mkami, H., Norman, D. G., and Owen-Hughes, T. (2011) The histone chaperones Nap1 and Vps75 bind histones H3 and H4 in a tetrameric conformation. *Mol Cell* **41**, 398-408
93. Keck, K. M., and Pemberton, L. F. (2011) Interaction with the histone chaperone Vps75 promotes nuclear localization and HAT activity of Rtt109 in vivo. *Traffic* **12**, 826-839
94. Bowman, A., Hammond, C. M., Stirling, A., Ward, R., Shang, W., El-Mkami, H., Robinson, D. A., Svergun, D. I., Norman, D. G., and Owen-Hughes, T. (2014) The histone chaperones Vps75 and Nap1 form ring-like, tetrameric structures in solution. *Nucleic Acids Res* **42**, 6038-6051
95. Orphanides, G., LeRoy, G., Chang, C. H., Luse, D. S., and Reinberg, D. (1998) FACT, a factor that facilitates transcript elongation through nucleosomes. *Cell* **92**, 105-116
96. Orphanides, G., Wu, W. H., Lane, W. S., Hampsey, M., and Reinberg, D. (1999) The chromatin-specific transcription elongation factor FACT comprises human SPT16 and SSRP1 proteins. *Nature* **400**, 284-288
97. Clark-Adams, C. D., Norris, D., Osley, M. A., Fassler, J. S., and Winston, F. (1988) Changes in histone gene dosage alter transcription in yeast. *Genes Dev* **2**, 150-159
98. Malone, E. A., Clark, C. D., Chiang, A., and Winston, F. (1991) Mutations in SPT16/CDC68 suppress cis- and trans-acting mutations that affect promoter function in *Saccharomyces cerevisiae*. *Molecular and cellular biology* **11**, 5710-5717
99. Wittmeyer, J., and Formosa, T. (1997) The *Saccharomyces cerevisiae* DNA polymerase alpha catalytic subunit interacts with Cdc68/Spt16 and with Pob3, a protein similar to an HMG1-like protein. *Molecular and cellular biology* **17**, 4178-4190
100. Formosa, T., Eriksson, P., Wittmeyer, J., Ginn, J., Yu, Y., and Stillman, D. J. (2001) Spt16-Pob3 and the HMG protein Nhp6 combine to form the nucleosome-binding factor SPN. *EMBO J* **20**, 3506-3517

101. Brewster, N. K., Johnston, G. C., and Singer, R. A. (2001) A bipartite yeast SSRP1 analog comprised of Pob3 and Nhp6 proteins modulates transcription. *Molecular and cellular biology* **21**, 3491-3502
102. Ruone, S., Rhoades, A. R., and Formosa, T. (2003) Multiple Nhp6 molecules are required to recruit Spt16-Pob3 to form yFACT complexes and to reorganize nucleosomes. *J Biol Chem* **278**, 45288-45295
103. Belotserkovskaya, R., Oh, S., Bondarenko, V. A., Orphanides, G., Studitsky, V. M., and Reinberg, D. (2003) FACT facilitates transcription-dependent nucleosome alteration. *Science* **301**, 1090-1093
104. Jamai, A., Puglisi, A., and Strubin, M. (2009) Histone chaperone spt16 promotes redeposition of the original h3-h4 histones evicted by elongating RNA polymerase. *Mol Cell* **35**, 377-383
105. Schwabish, M. A., and Struhl, K. (2004) Evidence for eviction and rapid deposition of histones upon transcriptional elongation by RNA polymerase II. *Molecular and cellular biology* **24**, 10111-10117
106. Formosa, T., Ruone, S., Adams, M. D., Olsen, A. E., Eriksson, P., Yu, Y., Rhoades, A. R., Kaufman, P. D., and Stillman, D. J. (2002) Defects in SPT16 or POB3 (yFACT) in *Saccharomyces cerevisiae* cause dependence on the Hir/Hpc pathway: polymerase passage may degrade chromatin structure. *Genetics* **162**, 1557-1571
107. John, S., Howe, L., Tafrov, S. T., Grant, P. A., Sternglanz, R., and Workman, J. L. (2000) The something about silencing protein, Sas3, is the catalytic subunit of NuA3, a yTAF(II)30-containing HAT complex that interacts with the Spt16 subunit of the yeast CP (Cdc68/Pob3)-FACT complex. *Genes Dev* **14**, 1196-1208
108. Biswas, D., Yu, Y., Prall, M., Formosa, T., and Stillman, D. J. (2005) The yeast FACT complex has a role in transcriptional initiation. *Molecular and cellular biology* **25**, 5812-5822
109. Mason, P. B., and Struhl, K. (2003) The FACT complex travels with elongating RNA polymerase II and is important for the fidelity of transcriptional initiation in vivo. *Molecular and cellular biology* **23**, 8323-8333
110. Duroux, M., Houben, A., Ruzicka, K., Friml, J., and Grasser, K. D. (2004) The chromatin remodelling complex FACT associates with actively transcribed regions of the Arabidopsis genome. *Plant J* **40**, 660-671
111. Saunders, A., Werner, J., Andrulis, E. D., Nakayama, T., Hirose, S., Reinberg, D., and Lis, J. T. (2003) Tracking FACT and the RNA polymerase II elongation complex through chromatin in vivo. *Science* **301**, 1094-1096
112. Costa, P. J., and Arndt, K. M. (2000) Synthetic lethal interactions suggest a role for the *Saccharomyces cerevisiae* Rtf1 protein in transcription elongation. *Genetics* **156**, 535-547
113. Krogan, N. J., Kim, M., Ahn, S. H., Zhong, G., Kobor, M. S., Cagney, G., Emili, A., Shilatifard, A., Buratowski, S., and Greenblatt, J. F. (2002) RNA polymerase II elongation factors of *Saccharomyces cerevisiae*: a targeted proteomics approach. *Molecular and cellular biology* **22**, 6979-6992
114. Shimojima, T., Okada, M., Nakayama, T., Ueda, H., Okawa, K., Iwamatsu, A., Handa, H., and Hirose, S. (2003) *Drosophila* FACT contributes to Hox gene expression through physical and functional interactions with GAGA factor. *Genes Dev* **17**, 1605-1616
115. Squazzo, S. L., Costa, P. J., Lindstrom, D. L., Kumer, K. E., Simic, R., Jennings, J. L., Link, A. J., Arndt, K. M., and Hartzog, G. A. (2002) The Paf1 complex physically and functionally associates with transcription elongation factors in vivo. *EMBO J* **21**, 1764-1774

116. Takahara, P. M., Rosenzweig, A. C., Frederick, C. A., and Lippard, S. J. (1995) Crystal structure of double-stranded DNA containing the major adduct of the anticancer drug cisplatin. *Nature* **377**, 649-652
117. Yarnell, A. T., Oh, S., Reinberg, D., and Lippard, S. J. (2001) Interaction of FACT, SSRP1, and the high mobility group (HMG) domain of SSRP1 with DNA damaged by the anticancer drug cisplatin. *J Biol Chem* **276**, 25736-25741
118. Sand-Dejmek, J., Adelmant, G., Sobhian, B., Calkins, A., Marto, J., Iglehart, D., and Lazaro, J.-B. (2011) Concordant and opposite roles of DNA-PK and the "facilitator of chromatin transcription" (FACT) in DNA repair, apoptosis and necrosis after cisplatin. *Molecular Cancer* **10**, 74
119. Keller, D. M., and Lu, H. (2002) p53 serine 392 phosphorylation increases after UV through induction of the assembly of the CK2.hSPT16.SSRP1 complex. *J Biol Chem* **277**, 50206-50213
120. Dinant, C., Ampatziadis-Michailidis, G., Lans, H., Tresini, M., Lagarou, A., Grosbart, M., Theil, A. F., van Cappellen, W. A., Kimura, H., Bartek, J., Fousteri, M., Houtsmuller, A. B., Vermeulen, W., and Marteijn, J. A. (2013) Enhanced chromatin dynamics by FACT promotes transcriptional restart after UV-induced DNA damage. *Mol Cell* **51**, 469-479
121. Wittmeyer, J., Joss, L., and Formosa, T. (1999) Spt16 and Pob3 of *Saccharomyces cerevisiae* form an essential, abundant heterodimer that is nuclear, chromatin-associated, and copurifies with DNA polymerase alpha. *Biochemistry* **38**, 8961-8971
122. Schlesinger, M. B., and Formosa, T. (2000) POB3 is required for both transcription and replication in the yeast *Saccharomyces cerevisiae*. *Genetics* **155**, 1593-1606
123. Foltman, M., Evrin, C., De Piccoli, G., Jones, R. C., Edmondson, R. D., Katou, Y., Nakato, R., Shirahige, K., and Labib, K. (2013) Eukaryotic replisome components cooperate to process histones during chromosome replication. *Cell reports* **3**, 892-904
124. O'Donnell, A. F., Brewster, N. K., Kurniawan, J., Minard, L. V., Johnston, G. C., and Singer, R. A. (2004) Domain organization of the yeast histone chaperone FACT: the conserved N-terminal domain of FACT subunit Spt16 mediates recovery from replication stress. *Nucleic Acids Res* **32**, 5894-5906
125. VanDemark, A. P., Blanksma, M., Ferris, E., Heroux, A., Hill, C. P., and Formosa, T. (2006) The structure of the yFACT Pob3-M domain, its interaction with the DNA replication factor RPA, and a potential role in nucleosome deposition. *Mol Cell* **22**, 363-374
126. Gunjan, A., Paik, J., and Verreault, A. (2005) Regulation of histone synthesis and nucleosome assembly. *Biochimie* **87**, 625-635
127. Winkler, D. D., and Luger, K. The histone chaperone Fact: Structural insights and mechanisms for nucleosome reorganization. *J Biol Chem*
128. Tsunaka, Y., Toga, J., Yamaguchi, H., Tate, S., Hirose, S., and Morikawa, K. (2009) Phosphorylated intrinsically disordered region of FACT masks its nucleosomal DNA binding elements. *J Biol Chem* **284**, 24610-24621
129. Stuwe, T., Hothorn, M., Lejeune, E., Rybin, V., Bortfeld, M., Scheffzek, K., and Ladurner, A. G. (2008) The FACT Spt16 "peptidase" domain is a histone H3-H4 binding module. *Proc Natl Acad Sci U S A* **105**, 8884-8889
130. VanDemark, A. P., Xin, H., McCullough, L., Rawlins, R., Bentley, S., Heroux, A., Stillman, D. J., Hill, C. P., and Formosa, T. (2008) Structural and functional analysis of the Spt16p N-terminal domain reveals overlapping roles of yFACT subunits. *J Biol Chem* **283**, 5058-5068

131. Maher, M. J., Ghosh, M., Grunden, A. M., Menon, A. L., Adams, M. W., Freeman, H. C., and Guss, J. M. (2004) Structure of the prolidase from *Pyrococcus furiosus*. *Biochemistry* **43**, 2771-2783
132. Winkler, D. D., Muthurajan, U. M., Hieb, A. R., and Luger, K. (2011) Histone chaperone FACT coordinates nucleosome interaction through multiple synergistic binding events. *J Biol Chem* **286**, 41883-41892
133. Park, Y.-J., Dyer, P. N., Tremethick, D. J., and Luger, K. (2004) A New Fluorescence Resonance Energy Transfer Approach Demonstrates That the Histone Variant H2AZ Stabilizes the Histone Octamer within the Nucleosome. *Journal of Biological Chemistry* **279**, 24274-24282
134. Ferreira, H., Somers, J., Webster, R., Flaus, A., and Owen-Hughes, T. (2007) Histone Tails and the H3 α N Helix Regulate Nucleosome Mobility and Stability. *Molecular and cellular biology* **27**, 4037-4048
135. Hondele, M., Stuwe, T., Hassler, M., Halbach, F., Bowman, A., Zhang, E. T., Nijmeijer, B., Kotthoff, C., Rybin, V., Amlacher, S., Hurt, E., and Ladurner, A. G. (2013) Structural basis of histone H2A-H2B recognition by the essential chaperone FACT. *Nature*
136. Kemble, D. J., Whitby, F. G., Robinson, H., McCullough, L. L., Formosa, T., and Hill, C. P. (2013) Structure of the Spt16 Middle Domain Reveals Functional Features of the Histone Chaperone FACT. *J Biol Chem* **288**, 10188-10194
137. Liu, Y., Huang, H., Zhou, B. O., Wang, S. S., Hu, Y., Li, X., Liu, J., Zang, J., Niu, L., Wu, J., Zhou, J. Q., Teng, M., and Shi, Y. Structural analysis of Rtt106p reveals a DNA binding role required for heterochromatin silencing. *J Biol Chem* **285**, 4251-4262
138. Xin, H., Takahata, S., Blanksma, M., McCullough, L., Stillman, D. J., and Formosa, T. (2009) yFACT induces global accessibility of nucleosomal DNA without H2A-H2B displacement. *Mol Cell* **35**, 365-376
139. Myers, C. N., Berner, G. B., Holthoff, J. H., Martinez-Fonts, K., Harper, J. A., Alford, S., Taylor, M. N., and Duina, A. A. (2011) Mutant versions of the *S. cerevisiae* transcription elongation factor Spt16 define regions of Spt16 that functionally interact with histone H3. *PLoS one* **6**, e20847
140. McCullough, L., Rawlins, R., Olsen, A., Xin, H., Stillman, D. J., and Formosa, T. (2011) Insight into the mechanism of nucleosome reorganization from histone mutants that suppress defects in the FACT histone chaperone. *Genetics* **188**, 835-846
141. Hainer, S. J., Charsar, B. A., Cohen, S. B., and Martens, J. A. (2012) Identification of Mutant Versions of the Spt16 Histone Chaperone That Are Defective for Transcription-Coupled Nucleosome Occupancy in *Saccharomyces cerevisiae*. *G3* **2**, 555-567
142. Yu, J. W., Mendrola, J. M., Audhya, A., Singh, S., Keleti, D., DeWald, D. B., Murray, D., Emr, S. D., and Lemmon, M. A. (2004) Genome-wide analysis of membrane targeting by *S. cerevisiae* pleckstrin homology domains. *Mol Cell* **13**, 677-688
143. Kasai, N., Tsunaka, Y., Ohki, I., Hirose, S., Morikawa, K., and Tate, S. (2005) Solution structure of the HMG-box domain in the SSRP1 subunit of FACT. *J Biomol NMR* **32**, 83-88
144. Masse, J. E., Wong, B., Yen, Y. M., Allain, F. H., Johnson, R. C., and Feigon, J. (2002) The *S. cerevisiae* architectural HMGB protein NHP6A complexed with DNA: DNA and protein conformational changes upon binding. *J Mol Biol* **323**, 263-284
145. Simic, R., Lindstrom, D. L., Tran, H. G., Roinick, K. L., Costa, P. J., Johnson, A. D., Hartzog, G. A., and Arndt, K. M. (2003) Chromatin remodeling protein Chd1 interacts with transcription elongation factors and localizes to transcribed genes. *EMBO J* **22**, 1846-1856

146. Flanagan, J. F., Mi, L. Z., Chruszcz, M., Cymborowski, M., Clines, K. L., Kim, Y., Minor, W., Rastinejad, F., and Khorasanizadeh, S. (2005) Double chromodomains cooperate to recognize the methylated histone H3 tail. *Nature* **438**, 1181-1185
147. Sims, R. J., 3rd, Chen, C. F., Santos-Rosa, H., Kouzarides, T., Patel, S. S., and Reinberg, D. (2005) Human but not yeast CHD1 binds directly and selectively to histone H3 methylated at lysine 4 via its tandem chromodomains. *J Biol Chem* **280**, 41789-41792
148. Kelley, D. E., Stokes, D. G., and Perry, R. P. (1999) CHD1 interacts with SSRP1 and depends on both its chromodomain and its ATPase/helicase-like domain for proper association with chromatin. *Chromosoma* **108**, 10-25
149. Xiao, T., Kao, C. F., Krogan, N. J., Sun, Z. W., Greenblatt, J. F., Osley, M. A., and Strahl, B. D. (2005) Histone H2B ubiquitylation is associated with elongating RNA polymerase II. *Molecular and cellular biology* **25**, 637-651
150. Rondon, A. G., Gallardo, M., Garcia-Rubio, M., and Aguilera, A. (2004) Molecular evidence indicating that the yeast PAF complex is required for transcription elongation. *EMBO reports* **5**, 47-53
151. Pavri, R., Zhu, B., Li, G., Trojer, P., Mandal, S., Shilatifard, A., and Reinberg, D. (2006) Histone H2B monoubiquitination functions cooperatively with FACT to regulate elongation by RNA polymerase II. *Cell* **125**, 703-717
152. Zhou, W., Zhu, P., Wang, J., Pascual, G., Ohgi, K. A., Lozach, J., Glass, C. K., and Rosenfeld, M. G. (2008) Histone H2A monoubiquitination represses transcription by inhibiting RNA polymerase II transcriptional elongation. *Mol Cell* **29**, 69-80
153. Heo, K., Kim, H., Choi, S. H., Choi, J., Kim, K., Gu, J., Lieber, M. R., Yang, A. S., and An, W. (2008) FACT-mediated exchange of histone variant H2AX regulated by phosphorylation of H2AX and ADP-ribosylation of Spt16. *Mol Cell* **30**, 86-97
154. Landais, I., Lee, H., and Lu, H. (2006) Coupling caspase cleavage and ubiquitin-proteasome-dependent degradation of SSRP1 during apoptosis. *Cell Death Differ* **13**, 1866-1878
155. Li, Y., Keller, D. M., Scott, J. D., and Lu, H. (2005) CK2 phosphorylates SSRP1 and inhibits its DNA-binding activity. *J Biol Chem* **280**, 11869-11875
156. Keller, D. M., Zeng, X., Wang, Y., Zhang, Q. H., Kapoor, M., Shu, H., Goodman, R., Lozano, G., Zhao, Y., and Lu, H. (2001) A DNA damage-induced p53 serine 392 kinase complex contains CK2, hSpt16, and SSRP1. *Mol Cell* **7**, 283-292
157. Spencer, J. A., Baron, M. H., and Olson, E. N. (1999) Cooperative transcriptional activation by serum response factor and the high mobility group protein SSRP1. *J Biol Chem* **274**, 15686-15693
158. Zeng, S. X., Dai, M. S., Keller, D. M., and Lu, H. (2002) SSRP1 functions as a co-activator of the transcriptional activator p63. *EMBO J* **21**, 5487-5497
159. Zeng, S. X., Li, Y., Jin, Y., Zhang, Q., Keller, D. M., McQuaw, C. M., Barklis, E., Stone, S., Hoatlin, M., Zhao, Y., and Lu, H. (2009) Structure-specific recognition protein 1 facilitates microtubule growth and bundling required for mitosis. *Molecular and cellular biology* **30**, 935-947
160. Li, Y., Zeng, S. X., Landais, I., and Lu, H. (2007) Human SSRP1 has Spt16-dependent and -independent roles in gene transcription. *J Biol Chem* **282**, 6936-6945
161. Ransom, M., Williams, S. K., Dechassa, M. L., Das, C., Linger, J., Adkins, M., Liu, C., Bartholomew, B., and Tyler, J. K. (2009) FACT and the proteasome promote promoter chromatin disassembly and transcriptional initiation. *J Biol Chem* **284**, 23461-23471

162. Kireeva, M. L., Walter, W., Tchernajenko, V., Bondarenko, V., Kashlev, M., and Studitsky, V. M. (2002) Nucleosome remodeling induced by RNA polymerase II: loss of the H2A/H2B dimer during transcription. *Mol Cell* **9**, 541-552
163. Jackson, V. (1990) In vivo studies on the dynamics of histone-DNA interaction: evidence for nucleosome dissolution during replication and transcription and a low level of dissolution independent of both. *Biochemistry* **29**, 719-731
164. Fraga, M. F., Ballestar, E., Villar-Garea, A., Boix-Chornet, M., Espada, J., Schotta, G., Bonaldi, T., Haydon, C., Ropero, S., Petrie, K., Iyer, N. G., Perez-Rosado, A., Calvo, E., Lopez, J. A., Cano, A., Calasanz, M. J., Colomer, D., Piris, M. A., Ahn, N., Imhof, A., Caldas, C., Jenuwein, T., and Esteller, M. (2005) Loss of acetylation at Lys16 and trimethylation at Lys20 of histone H4 is a common hallmark of human cancer. *Nat Genet* **37**, 391-400
165. Ozdag, H., Teschendorff, A. E., Ahmed, A. A., Hyland, S. J., Blenkiron, C., Bobrow, L., Veerakumarasivam, A., Burt, G., Subkhankulova, T., Arends, M. J., Collins, V. P., Bowtell, D., Kouzarides, T., Brenton, J. D., and Caldas, C. (2006) Differential expression of selected histone modifier genes in human solid cancers. *BMC Genomics* **7**, 90
166. Corpet, A., De Koning, L., Toedling, J., Savignoni, A., Berger, F., Lemaître, C., O'Sullivan, R. J., Karlseder, J., Barillot, E., Asselain, B., Sastre-Garau, X., and Almouzni, G. Asf1b, the necessary Asf1 isoform for proliferation, is predictive of outcome in breast cancer. *EMBO J* **30**, 480-493
167. Alekseev, O. M., Richardson, R. T., Tsuruta, J. K., and O'Rand, M. G. Depletion of the histone chaperone tNASP inhibits proliferation and induces apoptosis in prostate cancer PC-3 cells. *Reprod Biol Endocrinol* **9**, 50
168. Gasparian, A. V., Burkhart, C. A., Purmal, A. A., Brodsky, L., Pal, M., Saranadasa, M., Bosykh, D. A., Commane, M., Guryanova, O. A., Pal, S., Safina, A., Sviridov, S., Koman, I. E., Veith, J., Komar, A. A., Gudkov, A. V., and Gurova, K. V. Curaxins: anticancer compounds that simultaneously suppress NF- κ B and activate p53 by targeting FACT. *Sci Transl Med* **3**, 95ra74
169. Bradford, M. M. (1976) A rapid and sensitive method for the quantitation of microgram quantities of protein utilizing the principle of protein-dye binding. *Anal Biochem* **72**, 248-254
170. Gasteiger E., H. C., Gattiker A., Duvaud S., Wilkins M.R., Appel R.D., Bairoch A. (2005) Protein Identification and Analysis Tools on the ExPASy Server. in *The Proteomics Protocols Handbook* (Walker, J. M. E. ed.), Humana Press. pp pp. 571-607
171. Luger, K., Rechsteiner, T. J., and Richmond, T. J. (1999) Preparation of nucleosome core particle from recombinant histones. *Methods Enzymol* **304**, 3-19
172. Lambert, S. J., Nicholson, J. M., Chantalat, L., Reid, A. J., Donovan, M. J., and Baldwin, J. P. (1999) Purification of histone core octamers and 2.15 Å X-ray analysis of crystals in KCl/phosphate. *Acta Crystallogr D Biol Crystallogr* **55**, 1048-1051
173. Kabsch, W. (2010) Xds. *Acta Crystallogr D Biol Crystallogr* **66**, 125-132
174. Collaborative Computational Project, N. (1994) The CCP4 suite: programs for protein crystallography. *Acta Crystallogr D Biol Crystallogr* **50**, 760-763
175. Storoni, L. C., McCoy, A. J., and Read, R. J. (2004) Likelihood-enhanced fast rotation functions. *Acta Crystallogr D Biol Crystallogr* **60**, 432-438
176. Emsley, P., and Cowtan, K. (2004) Coot: model-building tools for molecular graphics. *Acta Crystallogr D Biol Crystallogr* **60**, 2126-2132
177. Adams, P. D., Grosse-Kunstleve, R. W., Hung, L. W., Ioerger, T. R., McCoy, A. J., Moriarty, N. W., Read, R. J., Sacchettini, J. C., Sauter, N. K., and Terwilliger, T. C. (2002)

- PHENIX: building new software for automated crystallographic structure determination. *Acta Crystallogr D Biol Crystallogr* **58**, 1948-1954
178. Konarev, P. V., Volkov, V. V., Sokolova, A. V., Koch, M. H. J., and Svergun, D. I. (2003) PRIMUS: a Windows PC-based system for small-angle scattering data analysis. *Journal of Applied Crystallography* **36**, 1277-1282
 179. Svergun, D. (1992) Determination of the regularization parameter in indirect-transform methods using perceptual criteria. *Journal of Applied Crystallography* **25**, 495-503
 180. Franke, D., and Svergun, D. I. (2009) DAMMIF, a program for rapid ab-initio shape determination in small-angle scattering. *Journal of Applied Crystallography* **42**, 342-346
 181. Volkov, V. V., and Svergun, D. I. (2003) Uniqueness of ab initio shape determination in small-angle scattering. *Journal of Applied Crystallography* **36**, 860-864
 182. Yang, J., Yan, R., Roy, A., Xu, D., Poisson, J., and Zhang, Y. (2015) The I-TASSER Suite: protein structure and function prediction. *Nature methods* **12**, 7-8
 183. Petoukhov, M. V., Franke, D., Shkumatov, A. V., Tria, G., Kikhney, A. G., Gajda, M., Gorba, C., Mertens, H. D. T., Konarev, P. V., and Svergun, D. I. (2012) New developments in the ATSAS program package for small-angle scattering data analysis. *Journal of Applied Crystallography* **45**, 342-350
 184. Kozin M.B., S. D. I. (2001) Automated matching of high- and low-resolution structural models. *J. Appl. Crystallogr.*, 33-41
 185. Laue T.M., S. B. D., R Ridgeway T.M., Peletier S.L. . (1992) Computer-aided interpretation of analytical sedimentation data for proteins. *Harding S.E.R.A., Horton J.C., editors. Analytical Ultracentrifugation in Biochemistry and Polymer Science. Society of Chemistry; Cambridge*, 99-125
 186. Schuck, P. (2000) Size-distribution analysis of macromolecules by sedimentation velocity ultracentrifugation and lamm equation modeling. *Biophys J* **78**, 1606-1619
 187. Vistica, J., Dam, J., Balbo, A., Yikilmaz, E., Mariuzza, R. A., Rouault, T. A., and Schuck, P. (2004) Sedimentation equilibrium analysis of protein interactions with global implicit mass conservation constraints and systematic noise decomposition. *Anal Biochem* **326**, 234-256
 188. Baker, N. A., Sept, D., Joseph, S., Holst, M. J., and McCammon, J. A. (2001) Electrostatics of nanosystems: Application to microtubules and the ribosome. *Proceedings of the National Academy of Sciences* **98**, 10037-10041
 189. Goldschmidt, L., Cooper, D. R., Derewenda, Z. S., and Eisenberg, D. (2007) Toward rational protein crystallization: A Web server for the design of crystallizable protein variants. *Protein science : a publication of the Protein Society* **16**, 1569-1576
 190. Smith, C. A. (1988) Estimation of Sedimentation Coefficients and Frictional Ratios of Globular Proteins. *Biomedical Education* **16**
 191. Dam, J., and Schuck, P. (2004) Calculating sedimentation coefficient distributions by direct modeling of sedimentation velocity concentration profiles. *Methods Enzymol* **384**, 185-212
 192. Zunder, R. M., Antczak, A. J., Berger, J. M., and Rine, J. (2012) Two surfaces on the histone chaperone Rtt106 mediate histone binding, replication, and silencing. *Proc Natl Acad Sci U S A* **109**, E144-153
 193. Laura McCullough, B. P., Zaily Connell, Hua Xin and Tim Formosa. (2013) The FACT Histone Chaperone Guides Histone H4 Into Its Nucleosomal Conformation in *Saccharomyces cerevisiae*. *Genetics* **195**, 101-113

194. Laura McCullough, R. R., * Aileen Olsen,† Hua Xin,* David J. Stillman,† and Tim Formosa. (2011) Insight Into the Mechanism of Nucleosome Reorganization From Histone Mutants That Suppress Defects in the FACT Histone Chaperone. *Genetics* **188**, 835-846
195. Lee, C. G., Hague, L. K., Li, H., and Donnelly, R. (2004) Identification of toposome, a novel multisubunit complex containing topoisomerase IIalpha. *Cell cycle* **3**, 638-647
196. Broderick, R., Nieminuszczy, J., Blackford, A. N., Winczura, A., and Niedzwiedz, W. (2015) TOPBP1 recruits TOP2A to ultra-fine anaphase bridges to aid in their resolution. *Nature communications* **6**, 6572